

Université Fédérale



Toulouse Midi-Pyrénées

THÈSE

En vue de l'obtention du **DOCTORAT DE L'UNIVERSITÉ DE TOULOUSE**

Délivré par l'Université Toulouse 3 - Paul Sabatier

Présentée et soutenue par

Viet PHAM

Le 24 juin 2020

Tracage de l'empreinte lithogénique en mers de Corail et des Salomon: apport des terres rares et de la composition isotopique du neodyme

Ecole doctorale : **SDUZE - Sciences de l'Univers, de l'Environnement et de l'Espace**

Spécialité : **Océan, Atmosphère, Climat**

Unité de recherche :

LEGOS - Laboratoire d'Etudes en Géophysique et Océanographie Spatiale

Thèse dirigée par

Catherine JEANDEL et Sophie CRAVATTE

Jury

Mme Cécile GUIEU, Rapporteur

M. Christophe COLIN, Rapporteur

M. Sylvain OUILLON, Examineur

Mme Thi Hue NGUYEN, Examinatrice

Mme Catherine JEANDEL, Directrice de thèse

Mme Sophie CRAVATTE, Co-directrice de thèse

“The sea is everything. It covers seven tenths of the terrestrial globe. Its breath is pure and healthy. It is an immense desert, where man is never lonely, for he feels life stirring on all sides. The sea is only the embodiment of a supernatural and wonderful existence. It is nothing but love and emotion; it is the Living Infinite.”

– Jules Verne, Twenty Thousand Leagues Under the Sea



Acknowledgement

From my point of view, my Ph.D. thesis was very formative and concentrate due to the opportunities I had to work with new things in which I had to dig on it, discovered so many new impressive things. I worked with marine geochemistry which did impress me at the beginning of the Ph.D. period. Since the Pandora project was conducted in 2012, I could not participate in it. However, the short trip to collect samples on the beach of Marseille and a winter school in Israel opened my mind about sampling campaigns. I was also able to train myself in the preparation and analysis of these samples in a clean room and then on various machines, particularly the mass spectrometers of the Midi-Pyrénées Observatory (OMP): ICMPS Agilent, ICPMS high-resolution Element-XR, MC-ICPMS Neptune and TIMS MAT-261. All of these training and information turn my thesis to a long road, a path filled with difficulties and stress. However, the encouragement from family, friends, and coworkers allowed me to reach the goal. That's why I want to thank them before continuing my journey toward the future.

Foremost, I would like to express my deepest gratitude to my two Ph.D. directors, Catherine and Sophie who I always called "Maman de these", for all of their patience, motivation, enthusiasm, and immense knowledge. They were the pillars of my thesis by providing me a privileged framework, wise counsel, and attentive ear. Their guidance helped me in all the time of research and writing of this Ph.D. thesis. I could not have imagined having a better advisor and mentor for my Ph.D. Overall, they instilled in me their passion for oceanography and geochemist.

I also want to thank all the jury members for their interest in my work, their thorough reading of this manuscript, and the remarks and suggestions relevant information. So thank you to Dr. Sylvain Ouillon for agreeing to chair the jury, my reviewers Christophe Colin and Cécile Guieu, my examiners Thi Hue Nguyen and Sylvain Ouillon. I am honored that you agreed to be part of my thesis jury.

I was lucky to get funded by the 911 fellowship program from the Ministry of Education and Training (MOET) and then sent to study in France from Water - Environment - Oceanography (WEO) department of the University of Science and Technology of Hanoi (-USTH). Here, I would like to thank the successive LEGOS director Alex Ganachaud who welcomed me into the laboratory, worried about my evolution, and sustained over the past three years. I extend my warmest thanks to the LEGOS managers, Martine, Nadine, Brigitte, and Agathe. I have many times appreciated their kindness, their indulgence, and their effectiveness in helping me through the various administrative procedures for my Ph.D.

I would like to sincerely thank the various people with whom I have been able to collaborate during my thesis. My special thanks to Prof. Sylvain Ouillon, head of WEO department, USTH for his meaningful supports in both mental and financial ways since my master and then my ph.D.

I have a special thought for the members of the TIM team who welcomed me in their small "family" during these 3 years. A special thank you to Kathy and Moustafa who guided me a lot in the "Salle Blanche". Thank you to Francois for his precious advice, his rigor, his availability,

and his good jokes, Pieter and Marc for their frequent encouragement, optimism, and good humor. Thanks to Lise and Marion who were the best of friends, quickly integrating me into a sacred group of friends! Thanks to Melanie for your supporting about the Pandora cruise and helping to purchase the stuff for my seaSLOW.

My thanks also go to the service of ICP-MS (Aurellie, Camile, G-rom..) and TIMS (Stephanie) for your presence during my measurement and helped me a lot to control these instruments. Thanks to Valerie Chavagnac for all of your advice and encouragement each time I had a chance to discuss with you.

Thanks to my many office colleagues Manon, Soo Yang, Xli, Nhu who all created in offices a pleasant, lively, relaxed atmosphere and friendly. I thank them for their tolerance and indulgence. Similarly, I thank the director of the SDU2E doctoral school Geneviève Soucail for your support during my Ph.D. I also extend my sincere thanks to executive assistants Marie-Claude Cathala and Tanya Robinson who helped me through the various administrative processes, allowing me to well to support my thesis on time.

It would be a truly miserable Ph.D. life without the companionship of my Vietnamese friends (Mr. Đa già, anh Kiên-Hoa, anh Hưng, anh Sơn, anh Đức, anh Cường-Lan ...) and LEGOS friends (Vandhna, Gabrielle, Audrey, Simon, Michael, Alice...). But above all, my honest thanks to Tùng béo and Bích béo to stay with me and sharing all of my valuable moments. You are an important part of my Toulouse life that I will never forget. My special thanks for the relaxing lunches with my dear friends (anh Thái, chị Ngọc, Tùng béo). Those fun moments with you guys helped to recharge my energy.

Finally, I extend very sincere thanks to my family, and in particular to my parents, who allowed me to leave the family nest and fly to France. They have always supported me, no matter how hard they struggled to see me settled so far from home, and have always given me advice in my moments of doubts and stress. They never stopped encouraging me to go through with my and I'm building a future that I like. Thank you to them, as well as to my older brother, Quốc Anh, my sister-in-law (chị Hường) and my two little nieces (Ngân Hà and Thảo Nguyên).

Abstract

The aim of this thesis was to better constrain the land-ocean fluxes using geochemical tracers, Rare Earth Element (REE) and Neodymium Isotopic Composition (Nd-IC). The studied area was the Coral and Solomon Seas, a part of the Southwest Pacific Ocean (SPO) where the waters feeding the Equatorial Pacific Ocean are circulating which confers an important role in the climate regulation to this area. The SPO is also a place where important hydrological and chemical modifications of the water masses occur.

A new dREE analytical protocol was developed to replace the one used for years in my research team. This “seaSLOW” manifold allows the simultaneous treatment of 8 seawater samples, dramatically reducing the analytical time, with a low matrix blank signal - less than 0.5% for dREE signal. Affordable detection limits (equal $\sim 1/40$ of the average seawater concentration) and high quantitative recoveries ($>90\%$) were obtained during the blank and performance tests, respectively. The strong points of seaSLOW are that it is low-cost (equal one fifteenth of the commercial product seaFAST) and easy to fabricate, making it accessible for other users, including developing countries

Vertical profiles of dissolved REE (dREE) concentrations for 143 samples collected in the Coral and Solomon Seas as part of the PANDORA cruise in summer 2012 were analyzed. dREE concentration –except the insoluble Ce– indicates the nutrient like profiles, i.e. low values at the surface increasing at depth (e.g. Nd concentrations range from ~ 5 pmol/kg at the surface to ~ 25 pmol/kg in the deepest layers). Local dREE enrichments are observed along the coast and in the three northern exiting straits of the Solomon Sea (a.k.a: Indispensable, Solomon and Vitiaz Straits). dREE variations in the different water layers were quantified using box models, pointing out a net enrichment of 145 ± 46 tNd/year in the lower thermocline. The basaltic material imprint was brought to light by positive Eu and Ce anomalies, especially in surface layer. The better correlation between heavy REE (HREE) and Si cycle than that observed for the LREE in the oceanic water was also confirmed. These results are published in Chemical Geology (Pham et al, 2019)

Dissolved Nd-IC were also measured on the same samples. The distributions of both Nd parameters (Nd concentration and Nd-IC) between the the Coral Sea, the entrance and the exit of the Solomon Sea were established as vertical profiles and as maps representing the layers transporting the different water bodies. All the vertical profiles show similar patterns with more radiogenic Nd-IC in the surface layer (up to $\epsilon_{Nd} = +3$), minimal ϵ_{Nd} values at Intermediate depths (~ 1100 m) before increasing again toward the bottom. On a regional scale, higher Nd-IC signals are observed at the northern exits than at the southern entrance of the Solomon Sea, likely reflecting the release of radiogenic material to the water masses during their pathways across the Solomon Sea. The occurrence of boundary exchange (BE) processes were suggested at many place within the sea, either at a local scale (e.g: surface water passing through Indispensable strait) or at the regional scale (e.g: deep water across the Solomon Sea). Quantification of BE via box models was conducted for the lower part of the Lower thermocline (LLTW) and the upper layer of the deep water layers (UCDW). As an illustration, the external input of Nd required to balance both the Nd-IC and Nd concentrations of the upper deep layer

(UCDW) between the southern entrance and the northern exits is of 105 ± 50 TNd/y. Applying Nd both parameters helped to better identify the sources of material and to reduce the uncertainties affecting the processes. Future studies of these parameter distributions on the suspended particles collected at the same stations will help to get a full picture of the processes governing the dissolved-particulate exchanges.

Résumé

Le but de cette thèse était de mieux contraindre les flux continent-océan à l'aide de traceurs géochimiques, les terres rares (REE) et la composition isotopique du néodyme (Nd-IC), en se focalisant sur les mers de Corail et des Salomon, région de l'Océan Pacifique Sud-Ouest (OPS) où circulent les eaux alimentant le Pacifique Equatorial et qui est le siège d'importantes modifications hydrologiques et géochimiques des masses d'eau.

Un nouveau protocole analytique des terres rares dissoutes (dREE) a été développé. Ce système 'seaSLOW' permet la préconcentration simultanée de 8 échantillons d'eau de mer, réduisant considérablement le temps d'analyse, avec un excellent blanc de chimie -moins de 0,5% du signal de dREE-, des limites de détection $\sim 1/40$ de la concentration moyenne d'eau de mer et des rendements $> 90\%$. Mais surtout, le seaSLOW est peu coûteux, facile à fabriquer, ce qui le rend accessible pour d'autres utilisateurs, en particulier des pays en développement

Les profils verticaux de dREE ont été réalisés pour 143 échantillons prélevés en mers de Corail et des Salomon (campagne PANDORA; été 2012). Les concentrations de dREE - à l'exception du Ce insoluble - montrent des profils de type nutriment soit de faibles valeurs en surface et plus riches en profondeur (ex: les concentrations de Nd varient de ~ 5 à 25 pmol / kg entre surface et fond) Des enrichissements locaux en dREE sont observés le long des côtes et dans les trois détroits, sorties de la mer Salomon. Des modèles en boîte révèlent un enrichissement net significatif de REE dans la thermocline inférieure (soit: 145 ± 46 tNd / an). L'empreinte basaltique a été mise en évidence par des anomalies positives Eu et Ce, en particulier dans la couche de surface. La très bonne corrélation entre les Terres Rares lourdes et le silicium dissous est confirmée. Ces résultats sont publiés dans Pham et al (2019)

Le Nd-IC dissous a également été mesuré sur les mêmes échantillons. Les distributions des deux paramètres Nd (concentration Nd et Nd-IC) entre la mer de Corail, l'entrée et la sortie de la mer Salomon ont été établies sous forme de profils verticaux et de cartes représentant les couches transportant les différentes masses d'eau. Les profils verticaux montrent tous plus de Nd-IC radiogénique dans la couche de surface (jusqu'à $\epsilon_{Nd} = +3$), des valeurs minimales de ϵ_{Nd} à des profondeurs intermédiaires (~ 1100 m) avant d'augmenter à nouveau en profondeur. À l'échelle régionale, des signaux de Nd-IC très positifs sont observés aux sorties nord de la mer Salomon, reflétant probablement la libération de matières radiogéniques dans les masses d'eau au cours de leur parcours à travers la mer Salomon. L'occurrence de processus d'échange aux frontières (BE) a été suggérée à de nombreux endroits, soit à l'échelle locale (ex: les eaux de surface traversant Indispensable Strait) ou à l'échelle régionale (ex: les eaux profondes à travers la mer Salomon). La quantification du BE via des modèles en boîtes a pu être réalisée pour la partie inférieure de la thermocline inférieure (LLTW) et la couche supérieure des couches d'eau profonde (UCDW). À titre d'illustration, l'apport externe de Nd nécessaire pour équilibrer à la fois les variations de Nd-IC et les concentrations de Nd de la couche profonde supérieure (UCDW) entre l'entrée sud et les sorties nord de la Mer des Salomon est de 105 ± 50 TNd / an. L'application des deux paramètres Nd a permis de mieux identifier les sources de matière et de réduire les incertitudes affectant les processus. Les études futures de ces distributions de

paramètres sur les particules en suspension collectées aux mêmes stations permettront d'obtenir une image complète des processus régissant les échanges entre particules et dissous.

Table of contents

Chapter 1 Introduction	8
1.1 General context – Why do we study the Solomon and Coral Seas?.....	9
1.2 The Southwest Pacific Ocean – hydrological context.....	12
1.3 Tracers in the sea- The Rare Earth Elements (REE) and Neodymium isotopic composition (Nd-IC).....	18
1.3.1 REE and their distribution.....	18
1.3.2 Neodymium and its isotopes.....	21
1.4 Land-ocean inputs: pathways and Boundary Exchange.....	23
1.5 Thesis objective.....	24
Chapter 2 Methodology	25
2.1 The Pandora Oceanographic cruise.....	26
2.2 Sampling procedure.....	27
2.3 Sample treatment and data analysis.....	28
2.3.1 Dissolved REE concentrations.....	28
2.3.2 Dissolved Nd-IC.....	31
Chapter 3 The ‘SeaSLOW’	34
3.1 Introduction.....	35
3.2 Material and procedure.....	36
3.2.1 Reagents.....	36
3.2.2 Pre-concentration system (seaSLOW).....	37
3.3 Method optimization.....	40
3.3.1 Column capacity and sample volume.....	40
3.3.2 The rinsing volume.....	41
3.4 Manifold validation.....	42
3.4.1 Blank and detection limit.....	44
3.4.2 Accuracy and precision.....	46
3.5 Conclusion.....	48
ANNEX A: MANIFOLD USER INSTRUCTION.....	50
Chapter 4 Dissolved rare earth element distribution in the Solomon Sea	58

4.1 Introduction.....	59
4.2 Published article: Dissolved rare earth elements distribution in the Solomon Sea.....	60
Chapter 5 The Southwest Pacific Ocean: Neodymium isotopic composition and rare earth element concentration variation	98
5.1 Introduction.....	99
5.2 Sampling and analytical procedure.....	100
5.3 Results.....	100
5.3.1 Vertical distribution	100
5.3.2 Comparison with previous studies	105
5.4 Discussion.....	106
5.4.1 Geochemical characteristics of the lithogenic source.....	106
5.4.2 Seawater modification through the Solomon Sea.....	109
5.4.3 Quantifying the Boundary exchange process.....	124
5.5 Conclusion	128
ANNEX B: LIST OF REFERENCES USED TO BUILD THE MAP OF LITHIOGENIC GEOCHEMICAL SIGNATURES AROUND AND AT THE BOTTOM OF THE CORAL AND SOLOMON SEAS.....	130
Chapter 6 Conclusion and Perspective.....	133
6.1 Conclusion	134
6.2 Perspectives.....	137
6.2.1 Better constraining the elemental fluxes at land-ocean interface and the fate of particles in seawater	137
6.2.2 Deep waters inside the Solomon Sea	138
6.2.3 Future collaboration between Vietnam-France: project PLUME	141
Reference	143

Table of figures

Figure 1-1 From South Equatorial Current (SEC) to Equatorial Undercurrent (EUC) of Western Pacific Ocean. From surface to intermediate depth currents, including Mindanao Current (MC), North Equatorial Current (NEC), North Equatorial Countercurrent (NECC), New Guinea Coastal Current (NGCC), and East Australia Current (EAC). The subsurface currents are New Guinea Coastal Undercurrent (NGCUC), Northern and Southern Subsurface Countercurrents (NSCC and SSCC), Mindanao Undercurrent (MUC), and Great Barrier Reef Undercurrent (GBRUC). Data from Fine et al (1994)..... 10

Figure 1-2 Average concentration of Pacific’s surface water of a) Nitrate (mmol/Kg), data from WOCE (<https://www.ewoce.org/>) and b) Chlorophyll (mg/m³), data from MODIS satellite (<https://oceancolor.gsfc.nasa.gov/>). Oval-shape with red line marks the HNLC zone while rectangle one indicate the Southwest pacific. 11

Figure 1-3 Main elements and regional structure of the SPICE field program, the background map and colorbar indicates ocean depth. Note that PIES=Pressure Inverted Echo Sounder; HR-XBT= High resolution XBTs; Q-IMOS= Integrated Marine Observing System (Queensland node); ECC= East Caledonian Current; EAC = East Australia Current. Data from (Ganachaud et al., 2014a)..... 12

Figure 1-4 Major surface (solid arrows) and subsurface (dashed arrows) currents of the Equatorial Pacific. Note that NEC =North Equatorial Current; nSEC and sSEC=north, south South Equatorial Currents; ME=Mindanao Eddy; HE=Halmahera Eddy). Blue shading areas indicate the subtropical subduction zones while green shading ones represent the equatorial/eastern upwelling. Magenta lines show the poleward pathways from central pacific. Numbers indicate water mass transport (Sv). Data from (Schott, Wang and Stammer, 2007). 13

Figure 1-5 Mean circulation of the Southwest Pacific Ocean. a) Topography with color scale in meters. Blue arrows denote the main currents while red arrows indicate the main surface counter currents. Data from Ganachaud et al., (2014). b) Zoom on the Solomon Sea during Pandora cruise (July-August 2012). Brown shading indicates shallow bathymetry (<1000m); Black and yellow dots represent station position and geochemical stations, respectively. Red arrows denote the main thermocline currents. GPC = Gulf of Papua Current; NVJ= North Vanuatu Jet; NGCU= New Guinea Coastal Undercurrent; NICU= New Ireland Coastal Undercurrent; NBCU= New Britain Coastal Undercurrent, SGU= Saint Georges Undercurrent. Data from Germaineaud et al., (2016) 15

Figure 1-6 a) The REE family in periodic table and b) the lanthanide contraction 18

Figure 1-7 Oddo-Hakkin Rule, REE group is shown under red rectangular 19

Figure 1-8 Examples of Post-Archean Australian Sedimentary (PAAS) –REE normalized patterns. (a) REE dissolved in seawater of station 60 – Pandora (b) REE of basaltic rock collected in Southwest Pacific Islands. According to Pham et al., (2019) 20

Figure 1-9 Schematic model of REE fractionation between particle seawater. Inside the oceanic particle, authigenic and lithogenic phases also are identified inside the particle. Data from (Sholkovitz, M. Landing and Lewis, 1994)	21
Figure 1-10 Extrapolation map of ϵ_{Nd} in continental rock. Extracted from Jeandel et al., (2007).	22
Figure 2-1 Pandora trajectory and sampling stations. Upper right corner is a picture of R/V L'Atalante	26
Figure 2-2 Nd-IC preconcentration on C18 cartridge during Pandora, a) modification of C18 cartridge by complexing agent, b) Multi-line preconcentrating with support device and peristaltic pump.....	28
Figure 2-3 Handcraft column for anionic resin AG 1- X8	30
Figure 2-4 A set of cationic column packed with AG50W-X8 resin. Column using here is a commercial product Poly-Prep® Chromatography Columns (Biorad™).....	31
Figure 2-5 a) Ln-Spec quartz column and b) Ln-Spec commercial resin.....	32
Figure 2-6 Measurement on TIMS, a) deposition of sample on the Re filament; b) inserting roller into sample introduction tray of TIMS and c) Schematic of Thermo-Ionization Mass Spectrometer (TIMS, Thermo Fisher®).....	33
Figure 3-1 seaSLOW preconcentration column with NOBIAS®-PA-1 chelate resin	37
Figure 3-2 seaSLOW manipulation scheme.....	38
Figure 3-3 Effect of rinsing buffer on the removal of salt content in the seaSLOW column	42
Figure 3-4 Analytical RSD(%) of different samples after seaSLOW and classical protocol.....	45
Figure 3-5 Normalization to PASS (Taylor and McLennan, 1985) of average REE concentration of seaSLOW compare with Classical protocol data published by Pham et al (2009).....	47
Figure 3-6 Pictures of seaSLOW system in ISO 2 clean laboratory of LEGOS, Toulouse, France	48
Figure 5-1 Vertical distribution of ϵ_{Nd} measured at all the stations shown in figure 5.0, as a function of a) depth and b) sigma	101
Figure 5-2 Location of the sampling stations dedicated to the Nd isotopic composition measurements during Pandora. Different colors are used to “cluster” the different sampling areas, as in Pham et al., (2019). The red points correspond to the southern entrance of the Solomon Sea. Samples collected in waters flowing through four straits (Indispensable, Vitiaz, St George's and Solomon), are colored with violet, black, green and dark blue, respectively. These color criteria will be kept all along this study. In addition, dissolved Nd concentration vertical profiles (pmol/kg) are also reported, using colors consistent with the sampling location ones.	105
Figure 5-3 Comparison of our data with those measured in the framework of preceding studies (Grenier et al., 2013).	106

Figure 5-4 (A) Suspended sediment runoff at estuary of New Georgia Island, Solomon archipelago. Mud distribution in Tetere Bay, Guadalcanal Island in (B) 1977 and in (C) 2016, 20 years' after Gold Ridge mine development. Data from Jupiter et al., (2018).	108
Figure 5-5 ϵNd value of samples of rocks and continent material extracted from the geochemical data set of EarthChem portal (http://www.earthchem.org). Recent active volcanoes are marked by green stars. The volcano names are also highlighted by green color. The areas where the bathymetry is shallower than 1000m depth are shaded in beige. Mine locations are displayed on the map by red pixel icon (Data from PNG Chamber of Mines and Petroleum, http://pngchamberminpet.com.pg/our-resource-industry/mining).....	108
Figure 5-6 ϵNd of sediment particles collected in different basins from Fiji to the north of New Britain Island. Data from the EarthChem portal (http://www.earthchem.org).	109
Figure 5-7 Neodymium data, hydrographic properties and main circulation scheme of the surface waters (5-40m). The data reported here are identified by the red dots on the adjacent θ -S plot. The ϵNd data of the potential geological sources (Figure 5-5) are also recalled at the right corner of the top panel. Main currents are determined from Ceccarelli et al., (2013) and represented by continuous dark blue arrow. In addition, water current observed during Pandora are represented by dashed-arrow.....	111
Figure 5-8 Zonal cross-section S-ADCP velocities from station 43 to station 47 on which we reported vertical data of ϵNd and Nd concentrations. Red numbers correspond to the sampled stations. Yellow color indicates positive value, representing northward and eastward directions. ϵNd values and Nd concentrations are reported on the sections by black and red numbers, respectively –courtesy of Gerard Eldin, Chief Scientist of PANDORA). Note that the currents here are dominated by tidal variability at semi-diurnal periods, and reverse.....	113
Figure 5-9 Plot of the Eu anomalies as a function of ϵNd of the surface waters, for all the stations documented during Pandora. Higher values ($Eu/Eu^* \geq 1.2$ and $\epsilon Nd > 0$) are observed for stations located inside the Solomon sea. Eu anomalies data are extracted from Pham et al., (2019).....	114
Figure 5-10 As figure 5.7 for UTW-Tropical Waters ($\sigma_\theta = 24-25.3 \text{ Kg/m}^3$). Value in bracket indicate possible contaminating sample.....	115
Figure 5-11 As figure 5.7, for ULTW-CW ($\sigma_\theta = 25.3-26.4 \text{ Kg/m}^3$)	117
Figure 5-12 As figure 5.7, for LLTW-SAMW ($\sigma_\theta = 26.4-26.9 \text{ Kg/m}^3$)	119
Figure 5-13 As figure 5.6, for Intermediate water ($\sigma_\theta = 26.9-27.4 \text{ Kg/m}^3$). The dark blue arrows (both continuous and dashed) indicate the AAIW current. The ϵNd data of the sediments (Figure 5-6) are also displayed at the right corner of the top panel.....	120
Figure 5-14 As figure 5.13, for UCDW ($\sigma_\theta = 27.4-27.76 \text{ Kg/m}^3$). The bathymetry shallower than 1200m is colored in light grey, in yellow if shallower than 2200 m. Value in bracket indicate possible contaminating sample	122
Figure 5-15 As Figure 5.14, for LCDW ($\sigma_\theta \geq 27.76 \text{ Kg/m}^3$. The bathymetry shallower than 3000m is colored in light grey, in yellow if shallower than 4750 m	124

Figure 5-16 Representations of the box models used to calculate the Nd exchanged fluxes at the land-ocean interface for a) local application (LLTW) and b) the whole Solomon Sea (UCDW). Note that for the later, Vitiaz Strait is closed.....	126
Figure 6-1 Authigenic and lithogenic phases of the particle during its sinking in oceanic water. Model taken from Sholkovitz et al., (1994)	137
Figure 6-2 Map of the bathymetry of a) the northern area of the Solomon Sea, from st.George to Solomon straits and b) the southern trench at eastern Woodlark basin. The red rectangular on the map located on the upper right corner shows the location of the working area in the Solomon Sea. The insets show the details of the bottom topography along the sections identified by the black lines on the maps.	139
Figure 6-3 Global maps of internal tide energy dissipation, lighter color reflects stronger waves created. Red rectangular highlight the southwest Pacific Ocean. Figure taken from de Lavergne et al., (2019).	140
Figure 6-4 Vertical distributions of dissolved inorganic carbon(DIC), pH and Silicate (SiO_4) between different stations located in the Coral Sea, at the entrance and in the core (st 60) of the Solomon Sea. Profile colors relate to the stations on the map, station 60 (middle of the Solomon Sea) is highlighted in red.....	141

Chapter 1

Introduction

1.1 General context – Why do we study the Solomon and Coral Seas?

My PhD topic fits into the broad framework of an international project in the Southwest Pacific Ocean (Solwara) which focuses on the water masses transportation and transformation during their northward transit towards the Equatorial Pacific. Indeed, a huge amount of water transits from the centre of the South Pacific tropical gyre to the Equatorial Undercurrent (EUC) via the Coral and Solomon Seas. A fraction of this water will later upwell along the equatorial “cold tongue” in the eastern Equatorial Pacific, preconditioning the El Niño Southern Oscillation (ENSO) variability and local biological activity there (*Figure 1-1 and 1-5a*). Determining the physical state and geochemical content of this fraction is of first importance.

Located on the western boundary, from 10°S to 5°S, the Solomon Sea is on the way between the tropical and equatorial regions. It is characterized by a complicated bathymetry and a complex circulation scheme; several water masses are converging and strong boundary currents occurs. In addition, the active weathering of the volcanic islands surrounding the Coral and Solomon Seas provide potential sources of nutrients and trace elements for the downstream waters of the EUC. Altogether the dynamics, biology and chemistry of the Solomon Sea, make this a key area for the Tropical Pacific. Thanks to the SOLWARA project (which includes the PANDORA cruise, field campaign of my thesis), recent studies brought to light some hydrological features characterizing the Solomon Sea (Cravatte, Kessler and Marin, 2012; Hristova and Kessler, 2012; Grenier *et al.*, 2013; Kessler and Cravatte, 2013b; Ganachaud *et al.*, 2014a, 2017; Gernineaud *et al.*, 2016). These studies described the main current pathways and provided water mass transports from the southern entrance of the Solomon Sea up to the three exiting straits in the north (Vitiaz Strait, Saint George’s Channel and Solomon Strait) and also established their relative contribution to the EUC (*Figure 1-1*). However, the distribution of the chemical species at the entrance, within and at the exit of the Solomon Sea needs to be understood. This comprises the distribution and behaviour of micronutrients (Fe, Zn, Cu, Ni...) as well as that of radionuclides and radiogenic tracers which allow quantification of some processes as dissolved-particulate exchange or land-ocean input quantification. Studying the latter is the major topic of my PhD.

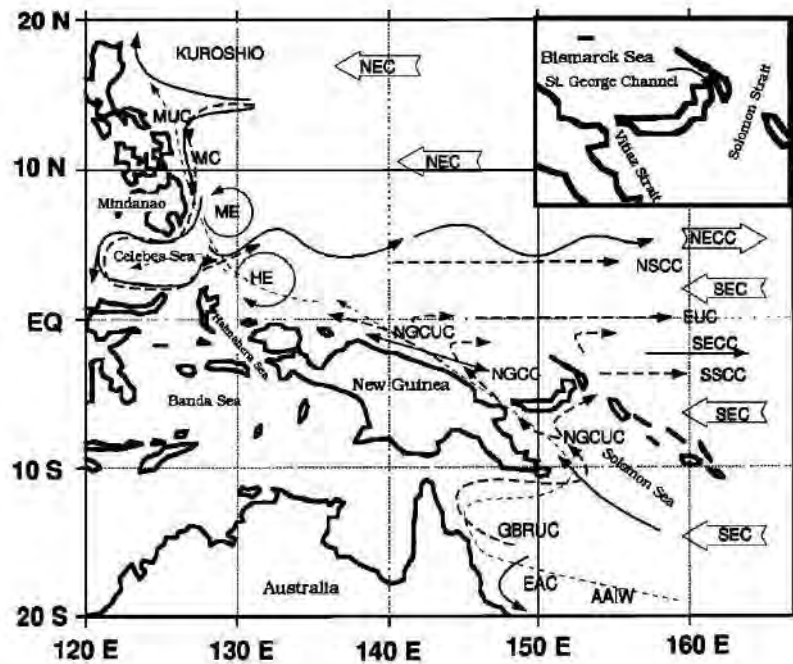


Figure 1-1 From South Equatorial Current (SEC) to Equatorial Undercurrent (EUC) of Western Pacific Ocean. From surface to intermediate depth currents, including Mindanao Current (MC), North Equatorial Current (NEC), North Equatorial Countercurrent (NECC), New Guinea Coastal Current (NGCC), and East Australia Current (EAC). The subsurface currents are New Guinea Coastal Undercurrent (NGCUC), Northern and Southern Subsurface Countercurrents (NSCC and SSCC), Mindanao Undercurrent (MUC), and Great Barrier Reef Undercurrent (GBRUC). Data from Fine *et al* (1994).

The Equatorial Pacific is an important oceanic area for the atmosphere to ocean carbon dioxide (CO₂) exchange. The equatorial cold tongue is the largest source of the CO₂ to the atmosphere. In the upper layers, the biological activity assimilates dissolved CO₂ via the photosynthesis process and transforms it into Particulate Organic Carbon (POC). While sinking towards the abyss, the POC is sequestered in the deep waters. While settling through the water column, a fraction of POC will be remineralized while the remaining one will reach the sediment. This sequestration contributes to the regulation of the atmospheric CO₂ concentration. Besides, while the equatorial region is rich in macronutrients (as NO₃⁻ or PO₄³⁻) the surface water chlorophyll level is surprisingly low. This region is then-called –High Nutrient Low Chlorophyll region (HNLC, *Figure 1-2*). The low productivity is likely due to the fact that these surface waters are depleted in micronutrients, among them Iron (Fe) which is an essential co-enzyme for the photosynthesis (Raven, Evans and Korb, 1999; Morel and Price, 2003; Schoffman *et al.*, 2016)). Because of the nature of the geological materials outcropping at the surface of the Australian continent and numerous islands characterizing this area, the high weathering rates and the occurrence of strong boundary currents, the southwest Pacific is likely a source lithogenic elements (e.g: Al, Mn, Th, REE) among them micronutrients (e.g. Fe, Zn, Ni...; (Johnson and McPhaden, 1999; Lacan and Jeandel, 2001, 2005; Grenier *et al.*, 2013)). The weathering of the rocks outcropping at the surface of the Australian continent and South Pacific islands as well as along their oceanic margins could modify the water mass trace element content, with consequences on the primary production and carbon biological pump along the cold tongue. The

“Boundary Exchange” (BE) process, which will be explained in the following section, is estimated as the major control of Rare Earth Element (REE) and Nd isotope distribution in the ocean (Jeandel, Bishop and Zindler, 1995; Tachikawa, 2003; Lacan and Jeandel, 2004, 2005; Jeandel *et al.*, 2007; Arsouze *et al.*, 2008, 2009; Grenier *et al.*, 2013). More recently, it was also established that BE is potentially an important source of micronutrients, “vita” to the life (e.g. Fe, Zn, Ni) (Mackey, O’Sullivan and Watson, 2002; Elrod *et al.*, 2004; Labatut *et al.*, 2014). Understanding and quantifying in detail the BE process in the southwest Pacific -thus in the Solomon Sea- is therefore an essential step to understand the connection between land-ocean interaction and climate.

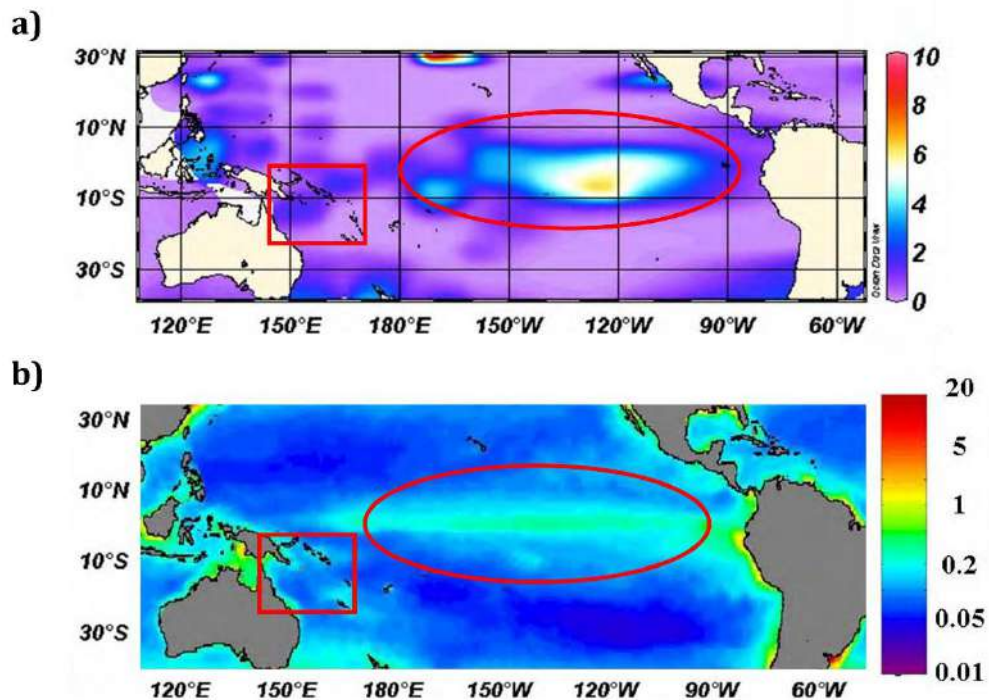


Figure 1-2 Average concentration of Pacific’s surface water of a) Nitrate (mmol/Kg), data from WOCE (<https://www.ewoce.org/>) and b) Chlorophyll (mg/m³), data from MODIS satellite (<https://oceancolor.gsfc.nasa.gov/>). Oval-shape with red line marks the HNLC zone while rectangle one indicate the Southwest Pacific.

SOLWARA- A cooperation between SPICE and GEOTRACES international programs

Up to present, various key aspects of the components driving the Southwest Pacific dynamic and biogeochemistry remained unknown. This motivated several countries to build the South West Pacific Ocean Circulation and Climate Experiment (SPICE), an international research program endorsed by the Climate and Ocean Variability, Predictability, and Change (CLIVAR). The key objectives of SPICE are to understand the Southwest Pacific Ocean circulation and the South Pacific Convergence Zone (SPCZ) dynamics, as well as their influence on regional and basin-scale climate patterns (Ganachaud *et al.*, 2014a, 2017). This program gathers scientists from France, Australia, USA, New Zealand, Japan, and Pacific Islands countries in order to build a broad observation network and to focus on modelling experiments (Ganachaud *et al.*, 2007; Ganachaud, 2008). From the Tasman Sea to the Equator, SPICE is coupling historical and new observations, providing a new modelling of the regional circulation. The field program helped to

validate the numerical simulations and vice versa, simulations being used to better adapt sampling strategy of unexplored areas. The French-USA “Solwara” project focus more specifically on the Coral and Solomon Seas. In order to collect in-situ measurements in the Solomon Sea area, two oceanographic cruises were launched in the framework of SPICE, named Pandora and MoorSPICE, respectively (Ganachaud *et al.*, 2014a, 2017). Their goal was to describe the dynamic and biogeochemistry of the Solomon and Bismarck Seas. More specifically, these programs aimed at understanding water mass transformation processes as well as the enrichment in micronutrients together with geochemical elements along the water transit described above. Interestingly, this geochemical cartography stands in the framework of the international GEOTRACES (<http://www.geotraces.org/>; SCOR, 2007). GEOTRACES focuses on the distribution and fate of the trace elements and their isotopes (TEIs) in seawater, as well as on their impact on ecosystems and the global carbon cycle. The main target of GEOTRACES is to provide the knowledge of the sources, sinks, internal cycling and chemical speciation of TEIs in the ocean. SPICE and GEOTRACES programs fruitfully collaborated in the Southwest Pacific Ocean in the framework of SOLWARA and as part of the 2 cruises (Ganachaud *et al.*, 2014, 2017) (<http://www.solomonseaoceanography.org/>)

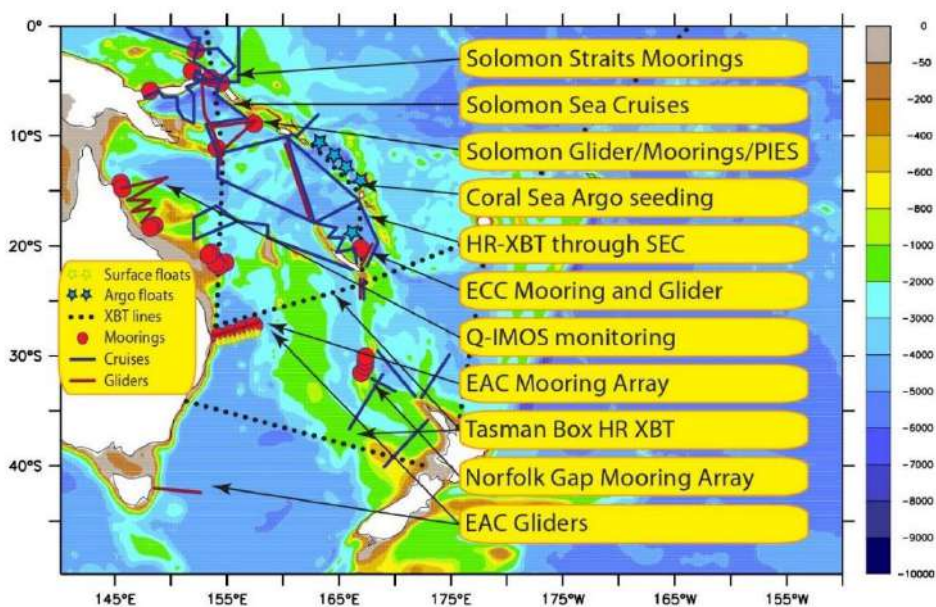


Figure 1-3 Main elements and regional structure of the SPICE field program, the background map and colorbar indicates ocean depth. Note that PIES=Pressure Inverted Echo Sounder; HR-XBT= High resolution XBTs; Q-IMOS= Integrated Marine Observing System (Queensland node); ECC= East Caledonian Current; EAC = East Australia Current. Data from (Ganachaud *et al.*, 2014a).

1.2 The Southwest Pacific Ocean – hydrological context

The mean Southwest Pacific Ocean circulation at large-scale had been studied for years and discussed in numerous studies since 1960’s (e.g: Tsuchiya, 1981; Tsuchiya *et al.*, 1989; Qu and Lindstrom, 2002; Grenier *et al.*, 2013; Kessler and Cravatte, 2013; Ganachaud *et al.*, 2014). Based on the data from Pandora (2012) and MoorSPICE (2014) cruises, Germaineaud *et al* (2016) provided a detailed description of the thermocline down to the intermediate layers of the Solomon Sea. Here, we propose the full description of the main hydrological features (currents,

water masses) from the Coral to the Solomon Seas. The mean circulation of the Coral and Solomon Seas is described by tracing the movement of South Equatorial Current (SEC) towards the Equator. Thereafter, all possible water masses which could be present in the Coral and Solomon sea are classified.

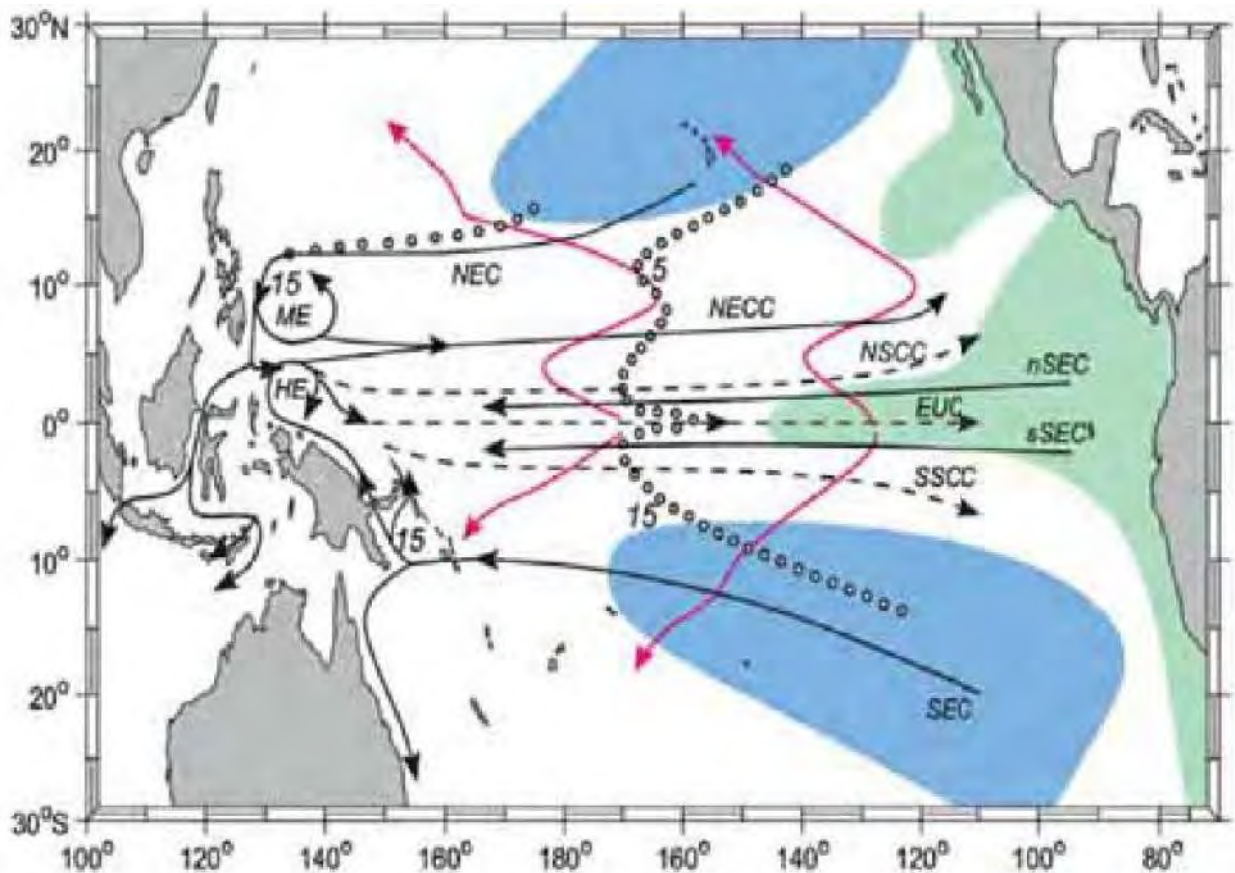


Figure 1-4 Major surface (solid arrows) and subsurface (dashed arrows) currents of the Equatorial Pacific. Note that NEC =North Equatorial Current; nSEC and sSEC=north, south South Equatorial Currents; ME=Mindanao Eddy; HE=Halmahera Eddy). Blue shading areas indicate the subtropical subduction zones while green shading ones represent the equatorial/eastern upwelling. Magenta lines show the poleward pathways from central pacific. Numbers indicate water mass transport (Sv). Data from (Schott, Wang and Stammer, 2007).

In the tropical Pacific Ocean, the trade winds blowing in the intertropical belt induce zonal currents with opposite directions (*Figure 1-5*). The two main currents here are the North and South Equatorial Current (NEC and SEC, respectively) driven by wind-forced, generally intensify down to thermocline layer; however, it could extent deeper to intermediate deep (up to 1000m). These currents flow westward and feed the western branch of the subtropical gyre in both hemispheres before turning into equatorward Western Boundary currents, or flowing equatorward into the ocean interior. In the southern hemisphere, the fast and intense Low Latitude Western Boundary current (LLWBC) is entering the Solomon Sea through two branches. The first branch of SEC enters the Coral Sea mainly South of Vanuatu, conveyed by the North Caledonian Jet (NCJ) (Gasparin, Ganachaud and Maes, 2011). This stream bifurcates when hitting the Australian coast where part of it flows northward and is conveyed by the Gulf of

Papua Current (GPC) and then enters the Solomon Sea by the New Guinea Coastal Undercurrent (NGCU). The second stream of SEC flows directly forming the North Vanuatu Jet (NVJ) and then joins the NGCU as it flows equatorward inside the Solomon Sea (Sokolov and Rintoul, 2000; Qu and Lindstrom, 2002; Kessler and Cravatte, 2013a; Germineaud *et al.*, 2016). Inside the Solomon Sea, the NGCU splits into two branches around Woodlark and then merge again in the northern side of this island. South of New Britain Island, the current bifurcates again into two streams that later exit the Solomon Sea to join the EUC (*Figure 1-5b*). The westward stream flows northward through the Vitiaz Strait while eastward stream is conveyed by the New Britain Coastal Undercurrent (NBCU). The NBCU flows equatorward and then splits into St Georges Undercurrent (SGU) and New Ireland Coastal Undercurrent (NICU), exiting the Solomon Sea through the St Georges and Solomon Strait, respectively. At the exit of Solomon Sea, New Ireland Coastal Undercurrent (NICU) with another branch of the SEC which also flows equatorward after having been deflected by the Solomon Island. (Melet *et al.*, 2010; Cravatte *et al.*, 2011; Germineaud *et al.*, 2016).

The different water masses transported by these currents through the Southwest Pacific Ocean will now be described from the surface to the bottom of the water column (*Figure 1-5*). Considering the non-consensus on the nomenclature of the thermocline water masses in this area, I used the water masses nomenclature proposed by Tomczak and Hao (1989) and Tsuchiya *et al* (1989).

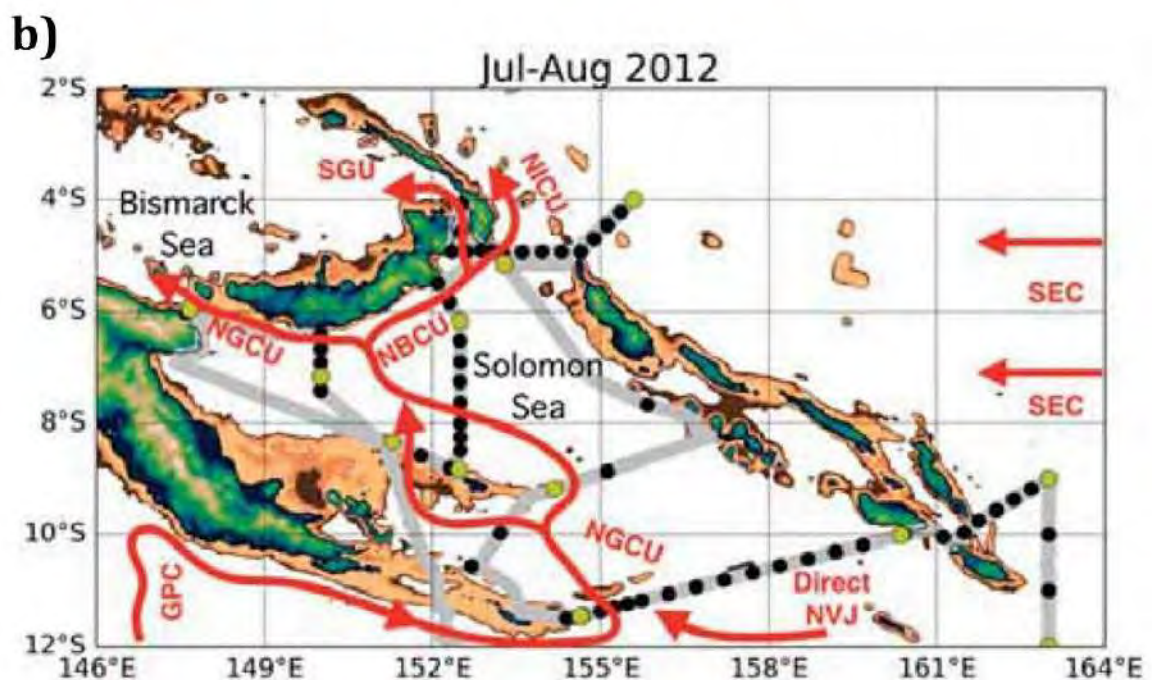
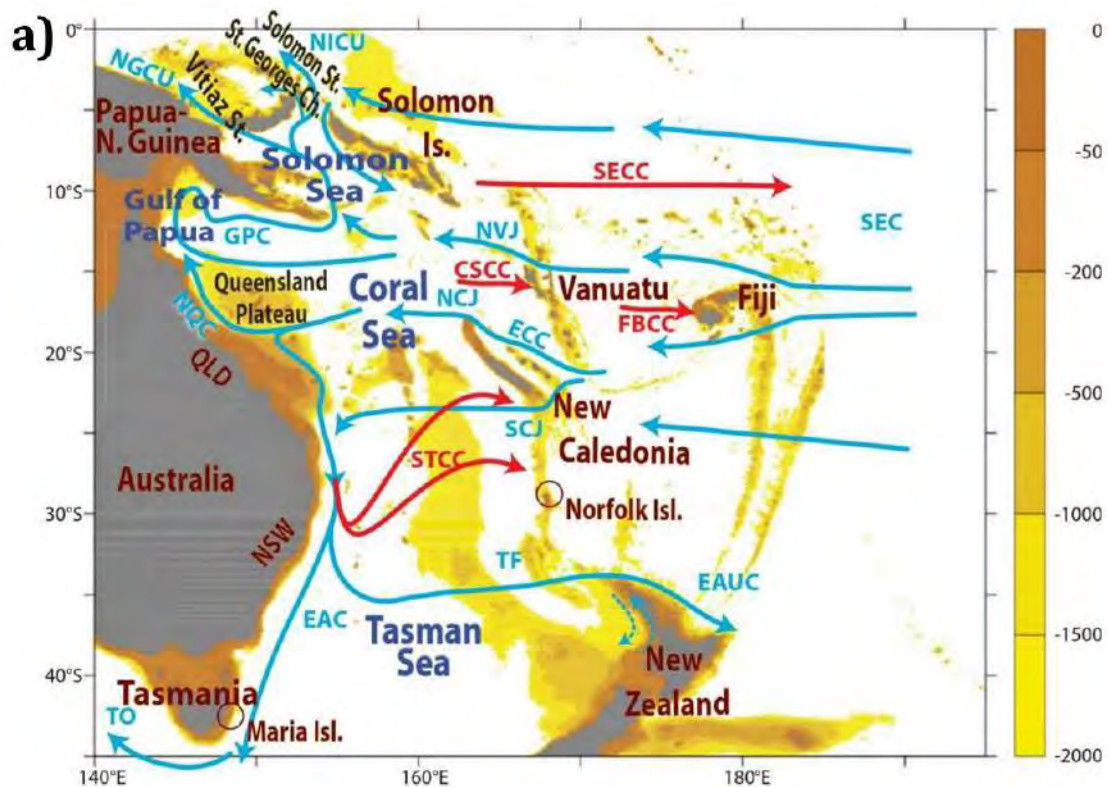


Figure 1-5 Mean circulation of the Southwest Pacific Ocean. a) Topography with color scale in meters. Blue arrows denote the main currents while red arrows indicate the main surface counter currents. Data from *Ganachaud et al., (2014)*. b) Zoom on the Solomon Sea during Pandora cruise (July-August 2012). Brown shading indicates shallow bathymetry (<1000m); Black and yellow dots represent station position and geochemical stations, respectively. Red arrows denote the main thermocline currents. GPC = Gulf of Papua Current; NVJ= North Vanuatu Jet; NGCU= New Guinea Coastal Undercurrent; NICU= New Ireland Coastal Undercurrent; NBCU= New Britain Coastal Undercurrent, SGU= Saint Georges Undercurrent. Data from *Germineaud et al., (2016)*

From top to bottom, the following water masses are identified:

- a. Surface Water: From the northern subtropical front to the equator, the Tropical Surface Water (TSW) is dominant. This water is characterized by high temperature and low salinity due to the intense solar radiation and precipitation. (Sokolov and Rintoul, 2000).
- b. Thermocline water: several water masses can be identified in the thermocline, and can be divided into two sublayers: upper ($\sim\sigma_\theta = 24.3 - 25.3 \text{ Kg/m}^3$) and lower thermocline ($\sim\sigma_\theta = 25.3 - 26.9 \text{ Kg/m}^3$).
 - The South Pacific Tropical Waters (SPTW) flow in the upper thermocline (Tsuchiya *et al.*, 1989; Qu and Lindstrom, 2002) and originates from the southeast Pacific Ocean (Kessler, 1999; Hasson *et al.*, 2012; Qu, Gao and Fine, 2013). This tropical water can be subdivided in two water masses while flowing towards the Coral Sea. The northern branch is called South Pacific Equatorial Water (SPEW) while the southern one keeps its original name (Tomczak and Hao, 1989; Tsuchiya *et al.*, 1989; Tomczak and Godfrey, 2003; Kessler and Cravatte, 2013b). The SPEW is originating from the subduction of “mode waters” in the subtropical central South Pacific (20°S, 110°W) in an area called the high surface evaporation zone (HSEA), characterized by a salinity maximum and relatively high oxygen content (see figure 5 of Pham *et al.*, 2019). The southern branch (SPTW) is conveyed by the North Caledonian Jet (NCJ) and enters into the Coral Sea mainly south of the Vanuatu island (Gasparin, Ganachaud and Maes, 2011; Grenier *et al.*, 2013; Ganachaud *et al.*, 2014a; Germaineaud *et al.*, 2016).
 - The upper part of the lower thermocline is occupied by the Western South Pacific Central Water (WSPCW). This water displays thermostat characteristic (Tsuchiya, 1981; Qu *et al.*, 2008; Grenier, Jeandel and Cravatte, 2014) and a very loose stratification at about 300m depth ($\sim\sigma_\theta = 26.0 \text{ Kg/m}^3$). Its potential density is centered around 26.4 Kg/m^3 and it displays a high salinity reflecting its origin (Tomczak and Hao, 1989; Tomczak and Godfrey, 2003). This water mass is formed at the latitude of the Subtropical Convergence in the Tasman Sea and partly north of New Zealand during winter (Tsuchiya, 1981; Qu *et al.*, 2008) and is then redistributed by the Subtropical Gyre. The WSPCW (mean $O_2=150 \text{ Kg/m}^3$) is conveyed into the southern part of the Coral Sea by the deep NCJ (Tsuchiya *et al.*, 1989; Sokolov and Rintoul, 2000; Tomczak and Godfrey, 2003). During its transportation through the Coral Sea, the Gulf of Papua and inside the Solomon Sea (Kessler and Cravatte, 2013b), this water mass keep losing its oxygen by mixing. Near the straits, it is mixed with older, deoxygenated water originating from the southeastern Pacific Ocean, and entering the Solomon Sea through Solomon Strait. Its dissolved oxygen concentration drops from $\sim 150 \text{ Kg/m}^3$ to $\sim 130 \text{ kg/m}^3$ by this mechanism.
 - Underneath the WSPCW, another mode water, with no salinity or oxygen extrema, is identified. It is named the Subantarctic Mode Water SAMW; ($\sim\sigma_\theta = 26.5 - 26.9 \text{ kg/m}^3$) and enters the Coral and Solomon Seas by the south, (McCartney, 1977; Jeandel *et al.*, 2013). It originates from the Southeastern Southern Ocean by subduction north of the Antarctic Circumpolar Current (Hanawa and D.Talley, 2001). This water mass is characterized by a low salinity (~ 34.5) and a high oxygen content ($\sim 175 \text{ kg/m}^3$) (Qu *et*

- al.*, 2009). In the Coral and Solomon Seas, SAMW is keeping its original characteristics and contributes to the formation of 13°C Water at the Equatorial Pacific (Qu *et al.*, 2009).
- c. Intermediate water: Southwest Pacific intermediate layer could be described by the incoming flow of two branches of the Antarctic Intermediate Water at the southern of the Solomon Sea. After taken a round trip at this sea, AAIW could mix with the Equatorial Pacific Intermediate Water which arrived from eastern Equatorial Pacific. Pathways of these two water masses were described in Bostock, Opdyke and Williams (2010) .
- The Antarctic Intermediate Water (AAIW) ($\sim\sigma_\theta = 27.2 \text{ Kg/m}^3$) is determined by a salinity minimum ($\sim S=34.3-34.5$) and an oxygen maximum ($\sim O_2= 200-300 \text{ }\mu\text{mol/kg}$). It was suggested that AAIW was formed by subduction of Antarctic Surface Waters below the Subantarctic Front (Deacon, 1937; McCartney, 1977; Bostock, Opdyke and Williams, 2010) in the vicinity of the Southern Chile Coast (Talley, 1996; Tsuchiya and Talley, 1998; Hanawa and D.Talley, 2001; Bostock, Opdyke and Williams, 2010). The AAIW flows northwestward in the subtropical gyre circulation and bifurcates equatorward through the Coral Sea. It enters the Solomon Sea through the LLWBCs (Tomczak and Godfrey, 2003; Qu and Lindstrom, 2004; Bostock, Opdyke and Williams, 2010; Germineaud *et al.*, 2016). Between the Coral Sea and the equator, the AAIW is becoming slightly denser and less oxygenated ($\sim\sigma_\theta = 27.26 \text{ Kg/m}^3$; $O_2=160-190 \text{ }\mu\text{mol/kg}$) due to remineralization of organic matter settling from the surface and isopycnal mixing with lower oxygenated waters arriving from the east.
 - The Equatorial Pacific Intermediate Water (EqPIW; $\sim\sigma_\theta = 27.3 \text{ kg.m}^{-3}$) is principally a combination of AAIW and upwelled Pacific Deep Water (Bostock, Opdyke and Williams, 2010) and flows within a complex intermediate current system (Grenier *et al.*, 2013; Pham *et al.*, 2019). It displays higher salinity than AAIW ($\sim S=34.5-34.6$) and much lower oxygen concentration ($O_2= 75-125 \text{ }\mu\text{mol/kg}$). It is found east of the Solomon Sea. The intrusion of this water in the Solomon Sea was described by Pham *et al.*, (2019)
- d. The deep and bottom waters within the Coral and Solomon Seas have been poorly documented since the first observations summarized in (Reid, 1986, 1997), and their pathways and fate are not clearly understood. Germineaud (2016) proposed a description of the circulation and mixing of the South Pacific deep waters in his thesis manuscript. In general, the bathymetry is the main driver of the waters displacements in this layer.
- The Upper Circumpolar Deep Water (UCDW) is observed between 1000m and 3500m. This water mass is depleted in oxygen since its origin in the Antarctic Circumpolar Current (ACC) (Reid, 1986; Wijffels, Toole and Davis, 2001; Talley, 2007). It has been suggested that UCDW in the Coral and Solomon Seas may originate from two pathways: one flowing northwards from the Tasman Sea, and one transiting through the Samoan Passage (10°S, 169°W) before passing through the channel between New Caledonia Trough and the South Fiji Basin (Orsi *et al.*, 1995; Sokolov and Rintoul, 2000; Grenier *et al.*, 2013; Germineaud, 2016). UCDW is characterized by relatively high salinity and a pronounced oxygen minimum (Pham *et al.*, 2019).

- The Lower Circumpolar Deep Water (LCDW) forms the deepest layer (Reid, 1997; Tsimplis, Bacon and Bryden, 1998; Kawabe and Fujio, 2010) It is identified by a salinity maximum reaching 34.72–34.73 and a decrease of its silicate content when compared to the UCDW (Orsi, Johnson and Bullister, 1999). From the known topography, the Solomon Sea is a sealed area at depths below 3500m, separated from the outer world by islands and sills (Germineaud, 2016). Curiously, we clearly identified the LCDW imprint in our profiles, and an unexpected oxygen concentration increase with depth, which underlines that the topography, and the possible pathways and fate of this water mass are still unclear.

1.3 Tracers in the sea- The Rare Earth Elements (REE) and Neodymium isotopic composition (Nd-IC)

1.3.1 REE and their distribution

Located in the 6th period of periodic table, Rare Earth Elements (REEs) belong to the lanthanide group and are a coherent set of elements regarding their chemical behaviour. REEs comprise 14 lanthanide elements, starting from lanthanum (La, Z=57) and ending with lutetium (Lu, Z=71; Figure 1-6). Notwithstanding their name, REEs are relatively abundant on Earth, specially the cerium which is more abundant than copper, with an average concentration of 68 part per million (ppm)(Bedinger, Kohler and Wallace, 2018). However, they are barely found concentrated in rare earth minerals, making difficult their economical extraction. The natural abundance of REEs follows the Oddo-Harkins rule, leading to even-numbered REEs roughly 5 times more abundant than the odd-numbered ones

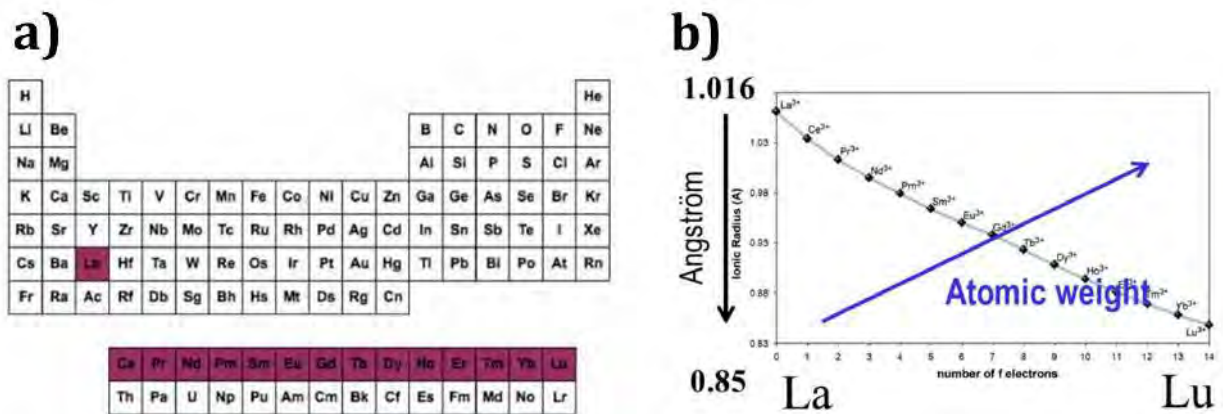


Figure 1-6 a) The REE family in periodic table and b) the lanthanide contraction

In addition, light REEs (La-Sm) are more abundant than heavy ones (Gd-Lu) and the difference of weight and ionic radius along the family lead to fractionation between the different REEs during the geochemical processes. Modern chemistry classified REE as light, middle and heavy REE referred to their atomic numbers. The increase of atomic number from light REE to heavy REE creates a gradual decrease in ionic radius (a.k.a lanthanide contraction) and lead to the fractionation of REE. Thus, the larger ionic radii of LREE make them compatible into a melt phase (e.g: magma) while the smaller HREE prefer to remain in the rock-forming minerals that make up Earth's mantle (eg: garnet) (Figure 1.6)(Winter, 2010). Common minerals containing

cerium and other LREE are monazite, parasite, lanthanite, etc. Among rare-earth-phosphate mineral, HREE is commonly found enriched in xenotime mineral while cerium and LREE incorporate with monazite mineral (Chelgani *et al.*, 2015).

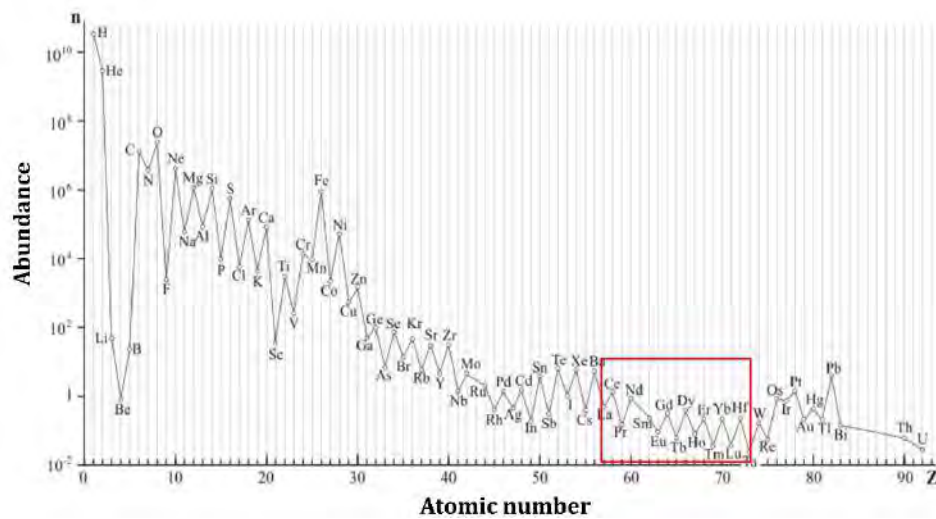


Figure 1-7 Oddo-Harkins Rule, REE group is shown under red rectangular

The REE properties allow applying them as proxies for different purposes in seawater. Thus, since they are of continental origin and poorly soluble, they can be used as lithogenic tracers. Indeed, only a small fraction of sediments discharged by the rivers and atmospheric dusts is dissolving at the seawater contact (Rousseau *et al.*, 2015). The particulate phase will thus keep the signature from the source. Marine geochemists will use this property to seek the sources of the REE measured in the ocean (Sholkovitz *et al.*, 1999; Chavagnac *et al.*, 2007, 2008).

However, once dissolved in seawater REEs occur as trivalent state excepted cerium and europium that could be at the IV state (Ce^{4+}) or the II state (Eu^{2+}). The lanthanide contraction makes that REEs are involved in particle-seawater exchange processes (e.g adsorption, remineralization, scavenging, etc...) leading to their fractionation. Conversely, the respective distribution of the REEs between the different phases in the water column could inform on the process(es) that result in their distribution. REEs are therefore used as proxies of particle-solution exchanges. In order to detect these fractionations while getting rid of the zig-zag pattern, the REE concentrations are normalized to a reference. Marine geochemists use the average composition of a shale representative of the average crustal value: The Post Archean Australian Shale (PAAS). A typical open-ocean shale-normalized REE pattern displays a HREE enrichment due to the fact that HREEs are more strongly complexed by the dissolved carbonates, leading to the lower solubility of the LREE; Thus, the latter are preferentially scavenged by marine particles (Byrne and Kim, 1990; Elderfield, Upstill-Goddard and Sholkovitz, 1990; Sholkovitz, Landing and Lewis, 1994; Tachikawa, Jeandel and Roy-Barman, 1999).

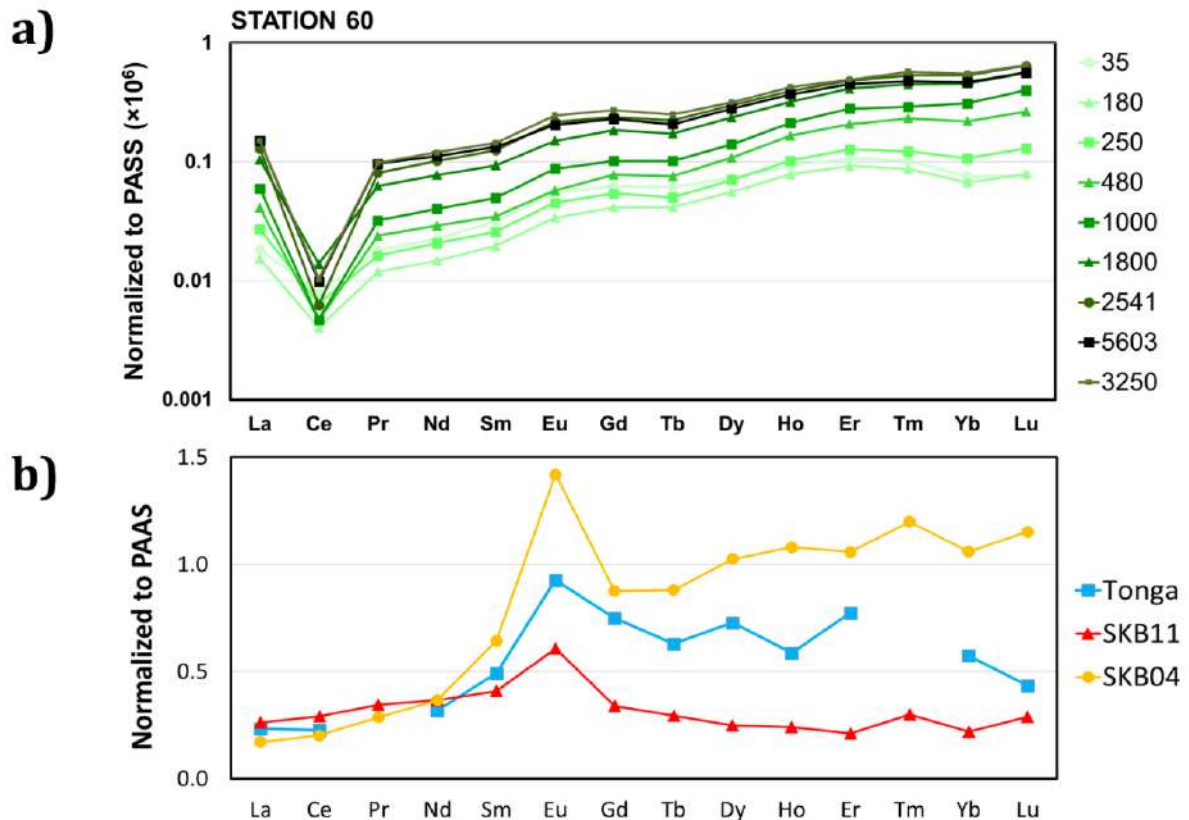


Figure 1-8 Examples of Post-Archean Australian Sedimentary (PAAS) –REE normalized patterns. (a) REE dissolved in seawater of station 60 – Pandora (b) REE of basaltic rock collected in Southwest Pacific Islands. According to Pham *et al.*, (2019)

A recent work also proposed that the dissolution of HREE-enriched diatom opal could contribute to this dissolved HREE relative enrichment (Akagi *et al.*, 2011; Garcia-Solsona *et al.*, 2014; Pham *et al.*, 2019). Because of the non-solubility of the Ce(IV), cerium is readily depleted by co-precipitation with Mn oxides (Moffett, 1990, 1994) and adsorption on the particles. This results in a cerium dissolved seawater-profile depleted in comparison with its REE neighbours. (Byrne and Kim, 1990; Elderfield, 1990; Moffett, 1990; Bertram and Elderfield, 1993; Tachikawa, Jeandel and Roy-Barman, 1999). Particulate REE profiles comprise lithogenic and authigenic fractions, depending on their origin. The lithogenic fraction –often represented as the refractory core of the particles- corresponds to the particulate matter produced by the mechanical erosion of continental/oceanic crust and brought by rivers and winds to the ocean (Figure 1-8). The authigenic fraction is formed by in situ processes within the water column, either biologically driven or not. This fraction may include materials like calcium carbonate, opal, organic matter and Fe/Mn oxy-hydroxide coatings (Sholkovitz, MLanding and Lewis, 1994; Tachikawa, Jeandel and Roy-Barman, 1999).

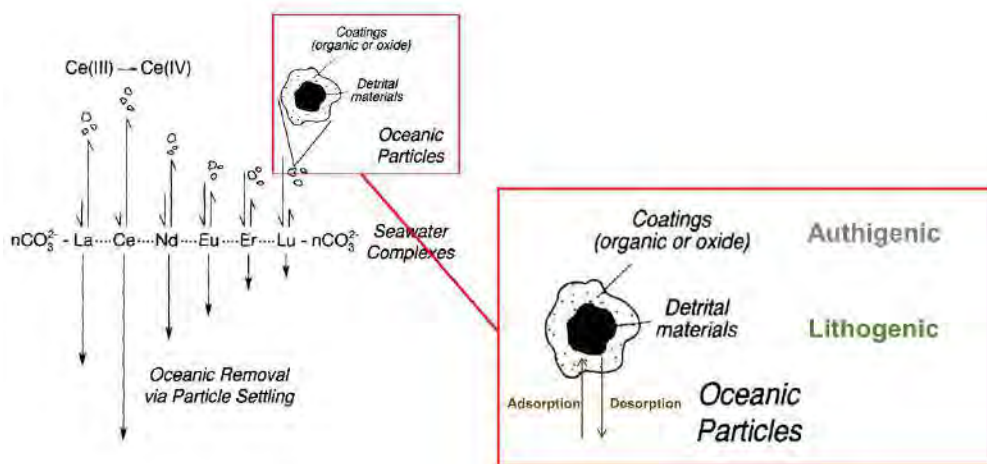


Figure 1-9 Schematic model of REE fractionation between particle and seawater. Inside the oceanic particle, authigenic and lithogenic phases also are identified inside the particle. Data from (Sholkovitz, M. Landing and Lewis, 1994)

More recently, the REE distributions could sometimes track the anthropogenic contamination in aquatic systems. This reflects the fact that modern technologies require more and more REEs due to their unique physical and chemical properties. The observed progressive increase of REE consumption is accompanied by their increasing release to the natural environment. Several studies proposed the impact of different REE to the ecosystems, including: i) La (Kulaksiz and Bau, 2011, 2013; Klaver *et al.*, 2014; Song *et al.*, 2017), ii) Ce (Olmez *et al.*, 1991), iii) Gd (Ogata and Terakado, 2006; Hatje, Bruland and Flegal, 2014; Johannesson *et al.*, 2017; Pedreira *et al.*, 2018), and iv) Sm (Olmez *et al.*, 1991; Kulaksiz and Bau, 2013; Song *et al.*, 2017). For example, Pedreira *et al.*, (2018) followed the trajectory of Gd released by hospitals (where Gd is commonly used as contrasting agent in radiology) to the Atlantic coastal water off the city of Salvador de Baia (Brazil). The key point here is that Gd is so strongly complexed in these contrasting agents that it passes through the Waste Water Treatment Plants (WWTPs) and then disperses in the ocean following the currents. Since the impact of REEs in human health is still poorly understood, their fate, behaviour, bioavailability and toxicological impacts become an urgent issue that need to be addressed.

Understanding the distribution and fate of REE in aquatic environment and more specifically in seawater becomes urgent to improve our knowledge of the dissolved-particulate exchanges and more globally of the interaction between land and ocean as well as potential REE impact to the ecosystems.

1.3.2 Neodymium and its isotopes

Neodymium, one of REE groups with atomic number 60, is naturally occurring with five stable isotopes (¹⁴²Nd, ¹⁴³Nd, ¹⁴⁵Nd, ¹⁴⁶Nd and ¹⁴⁸Nd) and two very long-lived radioisotopes (¹⁴⁴Nd and ¹⁵⁰Nd) which are assumed stable on the scales characterizing the modern ocean (Meija *et al.*, 2016). The most abundant isotope is ¹⁴²Nd with 27.2% while the second one is ¹⁴⁴Nd (23.8%). Many short-lived isotopes of Nd have also been characterized that contribute up to more than 30 isotopes (half-life ≤ 12 days). Among the 7 isotopes used in geochemistry, ¹⁴³Nd is particularly interesting as tracer. Indeed, it is produced by decay of the long-lived radioactive

isotope ^{147}Sm (α -decay, $t^{1/2}= 6.54 \times 10^{12}$ yr). Thus, its natural abundance varies and depends on the time-integrated Sm/Nd ratio of the rock which Nd is derived. The variations of the $^{143}\text{Nd}/^{144}\text{Nd}$ ratio is commonly express as ϵ_{Nd}

$$\epsilon_{\text{Nd}} = \left(\frac{(^{143}\text{Nd}/^{144}\text{Nd})_{\text{sample}}}{(^{143}\text{Nd}/^{144}\text{Nd})_{\text{CHUR}}} - 1 \right) \times 10^4$$

Where: CHUR = chondritic uniform reservoir, represents the average Earth value ($^{143}\text{Nd}/^{144}\text{Nd}_{\text{CHUR}}=0.512638$; Wasserburg *et al.*, 1981).

This ratio stays as a signature of the rock (a.k.a Nd isotopic composition value-Nd IC) and reflects the nature and age of the lithogenic material it originates from. The volcanic area where igneous rocks have been recently expelled from the mantle have more radiogenic ϵ_{Nd} values (ie greater than zero), whereas old continental crusts are characterized by values lower than -10. ϵ_{Nd} signatures of the sediments and rocks surrounding the ocean and along their margins is presented by Jeandel *et al.*, (2007).

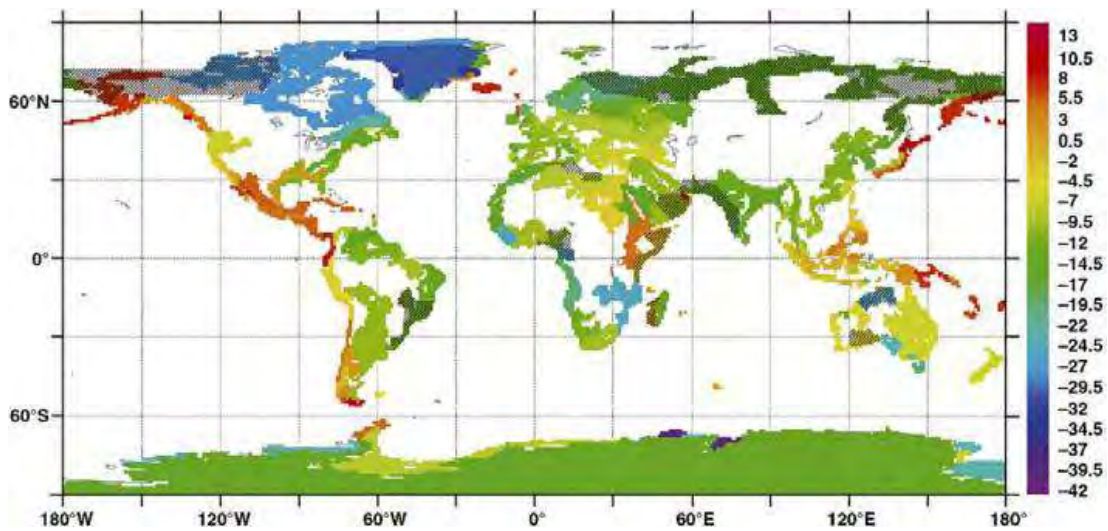


Figure 1-10 Extrapolation map of ϵ_{Nd} in continental rock. Extracted from Jeandel *et al.*, (2007).

Since Nd belongs to REEs group, this element is poorly soluble in seawater. It therefore interacts with marine particles though adsorption-desorption and scavenging-remineralization processes. Consequently, the vertical dissolved Nd profile shows low concentrations in surface waters which gradually increase with depth (De Baar, Brewer and Bacon, 1985; Jeandel, 1993; Alibo and Nozaki, 1999; Nozaki *et al.*, 1999). Contrastingly, ϵ_{Nd} of the different water masses display different vertical profiles, because this parameter is not directly influenced by Nd scavenging. It varies semi-independently from the concentration. Water mass ϵ_{Nd} signal can be modified by two main factors: external input and mixing. Thus, the ϵ_{Nd} of the water mass comprises the following information:

- i) Tracer of lithogenic sources, when getting closer to the ocean margins (Tachikawa *et al.*, 2017).
- ii) Quasi conservative tracer for mixing: far from any lithogenic source, the ϵ_{Nd} signal of the water mass becomes sub-conservative and is used to trace the current trajectory or mixing proportion of different water masses.

In addition, ϵ_{Nd} is a powerful tool to calculate the contribution of lithogenic material to a given location when coupled with the dissolved Nd concentration (Jeandel, Bishop and Zindler, 1995; Lacan and Jeandel, 2005; Garcia-Solsona *et al.*, 2014; Grenier, Jeandel and Cravatte, 2014; Lambelet *et al.*, 2016, etc). This lithogenic flux could be used as the preliminary step to estimate other parameter fluxes (e.g: NO_3^- ; PO_4^{3-} ; SiO_4^-). This is very useful since nutrient cycles are too dynamic and nutrient concentrations or isotopes do not preserve sufficient information on their sources or transformations. Thus, radiogenic isotopes as Nd one act as complementary tracers tracing not only the origin of the material but also its flux. Besides Nd isotopes, others 'hot tracers' also have been used including: ^{232}Th , 9Be , ϵ_{Nd} , Sr, Pb and Ra isotopes help quantifying land-ocean inputs. My thesis topic was more specifically dedicated to the use of REE and ϵ_{Nd} to trace land-ocean and particle-solution processes in the Coral and Solomon Seas.

1.4 Land-ocean inputs: pathways and Boundary Exchange

Materials from land are transported to ocean and then control the composition of seawater, influencing the element oceanic cycles. The variation in seawater composition is then directly linked to earth surface weathering and thus climate forcing. Jeandel, (2016) proposes five pathways for the solid material entering the seawater, including: 1) atmospheric source: aerosols deposits on the sea surface, either short or long distance; 2) river inputs: river water brings the chemical species to the seawater resulting from the continental crust weathering of continental crust. Material could be as suspended solid, dissolved or colloids form; 3) sediment remobilization: recent studies identified that the sediment deposited on the benthic floor –on the margins or at the bottom- can be a source of trace element and isotopes to the ocean (Haley, Klinkhammer and McManus, 2004; Lacan and Jeandel, 2005; Homoky *et al.*, 2013, 2016); 4) submarine ground water discharge(SGD): this term designs the subterranean estuaries which act as common river, could be a source of dissolved and particulate species to the oceanic water; 5) Mid-ocean ridges and volcanic arcs: hydrothermal fluids could modify the seawater composition by rapid removal of some chemical species (e.g: Mg) and loading it with others (e.g.: Fe, Zn). The roles of hydrothermal plumes are less understood but considering the size of the volcanic arcs and mid-oceanic ridges, the impact of this source could be significant (?) (Chavagnac *et al.*, 2018).

The boundary exchange (BE) process is occurring at the land-ocean interface where both the release (dissolution, desorption, etc) and removal (adsorption, scavenging, etc) of the same tracer happens simultaneously or in a relatively short timescale. Back to the study of Lacan and Jeandel, (2005), figure 2 shows the Nd signature modification of different water masses at various locations during their transports. the factors modifying the Nd concentrations and isotopic compositions are not the same. While concentrations are responding to both Nd inputs from an external source and its removal by scavenging, the isotopic signature change will reflect input only. On a world scale, this leads to changes of Nd-IC signature along the thermohaline circulation (reflecting external inputs) while the concentrations do not change between the Atlantic and Pacific oceans (van de Flierdt *et al.*, 2012). This was initially named as “the paradox of the Nd” (Bertram and Elderfield, 1993; Jeandel, Bishop and Zindler, 1995; Goldstein and

Hemming, 2003) which was solved by the BE hypothesis. Note that BE could happen in any layer of the water column (Lacan and Jeandel, 2005; Jeandel, 2016).

1.5 Thesis objective

The objective of my thesis stands among the main goals of the two programs- SPICE and GEOTRACES, which are to contribute to explain how the waters are transformed during their passage through the Coral and Solomon Seas and if these transformations reveal the influence of the surrounding lithogenic source to the oceanic water. When identified, my objective is also to quantify the importance of the external source fluxes. In details, my manuscript will provide information about:

- i) The dissolved REE distribution in the Southwest Pacific Ocean, allowing me to identify potential terrigenous material imprint in the water masses leaving the Solomon Sea and to quantify the net enrichment due to these inputs at the land-ocean interface. Using the relationship between some specific REEs and other elements, I also tried to disentangle different biological and chemical processes at play in the water column.
- ii) The ϵ_{Nd} signal of various water masses during their transportations towards the Equator, allowing me to identify and quantify the Boundary Exchange process, coupling ϵ_{Nd} with dissolved data to estimate geochemical processes inside the water masses.
- iii) The deep waters of the Solomon Sea. Below 3000m, the Solomon Sea is supposed to be isolated due to its specific bathymetry. However, our deep water data reveal that water from outside is penetrating deeper than what was thought before. Tracers allow the identification of tiny leak of deep water through a narrow strait.

Out of the Coral and Solomon seas, another objective of my thesis was to develop an adaptive method to analyse dREEs in aquatic sample in order to replace a 20 years-old method commonly used in the laboratory. This successful protocol is bringing stable yield, suitable blank level while it dramatically reduces time consumption: as a consequence, the data quality is improved.

Chapter 2

Methodology

2.1 The Pandora Oceanographic cruise

The Pandora cruise departed from Nouméa on June 28th, 2012 onboard the research vessel R/V L'Atalante. The strategy of Pandora was to document and sample the dynamic and chemical transformations of the water masses along a track covering the Coral to the Solomon Sea. It lasted 40 days and returned to Nouméa on August 6th. The Pandora cruise track is shown in *Figure 2-1*. A conductivity, temperature, and depth (CTD) system mounted with O₂ sensors was used to measure hydrological parameters at all stations. Samples to measure salinity, oxygen, nutrients (nitrate, phosphate, silica, etc.) and other biogeochemical parameters (e.g: carbonate chemistry) were collected using 12L Niskin bottles mounted on a standard rosette. Meanwhile, trace metals were sampled using a Clean sampling system (rosette, sensors, etc...) deployed down to 1300 m with a Kevlar cable to limit the sample contamination by the sampling device. A pair of RDI Lowered-Acoustic Doppler Current Profilers (L-ADCPs) were attached to the Standard Rosette to measure the currents along the PANDORA transects. The cruise followed a latitudinal transect along 163°E between 18°S and 9°S to document the westward SEC branches entering into the Coral Sea, including New Caledonia and North Vanuatu Jets. After passing the Indispensable Strait, the cruise track was closing the “southern entrance” of the Solomon Sea, joining the western coast of the Gulf of Papua New Guinea between 155-161°S along ~11°S. Three transects were conducted within the Solomon Sea (*Figure 2-1*). A transect allowed sampling water masses northeast of Bougainville Island, while two other transects were conducted via the Solomon Strait to St Georges Channel and across the Vitiaz Strait, to sample the exits of the Solomon Sea. As a whole, samples were collected at 83 stations including 170 casts, most of them down to 2000m, although ‘geochemical’ stations were reaching the bottom layers (Germineaud, 2016). Specifically, in the heart of the Solomon Sea, station #60 was sampled down to 5603m. This station was interesting because its deepest part below 3000-4000m was supposed to be isolated from the main Solomon Sea circulation thanks to the specific geological context and bathymetry of the Solomon Sea (Ganachaud *et al.*, 2014b, 2017).

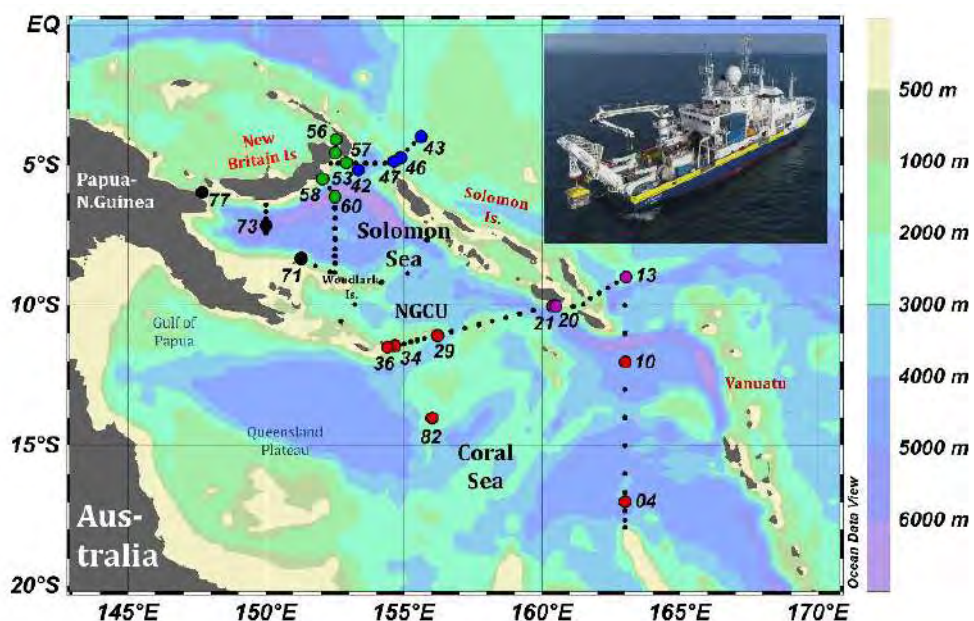


Figure 2-1 Pandora trajectory and sampling stations. Upper right corner is a picture of R/V L'Atalante

2.2 Sampling procedure

In the framework of this thesis, samples were collected with the aim to measure two parameters: dissolved rare earth concentrations and the isotopic composition of Nd (Nd-IC or ϵ_{Nd}) at 21 stations in total. The full sample list of all samples is shown in *table 2-1*.

Table 2-1 Sampled stations and sample depths during the Pandora cruise. Duplicate samples were also picked up for the validation of the analytical procedure

PN004	PN010	PN013	PN020	PN029	PN034	PN036	PN042
730m	4000m	2000m	1600m	2999m	1920m	901m	2500m
621m	2500m	1535m	900m	1534m	1750m	699m	2000m
351m	1735m	1335m	600m	1140m	1665m	401m	1750m
250m	1000m	685m	190m	934m	1550m	180m	1550m
166m	680m	600m	25m	737m	1065m	159m	1200m
30m	515m	300m		267m	735m	101m	1000m
	350m	160m	PN021		635m	24m	750m
	260m	40m	3280m		300m		500m
	185m	5m	2625m		180m		400m
	35m		2115m		40m		225m
			550m				180m
			400m				100m
			250m				50m
							5m
PN043	PN047	PN057	PN060	PN071	PN077	PN082	
1200m	635m	2201m	5603m	1100m	983m	2000m-NF	
700m	264m	1650m	5000m	600m	983m-NF	1350m-NF	
230m	156m	1302m	4750m	400m	701m	1200m-NF*	
150m	25m	850m	4500m	160m	701m-NF	1000m-NF	
5m		580m	4000m	50m	501m	800m-NF	
		450m	3250m		501m-NF	700m-NF	
PN046	PN053	250m	2541m		351m-NF	180m-NF	
1000m	719m	150m	1800m	PN073	180m	25m-NF	
700m	335m	25m	1600m	1650m*	180m-NF		
400m	149m		1000m	700m	101m-NF		
150m	25m		480m	25m	25m		
50m		PN058	250m	200m	25m-NF		
	PN056	1100m	180m	170m			
	1582m	215m	35m	50m			
							Total 21

NF = non-filtered sample

Samples were taken at different depths for each station using the 12L-Niskin bottles mounted on a CTD/rosette system. As soon as collected, the samples were filtered through 0.45 μ m pore size, 47mm diameter SUPOR membranes. An aliquot of 500mL was transferred into pre-cleaned low-density polyethylene (LDPE) bottles and 0.5mL concentrated d-HCl was added under a laminar flow hood to lower the pH of the samples to 2. Then, the surface of the LDPE bottle was wiped thoroughly to remove as much as possible any seawater trace and put into two zipped plastic bags. Meanwhile, approximately 10L of filtered seawater were collected into a precleaned HDPE container, acidified to pH \leq 2 with 10mL of acid and put on standby in the hood before being preconcentrated. Prior to be passed on the preconcentrating manifold, each sample pH was raised to 3.4-3.7 with the addition of small volume of suprapur NH₄OH (Merck®). The detailed REE preconcentration procedure was initially described by Shabani, Akagi and Masuda, (1992). Briefly, 10L of seawater (at pH \sim 3.6) was passed through two C18 cartridges which had been modified with a complexing agent right before manipulating. The precleaned C18 cartridge

were loaded with roughly 300mg of the mixture of 65% bi (2-ethylhexyl) hydrogen phosphate (HDEHP) and 35% 2-ethylhexyl dihydrogen phosphate (H₂MEHP) using a precleaned dropping bottle, sucking by a laboratory syringe (*Figure 2-2a*). A supporting device was applied to firm up the cartridge during the sample loading. Next, the sample was pumped through the cartridge at a flow rate of 20mL/min with the help of a peristaltic pump (*Figure 2-2b*). Seawater passing through the cartridges was thrown away. Once the preconcentration done, cartridges were disconnected from the circuit, sealed with Parafilm®, stored in a plastic bag and stored in a blind bag in order to avoid direct light exposal. REEs contained in the samples were quantitatively adsorbed by the complexing agent while major ions and a large amount of the Ba present in seawater were flowing through to the drain (Shabani, Akagi and Masuda, 1992). Due to the cartridge saturation capacity, 5L per cartridge is the maximum amount of seawater that can be passed through it.

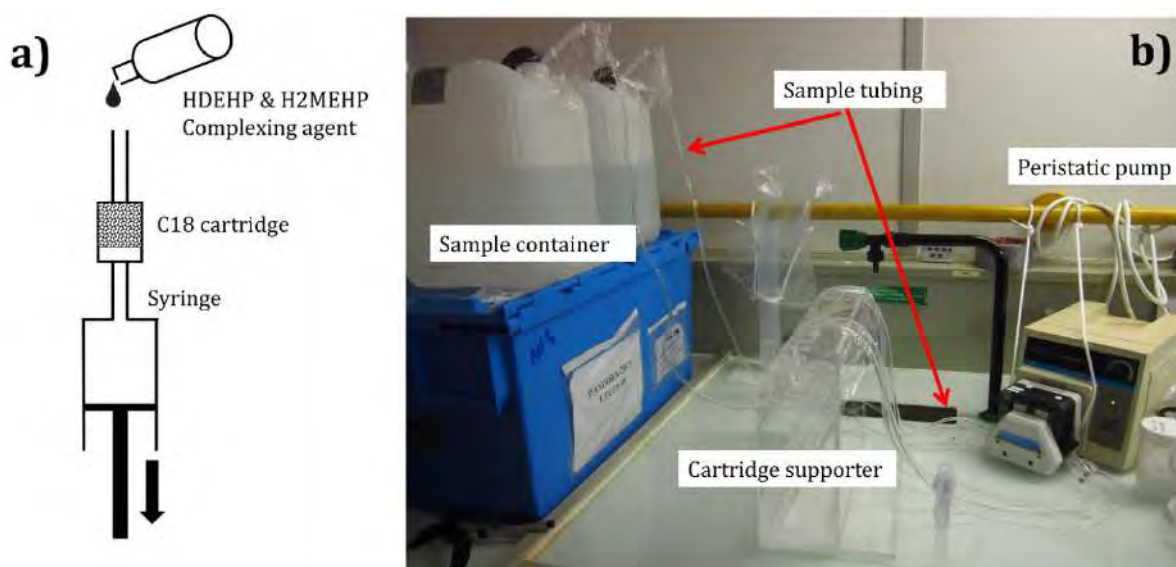


Figure 2-2 Nd-IC preconcentration on C18 cartridge during Pandora, a) modification of C18 cartridge by complexing agent, b) Multi-line preconcentrating with support device and peristaltic pump

2.3 Sample treatment and data analysis

2.3.1 Dissolved REE concentrations

Seawater dissolved REEs (dREE) concentrations were initially analyzed at LEGOS using a protocol that was established in the framework of Kazuyo Tachikawa and Francois Lacan thesis who used bispikes Nd and Yb (Tachikawa, Jeandel and Roy-Barman, 1999). In these studies, two spikes were added to the initial seawater sample to determine precisely the concentrations of two REEs (a light one, Nd and a heavy one, Yb) by using isotope dilution (ID). A comparison of the concentration obtained with ID calculation to those deduced from the external calibration allowed estimating the chemical recoveries for these two elements. These recoveries were then applied to the other REEs, using a linear interpolation between the Nd and Yb recoveries (Tachikawa, Jeandel and Roy-Barman, 1999; Lacan and Jeandel, 2001; Rousseau *et al.*, 2013). This strategy was completely suitable for most of the samples and was validated by analyzing

the reference solution provided by the Canadian National Research Council (CNRS): SLRS-5 riverine water and by the inter-calibration program in the framework of the GEOTRACES (van de Flierdt *et al.*, 2012). During my thesis, this protocol was improved by adding a europium (Eu) spike. This third spike was added due to the specific behavior of Eu together with the difficult analysis of this element. Indeed, recent works revealed that the marine behavior of dissolved Eu could differ from the other REE more than what was expected before (Grenier *et al.*, 2013; Garcia-Solsona *et al.*, 2014; Haley *et al.*, 2014). Dissolved positive Eu anomalies were detected in the Tropical Pacific, Northwest Pacific and Southern Atlantic and their origin and fate asks many questions, more specifically since Eu can occur under the +II oxidation state in the natural environments (Haley, Klinkhammer and McManus, 2004; Grenier *et al.*, 2011; Garcia-Solsona *et al.*, 2014). However, obtaining reliable Eu concentrations in seawater is a challenge for several reasons: 1) its natural concentration is at least ten times lower than the Nd one; 2) significant spectral interferences due to barium oxides can affect the Eu detection during the ICP-MS analytical process; 3) because of its possible +II oxidation state, it might behave differently from the other REE during the whole extraction procedure. In the framework of Mélanie Grenier thesis, desolvating nebulizer was added to the sample introducing line of the Quadrupole(Q)-ICP-MS, which improved the reliability of the Eu measurements by reducing the Ba oxide interferences (Grenier, 2012). The step further was to add an Eu spike into the sample. This means that we are now operating with 3 spikes. This allows us to determine Eu concentration using isotopic dilution, in parallel to Nd and Yb ones. The 3rd spike addition, and the validation for Eu application was tested during my master internship (Pham, 2015; Pham *et al.*, 2019)

In brief, the dREE analytical protocol is based on the co-precipitation of trivalent REE with Fe(OH)₃ in the seawater. The 0.5L aliquots of filtered seawater samples which were acidified on board to pH~2 were then spiked by the trispike solution containing ¹⁵⁰Nd (97.84%), ¹⁵¹Eu (97.79%) and ¹⁷²Yb (94.90%). The amount of spike added is determined by precisely weighing using a 7 digit-balance, and the amount of tri-spike solution added was adjusted based on REE data from previous studies (i.e: Zhang and Nozaki, 1996; Lacan and Jeandel, 2001; Grenier *et al.*, 2013). After ~36h and shaking again to ensure the spike homogenization, approximately 2.5mg of iron as FeCl₃ solution (5mg/mL purified) was added to the spiked sample. Few drops of H₂O₂ (30-32%, Fisher®) was added, vigorous shaking was then took using Stuart™-SSM1 placed at 90rpm for at least 24 hours to homogenize the samples, its pH was raised to 8±0.5 by adding NH₄OH. Then, the co-precipitation took place and left for 24h to complete. After decantation, two-third of sample supernatant was siphoned, and then REE-Fe precipitate was rinsed by continuous centrifugations. The supernatant was transferred to 50mL of polypropylene centrifugation tube, shaken rigorously and centrifuged at 3000 rpm in 30 minutes (Hettich-Rotina 380®). This rinsing-centrifugation procedure was repeated 5 to 7 times to remove as much as possible the salt content, for the sake of matrix-level guarantee of SF-ICP-MS. Rinsed co-precipitate was dissolved in 6M d-HCl, transferred to a 15mL Savillex® vial and then evaporated. The sample solution was evaporated down to become almost dry, to minimize sample loss since electrostatic Fe with the ambient environment could reduce the recoveries. Then 1mL of 6M HCl was added to the vial. Iron was removed from the sample by using an anion exchange column packed with 2mL of AG 1-X8 resin (handcraft quartz column, *Figure 2-3*). In

extreme acid condition (6M HCl), the REE are not adsorbed on the column, they are readily eluted while Fe is kept on the resin.

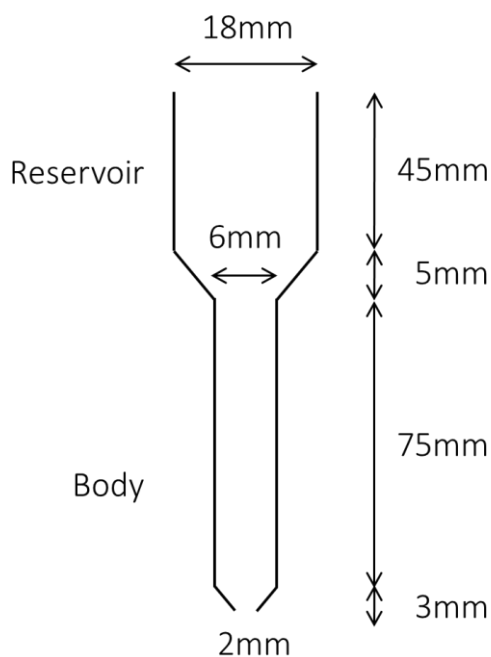


Figure 2-3 Handcraft column for anionic resin AG 1- X8

Thus, REEs were eluted from the column with 4mL of HCl 6M into a 7mL PTFE vial, evaporated to dryness and re-dissolved in an approximately 5-6mL of the 0.32M HNO₃ solution containing 0.1 ng/g of Indium and Rhenium as internal standard. Fe and remaining matrix were eluted after, during the cleaning procedure

The concentrations of REE in dissolved phases were measured with a SF-ICP-MS in a low resolution mode. REE concentrations in seawater and recoveries of analytical procedure were calculated using isotopic dilution and internal calibration method, respectively (Rousseau *et al.*, 2013). During the analysis, certified material standard and 0.1ng/g Cerium solution were also analyzed to calibrate the protocol and calculate the oxides formed which could generate interferences on the REE atomic masses. For example, barium which is 1000 times more concentrated than Nd in marine waters could interfere Eu151 and Eu153 by Ba135O16 and Ba137O16 oxides, respectively. A desolvating nebulizer (Aridus II) was coupled to the instrument in order to minimize oxide formations and consequent spectral interferences (Grenier *et al.*, 2011). Aridus considerably diminished the BaO interferences (down to less than 1%), yielding better conditions to measure Eu and middle REE concentrations. Blanks were lower than 1% for REE (III) and the mass fractionation was well monitored (Grenier *et al.*, 2011).

The REE concentrations were calculated simply by external calibration-EC, In and Re value were applied to correct the variations of instrumental sensitivity. The dREE data treatment was based on the coupling between ID and EC methods (Pham, 2015; Pham *et al.*, 2019)

2.3.2 Dissolved Nd-IC

Neodymium must be extracted from the sample and then separated from other elements to be measured with the solid source mass spectrometer. The pre-concentrated REEs stuck on the C18 cartridges (See section 2.2), were eluted in the clean laboratory. Handmade support allows connecting the cartridges to a peristaltic pump and then solutions were pushed via pre-cleaned tubing. Approximately 5mL of 0.01M HCl was first passed through the cartridge at 20mL/min to eliminate the remaining major salts and barium. Then, 20mL of 6M HCl at the same flow rate was used to elute the REEs (and/or remaining traces of other elements) into a 23mL PTFE vial. The eluted solution was evaporated to almost dryness and 2mL of aqua regia (mixing of HNO₃ and HCl) was added to deconstruct any organic matter. The mixing with aqua regia was placed on the hot plate at 120°C overnight and then completely evaporated. Subsequently, two chemical extractions were performed to purify Nd from other REEs: 1) a chromatographic extraction using a cationic column, this step separating REEs from other elements of the matrix and 2) a separation of Nd from other REEs using a specific anionic exchange column. In the first separation procedure, the deposit left in the vial after evaporation was re-dissolved in 1.5mL of 1M HCl and loaded on a column packed with 1.5mL of Dowex AG50W-X8 resin (200-400mesh, as shown in *Figure 2-4*). After loading, the column was first rinsed with 1mL of 1M d-HCl and then 2mL of 3M d-HCl to remove the iron and other major elements contained the sample. Next, 10mL of 2.5M d-HNO₃ was then added to extract the remaining matrix elements, the most important being the Ba. It is noted that two fractions of 0.5mL of MQW were added before and after HNO₃ fraction to avoid the formation of aqua regia that could affect the resin properties. The REEs were then eluted with 6mL of 6M d-HCl and collected into a 7mL PTFE vial.

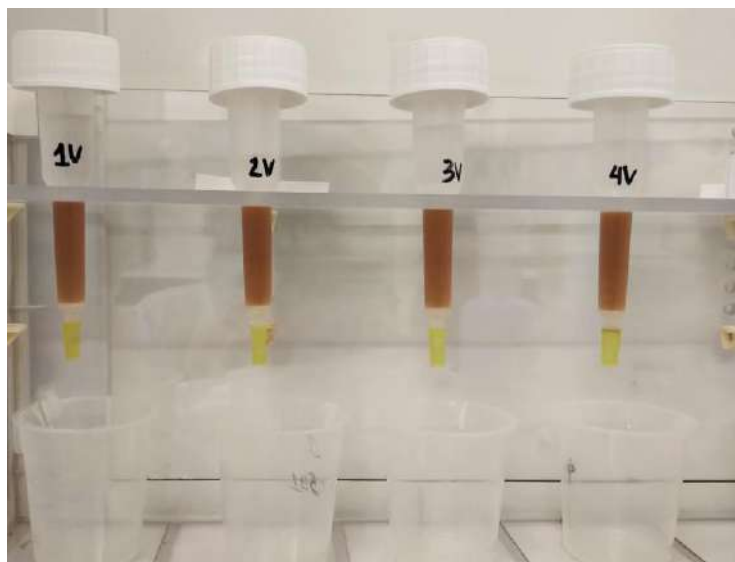


Figure 2-4 A set of cationic column packed with AG50W-X8 resin. Column using here is a commercial product Poly-Prep® Chromatography Columns (Biorad™)

After manipulation, the column was rinsed with 3mL of 6M d-HCl and stored in 1M d-HCl. The eluted solution was evaporated on the hotplate of the laminar flow hood. Once almost dry, the sample was taken up in 0.2mL of 0.05M d-HNO₃ for the second separation. In the following step, the sample was loaded onto a quartz column containing roughly 400mg Ln-spec resin

(Figure 2-5a). The column was successively rinsed with three small volumes (0.2mL) of 0.05M d-HNO₃ and then 3mL of the same acid. Subsequently, approximately 5mL of 0.23M d-HCl was added to the column to remove the REEs lighter than Nd, which was just after eluted by another 5mL fraction of 0.23M d-HCl. Note that the volume of acid used during these two steps had been calculated during the column calibrations and is not exactly the same for each column, due to their slightly different geometries. The Ln columns were cleaned with 7mL of 6M d-HCl, repeated 3 times and then stored in 0.05M d-HNO₃. The sample solution was then evaporated gradually to a small drop of 1-2µL which makes them ready for the mass spectrometry measurement.

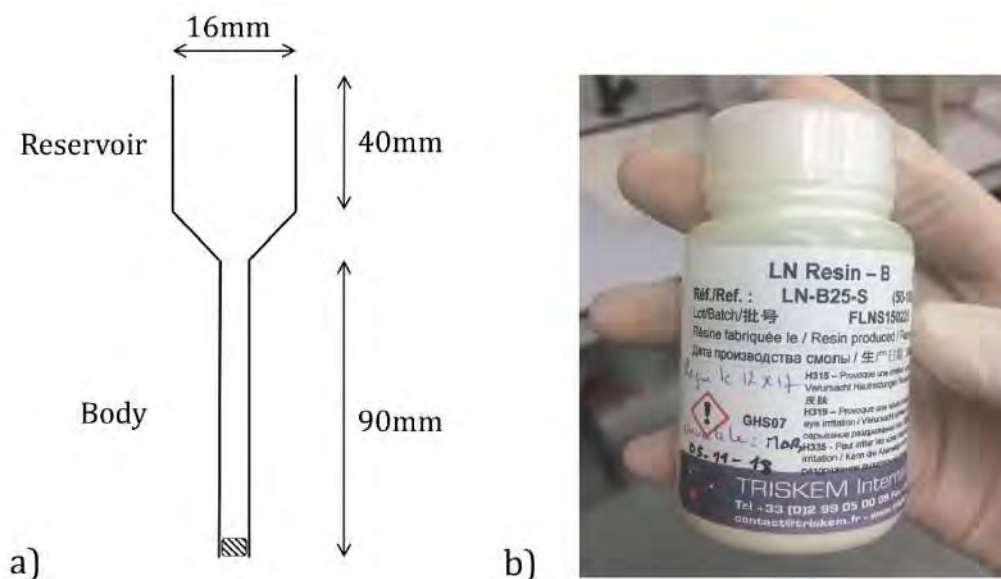


Figure 2-5 a) Ln-Spec quartz column and b) Ln-Spec commercial resin

The isotopic compositions of Nd were measured on the Thermo-Ionization Mass Spectrometer (TIMS, Thermo Fisher®) of the Midi-Pyrénées Observatory in Toulouse. The principle of TIMS is as follows: sample was deposited attentively onto a Rhenium filament, gently evaporated to dryness and placed in front of a second filament which is used for ionization. These filaments were subjected to electric current under a pronounced vacuum, allowing evaporation and ionization. The Nd isotopes were then accelerated by an electric field, deflected according to their mass and caught and counted in Faraday cups. The measurement was performed in static mode, ¹⁴³Nd/¹⁴⁴Nd ratio was normalized based on the ¹⁴⁶/¹⁴⁴Nd ratio to correct the mass fractionation of the instrument. The reference value ¹⁴⁶/¹⁴⁴Nd is 0.7219.

The accuracy and precision of TIMS were calculated automatically by the MatSpec software (Finnigan) and the reported data were taken with 2 standard errors (95%). The monitoring of the quality of the TIMS functioning was done by measuring 22 times of a La Jolla standard, at the beginning and the end of each measuring sequence. The instrument bias was set a value of 0.511848 ± 0.000010 for all the measurement. The reproducibility was evaluated by the analysis of triplicate sample, see measurement of Nd IC of station 82-1200m and 76-1650m. The blank contributions were also evaluated, with the average of 6pg which represents less than 1% of the signal

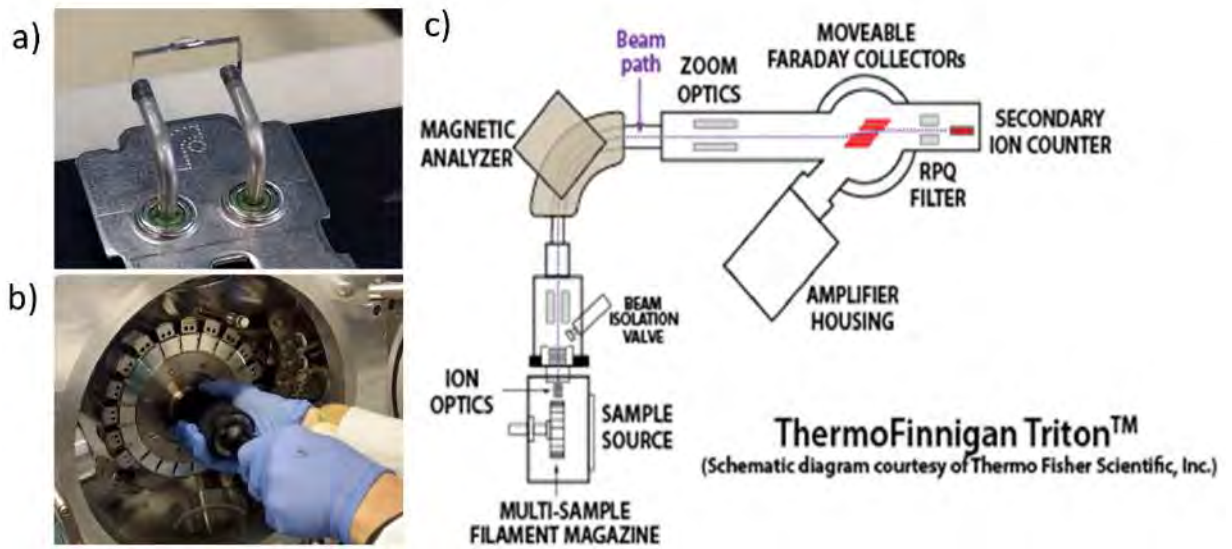


Figure 2-6 Measurement on TIMS, a) deposition of sample on the Re filament; b) inserting roller into sample introduction tray of TIMS and c) Schematic of Thermo-Ionization Mass Spectrometer (TIMS, Thermo Fisher®)

Chapter 3

The 'SeaSLOW'

3.1 Introduction

The Chapter 2 proposed a description of the analytical method for the analysis of dREE in seawater that I applied to the PANDORA samples, in the framework of this thesis. This method based on the REE co-precipitation with iron oxides had been used for years in the TIM-LEGOS laboratory and validated by many intercalibrations (e.g. van de Fliedrt *et al.*, 2012; Behrens *et al.*, 2018). However, it required a relatively long experimental time, a large sample volume requirement and an enhanced risk of contamination due to many different steps. More particularly, the number of centrifugation-rinsing steps required to eliminate the salt prior to the chromatographic purification and SF-ICP-MS analysis made the procedure quite long and tedious and added steps prone to recovery lost and contamination. During the 90's, other methods were developed including liquid-liquid extraction (Shabani, Akagi and Masuda, 1992; Nozaki and Alibo, 2003), ion chromatography (Bertram and Elderfield, 1993; Haley, Klinkhammer and McManus, 2004) and solid-phase extraction (SPE) (Zhang and Nozaki, 1998; Wen, Shan and Xu, 1999). Actually, none of these methods were satisfying for the REE analysis due to its huge time consumption and volume requirement. Recently, the NOBIAS-chelate PA-1® (Hitachi High-Technology) has become a 'hot' solid-phase sorbent for SPE due to its excellent performances for the preconcentration of trace metals (TM) from seawater (i.e: Sohrin *et al.*, 2008; Persson *et al.*, 2011; Biller and Bruland, 2012; Rousseau *et al.*, 2013; Hatje, Bruland and Flegal, 2014; Behrens *et al.*, 2016). In the last few years, a commercial preconcentration system named seaFAST® (Elemental Scientific Inc., Nebraska, USA) has become available for TM extraction from seawater, and adapted to the dREEs (Behrens *et al.*, 2016). This system provides the ability to work online, meaning that it can be connected directly to a SF-ICP-MS. Blanks, standards and samples are passed through the column in the same manner, and then elution solutions are injected immediately into the spray chamber of the SF-ICP-MS. The online process provides certain advantages, as reducing the preconcentration time, avoiding airborne contamination, reducing the sample volume and saving various vessel required for off-line preconcentration protocol (Hathorne *et al.*, 2012). The seaFAST® system can also be manipulated in "offline mode" which provides other advantages: 1) the system can be run over night unconnected to an ICP-MS, then saving argon gas and time, and 2) the sample signal is more constant than the peak signal due to online elution, allowing several measurement passes and, if required, re-analyses, thereby significantly increasing analytical precision (Behrens *et al.*, 2016). Notwithstanding the various advantages of the seaFAST®, this system cannot analyze seawater volumes larger than 40 ml. Thus, it does not allow analyzing the dCe reliably and leads to average precisions of ~12% (2σ) for most of the REEs for a 7 mL seawater sample (Hathorne *et al.*, 2012) or varying between 3 to 7% which can reach 86% for Ce (Behrens *et al.*, 2016). Hatje, Bruland and Flegal, (2014) developed an off-line method which improved some of

the seaFAST® weaknesses. It provided better precision, 5% for Ce (2σ , $n=5$) and less than 5% for others elements.

In the framework of this thesis, I was missioned by my advisor to develop an offline preconcentration system based on SPE and NOBIAS® resins that we named seaSLOW. I choose to start with the system developed by Hatje, Bruland and Flegal,(2014) for dREE extraction from seawater which I modified to allow more sample analysis in parallel. The seaSLOW is inexpensive, easy to set up and manipulate and allows processing 8 samples simultaneously. Sustainable blanks, yields and recoveries are obtained with this system that we used for the dREE analysis coupled to an isotopic dilution method. The reliability of this method was validated by analyzing replicates of samples collected at 2000 m in the Indian ocean in the framework of a GEOTRACES intercalibration with our Japanese colleagues and by the duplication of samples from the Solomon Sea (PANDORA cruise, Atalante, June-July 2012) which were initially measured by the classical method described in chapter 2.

3.2 Material and procedure

3.2.1 Reagents

We used high purity water ($>18\text{ M}\Omega\text{ cm}$) produced using a Milli-Q (MQW) system (Integral 5, Merck/Millipore). In-house distilled acids (d- HNO_3 and d- HCl) were prepared from commercial Trace Metal Grade (TMG) acid (Fisher Scientific®) and used to prepare all the reagents required by the experiment: the buffer solution to be loaded on the column, the elution solution (1N d- HNO_3) and the solution for the SF-ICP-MS analysis (0.32-0.37M d- HNO_3 spiked with 0.1 ppb of In and Re as internal standards). Another diluted d- HNO_3 (2%) solution was prepared for sample probe cleaning purpose. Finally, a 0.1M d- HCl solution was used for column rinsing and storage.

The preparation of the solution used to buffer the sample pH (referred as Sample Buffer in the following) was adapted for our experimental conditions from Hatje, Bruland and Flegal, (2014). 7M ammonium acetate stock solution was prepared by dissolving 150g of ultrapure ammonium acetate (NH_4AcO^- crystal form – VWR®) in 150g MQW, adjusted to $\text{pH}=8\pm 0.1$ with a small fraction of ultrapure glacial acetic acid and/or ammoniac solution (Merck®, depending if we needed to increase or decrease the resulting pH). The buffer used for the column pH conditioning (named Column Buffer) was made from 7.2mL of Sample Buffer diluted in 982.8 mL of MQW, adjusted to $\text{pH}=4.5\pm 0.2$ with ammoniac or hydrochloric acid solution prior to use. This buffer was also used to rinse the pre-concentrated sample once fixed on the column, in order to remove as much salt as possible.

The reagents and samples were stored in acid pre-washed high and low-density polyethylene (HDPE and LDPE) bottles, respectively. The cleaning procedure for reagent bottles included: 1) fill and submerge bottle in alkaline detergent (2% of RBS®-105), 2) rinse 3 times with MQW and fill with 1 M d-HNO₃ for a week) and 3) repeat the 2nd step but using 0.5M d-HCl. The rinsing process can be speed up by soaking at 80°C for one day. For sample bottles, we only used d-HCl because of the damage caused by nitric acid on the LDPE bottle walls. All cleaning processes and reagent preparations were performed under ISO 2 condition in the LEGOS clean laboratory.

3.2.2 Pre-concentration system (seaSLOW)

a) SPE Column

The column was built by packaging roughly 80µL of NOBIAS-chelate PA-1® resin which has two functional groups ethylenediaminetriacetic (EDTriA) and iminodiacetic acids (IDA) into a small PFA column (3 cm long PFA tubing; OD=3.175 mm, ID=1.587 mm, sealed by 2 porous polyethylene frits, 20µm pore size). The upper side of the column was attached directly to the top valve while the lower one was connected to the 1/16" OD PTFE tubing before connecting it to the bottom valve of the manifold. The column capacity will be discussed in section 3.3.1. All the connections were sealed with laboratory Parafilm® to avoid any air penetration into the column (See *Figure 3-1*). This column building allows saving up the cost for the commercial SPE column which could represent one third of seaSLOW cost.

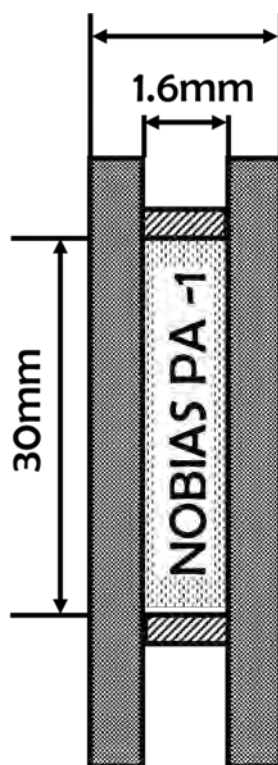


Figure 3-1 seaSLOW preconcentration column with NOBIAS®-PA-1 chelate resin

The stock resin was soaked prior to use and then decanted successively with 25 mL of each of the following solutions: acetone (reagent grade), methanol (reagent grade), MQW, 1M d-HCl-0.01M H₂O₂ (ultrapure), 1M HF, MQW, 1M HNO₃, MQW. The resin was finally rinsed and stocked in 0.1M HCl.

b) Manifold

In order to determine the REE concentration with the best precision, the volume of sample is increased up to 120 mL (maximum 250 mL) due to the low concentrations of dCe everywhere and dREE in the surface layers. We settled 8 columns in parallel, in order to pass 7 samples and a blank simultaneously.

As a compromise between the price and the performance of the manifold, we simplified the system described by Biller and Bruland, (2012) and Hatje, Bruland and Flegel, (2014). Instead of using one (or two) peristaltic pump for sample and rinsing buffer and N₂ gas pressure for elution, we used only 2 peristaltic pumps, named the Sample and Reagent pumps. The Sample pump allowed the sample loading while the Reagent pump was providing cleaning reagents for the different protocol steps (*Figure 3-2*). Tygon tubing was used to build the manifold thanks to its excellent chemical resistance. Prior to use, this tubing was cleaned carefully with the same cleaning procedure as for HDPE bottles. All the connections between the different tubes are made from pre-cleaned PTFE (OD=1.587mm; ID=0.793mm).

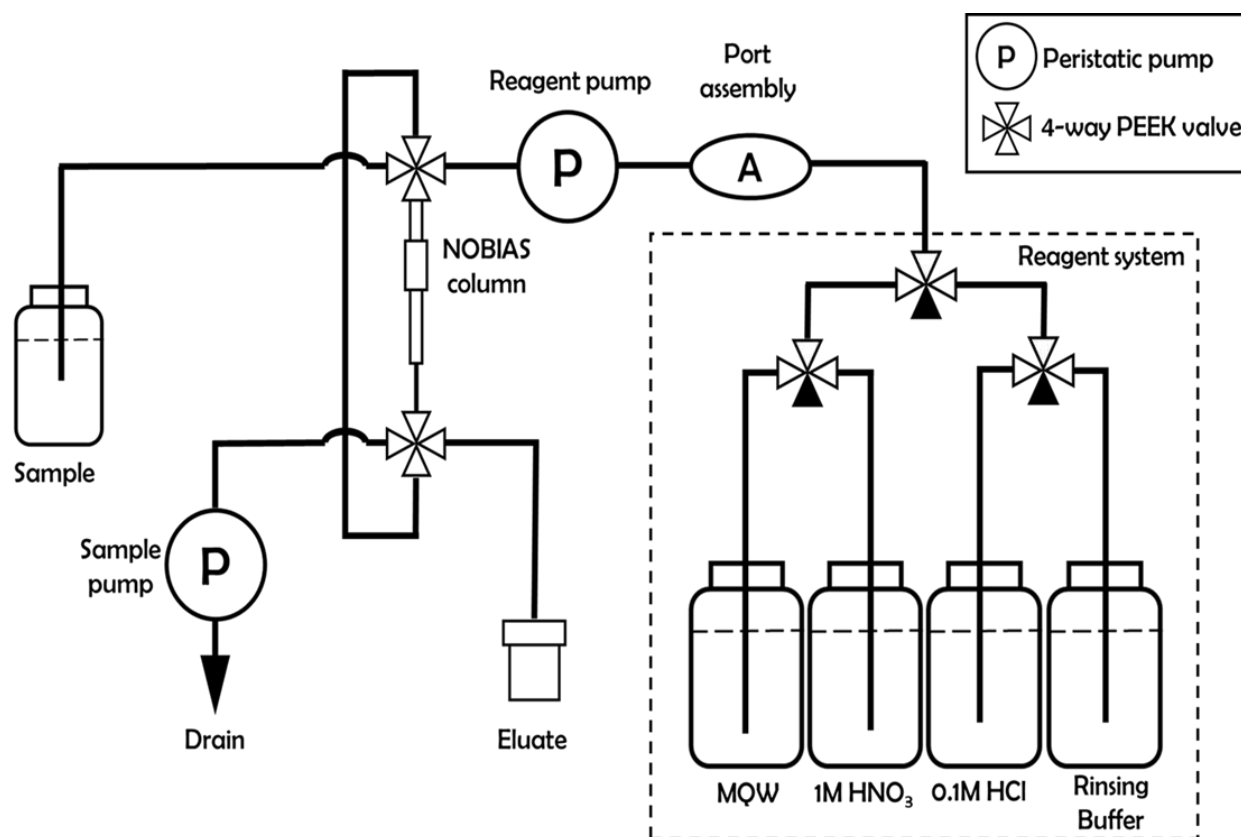


Figure 3-2 seaSLOW manipulation scheme

Figure 3-2 shows the seaSLOW manifold scheme. NOBIAS preconcentrating column was sandwiched between top and bottom 4-way PEEK valves (D-type). The different reagent solutions were pumped and brought to the top valve and then passed through column before flushing out of the system or to the collecting beaker. The sample was also introduced to the column from the top valve but via the sample pump.

c) Analytical procedure

Approximately 120 mL of pre-weighted samples are passed through the preconcentrating column. Prior to the loading, the sample was adjusted to $\text{pH}=4.5\pm 0.2$ as described above. Thus the final concentration of NH_4Ac in the sample was approximately 0.05M. Before loading the samples, all the columns were conditioned by flushing with Rinsing Buffer for 10 min (0.5 mL/min). This conditioning step allowed removing any acid left, thus ensuring the suitable column pH before loading the sample, and charged the exchange resin sites from H^+ form to NH_4^+ form (Biller and Bruland, 2012). The samples were then loaded with sample pump at a flow rate of 1 mL/min (roughly 2h for 120 mL sample). It is noted that the sample was not in contact with any Tygon tubing before passing through the column. Indeed, one of the numerous tests I did on this manifold revealed that dREE were adsorbed by the tubing, significantly lowering the recovery. Different experiment tests showed that sample flow rate could reach up to 1.2 mL/min without degrading the recovery; however, we applied 1 mL/min to our SeaSLOW to secure suitable reaction time for the resin. After loading, 3 mL of Rinsing Buffer were pushed through the column (see above). During this step, NH_4^+ replaced all the major cations (e.g. Na^+ K^+ Mg^{2+} and Ca^+) which had been adsorbed onto the resin during the previous step. Next, pre-cleaned PFA vial were placed into elution position and 3 mL of 1M d- HNO_3 (0.5 mL/min) were used to elute the REEs. Based on the study of Hatje, Bruland and Flegal, (2014), more than 99% of REE were eluted after the first 0.4 mL fraction, however, we collected 3 mL of eluent due to the larger size of our column compared to these author's study. The eluted solution was then evaporated to dryness and the residue was dissolved again into the 0.32M d- HNO_3 solution (see above) prior the SF-HR-ICPMS analysis. Columns were then rinsed by flushing with 10 mL of elution solution and MQW before storage in HCl 1M.

Table 3-1 Optimized preconcentration steps for eightfold system

Process	Step	Reagent Pump	Sample pump	Reagent	Flow rate	Time
					mL/min	min
Conditioning	1	On, tube on	Off, tube off	MQW	0.5	2
				Column Buffer	0.5	8
Sample loading	1	Off, tube on	On, tube on	Sample	1	Depend on sample volume (app. 120 min)
	2	On, tube on	Off, tube off	Column Buffer	0.5	
Elution	1	On, tube on	Off, tube off	1M HNO ₃	0.5	6
Cleaning	1	On, tube on	Off, tube off	MQW	1	2
	2			1M HNO ₃	1	10
	3			MQW	1	2
	4			0.1M HCl	1	6
Storage	1	Off, tube off	Off, tube off	0.1M HCl	-	-
Total time (min)						160

Tube on = connect tygon tubing to peristaltic pump, off = disconnect

The preconcentration procedure is summarized in *table 3-1* and a user guide of the manifold proposed in Annex A of this manuscript

3.3 Method optimization

When compared to the literature, the major changes in our system were focused on the column capacity and the optimization of the suitable rinsing volume after sample loading step. In addition, as for the classical procedure, we spiked all our samples with a triple spike made of ¹⁵⁰Nd, ¹⁵¹Eu and ¹⁷²Yb in order to constrain the experimental recoveries. The concentration Nd, Eu and Yb contained in the trispike were prepared at 6ppb, 1ppb and 4ppb, respectively.

3.3.1 Column capacity and sample volume

The column capacity was estimated to be consistent with the charge content of the volume of sample we need to analyze. Following Sohrin *et al.*, (2008), the adsorption capacity of the NOBIAS® Chelate-PA1 for Cu(II) is 0.16 ± 0.01 mmol/g. Thus, the exchange capacity of our column would be 48 mmol for this element. At a pH=4.5±0.2, we took into account all the chemical species present in any seawater sample that could

be preconcentrated together with our targeted REEs in order to calculate the amount of seawater that can be passed through the seaSLOW. The total concentration represents less than 150 nmol/Kg based on the average composition of the seawater (<https://www.mbari.org/science/upper-ocean-systems/chemical-sensor-group/periodic-table-of-elements-in-the-ocean/>). We thus estimated that our column can handle up to 2L of seawater, which could be very interesting for further development, as for example the preconcentration of deep water samples for isotopic composition measurements. For the dREE preconcentration, the range of volumes used span 120 ml (deep water) to 250mL (surface waters). These volumes are a compromise between different constraints: 1) The experimental time which is determined by the flowrate at 1ml/min, 2) Sample sensitivity and selectivity, since the REE dissolved concentrations are extremely low, especially for surface waters. This is even more crucial for dCe, which marked depletion compared to the other dREEs (expressed as a “negative anomaly”) has to be precisely determined. Thus, the volume of sample is calculated to get the best signal/noise ratio.

3.3.2 The rinsing volume

As discussed in chapter 2, the major cations and salt contained in seawater are generating interferences on the different masses we need to detect and/or could seriously hamper the sensitivity of the SF-HR-ICPMS by clogging the cones. In the classical protocol, the coprecipitate Fe-REE passed through a successive rinsing steps to minimize the salt content. With the SEASlow procedure salt and undesirable cations can simply be wiped out by an extra rinsing step with the buffer, just after the loading step. The rinsing volume should be optimized since redundant rinsing buffer can remain and generate noise during the spectrometric analysis and/or can affect the sample recovery. The rinsing step was carefully tested by checking salt content after each fraction of rinsing and results are shown in *Figure 3-3*. Substantial amount of salt was reduced after 1mL of rinsing, and decreased as the rinsing volume increased to 5mL. To ensure the best recovery, we determined an optimal rinsing volume of 3mL.

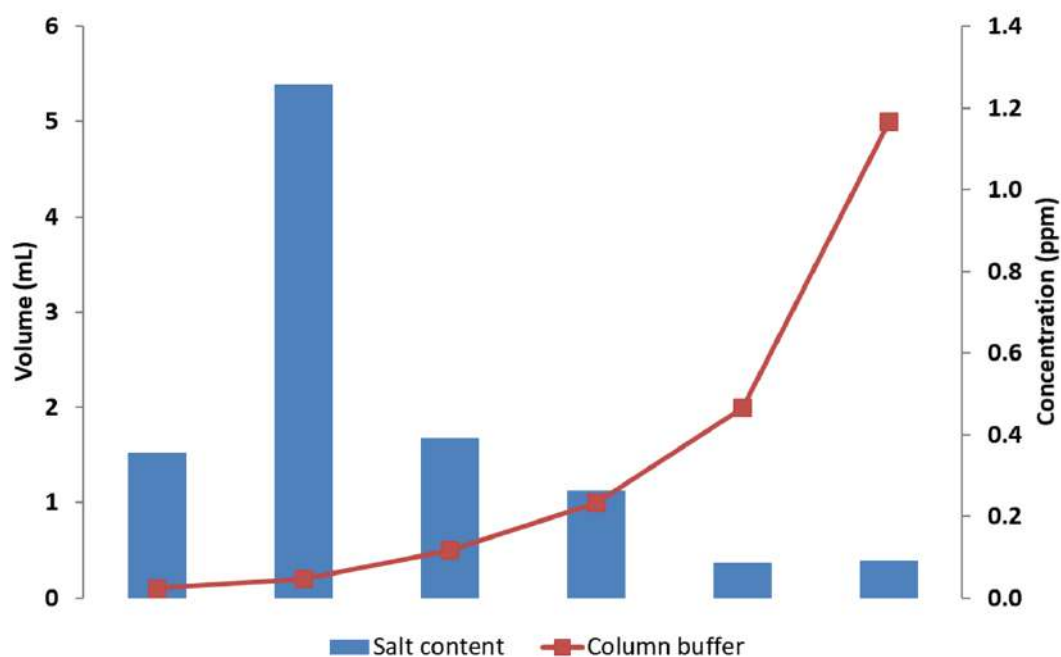


Figure 3-3 Effect of rinsing buffer on the removal of salt content in the seaSLOW column

3.4 Manifold validation

The performances of the seaSLOW were tested by duplicating Pandora samples of stations 13 at 600m (PAN13-600m), station 20 at 25 and 600m (PAN20-25m, PAN20-600m), station 73 1650m (PAN73-1650m). The reproducibility was established by measuring replicates of samples from the deep Indian Ocean collected by our Japanese colleagues in the framework of a GEOTRACES intercalibration. dREE recoveries were estimated by using isotopic dilution method with our trispike and were quantitative ($\geq 90\%$)

At a first glance, a diminution of the barium content of 400-1800pmol/Kg is observed in the eluted solution when using the seaSLOW compared to what we obtain with the classical protocol (*Table 3-2*). Eliminating Ba is important since its oxide BaO is interfering the europium mass during the mass spectrometric analysis.

Table 3-2 Dissolved REE concentrations (10^{-12} Kg) measured with the seaSLOW compared to the results obtained with the TIM classical protocol for different samples

	Ba	La	Ce	Pr	Nd	Sm	Eu	Gd	Th	Dy	Ho	Er	Tm	Yb	Lu
JAP2000m															
Average result using seaSLOW (n=7)	0.0	27.8	2.7	3.7	18.2	3.4	1.1	5.4	0.9	6.6	1.9	7.0	1.0	7.5	1.3
2 σ SD (pmol/Kg)	0.0	0.2	0.1	0.1	0.6	0.1	0.1	0.4	0.1	0.1	0.0	0.6	0.0	0.9	0.1
2 σ RSD (%)	0.0	0.5	0.2	0.1	1.2	0.1	0.2	0.9	0.1	0.2	0.0	1.1	0.0	1.7	0.2
Average result using classical protocol (n=3)	-	29.8	2.9	4.1	17.9	3.3	1.0	5.4	0.8	6.7	1.9	6.8	1.0	7.0	1.3
2 σ SD (pmol/Kg)	-	0.8	0.1	0.1	0.3	0.1	0.0	0.2	0.0	0.3	0.1	0.2	0.1	0.3	0.1
2 σ RSD (%)	-	2.8	2.8	2.6	1.9	3.3	3.7	3.9	2.6	4.0	3.3	2.9	5.9	4.8	4.3
PAN20-25m															
Average result using seaSLOW (n=1)	0.0	3.6	3.4	0.9	4.8	1.1	0.3	1.7	0.3	2.2	0.6	1.8	0.2	1.2	0.2
2 σ SD (pmol/Kg)	0.0	0.1	0.1	0.0	0.1	0.0	0.0	0.1	0.0	0.1	0.0	0.1	0.0	0.0	0.0
2 σ RSD (%)	0.0	3.2	2.5	2.7	2.5	3.9	2.7	3.7	2.9	3.1	3.2	3.6	3.5	2.7	3.0
Average result using classical protocol (n=1)	337.2	4.3	3.7	1.0	4.7	1.1	0.3	1.7	0.3	2.1	0.5	1.7	0.2	1.2	0.2
2 σ SD (pmol/Kg)	11.7	0.2	0.1	0.0	0.2	0.1	0.0	0.1	0.0	0.1	0.0	0.1	0.0	0.0	0.0
2 σ RSD (%)	3.5	4.3	4.0	4.2	3.4	5.8	3.6	5.9	3.6	4.5	3.8	4.4	4.5	3.2	4.5
PAN20-600m															
Average result using seaSLOW (n=1)	0.0	12.2	2.3	1.6	7.9	1.5	0.4	2.5	0.4	3.7	1.1	4.0	0.6	4.0	0.7
2 σ SD (pmol/Kg)	0.0	0.4	0.1	0.0	0.2	0.1	0.0	0.1	0.0	0.1	0.0	0.2	0.0	0.1	0.0
2 σ RSD (%)	0.0	3.5	2.5	2.9	2.4	3.6	2.6	3.7	2.6	3.1	3.5	4.2	3.6	2.5	3.1
Average result using classical protocol (n=1)	957.3	12.1	2.0	1.5	7.2	1.4	0.4	2.4	0.4	3.4	1.0	3.9	0.6	3.9	0.7
2 σ SD (pmol/Kg)	25.8	0.3	0.1	0.1	0.2	0.1	0.0	0.1	0.0	0.1	0.0	0.1	0.0	0.1	0.0
2 σ RSD (%)	2.7	2.8	3.7	3.3	2.7	4.4	4.8	3.3	2.8	3.4	3.6	3.1	3.2	2.6	2.9
PAN13-600m															
Average result using seaSLOW (n=1)	0.0	11.5	1.3	1.5	7.6	1.4	0.4	2.5	0.4	3.6	1.1	4.1	0.6	4.0	0.7
2 σ SD (pmol/Kg)	0.0	0.5	0.1	0.1	0.3	0.1	0.0	0.1	0.0	0.2	0.1	0.2	0.0	0.2	0.0
2 σ RSD (%)	0.0	4.7	4.1	3.9	4.2	4.9	3.9	4.5	4.2	4.6	4.6	4.5	4.4	3.9	4.6
Average result using classical protocol (n=1)	1021.1	11.8	1.0	1.5	7.2	1.4	0.5	2.5	0.4	3.5	1.1	4.0	0.6	4.1	0.8
2 σ SD (pmol/Kg)	16.9	0.2	0.0	0.0	0.1	0.0	0.0	0.1	0.0	0.1	0.0	0.1	0.0	0.1	0.0
2 σ RSD (%)	1.7	1.9	4.4	1.7	1.5	3.4	2.2	2.7	2.8	3.1	1.9	2.2	2.2	1.5	2.3
PAN73-1650m															
Average result using seaSLOW (n=1)	0.0	25.2	3.0	3.1	15.6	3.0	1.0	4.8	0.8	6.4	1.8	6.8	1.0	7.1	1.3
2 σ SD (pmol/Kg)	0.0	0.9	0.1	0.1	0.4	0.1	0.0	0.2	0.0	0.2	0.1	0.2	0.0	0.2	0.0
2 σ RSD (%)	0.0	3.5	2.5	3.1	2.4	3.5	2.5	4.0	3.1	3.7	3.5	3.5	3.7	2.4	3.4
Average result using classical protocol (n=1)	1736.8	25.2	2.8	3.2	14.9	3.0	1.0	4.7	0.7	6.1	1.8	6.5	1.0	7.1	1.3
2 σ SD (pmol/Kg)	77.2	1.3	0.1	0.2	0.5	0.1	0.0	0.2	0.0	0.3	0.1	0.3	0.0	0.2	0.1
2 σ RSD (%)	4.4	5.1	4.1	4.9	3.5	4.7	3.7	4.7	5.5	5.4	4.2	4.9	4.1	3.2	4.3

3.4.1 Blank and detection limit

The blanks are reported in *Table 3-3*.

Table 3-3 Average total procedural blank and detection limit for all REEs (n=26)

Element	Average Blank (10^{-12} mol/Kg)	Detection Limit (10^{-12} mol/Kg) ^a
La	0.4	1.1
Ce	0.5	1.1
Pr	0.08	0.22
Nd	0.2	0.6
Sm	0.03	0.13
Eu	0.03	0.13
Gd	0.06	0.11
Tb	0.01	0.03
Dy	0.06	0.29
Ho	0.01	0.08
Er	0.02	0.06
Tm	0.01	0.09
Yb	0.001	0.209
Lu	0.008	0.037

^a Three times of the standard deviation of total procedural blanks

The whole blanks comprise Sample Buffer together with rinsing solution, elution acid and other reagent and the manifold use: in other words, solutions without sample passing through the seaSLOW. Manifold blanks for each individual column, over multiple days, showed no significant variation, assessing the good constancy of the system.

In the deep waters, total procedural blanks represent less than 0.5% of the dREE signal with the exception for dCe which displays blanks $\leq 5.0\%$. In the surface waters, procedural blanks represent a higher proportion of the signal up to 1% for dREEs, except for Ce for which they range from 3.7% to 6.1%.

The resulting detection limit (DL) of the seaSLOW preconcentration procedure for dREEs, calculated as three times the standard deviation of the total procedural blanks (n=26) ranged between 0.03 pmol/Kg for Tb and 1.1 pmol/Kg for La and Ce. These DL are largely (~ 40 times) below the average seawater concentrations of these elements, of 1.1 pmol/Kg and 40 pmol/Kg, respectively.

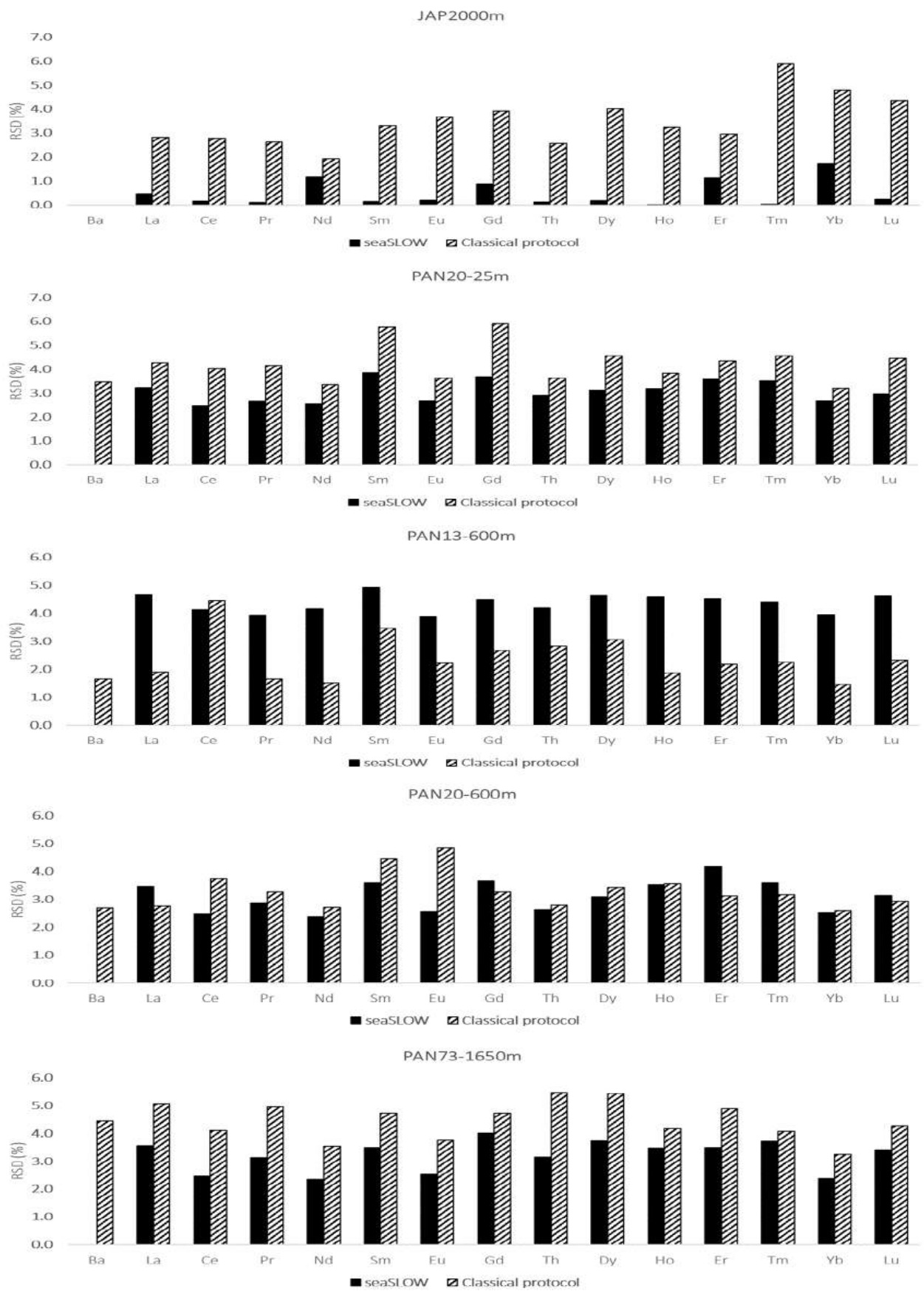


Figure 3-4 Analytical RSD(%) of different samples after seaSLOW and classical protocol

3.4.2 Accuracy and precision

As mentioned above, the accuracy of our seaSLOW was verified by repeated processing and analysis of JAP2000m (n=7) and duplicates of Pandora samples which were also compared with the results obtained for the same samples with the classical protocol, (Pham *et al.*, 2019). All the results are reported in *Table 3-2* seaSLOW analytical precision for JAP2000m (2σ RSD, n=7) was $\leq 1.1\%$ for all the REEs, except for Yb (1.7%) and Nd (1.2%). For other sample from PANDORA, the precision of seaSLOW show a similarity with classical protocol with an exception of sample PAN13-600m. The precision of the analytical methods using the seaSLOW are much better than those obtained with the classical protocol which provided dLREE concentrations agreeing within 8% for La, 14% for Ce and 4% for Pr and Nd; dMREE and dHREE concentrations agreeing within 8% for Sm, 11% for Eu and less than 4% for the remaining REEs (Pham *et al.*, 2019).

The mean dREE concentrations of the sample JAP2000m are well within the confidence interval of the classical protocol results (*Figure 3-5*).

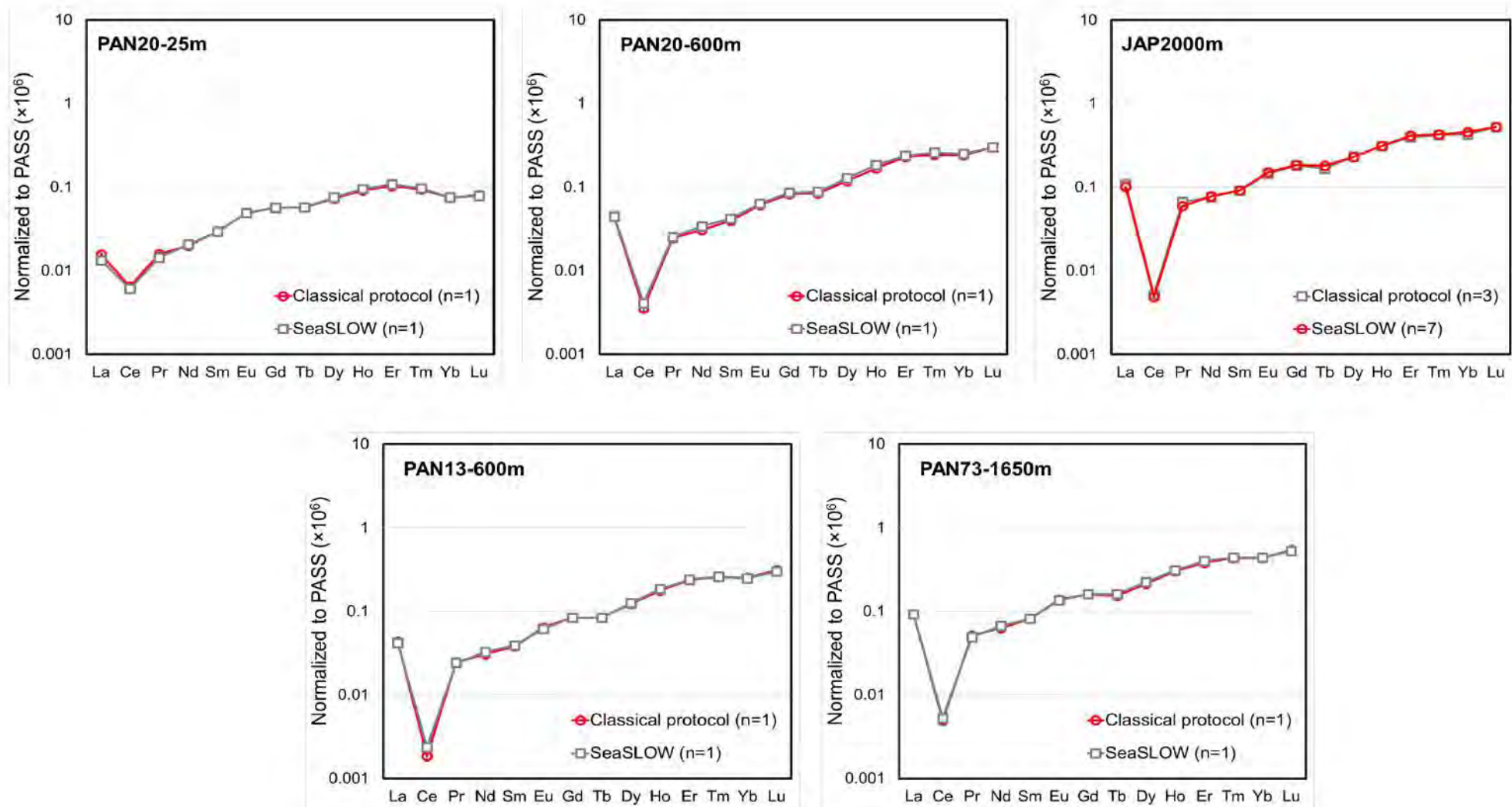


Figure 3-5 Normalization to PASS (Taylor and McLennan, 1985) of average REE concentration of seaSLOW compare with Classical protol data published by Pham et al (2009).

Duplicates of Pandora Sample using the seaSLOW also lead to satisfying results. The analytical precision averages 3% and stays better than what is obtained with the classical protocol. Analyzing the surface water from Pandora (PAN20-25m) shows good agreement with the published value, with less than 3.0% of deviation for almost all the REE, except for La (15.1%), Pr (9.2%) and Ce (6.2%). At 600m, samples from both station 13 and 20 (PAN13-600m, PAN20-600m) illustrate excellent agreement with published value, deviation between seaSLOW and classical protocol being lower than 5% for all the REE. Deepwater of Pandora sample, PAN73-1650m shows no difference between the two methodes, the highest deviation being observed for dCe (6.3%). Note that these Pandora samples were not analyzed by the same experimentalist which could introduce a bias. However, the highest deviation between the classical method and the seaSLOW one only happen in surface waters when the concentrations are low which makes the analysis more challenging. However, the deviation still stays at the confidence interval of both methods (*Figure 3-4*).

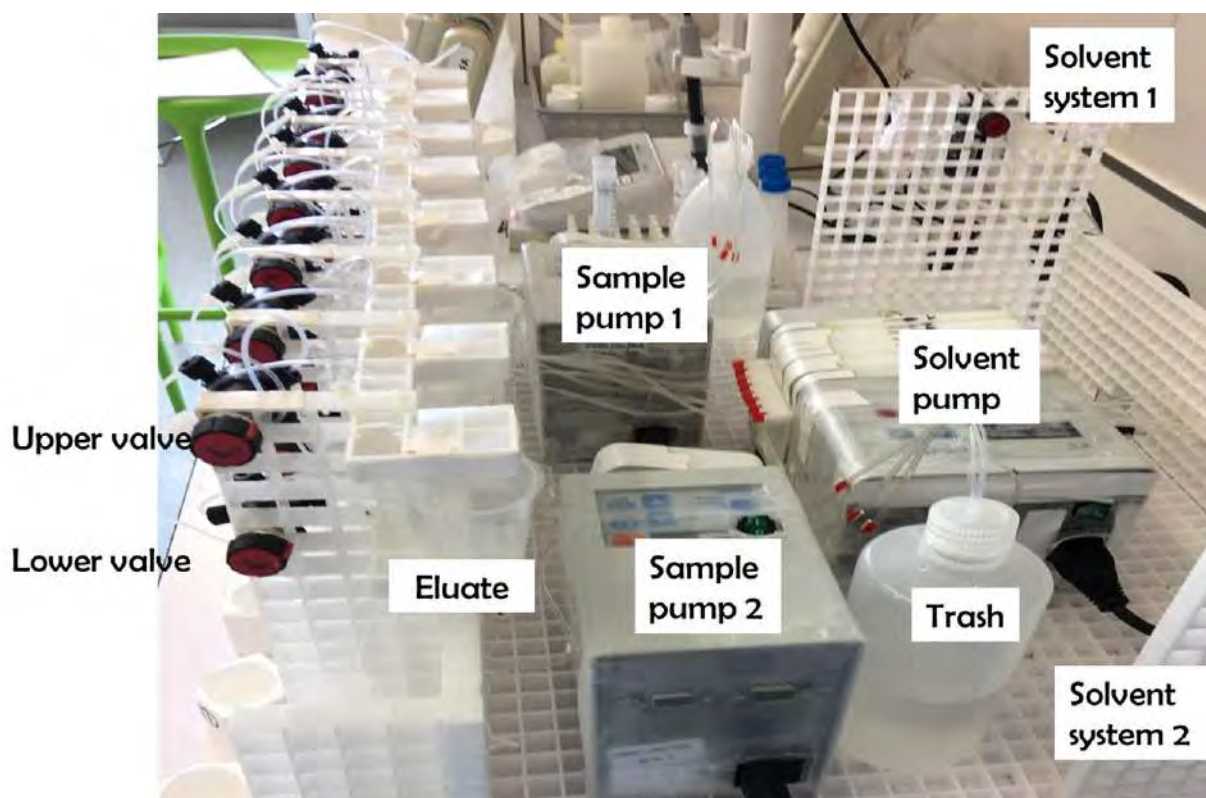


Figure 3-6 Pictures of seaSLOW system in ISO 2 clean laboratory of LEGOS, Toulouse, France

3.5 Conclusion

A new preconcentration system (seaSLOW) was built using NOBIAS® chelate resin to extract REE from seawater prior to be measured with SF-ICP-MS. This new seaSLOW allows us to simultaneous preconcentrate 8 samples in the same time which would be more applicable for research project requiring a high number of samples. One factor could make seaSLOW become available to be set up is that its cost to build up, typically

equal one fifteenth of seaFAST, commercial product price. The analytical method using seaSLOW displayed low blanks and detection limits couple with high quantitative recovery. More importantly, the Barium content in the seawater was eliminated together with others interference elements at suitable conditioning working. This aspect of seaSLOW allows better precision of the measurement of Eu which is one of our interest to trace Basalt source in seawater. Measurement of REES for GEOTRACE Indian Ocean collected by our Japanese colleagues (JAP2000m) and PANDORA samples indicated an excellent agreement between two methos, the seaSLOW and the Fe-coprecipitation (classical method in LEGOS). The applicability of seaSLOW will be demonstrated with proceeding studies which contain North Atlantic Ocean, Baltic Sea and other water area.

ANNEX A: MANIFOLD USER INSTRUCTION

This section describes in detail how to use the seaSLOW for dREE extraction from seawater summarized in *table 3-1* (Thesis Manuscript - Chapter 3). The protocol includes 4 main phases (conditioning, loading and rinsing, eluting and cleaning) as in *table 3-1* and divided here in 9 sub steps in total.

Figure A1 shows column attachment and all the connection between two main valves with the remaining parts of manifold. As indicated by the column-valve diagram, the preconcentration column was connected to the lower position of both upper and lower valve. The solution flowing direction was adjusted to be from top to bottom. The valve used here was a L-valve which provides only one-way direction for each movement of button.

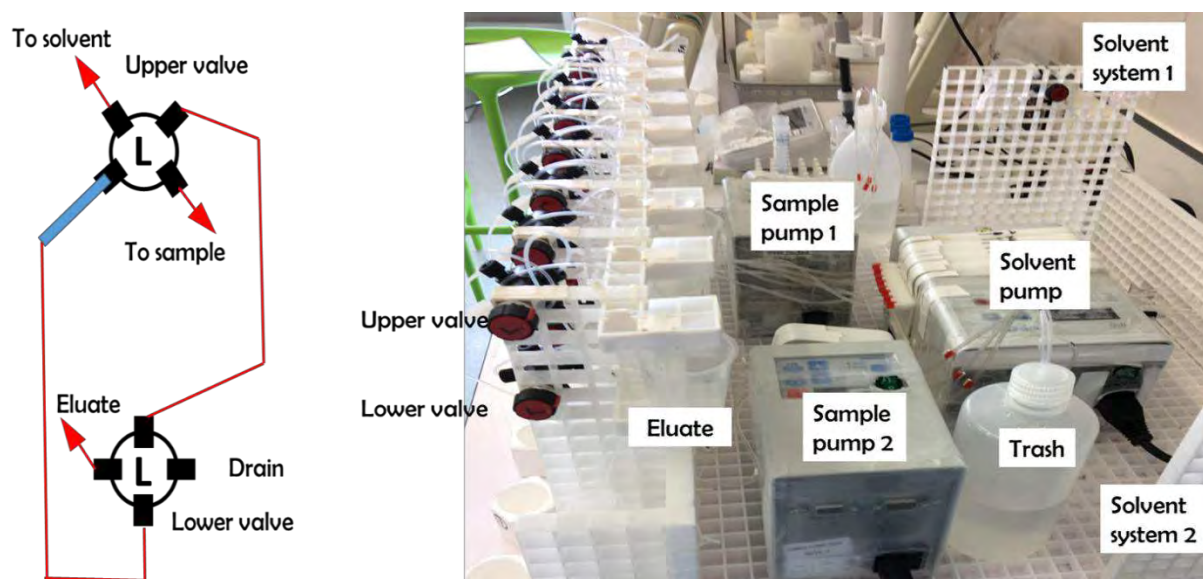


Figure A1 Valve and column connection (left) in the seaSLOW system (Right). 'L' symbol inside the valve indicates the L flow type of V101-L PEEK valve used in the manifold. Blue bar connected to lower position of upper valve represents the handcraft column with NOBIAS® resin. Solution is always flushed through the column via the upper valve and then discarded through lower valve

A.1 Main phase 1 - Conditioning

Conditioning phase procedure is resumed in *Figure A2*, detail as below:

- Lock peristaltic tubing to the roller of the Reagent Pump. It is noted that the tubings have to be settled carefully in the pump with the right order to ensure a good flow rate control.
- Check that the Sample pump has to be in OFF mode with all tubing are disconnected. Remaining connected tubing can result in backpressure for the seaSLOW and lead to leakage of connecting point.
- Set the column valve system as following the configuration shown on the left of the *Figure A2*.
- Adjust Reagent System to MWQ position, start Reagent pump for 2 minutes, at 0.5mL/min.

- Pause the Reagent pump, switch to Buffer position, continue pumping for 8 minutes at the same flowrate.

MANIFOLD MANIPULATION – STEP 1: CONDITIONING

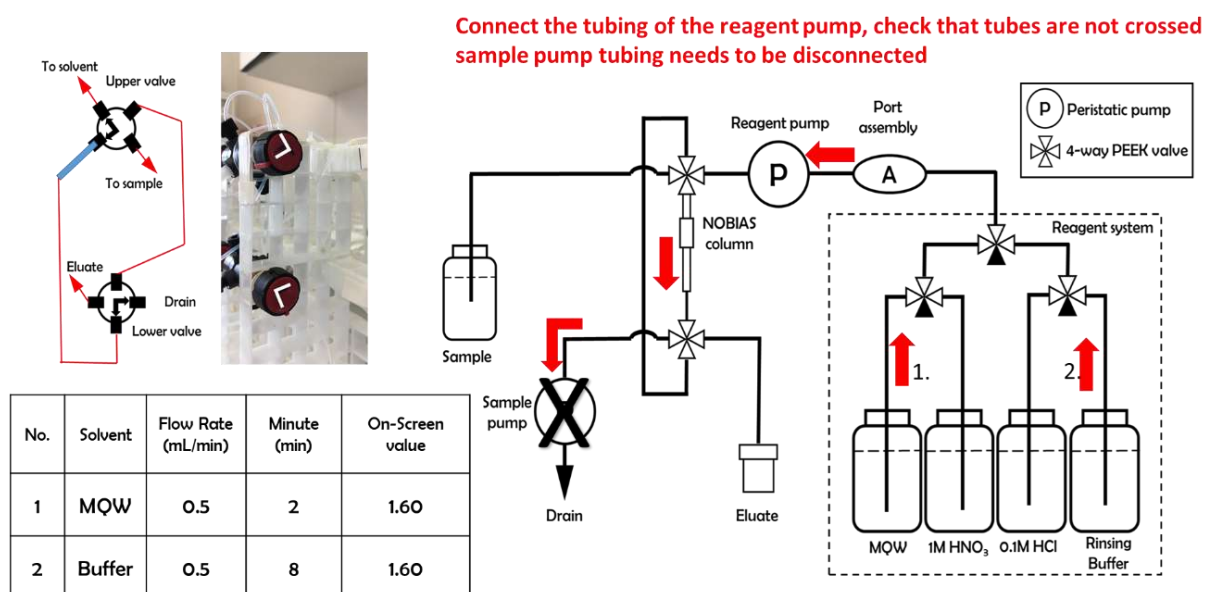


Figure A2 Conditioning phase. The arrows inside the valve shows the liquid ways; the red arrows above, also describe the trajectory of the different solutions.

A.2 Main phase 2 - Loading

This phase includes 4 steps (from step 2 to step 5) which will be demonstrated in *Figure A3, A4, A5, and A6*. For each step, the procedure is described as below:

❖ Loading – 1 (*Figure A3*)

The main purpose of this step is to get the system in preparation mode, get rid of all remaining acid inside the sampling needle.

- Turn OFF the Reagent Pump, tubings stay locked on the roller of the pump.
- Lock peristaltic tubing to the Sample Pump's rack. Check the tubing order.
- Set the column valve system as the configuration shown on the left of the *Figure A3*.
- Start the Sample Pump for just 15 s at 1 mL/min. The sample solution, at this moment, reaches the upper valve. Two onscreen values for the pumps are shown as a reference due to the application of a co-sample pump.

MANIFOLD MANIPULATION – STEP 2: LOADING -1

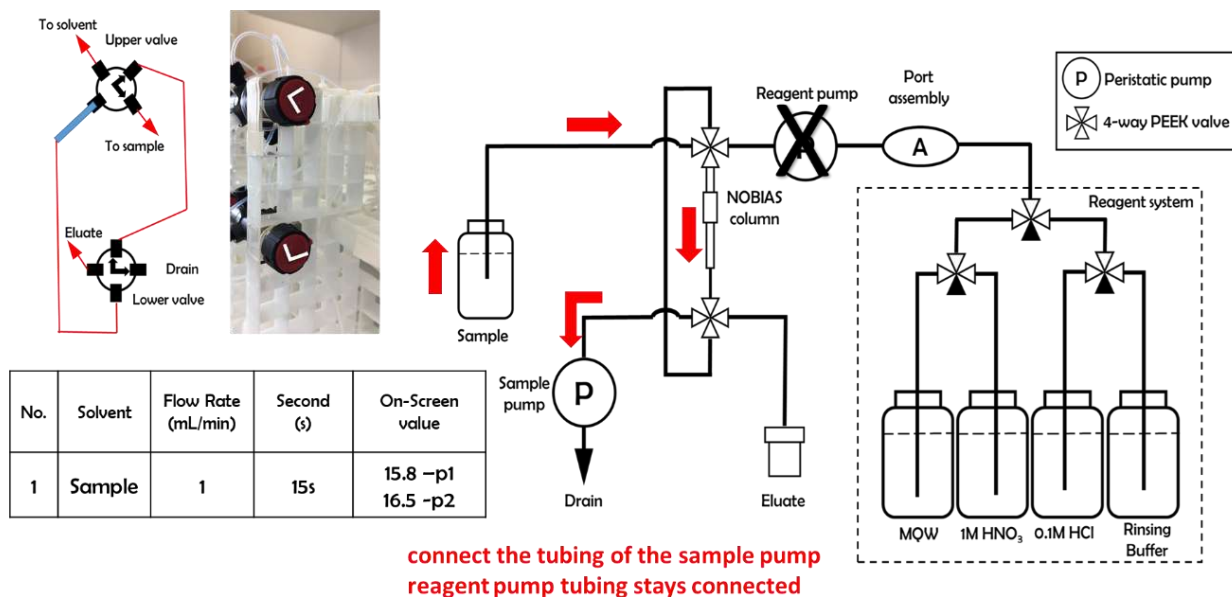


Figure A3 Loading phase – Step 1. Two sample pumps were installed lead to different onscreen values.

❖ Loading – 2 (Figure A4): Main loading steps

- Set valve configuration as shown on the left in figure A4.
- Continue flushing sample through the column at 1 mL/min.
- Check the drops at the drain or the bubble movement inside the tubing to ensure that the system is in working mode. Empty the drain after 60 minutes of manipulation.
- Due to the system properties, the flowrate of each line could differ from each other, leading to variation in loading time. In this case, pause the pump and set column's valves following the configuration shown for Loading-3, as soon as the sample aliquote was completely pumped out (see Figure A5). This action can ensure that the columns are not going to dry during stand by time.

MANIFOLD MANIPULATION – STEP 3: LOADING -2

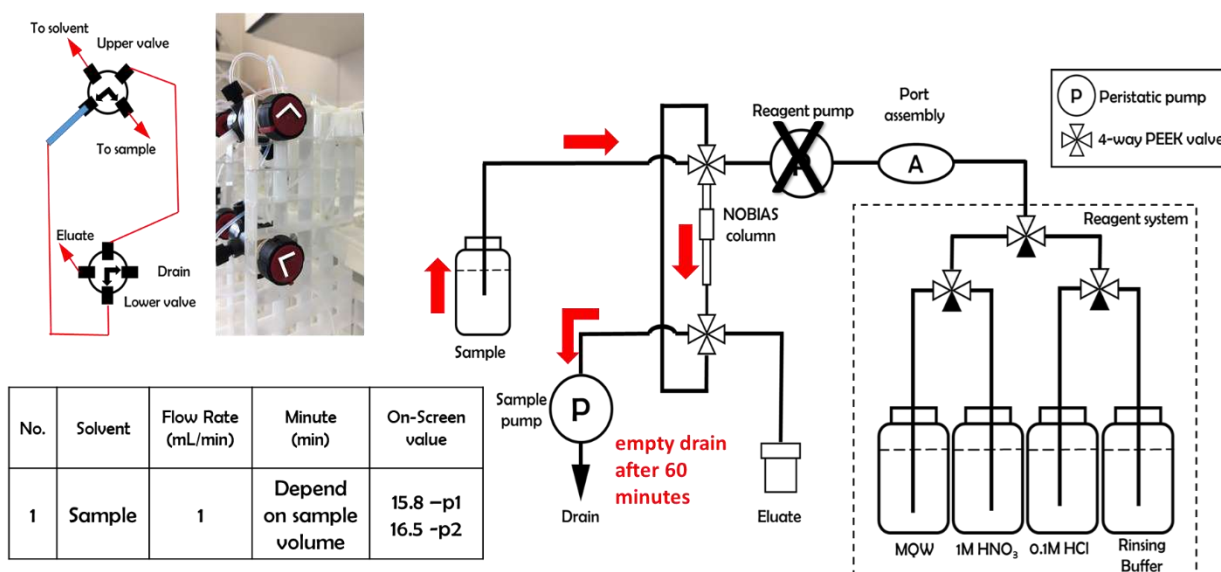


Figure A4 Loading phase – Step 2

❖ Loading – 3 (Figure A5): Sampling needle PreCleaning

- Replace sample bottle with clean 2% d-HNO₃ (rinsing solution)
- Set valve configuration as shown on the left of figure A5.
- Turn on the Sample Pump to keep pushing the rinsing solution via the system for 2-3 minutes, at 1mL/min to clean inner and outer surface of the sampling needle.
- Stop the sample pump.

MANIFOLD MANIPULATION – STEP 4: LOADING 3-PreCLEANING

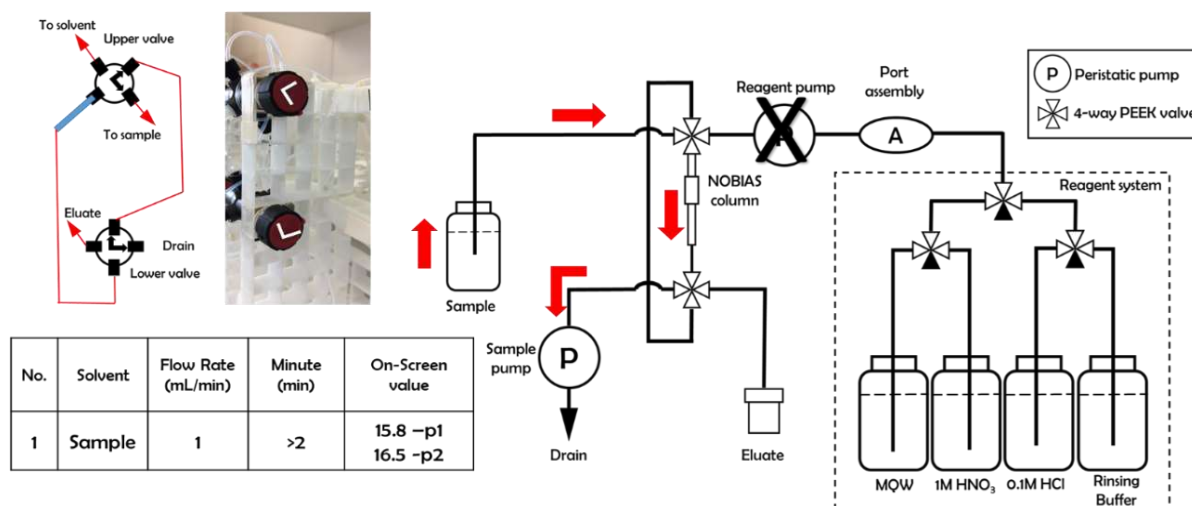


Figure A5 Loading phase – Step 3: Replace the empty sample bottle with the bottle with new 2% HNO₃. Then move this column into configuration above. Samples that are not done yet stay in Loading – Step 2 position.

❖ *Loading – 4 (Figure A6): Sample matrix removal*

All column matrix will be removed with in this step by flushing column with fresh buffer.

- Set valve configuration as shown on the left of figure A6.
- Disconnect peristaltic tubing from the sample pumps.
- Check the Reagent system to ensure that Buffer's position is still selected.
- Start Reagent pump for 6 minutes, at a speed of 0.5 mL/min.

MANIFOLD MANIPULATION – STEP 5: LOADING 4 - ELUTE MATRIX

(to remove matrix from columns)

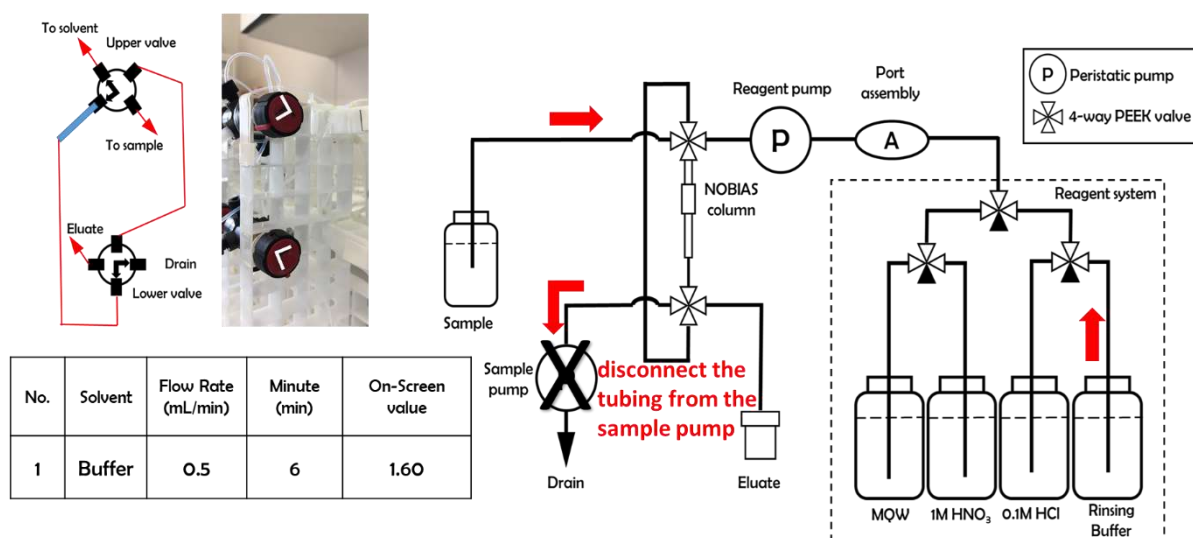


Figure A6 Loading phase -Step 4

A.3 Main phase 3 - Elution

❖ *Elution – 1 (Figure A7): Solution replacement*

This step is applied to replace the buffer solution inside the tubing by a fraction of elution solution. The detail is shown below:

- Set valve configuration as shown on the left of figure A7.
- Set Reagent System position to 1M d-HNO₃ (Elution solution).
- Start Reagent pump, flush solution for 2.5 minutes, at 0.5mL/min.
- Pause the pump

MANIFOLD MANIPULATION – STEP 6: ELUTION-1

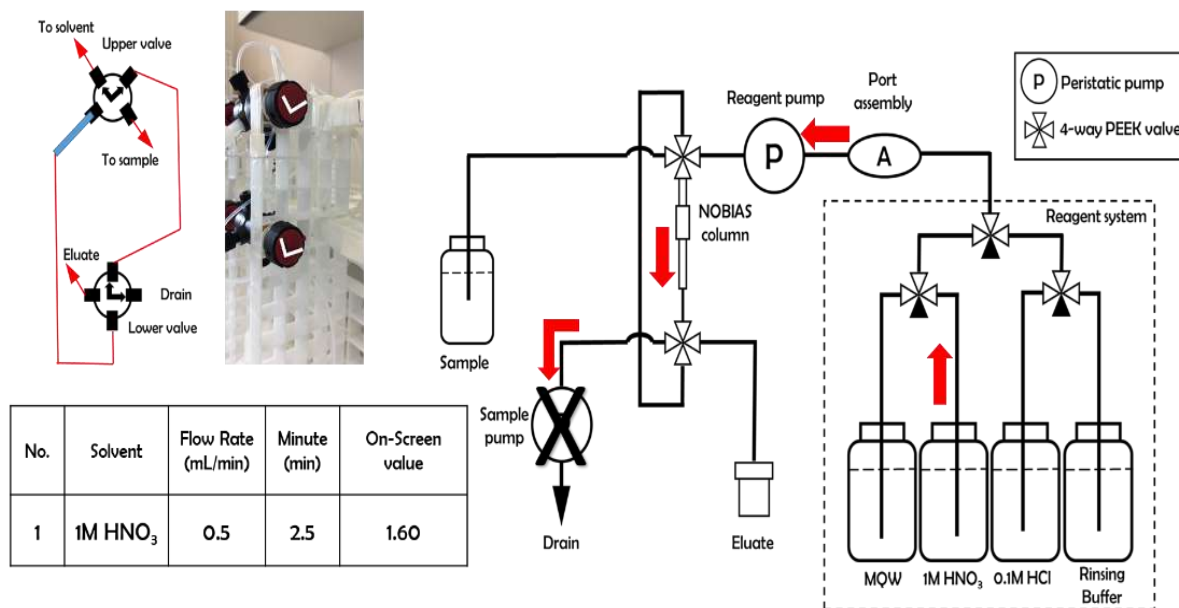


Figure A7 Elution phase - 1

❖ **Elution - 2 (Figure A8): Sample collection**

- Set valve configuration as shown on the left of figure A8.
- Put the preweight Savillex® vial into the collecting point.
- Start Reagent pump for 6 minutes, at 0.5mL/min

MANIFOLD MANIPULATION – STEP 7: ELUTION-2

(to recover sample)

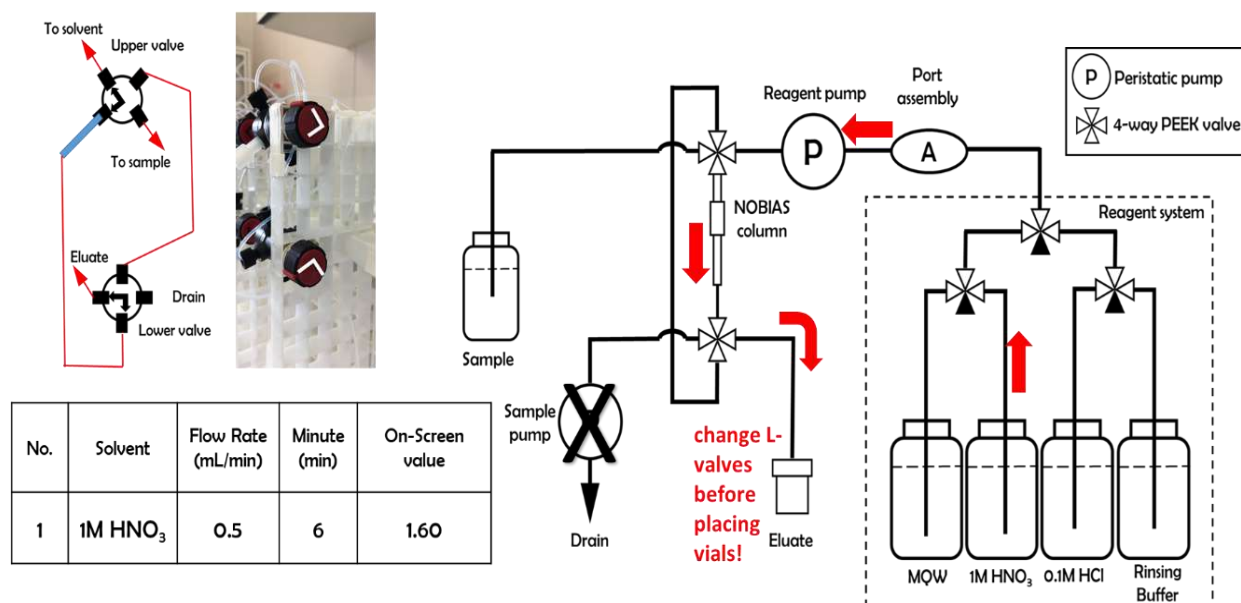


Figure A8 Elution phase - 2

A4 Main phase 4 - Cleaning and storage

In this step, the system is cleaned with various solutions to wipe out any contamination before a new sequence or long time storage.

- Collect sample vials, change with discard beaker.
- Valve configuration remains as previous step.
- Keep flushing the system with an elution solution during 10 minutes, at 1mL/min. Stop the pump.
- Switch reagent system to MQW position, keep pumping for 2.5 minutes, same flow rate.
- Switch to 0.1M d-HCl and flush for 6 minutes at 1mL/min.

MANIFOLD MANIPULATION – STEP 8: CLEANING

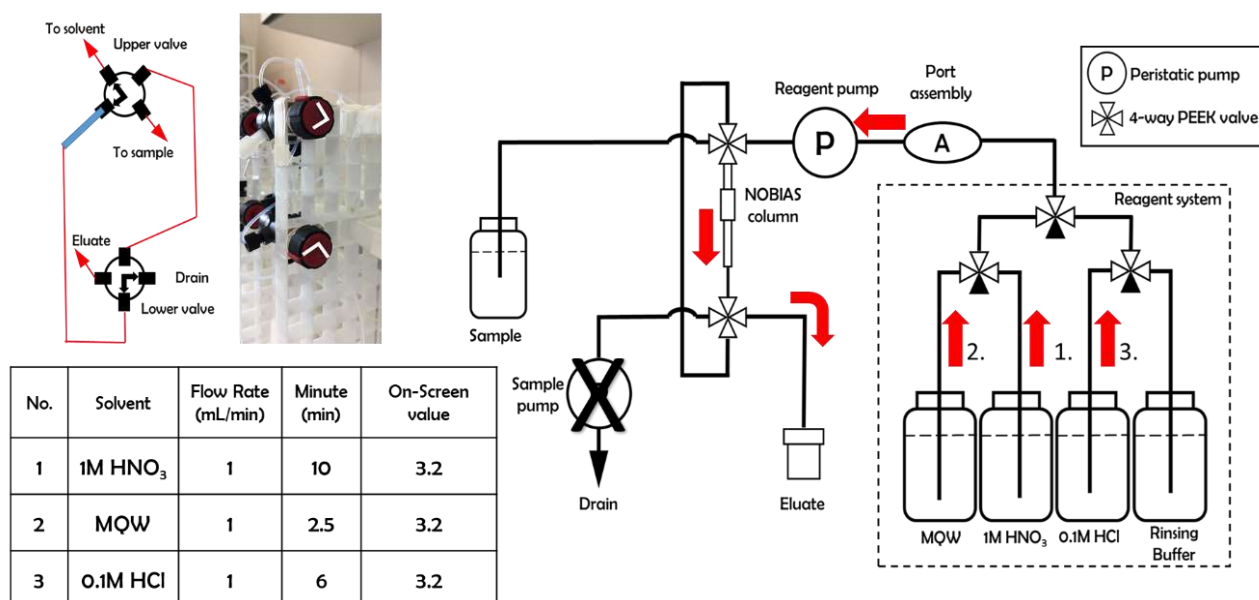
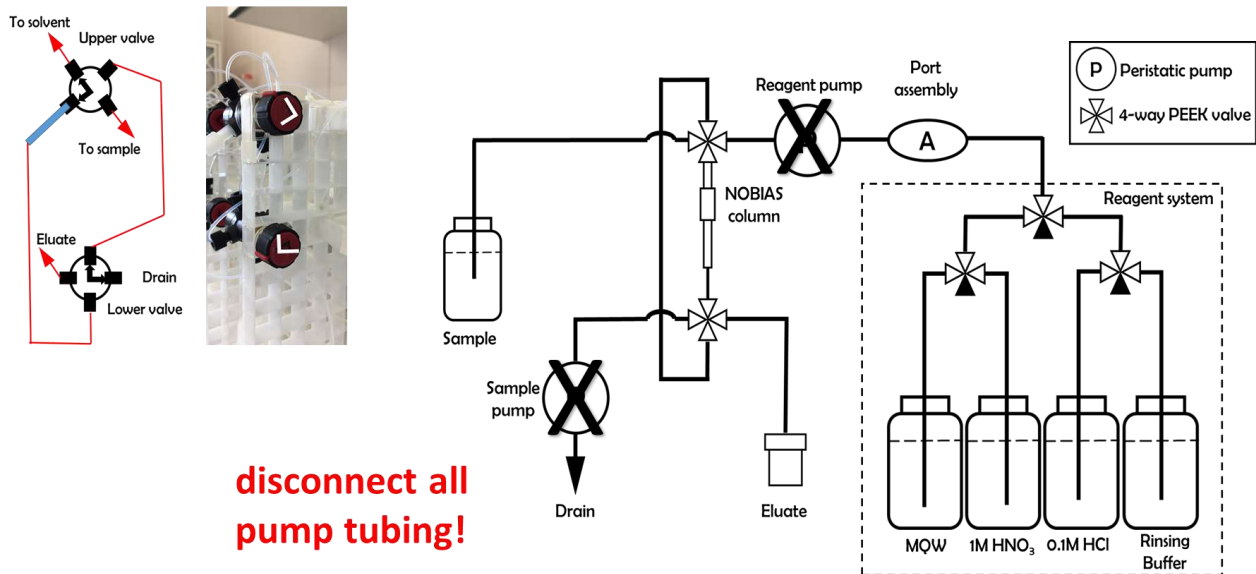


Figure A9 Cleaning phase

Another sequence can start right after the last rinsing solution. In the case of long period storage, set system as in figure A10.

- Turn off the pumps, unlock all the tubing from the rack.
- Set column valve configuration as shown on the left of figure A10.
- Empty all the drains and beakers.

MANIFOLD MANIPULATION – STEP 9: STORAGE



**disconnect all
pump tubing!**

Figure A10 Storage column in 0.1M d-HCl

Chapter 4

Dissolved rare earth element distribution in the Solomon Sea

4.1 Introduction

As explained in the introduction (*Chapter 1*), the main goal of my thesis is to improve our knowledge of the water mass transformation during the transit from the Southwest Pacific Ocean to the Equator. The geochemical modifications occurring in this key area for the global oceanic circulation could condition the structure and elemental composition of the Equatorial Undercurrent which itself is regulating the “High Nutrient Low Chlorophyll” properties of the remote eastern equatorial Pacific. According to the works of Johnson *et al.*, (1994; Lacan and Jeandel, (2001, 2005); Mackey, O’Sullivan and Watson, (2002); Slemons *et al.*, (2010) and Jeandel *et al.*, (2013), the PNG appears to play a major role in enrichment of macro nutrients (e.g dissolved silica) and micro nutrients (e.g. iron) in water flowing along its coast and submarine margin. However, what is precisely happening when water flows across the Solomon Sea remains to be described.

Indeed, despite the well-known role of dissolved Si (dSi) as limiting nutrient for phytoplankton growth in the marine waters (Officer and Ryther, 1980), the dSi oceanic source-sink balance is still not well constrained. Among others the Si flux contribution from lithogenic material to the oceanic dSi cycle is underestimated as recently discussed by Fabre *et al.*, (2019) In the Solomon Sea, the semi-closed topography makes this area potentially important for the dSi lithogenic flux. However, the direct measurement of the silicate fluxes experiences the difficulty of its rapid uptake by the marine biological activity- diatom, which is difficult to unravel. Other tracers, less biologically active, are therefore required to calculate and/or quantify the enrichment at land-ocean interface. REE in general and Nd for its specific property thanks to its isotopic composition could be used as tracers to quantify the water body enrichment due to land-ocean inputs, which then can contribute to estimate the flux of dSi or other nutrients (Jeandel, 2016) . Furthermore, oceanic processes that involve dissolved-particle exchanges can be revealed by the distribution and behavior of the REE within the seawater column. These key questions were discussed in a published article in *Chemical Geology* as summarized below.

i. What is the dREE distribution in the Southwest Pacific Ocean and more specifically in the SS?

In this article, vertical profiles of dREE concentrations were displayed together with corresponding water masses. The dataset was qualified by successful comparisons with preceding results from Zhang and Nozaki, (1996); Grenier *et al.*, (2013). The outstanding similarity between studies highlighted the possible ‘buffering’ feature of Nd concentration at the Vitiaz Strait.

ii. Is there dREE enrichment during the northward transfer of the water masses across the SS? In which layer does it happen? Is it possible to quantify the seawater enrichment with dREE data?

Due to the complex bathymetry and circulation schemes of the Southwest Pacific, revealing dREE enrichment for each water layer was a difficult task. For this purpose, we built a simple box model, named “Pandora box” to describe, for each layer of interest, the incoming and exiting fluxes between the southern entrance of the Solomon Sea and the three northern straits. Under the hypothesis of a negligible influence of diapycnal mixing and considering balanced water transports, the net fluxes of dREE were calculated for the following layers: Upper thermocline water (UTW; $\sigma_\theta = 24\text{--}25.3 \text{ Kg/m}^3$); Lower thermocline water (LTW; $\sigma_\theta = 25.3\text{--}26.9 \text{ Kg/m}^3$); Intermediate water (IW; $\sigma_\theta = 26.9\text{--}27.4 \text{ Kg/m}^3$); Upper Circumpolar Deep Water (UCDW) - upper extent ($\sigma_\theta = 27.4\text{--}26.65 \text{ Kg/m}^3$); Upper Circumpolar Deep Water (UCDW) - lower extent ($\sigma_\theta = 27.65\text{--}27.76 \text{ Kg/m}^3$). Obtained results indicate positive flux suggesting REE inputs for almost all the layers, except in the Intermediate Water. However, only one positive net flux was significant within the uncertainty, calculated using a Monte Carlo statistic method. This flux affects the lower thermocline, suggesting a net gain of dNd in this layer while crossing the Solomon Sea. Note that Grenier, Jeandel and Cravatte, (2014) who studied the water modifications with the same tracers outside of the Solomon Sea also detected a significant enrichment in the lower thermocline, to which we compare our results.

iii. How oceanic processes influence the individual dREE distribution in the water column?

The fractionation of the REEs group by various oceanic processes (particulate scavenging, remineralization, or input of fresh continental weathering) was identified using the normalization of dREE concentrations in seawater to those of a reference, - the Post-Archean Australian Shale or “PAAS”. This led to the construction of dREE patterns. Next, the dREE anomalies (La, Ce, Eu, Yb) calculated using the PAAS normalized data were presented as vertical profiles, providing the following information: i) the dLa shows a station to station correlation with dBa concentrations, which could indicate that barite-barium plays a role in the LREE cycle; however, the observed link between both tracers was not strong enough to conclude further ii) the impact of volcanic particle – basaltic material resulting in a significant Eu anomaly, mostly in the surface waters was also highlighted; iii) lithogenic imprint into seawater was revealed by pronounced Ce anomalies data; iv) the correlation with dSi cycle also assessed by coupling of dHREE profile and Nd_n/Yb_n slope.

This work provides the first observation on the dREE behavior in the water masses during their transit via the Solomon Sea. The box model quantification applied to each layer revealed that the net enrichment was more significant in the lower thermocline. However, although we suspect a basaltic source marked by the Eu anomaly, we are not able to precisely define the enrichment mechanism yet. In the next step, the dNd isotopic composition will be measured as necessary parameter in order to go deeper in assessing the contribution of various oceanic processes into this observed net enrichment. Consequently, this chapter provides the first picture about the dREE distribution and enrichment quantification of water passing through the Coral and Solomon seas.

4.2 Published article: Dissolved rare earth elements distribution in the Solomon Sea



Cycles of trace elements and isotopes in the ocean - GEOTRACES and beyond

Dissolved rare earth elements distribution in the Solomon Sea

V.Q. Pham^{a,c,*}, M. Grenier^a, S. Cravatte^a, S. Michael^b, S. Jacquet^c, M. Belhadj^a, Y. Nachez^a, C. Germaineaud^d, C. Jeandel^a^a LEGOS, Université de Toulouse, (CNRS, UPS, IRD, CNES), Toulouse, France^b School of Oceanography, University of Washington, Seattle, WA 98105, USA^c Aix Marseille Université, CNRS/INSU, Université de Toulon, IRD, Mediterranean Institute of Oceanography (MIO), UM 110, 13288 Marseille, France^d Université Grenoble Alpes, CNRS, IRD, Grenoble-INP, IGE, Grenoble, France^e Department of Water-Environment-Oceanography, University of Science and Technology of Hanoi, 18 Hoang Quoc Viet, Cau Giay, Hanoi, Vietnam

ARTICLE INFO

Editor: Michael E. Böttcher

Keywords:

Solomon Sea

Coral Sea

Dissolved rare Earth Element distribution

Lithogenic inputs

GEOTRACES

ABSTRACT

Trace Elements and Isotopes (TEIs) were measured as part of the GEOTRACES PANDORA cruise (July–August 2012, R/V *Atalante*), among them Rare Earth Elements (REEs) as pertinent tracers of land-ocean inputs and water mass transformations. This work discusses results of 19 dissolved REE (dREE) profiles measured using a trispike method in the Coral Sea and inside and at the exits of the Solomon Sea, a semi-enclosed sea with complex topography and straits. Overall, dREEs –except the insoluble Ce– show nutrient like profiles, i.e. depleted at the surface and enriched at depth. Illustrative Nd concentrations range from ~5 pmol/kg at the surface to > 25 pmol/kg at 5000 m depth. However, local dREE enrichments are observed, mostly in the Straits (Indispensable, Solomon and Vitiav Straits) and along the island coasts. A box model allows calculating and discussing the fate of the dREEs in the different water layers flowing through the Solomon Sea. Finally, subtle variations revealed by La, Ce, Eu anomalies and the normalized light versus heavy REE ratio (expressed as Nd_o/Yb_o) allows the identification of specific mechanisms affecting the distribution of the different dREEs. The positive Eu anomaly observed in the surface layers reflects the basaltic origin of external inputs, consistent with the intensive weathering and/or volcanic activity affecting the surrounding islands. These data also confirm that the distributions of heavy dREEs (like Yb) are better correlated to the dSi concentrations than that of the other REEs.

This article is part of a special issue entitled: “Cycles of trace elements and isotopes in the ocean – GEOTRACES and beyond” - edited by Tim M. Conway, Tristan Horner, Yves Plancherel, and Aridane G. González.

1. Introduction

In the southwest Pacific Ocean, the northern branch of the westward South Equatorial Current is conveyed equatorward by the low-latitude western boundary currents (LLWBCs, Fig. 1). These currents flow through the semi-enclosed Solomon Sea as a final pathway between the subtropical Pacific and the Equator (Fine et al., 1994; Grenier et al., 2014; Ganachaud et al., 2014). The LLWBCs join the equatorial current system, in particular the eastward Equatorial Undercurrent feeding the “cold equatorial tongue” in the eastern equatorial Pacific. The properties of the water masses they transport have thus the potential to impact the equatorial thermocline stratification as well as native ecosystems of the western Pacific with potential downstream effects on the eastern Pacific ones (Slemons et al., 2010; Qin et al., 2016). Hence, the Solomon Sea is a hot spot to study the water modifications when flowing from the Subtropical to the Equatorial region.

The Solomon Sea is surrounded by high and intensively weathered islands (Milliman et al., 1999). Together with its complex topography and hydrography, these characteristics make this area a potential source of trace elements to the waters flowing through it. Preceding studies aimed at characterizing the chemistry of the LLWBCs upstream and downstream of the Solomon Sea (i.e. Grenier et al., 2013, 2014; Slemons et al., 2010; Mackey et al., 2002; Zhang and Nozaki, 1996). However, the Solomon Sea itself has not been documented so far, becoming with time a sort of “missing piece” of the geochemical map of this area.

Two exploratory oceanographic cruises were undertaken in the framework of the SPICE (Southwest Pacific Ocean Circulation and Climate Experiment) and GEOTRACES (www.geotraces.org) programs (Ganachaud et al., 2014; Ganachaud et al., 2017). The Pandora cruise (July–August 2012) documented a large number of hydrographic and biogeochemical parameters in the Coral and Solomon Seas while the

* Corresponding author.

E-mail address: vier.pham@legos.obs-mip.fr (V.Q. Pham).<https://doi.org/10.1016/j.chemgeo.2019.05.012>

Received 31 May 2018; Received in revised form 19 April 2019; Accepted 9 May 2019

Available online 28 May 2019

0009-2541/© 2019 Elsevier B.V. All rights reserved.

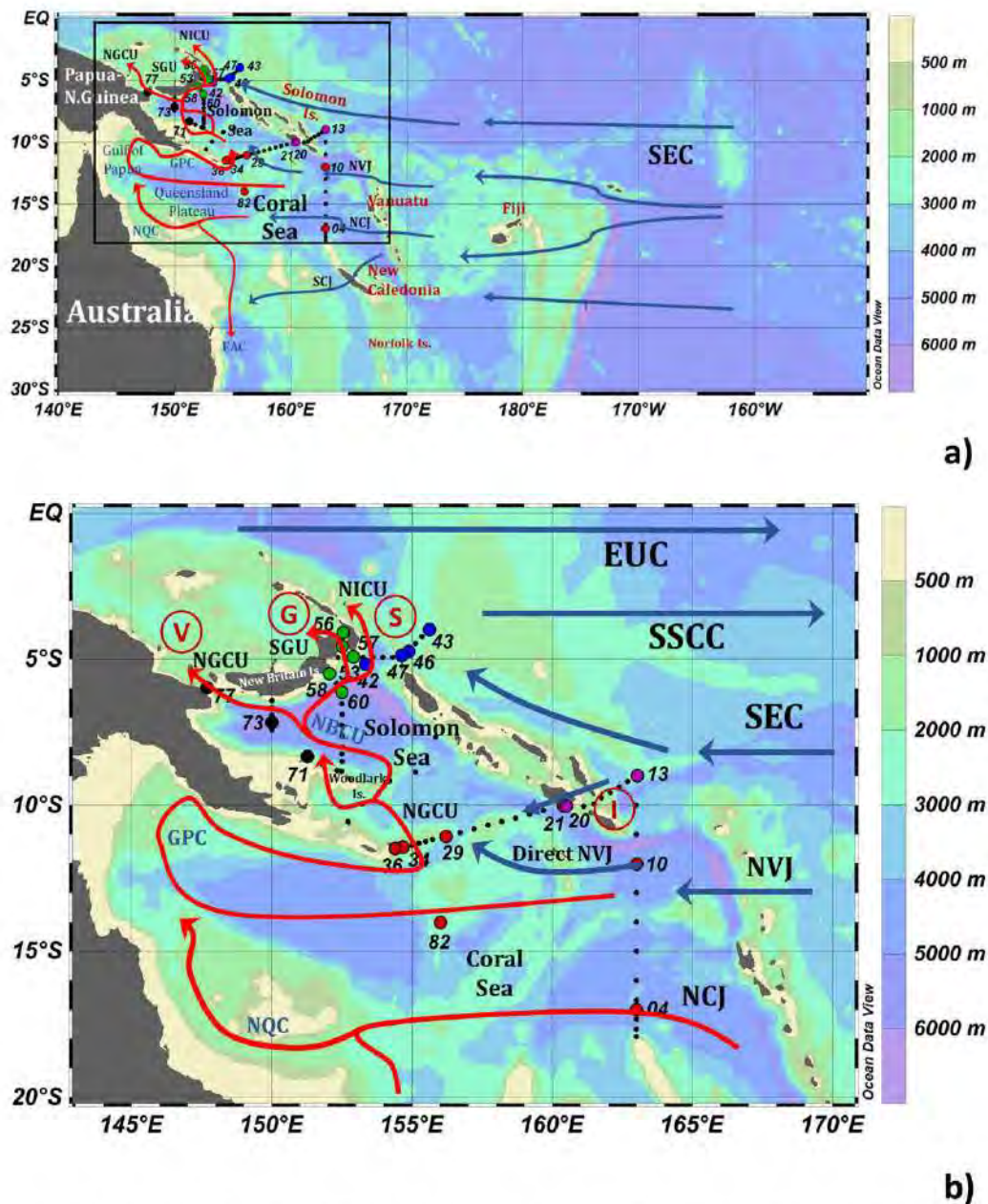


Fig. 1. General map of the studied area (a) and zoom panel in the Coral and Solomon Seas allowing the identification of the sampling locations. Red arrows indicate the LLWBCs (b). The sampling locations are represented by circles and different colors associated with distinct regions. The red circles correspond the Coral Sea and Southern entrance of the Solomon Sea. Samples collected in waters flowing through four straits (Indispensable, Vitiaz, St George's and Solomon), are colored with dark violet, black, green and dark blue, respectively. These color criteria will be kept throughout this work. The main currents flowing in the South Western Pacific Ocean are shown by solid arrow (Grenier et al., 2011, 2013). SEC: South Equatorial Current, NVJ: New Vanuatu Jet, NCJ: New Caledonia Jet, GPC: eastward Gulf of Papua Current, NQC: polarward New Queensland Current, NGCU: New Guinea Coastal Undercurrent, NBCU: New Britain Coastal Undercurrent, NICU: New Ireland Coastal Undercurrent, SSCC: South Subsurface Countercurrent, EUC: Equatorial Undercurrent. The main archipelago and islands are also reported in the map. Straits are identified by a character covered by red circle: Indispensable, Vitiaz, St. George and Solomon Strait also highlighted in the map as V, G and S, correspondingly.

MoorSPICE cruise repeated the hydrographic measurements in March 2014.

Dissolved chemical elements and their isotopes (geochemical tracers) provide key information that allow us to better understand and characterize water mass histories and sources of key nutrient species to the oceans (Crusius et al., 1996; Elrod et al., 2004; Haley et al., 2004; Johnson et al., 2003; Nozaki, 1986). Among the “tracer world”, REEs and isotopic composition of neodymium are used to determine water mass pathways and quantify lithogenic enrichments and scavenging processes that potentially occur along these pathways (Goldstein and

Hemming, 2003; Jeandel et al., 2013; Lacan and Jeandel, 2001; Tachikawa et al., 2003). REEs are a group of 14 elements displaying coherent characteristics from lanthanum (La) to lutetium (Lu). The light REEs (LREEs) refer to the lower atomic number REEs from 57 (La) to 61 (Nd); Samarium (Sm) Europium (Eu) and Gadolinium (Gd) stand for medium REEs (MREEs), while Dysprosium (Dy) to Lutetium are heavy REEs (HREEs). Within this group, the atomic weight increases while the atomic size decreases, yielding chemical fractionation to occur during geochemical processes. In the oceanic environment, most of the previous studies concluded that not only internal processes (i.e.: Akagi,

2013; Akagi et al., 2011; Byrne and Kim, 1990; De Baar et al., 1985a; Lee and Byrne, 1993; Schiff et al., 2015; Tachikawa et al., 1999) but also external ones including suspended sediments in estuaries, groundwater and porewater (i.e.: Nozaki and Alibo, 2003a; Nozaki and Alibo, 2003b; Sholkovitz et al., 1994; Rousseau et al., 2015; Wang and Yamada, 2007; Abbott et al., 2015) could fractionate the REEs. The internal processes can be resumed as dissolved-particulate exchanges over the water column that result from biological uptake-remobilization and/or adsorption-desorption onto reactive particle coatings and/or (co)precipitation-dissolution (Sholkovitz et al., 1994). In addition, dREEs could be released to the open ocean from river discharge, atmospheric dust, hydrothermal plume or exchange at the land-ocean interface, considered as external inputs (Elderfield, 1990; Elderfield and Sholkovitz, 1987; German and Elderfield, 1989; Johannesson et al., 2011; Haley et al., 2004; Sholkovitz and Szymczak, 2000). Clearly identifying these processes and their consequences on the oceanic REE distribution is therefore a key issue.

This work characterizes the dREE concentrations from surface to bottom at 21 stations collected between the entrance of the Coral Sea and the exiting straits of the Solomon Sea. The geochemical data are coupled with the associated hydrological parameters and the water mass transports to permit the discrimination and fine characterization of key processes occurring along the water mass pathways. This strategy allows us to describe and quantify the modification of geochemical parameters during equatorward transit of the waters through the Solomon Sea. Our results are also compared with other geochemical parameters (e.g. Al, Mn) which helps to validate the enrichment of lithogenic origin observed in the Solomon Sea. Relationships between dREEs and nutrient data are also discussed.

Section 2 describes the sampling procedure, sample preservation and analytical protocol while Section 3 presents the hydrological context. Section 4 presents the resulting dREE profiles and their PAAS-normalized patterns. Results are discussed in Section 5. A simple box model allows estimating the dREE Solomon Sea budgets in different density layers, and the water enrichment along their pathways. This section also presents a discussion around the fractionation observed in the REE patterns and the presumed associated mechanisms.

2. Material and methods

2.1. Sample collection

143 seawater samples were collected at 21 stations (19 dREE full profiles, one station with one deep sample and one total dissolved REE profile) during the PANDORA cruise (July–August 2012, onboard R/V *Atalante*). The sampling locations are reported in Fig. 1b. Nine stations (stations 04, 10, 13, 20, 21, 29, 34, 36 and 82) were located in the Coral Sea and at the southern entrance of the Solomon Sea. Stations 04 and 10 were sampled to characterize the North Vanuatu Jet (NVJ) and North Caledonia Jet (NCJ), respectively. Stations 13, 20 and 21 were collected before and after the Indispensable Strait in order to identify potential modifications of the water properties when flowing through this strait. Stations 29, 34 and 36 tried to catch the complex hydrological features at the entrance of the Solomon Sea (Cravatte et al., 2011; Davis et al., 2012; Gernineaud et al., 2016). The remaining 12 stations are located in the “body” of the Solomon Sea as well as in the 3 straits through which waters flow out (i.e. Vitiaz Strait, St George's Channel and Solomon Strait).

Salinity (S), potential temperature (θ) and dissolved oxygen (dO_2) were measured on board using sensors mounted at the base of the rosette. Salinity and oxygen sensors were calibrated and adjusted after the cruise using the measurements of these parameters on discrete samples (Ganachaud et al., 2017). Shipboard and Lowered Acoustic Doppler Current Profiler (L-ADCP) data and other samples for various chemical analyses were also acquired during the cruise for the seawater characterization in trace metals, nutrients and other biological and chemical

parameters. The online cruise report (<http://www.obs-vlfr.fr/proof/php/pandora/xdata1st1.php?xxop=pandora&xxcamp=pandora>) and the synthesis article of Ganachaud et al. (2017) provide more details on the numerous operations conducted in the framework of PANDORA.

Seawater samples dedicated to dREE analysis were collected using 12 L-Niskin bottles mounted on a standard rosette. Aliquots of 500 mL were rapidly filtered through 0.4 μ m pore size, 47 mm diameter SUPOR membranes in the R/V *Atalante* humid laboratory. Filtered water was transferred into pre-cleaned low density polyethylene (LDPE) bottles and immediately acidified to pH ≤ 2 by addition of suprapur 30% HCl. All consumable material was acid-cleaned before the cruise. Note that samples from station 82 and some duplicates from station 73 and 77 were not filtered. Replicate samples were also taken at some stations in order to validate the data, identify particle-dissolved interaction and control the blank of the filtration system (e.g. at station 73).

2.2. Analytical procedure

dREE concentrations were determined using the LEGOS protocol (Lacan and Jeandel, 2001; Tachikawa et al., 1999). Briefly, dREEs were extracted from the seawater aliquot by a co-precipitation with iron hydroxides, followed by purification through ion-exchange column and measured with a High Resolution Inductively Coupled Plasma Mass Spectrometer (HR-ICP-MS). In details, a trispike solution containing ^{150}Nd (97.84%), ^{151}Eu (97.84%), and ^{172}Yb (94.9%) was added to the acidified seawater aliquots of 250 mL or 500 mL. Approximately 2.5 mg of purified FeCl_3 diluted in 0.1 M HCl was then added to the samples. The homogenization was ensured by a continuous shaking of the sample during 24 h and a subsequent 24 h resting state before performing the co-precipitation. Then, the pH was increased to 8 ± 0.5 by adding suprapur NH_4OH yielding the iron hydroxides to co-precipitate the dREEs. The dREE-Fe precipitate was then rinsed and separated from the seawater by successive centrifugations. This rinsing step was repeated up to 7 times and the precipitate was later dissolved in 1 mL of 6 M HCl and then loaded on an anion exchange column packed with 2 mL of AG1-X8 resin, in order to purify the dREE fraction from Fe. dREEs were then eluted from the column using 4 mL of 6 M HCl and evaporated to dryness. Finally, the residue was dissolved again with 5 mL 0.32 M HNO_3 spiked with an internal standard (In–Re, 100 ppt), which is the appropriate solution to measure the concentrations on a sector field Inductively Coupled Plasma Mass Spectrometer (THERMO ELEMENT XR™ ICP-MS).

Recoveries of the whole experiment (including sensitivity variations during the ICP-MS sequence) were precisely determined by comparing the Nd, Eu and Yb concentrations calculated by Isotopic Dilution (ID-CONC) with that measured by external calibration (EXT-CONC). The ratio (EXT-CONC)/(ID-CONC) for these 3 elements were then linearly interpolated and extrapolated to be applied to the remaining dREE concentrations, measured by external calibration only. On the average, recoveries of $> 80\%$ were obtained for the light REEs, and around 77% for the middle and heavy REEs. Our method, based on 2 or 3 spikes followed by interpolation (and extrapolation), was validated by comparing results obtained using 10 spikes on the same seawater samples, either in the framework of T. Rousseau thesis (Rousseau et al., 2013) or in the recent work of M. Behrens (Behrens et al., 2016). During the ICP-MS analysis, the use of a desolvating nebulizer system (ARIDUS II) considerably minimized the oxide interference formation (Chung et al., 2009; Grenier et al., 2013; Pahnke et al., 2012). This is notably effective for the barium oxide formation reduction, which subsequently improves the analytical accuracy for ^{151}Eu and ^{153}Eu .

Replicate measurements were conducted on filtered (4 replicates, station 73, 1650 m) and non-filtered samples (3 replicates at 1650 m of station 73 and 4 replicates at 1200 m of station 82). Filtered light REE (dLREE) concentrations agree within 8% for La, 14% for Ce and 4% for Pr and Nd; filtered middle (dMREE) and heavy (dHREE) concentrations agree within 8% for Sm, 11% for Eu and $< 4\%$ for the remaining REEs.

Non-filtered concentrations agree within < 4% for all the LREEs (including Ce) and 7% for MREEs and HREEs.

The average chemical blank values were established on 20 measurements. Blank levels represent < 2% of the LREE signals and < 0.7% for MREE and HREE ones. Due to the very low Ce concentrations in our samples, the dCe blanks represent $14 \pm 9\%$ of the sample signal. In addition, the blank of our on-board filtration system was checked by filtering twice the same samples. No noticeable variation of concentration was observed, assessing the cleanliness of our systems. Finally, our full dREE analytical procedure was validated by our successful participation to two GEOTRACES intercalibration exercises (Behrens et al., 2016; van de Fliedert et al., 2012).

Together with dREE analysis, the dissolved Ba were also measured following this protocol: 15 mL of unfiltered seawater were collected in pre-cleaned polypropylene bottles (rinsed three times with the same seawater sample), acidified with 15 μ L of HCl (10 M, Optima grade) and kept at room temperature for later analysis. Dissolved Ba concentrations were measured using an isotope dilution (ID) method (Freydier et al., 1995; Klinkhammer and Chan, 1990) by high resolution inductively coupled plasma-mass spectrometry (HR-ICP-MS), operated at low resolution mode. This method was adapted to a Thermo Finnigan Element XR[™] instrument (MIO, Marseille). The dissolved Ba measurements presented here are the sum of dissolved Ba and a very small fraction (generally < 1% of total Ba) that is generated from the particulate Ba pool as a result of the acidification (Jacquet et al., 2005). For the sake of simplicity, we use the term of dissolved Ba and dBa data are reported in the Table B of Supplementary material. Samples (0.5 mL) were spiked with 300 μ L of a ¹³⁵Ba-enriched solution (93% ¹³⁵Ba; 95 nmol/kg) and diluted with 15 mL of acidified (2% HNO₃, 14 M, Optima grade) Milli-Q grade water (Millipore). The amounts of sample, spike and dilution water were assessed by weighing. Reproducibility of this method is 1.5% (1 RSD) as tested on repeated preparations of the reference solution SLRS-5 (NRC-CNRC river water reference material for trace metals; 101.9 ± 3.6 nmol/kg). The limit of detection, calculated as three times the standard deviation of the procedural blank, is 0.09 nmol/kg.

3. Hydrological context

Coral and Solomon Sea hydrological properties have been the subject of several surveys since the early 1960s. Water mass properties were discussed in miscellaneous works since then (e.g. Tsuchiya, 1981; Tsuchiya et al., 1989; Qu and Lindstrom, 2002; Grenier et al., 2013; Kessler and Cravatte, 2013; Ganachaud et al., 2014). Germineaud et al. (2016) presented a detailed description of the currents and water mass properties from the surface down to 1000 m depth based on both the PANDORA (2012) and MoorSPICE (2014) cruise data. The description proposed here is mostly based on this last work together with the thorough description given in Southwest Pacific currents conducted by Grenier et al. (2011, 2013, 2014). The water mass nomenclatures vary among authors; the names used in this study follow those proposed by Tomczak and Hao (1989) and adopted by Grenier et al. (2013) in order to avoid any confusion when describing the water masses, especially in the layers characterizing the thermocline.

The general circulation scheme, current names and sampling details of the different stations used in this study are given in Fig. 1. Fig. 2 proposes a compilation of hydrological property plots observed at the different stations, together with the identification of the main water masses sampled during the cruise. The last column of Table 1 recalls the water masses corresponding to the collected seawater samples.

Water properties in the Southwest Pacific can be traced from the Coral Sea to the Solomon Sea, in part through the Low Latitude Western Boundary Currents (LLWBCs) flowing toward the Equator (Fig. 1). The LLWBCs are initially fed by the westward South Equatorial Current (SEC; Qu and Lindstrom, 2002; Tsuchiya et al., 1989), dividing into several zonal currents when encountering islands in the Coral Sea.

These zonal currents -some of them extending as deep as 1000 m-transport several water masses that we choose to describe here following increasing density.

3.1. Thermocline waters

3.1.1. Upper thermocline: tropical and equatorial waters

In the Coral and Solomon Seas, the upper thermocline is made of salty South Pacific Tropical Waters (SPTW) ($-\sigma_\theta = 24.3\text{--}25.3$ kg/m³). This tropical water can be divided into two main branches.

The northern branch of the SPTW is called the South Pacific Equatorial Water (SPEW) and enters the Coral Sea north of the Vanuatu Archipelago, transported by the North Vanuatu Jet (NVJ) (Kessler and Cravatte, 2013; Tomczak and Godfrey, 2003; Tomczak and Hao, 1989; Tsuchiya et al., 1989). The SPEW originates from the subtropical central South Pacific ($\sim 20^\circ\text{S}$, 110°W), characterized by high evaporation and a maximum in sea surface salinity (see Fig. 1 of Grenier et al., 2013). The SPEW is thus marked by a maximum in salinity ($-\text{S} = 36.0$) at $-\sigma_\theta = 24.5$ kg/m³ (Kessler, 1999; Qu and Lindstrom, 2002) and relative high oxygen (~ 135 μ mol/kg; Grenier et al., 2013). It enters the Solomon Sea both through a direct pathway in the middle of the southern entrance, and through the NGCU flowing along the coast. During Pandora, SPEW was well identified at station 10 (Fig. 2).

The southern branch of the SPTW enters the Coral Sea mainly south of the Vanuatu Archipelago, conveyed by the North Caledonian Jet (NCJ; Ganachaud et al., 2014; Gasparin et al., 2011; Germineaud et al., 2016; Grenier et al., 2013). At the entrance of the Coral Sea, this water mass is slightly denser ($-\sigma_\theta = 24.8$ kg/m³), less saline ($\text{S} \sim 35.6$) and richer in oxygen (~ 165 μ mol/kg¹) than those of the northern branch (see station 04, Fig. 2). It enters the Solomon Sea through the NGCU.

Inside the Solomon Sea, the NGCU splits south of Woodlark Island and then reemerges at its northern side, to finally bifurcate again into two branches south of New Britain Island. The first branch flows westward toward the Bismarck Sea through Vitiaz Strait while the second one is conveyed eastward by the New Britain Coastal Undercurrent. It exits the Solomon Sea northward by the St George's Undercurrent (SGU) and the New Ireland Coastal Undercurrent (NICU) through St George's Channel and Solomon Strait, respectively (Cravatte et al., 2011; Ganachaud et al., 2014; Ganachaud et al., 2017; Germineaud et al., 2016). Since the SPTW in the Solomon Sea results from the mixing between two water masses of minor differences which are referred above, its characteristics are fairly high oxygen content (140–145 μ mol/kg¹) and high salinity level ($-\text{S} = 35.7$, see stations 34, 36, 42, 43, 57, 60, 71, 73 and 77 in Fig. 2).

3.1.2. Lower thermocline: central water and mode water

Lying just underneath the upper thermocline water, the Western South Pacific Central Water (WSPCW), displays very loose stratification at about 300 m depth (Grenier et al., 2014; Qu et al., 2008; Tsuchiya, 1981). WSPCW is described by potential density centered at 26.4 kg/m³ and high salinity due to its origin, north of New Zealand (Tomczak and Hao, 1989). Rich in oxygen (mean O₂ = 160 kg/m³), the WSPCW is conveyed into the Coral Sea in its southern part, through the deep NCJ (Gasparin et al., 2011; Sokolov and Rintoul, 2000; Tomczak and Godfrey, 2003; Tsuchiya et al., 1989). While crossing the Solomon Sea, this water mass may become depleted in oxygen by mixing with water originating from the southeastern Pacific Ocean (Kessler and Cravatte, 2013).

Below the WSPCW flows a mode water. The Subantarctic Mode Water (SAMW; $-\sigma_\theta = 26.5\text{--}27$ kg/m³; no salinity or oxygen extremum) enters the Coral and Solomon Seas from the south (Grenier et al., 2013; McCartney, 1977). It originates from the Southern Ocean by subduction north of the Antarctic Circumpolar Current (Hanawa and Talley, 2001). This water mass is centered on $-\sigma_\theta = 27$ kg/m³ and is characterized by a low salinity (~ 34.5) and high oxygen content (~ 175 kg/m³) because of its origin (Qu et al., 2009). In the Coral and Solomon Seas, the SAMW

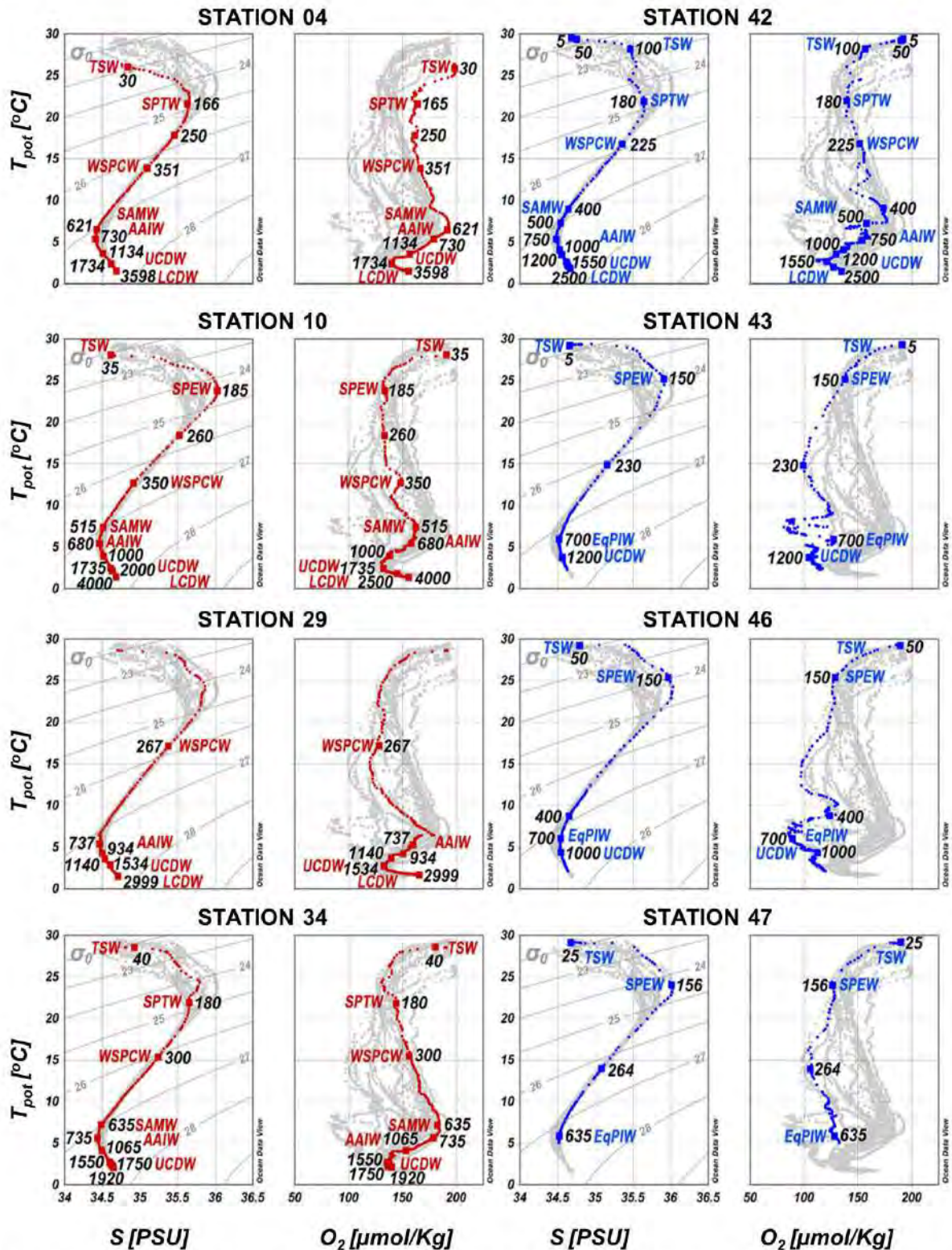


Fig. 2. Potential temperature (θ) versus salinity (S; right) and potential temperature (θ) versus dissolved oxygen (O_2 ; left) plots for the stations. The curve colors correspond to the different locations denoted in Fig. 1. The grey curves are representing the same properties at all the hydrographic stations sampled as part of PANDORA. In the left plots, potential density anomaly contours are shown as solid grey lines. Each depth sampled for dissolved REE measurement is identified by a rectangle and its value (m). All the data characterizing the stations represented here are provided in Table 1. The water masses at the sampling depth are also highlighted by their notation: TSW: Tropical Surface Water, SPTW: South Pacific Tropical Water, SPEW: South Pacific Equatorial Water, WSPCW: Western South Pacific Central Water, SAMW: Subantarctic Mode Water, AAIW: Antarctic Intermediate Water, EqPIW: Equatorial Pacific Intermediate Water, UCDW and LCDW: Upper and Lower Circumpolar Deep Water.

Table 1

Station number and locations, depths, hydrological properties, dREE anomalies of the analyzed samples; the corresponding water masses are identified.

Depth	Salinity	Pot. temp	O ₂	Pot. dens	La/La*	Ce/Ce*	Eu/Eu*	Yb/Yb*	(Nd/Yb) _d	Water mass
(m)	(PSU)	[°C]	($\mu\text{mol/kg}$)	(σ_θ) (kg/m ³)						
Station 004 (July 01, 2012; 17° 0' 10.8" S; 162° 59' 45.6" E; depth: 4680 m)										
30	34.840	25.931	199	22.94	2.08	0.60	1.21	0.50	0.25	TSW
166	35.631	21.533	164	24.83	1.81	0.51	1.12	0.50	0.22	SPTW
250	35.462	17.831	161	25.67	2.31	0.46	1.11	0.55	0.21	
351	35.095	13.923	167	26.28	2.04	0.23	1.09	0.59	0.17	WSPCW
621	34.426	6.496	192	27.04	2.11	0.12	1.00	0.66	0.14	SAMW
730	34.415	5.375	179	27.17	2.21	0.10	1.11	0.70	0.13	AAIW
1134	34.510	3.573	157	27.44	2.20	0.41	1.05	0.74	0.13	
1734	34.620	2.410	140	27.64	–	–	–	–	–	UCDW
3598	34.687	1.546	156	27.76	5.48	0.09	1.12	0.77	0.22	LCDW
Station 010 (July 03, 2012; 12° 0' 0" S; 162° 59' 56.4" E; depth: 5092 m)										
35	34.616	28.053	191	22.09	2.13	0.51	1.21	0.50	0.26	TSW
185	36.029	24.496	134	24.50	–	–	–	–	–	SPEW
260	35.523	18.403	133	25.58	2.12	0.29	1.21	0.54	0.20	
350	34.918	12.675	148	26.40	2.68	0.27	1.05	0.60	0.18	WSPCW
515	34.510	7.400	163	26.98	–	–	–	–	–	SAMW
680	34.458	5.395	158	27.20	2.61	0.10	0.95	0.72	0.12	AAIW
1000	34.520	3.960	139	27.41	–	–	–	–	–	
1735	34.613	2.435	133	27.63	2.62	0.14	1.12	0.77	0.13	UCDW
2500	34.669	1.777	145	27.73	2.26	0.07	1.13	0.75	0.17	LCDW
4000	34.685	1.443	153	27.77	2.14	0.13	1.08	0.77	0.20	
Station 013 (July 04, 2012; 9° 0' 10.8" S; 162° 59' 56.4" E; depth: 3853 m)										
5	34.651	29.182	191	21.74	1.74	0.61	1.14	0.45	0.34	TSW
40	34.675	29.157	191	21.77	1.77	0.54	1.05	0.44	0.29	
160	35.830	24.121	129	24.24	3.32	0.74	1.26	0.53	0.19	SPEW
300	35.188	15.244	106	26.07	2.54	0.26	0.96	0.57	0.18	–
600	34.515	6.128	138	27.16	3.52	0.10	1.08	0.72	0.12	EqPIW
685	34.503	5.528	138	27.22	2.89	0.14	1.18	0.71	0.12	
1335	34.574	3.108	126	27.54	4.01	0.15	1.02	0.75	0.11	UCDW
1535	34.595	2.709	129	27.60	4.86	0.10	1.11	0.78	0.12	
2000	34.640	2.023	133	27.69	3.19	0.11	1.21	0.80	0.14	
Station 020 (July 06, 2012; 9° 59' 56.4" S; 160° 25' 1.2" E; depth: 2910 m)										
25	34.832	28.896	189	21.97	2.09	0.56	1.21	0.56	0.27	TSW
190	35.822	22.620	127	24.67	–	–	–	–	–	SPEW
600	34.485	6.223	162	27.12	3.49	0.19	1.02	0.71	0.13	AAIW
900	34.490	4.787	151	27.30	3.53	0.12	1.08	0.72	0.12	
1600	34.599	2.720	133	27.60	–	–	–	–	–	UCDW
Station 021 (July 07, 2012; 10° 0' 46.8" S; 160° 21' 25.2" E; depth: 3342 m)										
250	35.388	17.226	127	25.76	3.05	0.35	1.08	0.53	0.20	WSPCW
400	34.675	9.036	140	26.86	3.24	0.19	1.07	0.69	0.13	SAMW
550	34.491	6.382	163	27.10	3.06	0.11	1.06	0.71	0.12	AAIW
2115	34.644	2.075	139	27.69	3.48	0.10	1.20	0.80	0.16	UCDW
2625	34.677	1.787	150	27.74	3.52	0.09	1.14	0.79	0.15	LCDW
3280	34.700	1.614	165	27.77	3.07	0.09	1.14	0.76	0.18	
Station 029 (July 09, 2012; 11° 3' 39.6" S; 156° 12' 54" E; depth: 3856 m)										
267	35.378	17.122	128	25.78	2.49	0.35	1.10	0.53	0.20	–
737	34.465	5.346	160	27.21	3.32	0.18	1.07	0.73	0.12	AAIW
934	34.497	4.281	150	27.36	3.29	0.28	1.08	0.74	0.13	
1140	34.535	3.704	139	27.45	3.37	0.16	1.16	0.74	0.12	
1534	34.593	2.817	133	27.59	3.65	0.08	1.16	0.76	0.13	UCDW
2999	34.699	1.687	166	27.77	3.02	0.10	1.14	0.77	0.17	LCDW
Station 034 (July 10, 2012; 11° 27' 7.2" S; 154° 39' 54" E; depth: 2005 m)										
40	34.932	28.522	181	22.17	2.47	0.54	1.21	0.55	0.23	TSW
180	35.656	21.834	144	24.77	3.76	0.50	1.21	0.57	0.20	SPTW
300	35.247	15.416	156	26.08	2.46	0.30	1.14	0.60	0.18	WSPCW
635	34.485	7.121	183	27.00	2.19	0.23	1.01	0.67	0.14	SAMW
735	34.439	5.649	179	27.16	1.94	0.39	1.04	0.69	0.15	AAIW
1065	34.493	4.140	154	27.37	3.23	0.24	1.05	0.71	0.13	
1550	34.600	2.730	136	27.60	3.02	0.15	1.05	0.73	0.14	UCDW
1665	34.613	2.558	137	27.62	3.42	0.09	1.11	0.74	0.14	
1750	34.625	2.385	136	27.65	2.88	0.10	1.11	0.74	0.15	
1920	34.645	2.140	140	27.69	–	–	–	–	–	
Station 036 (July 11, 2012; 11° 30' 7.2" S; 154° 23' 24" E; depth: 1168 m)										
24	34.489	27.756	195	22.09	1.52	0.54	1.25	0.59	0.34	TSW
101	35.431	24.271	163	23.89	2.31	0.56	1.18	0.55	0.22	
159	35.609	22.290	141	24.60	2.28	0.50	1.22	0.54	0.22	SPTW
180	35.639	21.074	144	24.96	2.60	0.56	1.11	0.55	0.22	
401	34.943	12.203	167	26.51	2.37	0.23	1.08	0.63	0.16	WSPCW
699	34.460	6.285	182	27.09	2.75	0.12	0.98	0.69	0.13	AAIW

(continued on next page)

Table 1 (continued)

Depth	Salinity	Pot. temp	O ₂	Pot. dens	La/La ^c	Ce/Ce ^c	Eu/Eu ^c	Yb/Yb ^c	(Nd/Yb) _n	Water mass
(m)	(PSU)	[°C]	(μmol/kg)	(σ _θ) (kg/m ³)						
901	34.458	5.126	170	27.24	3.03	0.12	1.07	0.71	0.12	
Station 042 (July 15, 2012; 5° 8' 42" S; 153° 17' 24" E; depth: 3081 m)										
5	34.691	29.381	192	21.71	2.50	0.61	1.26	0.50	0.29	TSW
50	34.753	29.380	192	21.75	–	–	–	–	–	
100	35.464	28.210	157	22.68	–	–	–	–	–	
180	35.648	21.971	140	24.72	2.62	0.50	1.21	0.55	0.20	SPTW
225	35.353	16.762	152	25.85	2.99	0.26	0.79	0.57	0.17	WSPCW
400	34.644	9.024	174	26.84	2.99	0.19	0.98	0.67	0.14	SAMW
500	34.538	7.266	158	27.02	2.79	0.16	1.03	0.70	0.13	
750	34.484	5.316	154	27.23	3.24	0.15	1.06	0.73	0.12	AAIW
1000	34.526	4.032	137	27.41	3.01	0.14	1.07	0.73	0.13	
1200	34.557	3.501	130	27.49	3.31	0.18	1.22	0.77	0.13	
1550	34.610	2.607	123	27.62	3.15	0.22	1.22	0.78	0.15	UCDW
1750	34.621	2.419	124	27.64	3.99	0.20	1.16	0.78	0.15	
2000	34.639	2.132	126	27.68	3.03	0.13	1.22	0.76	0.16	
2500	34.660	1.782	133	27.73	3.02	0.15	1.20	0.78	0.18	LGDW
Station 043 (July 17, 2012; 3° 59' 52.8" S; 155° 35' 38.4" E; depth: 1925 m)										
5	34.659	29.274	191	21.72	2.34	0.57	1.13	0.44	0.29	TSW
150	35.914	25.138	138	23.99	2.65	0.49	1.12	0.55	0.20	SPEW
230	35.161	14.819	99	26.14	[6.85]	[1.32]	[1.19]	[0.64]	[0.17]	–
700	34.513	5.914	128	27.18	3.35	0.16	1.24	0.72	0.13	EqPIW
1200	34.564	3.737	105	27.47	3.31	0.13	1.15	0.79	0.12	UCDW
Station 046 (July 18, 2012; 4° 42' 0" S; 154° 52' 48" E; depth: 3117 m)										
50	34.794	29.190	190	21.85	2.67	0.49	1.19	0.42	0.30	TSW
150	35.974	25.365	129	23.97	3.29	0.36	1.11	0.52	0.18	SPEW
400	34.649	8.724	124	26.89	3.52	0.26	1.11	0.68	0.14	–
700	34.542	6.028	89	27.19	3.34	0.09	1.10	0.72	0.12	EqPIW
1000	34.540	4.326	112	27.39	3.43	0.15	1.07	0.75	0.13	UCDW
Station 047 (July 18, 2012; 4° 56' 2.4" S; 154° 38' 52.8" E; depth: 1004 m)										
25	34.670	29.108	190	21.78	1.99	0.50	1.27	0.51	0.30	TSW
156	36.017	24.025	126	24.41	3.80	0.63	0.99	0.51	0.18	SPEW
264	35.082	13.952	106	26.27	2.71	0.22	1.05	0.63	0.16	–
635	34.522	5.856	129	27.20	2.92	0.21	1.09	0.72	0.13	EqPIW
Station 053 (July 19, 2012; 4° 54' 18" S; 152° 52' 12" E; depth: 733 m)										
25	34.879	28.959	189	21.99	2.55	0.57	1.27	0.57	0.26	TSW
149	35.610	21.864	142	24.72	3.30	0.89	1.12	0.55	0.23	SPTW
335	34.977	12.632	161	26.45	2.57	0.21	1.10	0.65	0.16	WSPCW
719	34.480	5.424	158	27.22	3.17	0.12	1.07	0.71	0.13	AAIW
Station 056 (July 20, 2012; 4° 4' 37.2" S; 152° 32' 20.4" E; depth: 1580 m)										
1582	34.599	2.818	125	27.59	3.20	0.18	1.08	0.72	0.15	UCDW
Station 057 (July 20, 2012; 4° 34' 12" S; 152° 31' 22.8" E; depth: 2552 m)										
25	34.767	28.952	192	21.91	3.16	0.59	1.39	0.55	0.27	TSW
150	35.583	23.624	139	24.20	2.52	0.52	1.19	0.55	0.21	SPTW
250	35.268	15.802	152	26.00	2.45	0.32	1.09	0.58	0.18	WSPCW
450	34.650	8.974	171	26.85	2.94	0.16	1.02	0.71	0.14	
580	34.509	7.083	177	27.02	2.85	0.22	1.06	0.69	0.13	SAMW
850	34.503	4.623	143	27.33	3.53	0.14	1.15	0.76	0.12	AAIW
1302	34.565	3.374	129	27.51	4.17	0.18	1.18	0.77	0.13	UCDW
1650	34.611	2.610	124	27.62	–	–	–	–	–	
2201	34.654	1.992	135	27.71	3.77	0.13	1.20	0.79	0.17	LCDW
Station 058 (July 21, 2012; 5° 30' 10.8" S; 152° 5' 52.8" E; depth: 1142 m)										
215	35.500	18.602	135	25.51	2.74	0.40	1.16	0.56	0.20	WSPCW
1100	34.547	3.675	133	27.47	3.77	0.20	1.07	0.76	0.13	UCDW
Station 060 (July 22, 2012; 6° 10' 1.2" S; 152° 29' 49.2" E; depth: 5609 m)										
35	34.737	28.022	193	22.19	2.03	0.59	1.30	0.54	0.30	TSW
180	35.733	22.267	135	24.70	2.40	0.44	1.18	0.52	0.22	SPTW
250	35.325	16.605	124	25.86	3.65	0.55	1.22	0.58	0.19	WSPCW
480	34.531	7.193	173	27.03	2.97	0.25	1.08	0.72	0.13	SAMW
1000	34.530	3.930	138	27.43	3.68	0.19	1.20	0.74	0.13	AAIW
1600	34.611	2.604	124	27.62	3.08	0.22	1.18	0.79	0.15	UCDW
1800	34.631	2.263	125	27.67	3.11	0.29	1.16	0.77	0.17	
2541	34.661	1.724	132	27.73	3.21	0.10	1.28	0.81	0.19	LCDW
3250	34.692	1.673	155	27.76	2.81	0.14	1.31	0.83	0.22	
4000	34.696	1.665	158	27.77	2.62	0.13	1.28	0.81	0.23	
4500	34.696	1.660	160	27.77	2.31	0.16	1.34	0.79	0.23	
4750	34.697	1.656	160	27.77	2.26	0.27	1.29	0.75	0.25	
5000	34.697	1.653	161	27.77	3.43	0.15	1.29	0.72	0.22	
5603	34.697	1.649	162	27.77	2.30	0.12	1.19	0.75	0.24	

(continued on next page)

Table 1 (continued)

Depth	Salinity	Pot. temp	O ₂	Pot. dens	La/La ⁻	Ce/Ce ⁺	Eu/Eu ⁺	Yb/Yb ⁺	(Nd/Yb) _n	Water mass
(m)	(PSU)	[°C]	(μmol/kg)	(σ _θ) (kg/m ³)						
Station 071 (July 25, 2012; 8° 19' 55.2" S; 151° 17' 27.6" E; depth: 1563 m)										
50	34.797	27.552	192	22.39	2.14	0.46	1.26	0.52	0.24	TSW
160	35.659	22.424	138	24.60	5.68	1.37	1.09	0.52	0.22	SPTW
400	34.977	12.552	165	26.47	4.17	0.67	1.08	0.63	0.17	WSPCW
600	34.493	6.699	178	27.06	3.00	0.17	1.00	0.71	0.13	AAIW
1100	34.522	4.051	143	27.41	5.89	0.36	1.17	0.74	0.13	UCDW
Station 073 (July 26, 2012; 7° 9' 57.6" S; 149° 59' 56.4" E; depth: 5253 m)										
50	35.058	27.325	171	22.66	2.40	0.55	1.22	0.55	0.24	TSW
170	35.586	21.658	141	24.76	2.40	0.44	1.33	0.55	0.21	SPTW
200	35.602	21.191	140	24.90	2.85	0.36	1.15	0.53	0.19	
700	34.474	5.882	169	27.16	3.24	0.11	1.12	0.71	0.12	AAIW
1650	34.609	2.604	123	27.62	3.35	0.13	1.18	0.77	0.14	UCDW
Station 077 (July 28, 2012; 5° 57' 3.6" S; 147° 39' 36" E; depth: 1045 m)										
25	34.767	27.606	191	22.35	4.19	0.53	1.24	0.57	0.26	TSW
180	35.609	21.401	140	24.85	2.52	0.48	1.12	0.53	0.21	SPTW
501	34.572	8.016	178	26.94	2.43	0.37	1.09	0.71	0.16	SAMW
701	34.477	5.536	159	27.20	3.00	0.13	1.05	0.71	0.13	AAIW
983	34.505	4.473	145	27.35	3.73	0.19	1.13	0.74	0.13	
Station 082- non-filtrated (August 03, 2012; 13° 59' 49.2" S; 156° 0' 25.2" E; depth: 2586 m)										
25	34.927	26.195	197	22.92	2.68	0.72	1.40	0.53	0.26	TSW
180	35.789	22.612	129	24.65	3.06	0.82	1.04	0.53	0.21	SPTW
700	34.469	6.035	165	27.13	2.55	0.32	1.00	0.67	0.14	AAIW
800	34.451	5.083	163	27.23	2.65	0.29	1.02	0.68	0.13	
1000	34.498	4.114	151	27.38	3.14	0.92	1.04	0.71	0.13	
1200	34.539	3.454	145	27.48	3.60	0.44	1.05	0.74	0.12	UCDW
1350	34.565	3.159	140	27.53	3.45	0.17	0.98	0.73	0.13	
2000	34.636	2.226	141	27.67	2.29	0.37	1.18	0.77	0.14	

keeps its original characteristics and contributes to the formation of 13°C Water (Qu et al., 2009).

3.2. Intermediate waters

The Antarctic Intermediate Water (AAIW; $\sigma_{\theta} \sim 27.2 \text{ kg/m}^3$) is identified in the southern part of the studied region by a salinity minimum ($-S = 34.3\text{--}34.5$) and an oxygen maximum ($\sim O_2 = 200\text{--}300 \mu\text{mol/kg}$, Qu and Lindstrom, 2004). It enters the Solomon Sea via the NGCU (Bostock et al., 2010; Germaineaud et al., 2016; Qu and Lindstrom, 2004; Tomczak and Godfrey, 2003). From the Coral Sea to the equator, the AAIW becomes slightly denser and less oxygenated ($-\sigma_{\theta} = 27.26 \text{ kg/m}^3$; $O_2 = 160\text{--}190 \mu\text{mol/kg}$) due to remineralization of organic material settling from the surface and to diapycnal mixing with lower oxygenated waters.

The Equatorial Pacific Intermediate Water (EqPIW; $-\sigma_{\theta} = 27.3 \text{ kg/m}^3$), originally formed from a combination of AAIW and upwelled Pacific Deep Water (Bostock et al., 2010), is also identified. It is suggested that part of this water mass enters the Solomon Sea from the north-east through Solomon Strait (Germaineaud et al., 2016) and mixes then with AAIW as proposed in Fig. 1 of Bostock et al. (2010). The distinct characteristics of this water mass is a salinity higher than that of AAIW ($-S = 34.5\text{--}34.6$) and a significantly lower oxygen concentration ($\sim O_2 = 75\text{--}125 \mu\text{mol/kg}$). It is found at a density of 27 kg/m^3 at station 43 and 46. Moreover, the oxygen plot of station 43 shows that EqPIW and AAIW form interleaving near 700 m depth (see Fig. 2).

3.3. Deep and bottom waters

The deep and bottom waters within the Coral and Solomon Seas have been poorly documented since the first observations summarized in Reid (1986, 1997) and their pathways and fates are not clearly understood. They are strongly constrained by the topography (Johnson and Toole, 1993; Kawabe and Fujio, 2010; Roemmich et al., 1996; Tsimplis et al., 1998). Their pathways, origins and properties are the

topic of an ongoing work.

The Upper Circumpolar Deep Water (UCDW) is observed between 1000 m and around 3500 m in the studied area. This water mass has been depleted in oxygen since its origin in the Antarctic Circumpolar Current (ACC; Reid, 1986; Talley, 2007; Wijffels et al., 2001). In this study, the UCDW is characterized by a relatively high salinity and a low oxygen content with a pronounced minimum ($-S = 34.6$, $\sim O_2 = 140 \mu\text{mol/kg}$) at $-\sigma_{\theta} = 27.65 \text{ kg/m}^3$ at almost all of our stations (Fig. 2). Germaineaud et al. (2016) suggests that the UCDW can be divided into two sublayers, the upper extent ($\sigma_{\theta} \sim 27.4\text{--}27.65 \text{ kg/m}^3$) and lower extent UCDW ($\sigma_{\theta} \sim 27.65\text{--}27.76 \text{ kg/m}^3$).

Just beneath the UCDW, the Lower Circumpolar Deep Water (LCDW; Kawabe and Fujio, 2010; Reid, 1997; Tsimplis et al., 1998) is identified by a salinity maximum reaching 34.72–34.73 and a decrease of its silicate content when compared to the UCDW (Orsi et al., 1999).

4. Results

4.1. Dissolved REE concentrations

The dissolved concentrations measured for the 14 REEs at the different stations are compiled in Table 2. For simplicity, only the vertical distributions of dissolved lanthanum (dLa), neodymium (dNd), europium (dEu) and ytterbium (dYb) are shown in Fig. 3. dLa and dNd represent the dissolved LREEs while dEu and dYb represent the dMREEs and dHREEs, respectively.

The dREE concentrations display low values at the surface and increase with depth, showing a vertical profile shape similar to that of nutrients although not completely depleted in the surface waters (Fig. 3). dLa concentrations increase from $\sim 4 \text{ pmol/kg}$ in the surface water to $\sim 15 \text{ pmol/kg}$ at $\sim 1000 \text{ m}$; dNd profiles vary from $\sim 5 \text{ pmol/kg}$ in the surface to $\sim 10 \text{ pmol/kg}$ at intermediate layer followed by a ~ 2.5 -fold increase toward the bottom. Typical dEu and dYb profiles show the same kind of gradients as dLa and dNd, although with lower concentrations ($< 1 \text{ pmol/kg}$ for dEu and $< 10 \text{ pmol/kg}$ for dYb).

Table 2
Dissolved REE concentrations (pmol/kg). Data are reported with daily confidence interval (2σ).

Depth (m)	Salinity (PSU)	O ₂ (μmol/kg)	σ _t (kg·m ⁻³)	La (pmol/kg)	Ce	Pr	Nd	Sm	Eu	Gd	Tb	Dy	Ho	Er	Tm	Yb	Lu
Station 004 [July 01, 2012; 17° 0' 10.8" S; 162° 59' 45.6" E; depth: 4680 m]																	
30	34.84	199	22.94	3.7 ± 0.1	3.3 ± 0.1	0.8 ± 0	3.8 ± 0.1	0.9 ± 0	0.3 ± 0	1.5 ± 0.1	0.2 ± 0	1.8 ± 0.1	0.5 ± 0	1.6 ± 0.1	0.2 ± 0	1 ± 0	0.2 ± 0
166	35.63	164	24.83	3.3 ± 0.1	2.6 ± 0.1	0.7 ± 0	3.2 ± 0.1	0.8 ± 0	0.2 ± 0	1.2 ± 0.1	0.2 ± 0	1.5 ± 0.1	0.4 ± 0	1.5 ± 0.1	0.2 ± 0	1 ± 0	0.2 ± 0
250	35.46	161	25.67	4.1 ± 0.2	2.4 ± 0.1	0.7 ± 0	3.4 ± 0.1	0.8 ± 0	0.2 ± 0	1.2 ± 0	0.2 ± 0	1.6 ± 0.1	0.4 ± 0	1.5 ± 0.1	0.2 ± 0	1.1 ± 0	0.2 ± 0
351	35.10	167	26.28	6.2 ± 0.2	1.8 ± 0	1 ± 0	4.5 ± 0.1	0.9 ± 0	0.3 ± 0	1.6 ± 0.1	0.2 ± 0	2 ± 0.1	0.6 ± 0	2.2 ± 0.1	0.3 ± 0	1.8 ± 0	0.3 ± 0
621	34.43	192	27.04	11.8 ± 0.5	1.5 ± 0.1	1.7 ± 0.1	7.3 ± 0.2	1.7 ± 0.1	0.4 ± 0	2.5 ± 0.1	0.4 ± 0	3.4 ± 0.1	1 ± 0	3.9 ± 0.3	0.6 ± 0	3.7 ± 0.1	0.7 ± 0
730	34.42	179	27.17	12.3 ± 0.6	1.3 ± 0.1	1.8 ± 0.1	7.7 ± 0.4	1.5 ± 0.1	0.5 ± 0	2.8 ± 0.1	0.4 ± 0	3.6 ± 0.2	1.1 ± 0.1	4.2 ± 0.2	0.7 ± 0	4.1 ± 0.1	0.8 ± 0
1134	34.51	157	27.44	19 ± 0.7	8.3 ± 0.3	2.5 ± 0.1	10.3 ± 0.3	2 ± 0.1	0.6 ± 0	3.5 ± 0.2	0.5 ± 0	4.7 ± 0.3	1.4 ± 0.1	5.4 ± 0.3	0.9 ± 0	5.7 ± 0.2	1.1 ± 0
1734	34.62	140	27.64	—	—	—	—	—	—	—	—	—	—	—	—	—	—
3598	34.69	156	27.76	33.5 ± 1.3	2.4 ± 0.1	4.8 ± 0.2	24.1 ± 0.7	3.8 ± 0.2	1.1 ± 0	6 ± 0.3	0.9 ± 0	7.4 ± 0.3	2.1 ± 0.1	7.4 ± 0.4	1.2 ± 0.1	7.7 ± 0.3	1.4 ± 0.1
Station 010 [July 03, 2012; 12° 0' 0" S; 162° 59' 56.4" E; depth: 5092 m]																	
35	34.62	191	22.09	3.4 ± 0.1	2.6 ± 0.1	0.8 ± 0	3.6 ± 0.1	0.8 ± 0	0.3 ± 0	1.5 ± 0.1	0.2 ± 0	1.7 ± 0.1	0.5 ± 0	1.5 ± 0.1	0.2 ± 0	1 ± 0	0.2 ± 0
185	36.03	134	24.50	—	—	—	—	—	—	—	—	—	—	—	—	—	—
260	35.52	133	25.58	5.2 ± 0.2	1.8 ± 0.1	0.8 ± 0	3.6 ± 0.1	0.7 ± 0	0.2 ± 0	1.2 ± 0.1	0.2 ± 0	1.6 ± 0.1	0.5 ± 0	1.6 ± 0.1	0.2 ± 0	1.2 ± 0	0.2 ± 0
350	34.92	148	26.40	7.4 ± 0.3	2.1 ± 0.1	1.1 ± 0	4.9 ± 0.2	0.9 ± 0	0.3 ± 0	1.7 ± 0.1	0.3 ± 0	2.2 ± 0.1	0.6 ± 0	2.3 ± 0.1	0.3 ± 0	1.9 ± 0.1	0.3 ± 0
515	34.51	163	26.98	—	—	—	—	—	—	—	—	—	—	—	—	—	—
680	34.46	158	27.20	13 ± 0.5	1.3 ± 0.1	1.7 ± 0.1	7.7 ± 0.2	1.5 ± 0.1	0.4 ± 0	2.6 ± 0.1	0.4 ± 0	3.7 ± 0.2	1.1 ± 0.1	4.2 ± 0.2	0.7 ± 0	4.3 ± 0.1	0.8 ± 0.1
1000	34.52	139	27.41	—	—	—	—	—	—	—	—	—	—	—	—	—	—
1735	34.61	133	27.63	24.4 ± 1	3.2 ± 0.1	3 ± 0.1	13.1 ± 0.3	2.4 ± 0.1	0.8 ± 0	4.3 ± 0.2	0.7 ± 0	5.7 ± 0.3	1.7 ± 0.1	6.3 ± 0.3	1 ± 0	6.8 ± 0.2	1.3 ± 0.1
2500	34.67	145	27.73	31 ± 1.5	2.2 ± 0.1	4.3 ± 0.2	18.5 ± 0.6	3.5 ± 0.2	1.1 ± 0.1	5.6 ± 0.3	0.9 ± 0	7.1 ± 0.4	2.1 ± 0.1	7.3 ± 0.4	1.1 ± 0.1	7.6 ± 0.3	1.4 ± 0.1
4000	34.69	153	27.77	39.1 ± 1.3	5.9 ± 0.2	5.8 ± 0.2	24.6 ± 0.7	4.7 ± 0.2	1.3 ± 0.1	7.2 ± 0.3	1.1 ± 0	8.5 ± 0.4	2.4 ± 0.1	8.3 ± 0.4	1.3 ± 0	8.6 ± 0.3	1.6 ± 0.1
Station 013 [July 04, 2012; 9° 0' 10.8" S; 162° 59' 56.4" E; depth: 3853 m]																	
5	34.65	191	21.74	4 ± 0.1	3.8 ± 0.1	0.9 ± 0	3.9 ± 0.1	0.8 ± 0.1	0.2 ± 0	1.3 ± 0.1	0.2 ± 0	1.6 ± 0.1	0.4 ± 0	1.4 ± 0	0.2 ± 0	0.8 ± 0	0.1 ± 0
40	34.68	191	21.77	3.3 ± 0.1	2.8 ± 0.1	0.7 ± 0	3.3 ± 0	0.7 ± 0	0.2 ± 0	1.2 ± 0	0.2 ± 0	1.5 ± 0	0.4 ± 0	1.4 ± 0	0.2 ± 0	0.8 ± 0	0.1 ± 0
160	35.83	129	24.24	4 ± 0.1	2.9 ± 0.1	0.6 ± 0	2.8 ± 0.1	0.6 ± 0	0.2 ± 0	1.1 ± 0	0.2 ± 0	1.4 ± 0.1	0.4 ± 0	1.4 ± 0	0.2 ± 0	1 ± 0	0.2 ± 0
300	35.19	106	26.07	5.6 ± 0.1	1.6 ± 0.1	0.8 ± 0	3.7 ± 0.1	0.7 ± 0	0.2 ± 0	1.3 ± 0	0.2 ± 0	1.7 ± 0.1	0.5 ± 0	1.9 ± 0.1	0.3 ± 0	1.5 ± 0	0.3 ± 0
600	34.52	138	27.16	11.8 ± 0.2	1.1 ± 0.1	1.5 ± 0	7.2 ± 0.1	1.4 ± 0	0.5 ± 0	2.5 ± 0.1	0.4 ± 0	3.5 ± 0.1	1.1 ± 0	4 ± 0.1	0.6 ± 0	4.1 ± 0.1	0.8 ± 0
685	34.50	138	27.22	12.2 ± 0.5	1.6 ± 0.1	1.6 ± 0.1	7.2 ± 0.2	1.4 ± 0.1	0.5 ± 0	2.4 ± 0.1	0.4 ± 0	3.4 ± 0.2	1.1 ± 0	4.1 ± 0.2	0.6 ± 0	4.2 ± 0.1	0.8 ± 0
1335	34.57	126	27.54	18.3 ± 0.5	2.1 ± 0.1	2 ± 0.1	9.6 ± 0.2	2 ± 0.1	0.6 ± 0	3.1 ± 0.1	0.5 ± 0	4.7 ± 0.2	1.3 ± 0	5.5 ± 0.2	0.8 ± 0	5.9 ± 0.1	1 ± 0
1535	34.60	129	27.60	20 ± 0.7	1.4 ± 0.1	2.2 ± 0.1	10.6 ± 0.3	1.9 ± 0.1	0.6 ± 0	3.5 ± 0.2	0.5 ± 0	4.9 ± 0.2	1.4 ± 0.1	5.6 ± 0.2	0.9 ± 0	6.2 ± 0.2	1.2 ± 0.1
2000	34.64	133	27.69	26.8 ± 1.1	2.6 ± 0.1	3.3 ± 0.1	14.8 ± 0.4	2.8 ± 0.1	0.9 ± 0	4.7 ± 0.2	0.7 ± 0	6.1 ± 0.4	1.7 ± 0.1	6.6 ± 0.3	1 ± 0	7.3 ± 0.2	1.4 ± 0.1
Station 020 [July 06, 2012; 9° 59' 56.4" S; 160° 25' 1.2" E; depth: 2910 m]																	
25	34.83	189	21.97	4.3 ± 0.2	3.7 ± 0.1	1 ± 0	4.7 ± 0.2	1.1 ± 0.1	0.3 ± 0	1.7 ± 0.1	0.3 ± 0	2.1 ± 0.1	0.5 ± 0	1.7 ± 0.1	0.2 ± 0	1.2 ± 0	0.2 ± 0
190	35.82	127	24.67	—	—	—	—	—	—	—	—	—	—	—	—	—	—
600	34.49	162	27.12	0 ± 0	0 ± 0	0 ± 0	0 ± 0	0 ± 0	0 ± 0	0 ± 0	0 ± 0	0 ± 0	0 ± 0	0 ± 0	0 ± 0	0 ± 0	0 ± 0
900	34.49	151	27.30	14.1 ± 0.6	1.5 ± 0.1	1.8 ± 0.1	8.2 ± 0.3	1.6 ± 0.1	0.5 ± 0	2.8 ± 0.2	0.4 ± 0	3.8 ± 0.2	1.2 ± 0	4.5 ± 0.2	0.7 ± 0	4.7 ± 0.2	0.9 ± 0
1600	34.60	133	27.60	—	—	—	—	—	—	—	—	—	—	—	—	—	—
Station 021 [July 07, 2012; 10° 0' 46.8" S; 160° 21' 25.2" E; depth: 3342 m]																	
250	35.39	127	25.76	5.6 ± 0.2	2 ± 0.1	0.9 ± 0	4.1 ± 0.1	0.7 ± 0	0.2 ± 0	1.4 ± 0.1	0.2 ± 0	1.8 ± 0.1	0.5 ± 0	1.9 ± 0.1	0.3 ± 0	1.4 ± 0	0.3 ± 0
400	34.68	140	26.86	8.2 ± 0.2	1.5 ± 0	1.1 ± 0	5.3 ± 0.1	1.1 ± 0	0.3 ± 0	1.8 ± 0.1	0.3 ± 0	2.6 ± 0.1	0.8 ± 0	2.9 ± 0.1	0.4 ± 0	2.8 ± 0.1	0.5 ± 0
550	34.49	163	27.10	10.3 ± 0.2	1.2 ± 0	1.5 ± 0	6.8 ± 0.1	1.4 ± 0	0.4 ± 0	2.4 ± 0.1	0.4 ± 0	3.4 ± 0.1	1 ± 0	3.8 ± 0.1	0.6 ± 0	3.8 ± 0.1	0.7 ± 0
1115	34.64	139	27.69	27.7 ± 0.6	2.4 ± 0.1	3.5 ± 0.1	16.5 ± 0.3	3.1 ± 0.1	1 ± 0	5.1 ± 0.2	0.8 ± 0	6.4 ± 0.2	1.8 ± 0	6.5 ± 0.2	1 ± 0	7 ± 0.1	1.3 ± 0
2625	34.68	150	27.74	26.4 ± 0.4	2.1 ± 0.1	3.4 ± 0.1	15.9 ± 0.2	2.9 ± 0.1	0.9 ± 0	5.1 ± 0.2	0.8 ± 0	6.6 ± 0.2	1.9 ± 0	6.9 ± 0.2	1.1 ± 0	7.6 ± 0.1	1.4 ± 0
3280	34.70	165	27.77	31.1 ± 2	2.7 ± 0.2	4.1 ± 0.2	19 ± 0.7	3.5 ± 0.2	1.1 ± 0.1	5.5 ± 0.4	0.8 ± 0.1	6.8 ± 0.6	1.9 ± 0.1	6.9 ± 0.6	1 ± 0.1	7.1 ± 0.3	1.3 ± 0.1
Station 029 [July 09, 2012; 11° 3' 39.6" S; 156° 12' 54" E; depth: 3856 m]																	
267	35.38	128	25.78	5.2 ± 0.2	2.2 ± 0.1	0.9 ± 0	4 ± 0.1	0.8 ± 0	0.2 ± 0	1.4 ± 0.1	0.2 ± 0	1.8 ± 0.1	0.5 ± 0	1.9 ± 0.1	0.3 ± 0	1.4 ± 0	0.3 ± 0
737	34.47	160	27.21	11.4 ± 0.4	1.9 ± 0.1	1.6 ± 0	7.2 ± 0.2	1.4 ± 0.1	0.4 ± 0	2.5 ± 0.1	0.4 ± 0	3.5 ± 0.1	1 ± 0	4 ± 0.2	0.6 ± 0	4.1 ± 0.1	0.8 ± 0
934	34.50	150	27.36	15.3 ± 0.6	3.8 ± 0.1	1.9 ± 0.1	8.6 ± 0.2	1.6 ± 0.1	0.5 ± 0	2.8 ± 0.1	0.5 ± 0	3.9 ± 0.2	1.1 ± 0	4.5 ± 0.2	0.7 ± 0	4.7 ± 0.1	0.9 ± 0
1140	34.54	139	27.45	16.2 ± 0.5	2.2 ± 0	2 ± 0	9.2 ± 0.2	1.8 ± 0.1	0.6 ± 0	3.2 ± 0.1	0.5 ± 0	4.2 ± 0.2	1.3 ± 0	4.9 ± 0.2	0.8 ± 0	5.3 ± 0.1	1 ± 0
1534	34.59	133	27.59	18.9 ± 0.7	1.3 ± 0.1	2.4 ± 0.1	11.4 ± 0.3	2.2 ± 0.1	0.7 ± 0	3.8 ± 0.2	0.6 ± 0	5.2 ± 0.3	1.5 ± 0.1	5.8 ± 0.2	0.9 ± 0	6.2 ± 0.2	1.2 ± 0.1

(Continued on next page)

Table 2 (continued)

Depth (m)	Salinity (PSU)	O ₂ (μmol/kg)	σ _θ (kg/m ³)	La (pmol/kg)	Ce	Pr	Nd	Sm	Eu	Gd	Tb	Dy	Ho	Er	Tm	Yb	Lu
2999	34.70	166	27.77	27.1 ± 2	2.7 ± 0.2	3.7 ± 0.2	16.9 ± 0.9	3.2 ± 0.3	1 ± 0.1	5.1 ± 0.4	0.8 ± 0	6.5 ± 0.4	1.8 ± 0.1	6.6 ± 0.4	1 ± 0.1	6.9 ± 0.4	1.3 ± 0.1
Station 034 (July 10, 2012; 11° 27' 7.2" S; 154° 39' 54" E; depth: 2005 m)																	
40	34.93	181	22.17	4 ± 0.1	3 ± 0.1	0.9 ± 0	4.2 ± 0.1	1 ± 0	0.3 ± 0	1.7 ± 0	0.3 ± 0	2 ± 0	0.6 ± 0	1.8 ± 0	0.2 ± 0	1.3 ± 0	0.2 ± 0
180	35.66	144	24.77	3.7 ± 0.1	2.1 ± 0	0.7 ± 0	3.4 ± 0	0.7 ± 0	0.3 ± 0	1.3 ± 0	0.3 ± 0	1.7 ± 0	0.5 ± 0	1.6 ± 0.1	0.2 ± 0	1.2 ± 0	0.2 ± 0
300	35.25	156	26.08	5.8 ± 0.1	2.1 ± 0.1	1 ± 0	4.5 ± 0.1	1 ± 0	0.3 ± 0	1.6 ± 0	0.3 ± 0	2.1 ± 0.1	0.6 ± 0	2.2 ± 0.1	0.3 ± 0	1.8 ± 0	0.3 ± 0
635	34.49	183	27.00	11.8 ± 0.5	3.1 ± 0.1	1.7 ± 0	7.2 ± 0.1	1.4 ± 0.1	0.4 ± 0	2.3 ± 0.1	0.4 ± 0	3.3 ± 0.1	1 ± 0	3.7 ± 0.1	0.6 ± 0	3.5 ± 0.1	0.7 ± 0
1065	34.49	179	27.35	14 ± 0.6	6.5 ± 0.2	2.1 ± 0.1	8.6 ± 0.2	1.5 ± 0.1	0.5 ± 0	2.5 ± 0.1	0.4 ± 0	3.5 ± 0.1	1.1 ± 0	4.1 ± 0.1	0.6 ± 0	4 ± 0.1	0.7 ± 0
1550	34.60	136	27.37	16.5 ± 0.6	3.5 ± 0.1	2 ± 0.1	9.3 ± 0.2	1.8 ± 0.1	0.5 ± 0	3.2 ± 0.1	0.5 ± 0	4.3 ± 0.1	1.3 ± 0	4.9 ± 0.2	0.7 ± 0	4.9 ± 0.1	0.9 ± 0
1665	34.61	137	27.62	24.8 ± 0.9	11.9 ± 0.1	3 ± 0.1	13.3 ± 0.5	2.5 ± 0.1	0.7 ± 0	4.3 ± 0.2	0.7 ± 0	5.5 ± 0.3	1.6 ± 0.1	6.3 ± 0.3	0.9 ± 0	6.6 ± 0.3	1.2 ± 0.1
1750	34.63	136	27.65	26.3 ± 0.9	2.5 ± 0.1	3.4 ± 0.1	15 ± 0.4	3 ± 0.1	0.9 ± 0	4.7 ± 0.2	0.8 ± 0	6.1 ± 0.2	1.9 ± 0.1	6.7 ± 0.3	1 ± 0	7 ± 0.2	1.3 ± 0
1920	34.65	140	27.69	-	-	-	-	-	-	-	-	-	-	-	-	-	-
Station 036 (July 11, 2012; 11° 30' 7.2" S; 154° 23' 24" E; depth: 1168 m)																	
25	34.49	195	22.09	7 ± 0.1	7.1 ± 0.1	1.8 ± 0	8.2 ± 0.1	2 ± 0.1	0.6 ± 0	2.8 ± 0.1	0.4 ± 0	3.1 ± 0.1	0.8 ± 0	2.4 ± 0.1	0.3 ± 0	1.7 ± 0	0.3 ± 0
100	35.43	163	23.89	3.7 ± 0.1	3 ± 0	0.8 ± 0	3.9 ± 0	1 ± 0	0.3 ± 0	1.5 ± 0.1	0.2 ± 0	1.9 ± 0	0.5 ± 0	1.7 ± 0.1	0.2 ± 0	1.2 ± 0	0.2 ± 0
160	35.61	141	24.60	4.1 ± 0.1	2.8 ± 0.1	0.8 ± 0	3.8 ± 0	0.9 ± 0	0.3 ± 0	1.4 ± 0.1	0.2 ± 0	1.8 ± 0.1	0.5 ± 0	1.7 ± 0.1	0.2 ± 0	1.2 ± 0	0.2 ± 0
180	35.64	144	24.96	4.4 ± 0.1	3.1 ± 0	0.8 ± 0	3.8 ± 0	0.9 ± 0	0.3 ± 0	1.4 ± 0	0.2 ± 0	1.8 ± 0.1	0.5 ± 0	1.7 ± 0	0.2 ± 0	1.2 ± 0	0.2 ± 0
400	34.94	167	26.51	7.2 ± 0.2	1.9 ± 0.1	1.1 ± 0	5.2 ± 0.1	1.1 ± 0	0.3 ± 0	1.7 ± 0.1	0.3 ± 0	2.4 ± 0.1	0.7 ± 0	2.5 ± 0.1	0.4 ± 0	2.2 ± 0	0.4 ± 0
700	34.46	182	27.09	11.4 ± 0.4	11.4 ± 0.1	1.6 ± 0	7.2 ± 0.1	1.5 ± 0.1	0.4 ± 0	2.4 ± 0.1	0.4 ± 0	3.4 ± 0.1	1 ± 0	3.8 ± 0.1	0.6 ± 0	3.7 ± 0.1	0.7 ± 0
900	34.46	170	27.24	12.6 ± 0.4	1.4 ± 0	1.6 ± 0	7.5 ± 0.1	1.5 ± 0.1	0.5 ± 0	2.5 ± 0.1	0.4 ± 0	3.6 ± 0.1	1.1 ± 0	4.1 ± 0.1	0.6 ± 0	4.2 ± 0.1	0.8 ± 0
Station 042 (July 15, 2012; 5° 8' 42" S; 153° 17' 24" E; depth: 3081 m)																	
5	34.69	192	21.71	3.6 ± 0.2	3.1 ± 0.2	0.8 ± 0	3.9 ± 0.2	0.8 ± 0	0.3 ± 0	1.4 ± 0.1	0.2 ± 0	1.7 ± 0.1	0.5 ± 0	1.5 ± 0.1	0.2 ± 0	0.9 ± 0	0.2 ± 0
50	34.75	192	21.75	-	-	-	-	-	-	-	-	-	-	-	-	-	-
100	35.46	157	22.68	-	-	-	-	-	-	-	-	-	-	-	-	-	-
180	35.65	140	24.72	4.2 ± 0.2	2.5 ± 0.1	0.7 ± 0	3.4 ± 0.1	0.8 ± 0	0.3 ± 0	1.3 ± 0.1	0.2 ± 0	1.7 ± 0.1	0.5 ± 0	1.7 ± 0.1	0.2 ± 0	1.2 ± 0	0.2 ± 0
225	35.35	152	25.85	4.9 ± 0.2	11.4 ± 0.1	0.8 ± 0	3.8 ± 0.1	1.5 ± 0.1	0.3 ± 0	1.4 ± 0.1	0.2 ± 0	2 ± 0.1	0.5 ± 0	2 ± 0.1	0.3 ± 0	1.6 ± 0	0.3 ± 0
400	34.64	174	26.84	9.8 ± 0.2	11.8 ± 0.1	1.3 ± 0.1	6.1 ± 0.1	1.2 ± 0.1	0.4 ± 0	2.1 ± 0.1	0.3 ± 0	3 ± 0.1	0.9 ± 0	3.3 ± 0.1	0.5 ± 0	3.1 ± 0.1	0.6 ± 0
500	34.54	158	27.02	11 ± 0.3	1.7 ± 0	1.5 ± 0	6.8 ± 0.1	1.4 ± 0	0.4 ± 0	2.3 ± 0.1	0.4 ± 0	3.2 ± 0.1	1 ± 0	3.6 ± 0.2	0.6 ± 0	3.6 ± 0.1	0.7 ± 0
750	34.48	154	27.23	11.9 ± 0.3	11.6 ± 0.1	1.6 ± 0	7.3 ± 0.1	1.5 ± 0	0.4 ± 0	2.5 ± 0.1	0.4 ± 0	3.5 ± 0.1	1.1 ± 0	4 ± 0.1	0.6 ± 0	4.1 ± 0	0.8 ± 0
1000	34.53	137	27.41	15.8 ± 0.8	2.1 ± 0.1	2.1 ± 0.1	9.4 ± 0.3	1.9 ± 0.1	0.6 ± 0	3.2 ± 0.2	0.5 ± 0	4.5 ± 0.3	1.3 ± 0.1	5 ± 0.3	0.7 ± 0	5.1 ± 0.2	1 ± 0.1
1200	34.56	130	27.49	17.9 ± 0.6	2.8 ± 0.1	2.3 ± 0.1	10.4 ± 0.2	2 ± 0.1	0.7 ± 0	3.5 ± 0.2	0.6 ± 0	4.6 ± 0.2	1.4 ± 0.1	5.1 ± 0.2	0.8 ± 0	5.6 ± 0.1	1.1 ± 0
1550	34.61	123	27.62	24.8 ± 0.7	5.1 ± 0.1	3.2 ± 0.1	14.5 ± 0.3	2.8 ± 0.1	0.9 ± 0	4.4 ± 0.2	0.7 ± 0	5.7 ± 0.2	1.7 ± 0.1	6.1 ± 0.3	1 ± 0	6.6 ± 0.2	1.2 ± 0
1750	34.62	124	27.64	28.6 ± 0.9	4.6 ± 0.2	3.3 ± 0.1	15.8 ± 0.5	3.1 ± 0.1	1 ± 0	5.2 ± 0.2	0.8 ± 0	6.5 ± 0.2	1.8 ± 0.1	6.7 ± 0.2	1.1 ± 0	7.2 ± 0.2	1.3 ± 0
2000	34.64	126	27.68	29.1 ± 1.6	3.6 ± 0.2	3.9 ± 0.2	18 ± 0.8	3.4 ± 0.2	1.1 ± 0.1	5.7 ± 0.3	0.9 ± 0	6.8 ± 0.4	1.9 ± 0.1	7.3 ± 0.5	1.1 ± 0.1	7.7 ± 0.4	1.4 ± 0.1
2500	34.66	133	27.73	32.5 ± 2.6	4.8 ± 0.2	4.7 ± 0.3	21.8 ± 0.9	4.2 ± 0.3	1.3 ± 0.1	6.7 ± 0.4	1 ± 0.1	7.9 ± 0.6	2.2 ± 0.2	8 ± 0.6	1.3 ± 0.1	8.5 ± 0.4	1.5 ± 0.1
Station 043 (July 17, 2012; 3° 59' 52.8" S; 155° 35' 38.4" E; depth: 1925 m)																	
5	34.66	191	21.72	3.6 ± 0.2	2.8 ± 0.2	0.7 ± 0	3.5 ± 0.1	0.7 ± 0	0.2 ± 0	1.3 ± 0.1	0.2 ± 0	1.6 ± 0.1	0.5 ± 0	1.4 ± 0.1	0.2 ± 0	0.8 ± 0	0.1 ± 0
150	35.91	138	23.99	4.5 ± 0.1	2.6 ± 0.1	0.8 ± 0	3.7 ± 0.1	0.7 ± 0	0.2 ± 0	1.3 ± 0.1	0.2 ± 0	1.7 ± 0.1	0.5 ± 0	1.7 ± 0.1	0.2 ± 0	1.2 ± 0	0.2 ± 0
230	35.16	99	26.14	25.5 ± 0.8	112.3 ± 0.3	11.2 ± 0.1	5.2 ± 0.1	10.9 ± 0.1	10.3 ± 0.1	11.6 ± 0.1	10.3 ± 0.1	12.2 ± 0.1	10.6 ± 0.1	12.3 ± 0.1	10.3 ± 0.1	12.1 ± 0.1	10.4 ± 0.1
700	34.51	128	27.18	13.1 ± 0.3	1.8 ± 0	1.7 ± 0	7.6 ± 0.1	1.5 ± 0	0.5 ± 0	2.5 ± 0.1	0.4 ± 0	3.4 ± 0.1	1.1 ± 0	4 ± 0.1	0.6 ± 0	4.2 ± 0.1	0.8 ± 0
1200	34.56	105	27.47	16.4 ± 0.5	1.9 ± 0	2.1 ± 0	9.6 ± 0.2	1.9 ± 0.1	0.6 ± 0	3.2 ± 0.1	0.5 ± 0	4.4 ± 0.1	1.3 ± 0	4.9 ± 0.2	0.8 ± 0	5.5 ± 0.1	1 ± 0
Station 045 (July 18, 2012; 4° 42' 0" S; 154° 52' 48" E; depth: 3117 m)																	
50	34.79	190	21.85	3.6 ± 0.1	2.2 ± 0.1	0.7 ± 0	3.3 ± 0	0.7 ± 0	0.2 ± 0	1.3 ± 0	0.2 ± 0	1.5 ± 0	0.4 ± 0	1.4 ± 0	0.2 ± 0	0.8 ± 0	0.1 ± 0
150	35.97	129	23.97	3.5 ± 0.1	1.3 ± 0	0.6 ± 0	2.6 ± 0	0.6 ± 0	0.2 ± 0	1.1 ± 0	0.2 ± 0	1.5 ± 0	0.4 ± 0	1.5 ± 0	0.2 ± 0	1 ± 0	0.2 ± 0
400	34.65	124	26.89	11.3 ± 0.3	2.5 ± 0.1	1.4 ± 0	6.5 ± 0.1	1.3 ± 0.1	0.4 ± 0	2.1 ± 0.1	0.4 ± 0	3 ± 0.1	0.9 ± 0	3.4 ± 0.1	0.5 ± 0	3.3 ± 0.1	0.6 ± 0
700	34.54	89	27.19	12.5 ± 0.3	0.9 ± 0	1.6 ± 0	7.2 ± 0.2	1.4 ± 0.1	0.5 ± 0	2.5 ± 0.1	0.4 ± 0	3.5 ± 0.1	1 ± 0	4 ± 0.1	0.6 ± 0	4.1 ± 0.1	0.8 ± 0
1000	34.54	112	27.39	15.6 ± 0.5	2 ± 0.1	1.9 ± 0	8.9 ± 0.2	1.8 ± 0.1	0.5 ± 0	3.1 ± 0.1	0.5 ± 0	4.2 ± 0.1	1.2 ± 0	4.7 ± 0.1	0.7 ± 0	4.9 ± 0.1	0.9 ± 0
Station 047 (July 18, 2012; 4° 56' 2.4" S; 154° 38' 52.8" E; depth: 1004 m)																	
25	34.67	190	21.78	4.4 ± 0.1	3.3 ± 0.1	1 ± 0	4.4 ± 0.1	1 ± 0	0.3 ± 0	1.6 ± 0	0.2 ± 0	1.9 ± 0.1	0.5 ± 0	1.6 ± 0	0.2 ± 0	1 ± 0	0.2 ± 0
156	36.02	126	24.41	4.6 ± 0.1	2.6 ± 0	0.6 ± 0	3 ± 0	0.6 ± 0	0.2 ± 0	1.2 ± 0	0.2 ± 0	1.6 ± 0	0.5 ± 0	1.7 ± 0	0.2 ± 0	1.2 ± 0	0.2 ± 0

(Continued on next page)

Table 2 (continued)

Depth (m)	Salinity (PSU)	O ₂ (μmol/kg)	SiO ₂ (kg/m ³)	La (pmol/kg)	Ce	Pr	Nd	Sm	Eu	Gd	Tb	Dy	Ho	Er	Tm	Yb	Lu
264	35.08	106	26.27	17.4 ± 0.1	1.7 ± 0	1.1 ± 0	4.8 ± 0.1	0.9 ± 0	0.3 ± 0	1.6 ± 0.1	0.3 ± 0	2.2 ± 0.1	0.7 ± 0	2.4 ± 0.1	0.3 ± 0	2.1 ± 0	0.4 ± 0
635	34.52	129	27.20	13.3 ± 0.3	2.6 ± 0.2	1.7 ± 0	7.7 ± 0.1	1.5 ± 0	0.5 ± 0	2.6 ± 0.1	0.4 ± 0	3.6 ± 0.2	1.1 ± 0	4.1 ± 0.1	0.7 ± 0	4.2 ± 0.1	0.8 ± 0
Station 053 (July 19, 2012; 4° 54' 18" S; 152° 52' 12" E; depth: 733 m)																	
25	34.88	189	21.99	4.9 ± 0.2	4.1 ± 0.2	1.2 ± 0.1	5.7 ± 0.3	1.4 ± 0.1	0.5 ± 0	2.1 ± 0.1	0.3 ± 0	2.5 ± 0.1	0.7 ± 0	2.1 ± 0.1	0.3 ± 0	1.5 ± 0.1	0.2 ± 0
149	35.61	142	24.72	6.3 ± 0.2	5.2 ± 0.1	0.9 ± 0	4 ± 0.1	0.9 ± 0	0.3 ± 0	1.5 ± 0.1	0.2 ± 0	1.8 ± 0.1	0.5 ± 0	1.7 ± 0	0.2 ± 0	1.2 ± 0	0.2 ± 0
335	34.98	161	26.45	17.6 ± 0.1	1.8 ± 0	1.2 ± 0	5.3 ± 0.1	1.1 ± 0	0.3 ± 0	1.8 ± 0.1	0.3 ± 0	2.5 ± 0.1	0.7 ± 0	2.6 ± 0.1	0.4 ± 0	2.3 ± 0	0.4 ± 0
719	34.48	158	27.22	12.6 ± 0.5	1.5 ± 0	1.7 ± 0	7.8 ± 0.1	1.5 ± 0	0.5 ± 0	2.6 ± 0.1	0.4 ± 0	3.7 ± 0.1	1.1 ± 0	4.2 ± 0.1	0.6 ± 0	4.2 ± 0.1	0.8 ± 0
Station 055 (July 20, 2012; 4° 37.2" S; 152° 32' 20.4" E; depth: 1580 m)																	
1582	34.60	125	27.59	23.4 ± 0	3.8 ± 0	3.1 ± 0	14.3 ± 0	2.8 ± 0	0.8 ± 0	4.8 ± 0	0.7 ± 0	5.9 ± 0	1.8 ± 0	6.6 ± 0	0.9 ± 0	6.7 ± 0	1.2 ± 0
Station 057 (July 20, 2012; 4° 30' 12" S; 152° 31' 22.8" E; depth: 2552 m)																	
25	34.77	192	21.91	4.1 ± 0.1	3.5 ± 0.1	1 ± 0	5.2 ± 0.1	1.3 ± 0.1	0.5 ± 0	2.1 ± 0.1	0.3 ± 0	2.3 ± 0.1	0.6 ± 0	2 ± 0.1	0.3 ± 0	1.3 ± 0	0.2 ± 0
150	35.58	139	24.20	3.8 ± 0.2	2.6 ± 0.1	0.8 ± 0	3.7 ± 0.1	0.9 ± 0.1	0.3 ± 0	1.4 ± 0.1	0.2 ± 0	1.8 ± 0.1	0.5 ± 0	1.7 ± 0.1	0.2 ± 0	1.2 ± 0	0.2 ± 0
250	35.27	152	26.00	5.4 ± 0.2	2.1 ± 0.1	0.9 ± 0.1	4.2 ± 0.1	0.9 ± 0.1	0.3 ± 0	1.5 ± 0.1	0.2 ± 0	2 ± 0.1	0.6 ± 0	2.1 ± 0.1	0.3 ± 0	1.7 ± 0	0.3 ± 0
450	34.65	171	26.85	9.3 ± 0.2	1.5 ± 0	1.3 ± 0	6.2 ± 0.1	1.2 ± 0.1	0.4 ± 0	2.1 ± 0.1	0.3 ± 0	2.9 ± 0.1	0.9 ± 0	3.1 ± 0.1	0.5 ± 0	3.1 ± 0	0.6 ± 0
580	34.51	177	27.02	12.1 ± 0.3	2.5 ± 0.1	1.5 ± 0	6.8 ± 0.1	1.3 ± 0	0.4 ± 0	2.2 ± 0.1	0.4 ± 0	3.1 ± 0.1	0.9 ± 0	3.6 ± 0.1	0.5 ± 0	3.6 ± 0.1	0.7 ± 0
850	34.50	143	27.33	13.7 ± 0.4	1.6 ± 0	1.7 ± 0	8.1 ± 0.2	1.6 ± 0.1	0.5 ± 0	2.9 ± 0.1	0.5 ± 0	3.9 ± 0.1	1.2 ± 0	4.4 ± 0.1	0.7 ± 0	4.8 ± 0.1	0.9 ± 0
1302	34.57	129	27.51	19.2 ± 0.5	2.8 ± 0.1	2.4 ± 0.1	11.5 ± 0.3	2.2 ± 0.1	0.7 ± 0	3.9 ± 0.2	0.6 ± 0	5.1 ± 0.2	1.5 ± 0	5.5 ± 0.2	0.9 ± 0	6 ± 0.1	1.1 ± 0
1650	34.61	124	27.62	—	—	—	—	—	—	—	—	—	—	—	—	—	—
2201	34.65	135	27.71	31.2 ± 0.9	3.5 ± 0.1	4.2 ± 0.1	20 ± 0.5	3.9 ± 0.2	1.3 ± 0	6.3 ± 0.3	1 ± 0	7.9 ± 0.3	2.1 ± 0	7.7 ± 0.2	1.2 ± 0	8.2 ± 0.2	1.5 ± 0
Station 058 (July 21, 2012; 5° 30' 10.8" S; 152° 5' 52.8" E; depth: 1142 m)																	
215	35.50	135	25.51	4.8 ± 0.2	2.2 ± 0.1	0.8 ± 0	3.9 ± 0.1	0.8 ± 0	0.3 ± 0	1.4 ± 0.1	0.2 ± 0	1.8 ± 0.1	0.5 ± 0	1.8 ± 0.1	0.3 ± 0	1.4 ± 0	0.2 ± 0
1100	34.55	133	27.47	18.9 ± 0.7	3.1 ± 0.1	2.3 ± 0.1	11 ± 0.3	2.2 ± 0.1	0.7 ± 0	3.7 ± 0.2	0.6 ± 0	4.9 ± 0.2	1.4 ± 0.1	5.4 ± 0.2	0.8 ± 0	5.7 ± 0.2	1 ± 0
Station 060 (July 22, 2012; 6° 10' 1.2" S; 152° 29' 49.2" E; depth: 5609 m)																	
35	34.74	193	22.19	5 ± 0.1	4.5 ± 0.1	1.1 ± 0	5.3 ± 0.1	1.2 ± 0	0.4 ± 0	1.8 ± 0.1	0.3 ± 0	2.1 ± 0.1	0.6 ± 0	1.8 ± 0.1	0.2 ± 0	1.2 ± 0	0.2 ± 0
180	35.73	135	24.70	4.2 ± 0.2	2.3 ± 0.1	0.7 ± 0	3.4 ± 0.1	0.7 ± 0	0.2 ± 0	1.2 ± 0.1	0.2 ± 0	1.6 ± 0.1	0.5 ± 0	1.6 ± 0.1	0.2 ± 0	1.1 ± 0	0.2 ± 0
250	35.33	124	25.86	7.4 ± 0.1	3.7 ± 0.1	1 ± 0	4.9 ± 0.1	1 ± 0	0.3 ± 0	1.6 ± 0.1	0.2 ± 0	2 ± 0.1	0.6 ± 0	2.2 ± 0.1	0.3 ± 0	1.7 ± 0	0.3 ± 0
480	34.53	173	27.03	11.2 ± 0.3	2.6 ± 0.1	1.5 ± 0.1	6.8 ± 0.1	1.3 ± 0.1	0.4 ± 0	2.3 ± 0.1	0.4 ± 0	3.1 ± 0.1	1 ± 0	3.5 ± 0.1	0.6 ± 0	3.6 ± 0.1	0.7 ± 0
1000	34.53	138	27.43	16.3 ± 0.3	2.7 ± 0.1	2 ± 0	9.4 ± 0.1	1.8 ± 0.1	0.6 ± 0	3 ± 0.1	0.5 ± 0	4 ± 0.1	1.3 ± 0	4.8 ± 0.2	0.7 ± 0	5 ± 0.1	1 ± 0
1600	34.61	124	27.62	23.9 ± 0.9	5 ± 0.2	3.2 ± 0.1	14.5 ± 0.3	2.8 ± 0.1	0.9 ± 0	4.6 ± 0.2	0.7 ± 0	5.8 ± 0.2	1.8 ± 0	6.2 ± 0.2	1 ± 0	6.8 ± 0.1	1.3 ± 0
1800	34.63	125	27.67	28.4 ± 0.6	7.8 ± 0.2	3.9 ± 0.1	18.1 ± 0.3	3.4 ± 0.1	1.1 ± 0	5.4 ± 0.2	0.8 ± 0	6.8 ± 0.3	1.9 ± 0.1	7 ± 0.2	1.1 ± 0	7.4 ± 0.2	1.4 ± 0
2541	34.66	132	27.73	35.4 ± 1	3.5 ± 0.1	5.1 ± 0.1	23.8 ± 0.5	4.6 ± 0.2	1.5 ± 0	7 ± 0.3	1.1 ± 0	8.6 ± 0.4	2.3 ± 0.1	8.1 ± 0.4	1.3 ± 0.1	8.7 ± 0.2	1.6 ± 0.1
3250	34.69	155	27.76	41.1 ± 1.1	5.8 ± 0.2	6.1 ± 0.2	28.1 ± 0.6	5.3 ± 0.2	1.7 ± 0	8 ± 0.3	1.2 ± 0	9.1 ± 0.4	2.6 ± 0.1	8.3 ± 0.3	1.4 ± 0	8.9 ± 0.2	1.6 ± 0.1
4000	34.70	158	27.77	41 ± 1.4	5.6 ± 0.2	6.3 ± 0.2	28.8 ± 0.8	5.9 ± 0.2	1.8 ± 0.1	8.2 ± 0.3	1.2 ± 0	9.5 ± 0.3	2.5 ± 0.1	8.7 ± 0.3	1.3 ± 0	8.9 ± 0.2	1.6 ± 0.1
4500	34.70	160	27.77	41.9 ± 1.6	8 ± 0.3	6.8 ± 0.3	30.2 ± 1	6 ± 0.3	1.9 ± 0.1	8.4 ± 0.5	1.3 ± 0.1	9.6 ± 0.6	2.6 ± 0.1	8.8 ± 0.5	1.4 ± 0.1	8.9 ± 0.3	1.6 ± 0.1
4750	34.70	160	27.77	47.3 ± 1	14.6 ± 0.3	7 ± 0.2	30.4 ± 0.4	5.6 ± 0.2	1.8 ± 0	7.8 ± 0.3	1.2 ± 0	8.9 ± 0.4	2.4 ± 0.1	8.4 ± 0.3	1.2 ± 0	8.3 ± 0.1	1.6 ± 0
5000	34.70	161	27.77	39.3 ± 0.9	5.3 ± 0.1	5.4 ± 0.1	25.4 ± 0.3	4.8 ± 0.2	1.5 ± 0	7 ± 0.2	1.1 ± 0	8.1 ± 0.3	2.3 ± 0.1	8 ± 0.3	1.2 ± 0	7.8 ± 0.1	1.5 ± 0
5603	34.70	162	27.77	41.2 ± 1.5	5.6 ± 0.2	6 ± 0.2	26.3 ± 0.7	4.9 ± 0.2	1.4 ± 0.1	6.8 ± 0.4	1 ± 0.1	8 ± 0.4	2.2 ± 0.1	7.6 ± 0.4	1.1 ± 0.1	7.6 ± 0.2	1.4 ± 0
Station 071 (July 25, 2012; 8° 19' 55.2" S; 151° 17' 27.6" E; depth: 1563 m)																	
50	34.80	192	22.39	3.8 ± 0.3	2.6 ± 0.2	0.8 ± 0.1	4 ± 0.2	1 ± 0.1	0.3 ± 0	1.5 ± 0.1	0.2 ± 0	1.8 ± 0.1	0.5 ± 0	1.7 ± 0.1	0.2 ± 0	1.1 ± 0	0.2 ± 0
160	35.66	138	24.60	4.6 ± 0.3	5.9 ± 0.4	0.8 ± 0	3.9 ± 0.2	0.7 ± 0.1	0.2 ± 0	1.3 ± 0.1	0.2 ± 0	1.7 ± 0.1	0.5 ± 0	1.7 ± 0.1	0.2 ± 0	1.2 ± 0.1	0.2 ± 0
400	34.98	165	26.47	7.9 ± 0.6	4.6 ± 0.2	1.1 ± 0.1	5.2 ± 0.2	1.1 ± 0.1	0.3 ± 0	1.8 ± 0.1	0.3 ± 0	2.5 ± 0.2	0.7 ± 0	2.5 ± 0.1	0.4 ± 0	2.2 ± 0.1	0.4 ± 0
600	34.49	178	27.06	12 ± 0.9	11.9 ± 0.2	1.5 ± 0.1	6.9 ± 0.4	1.3 ± 0.1	0.4 ± 0	2.3 ± 0.2	0.4 ± 0	3.3 ± 0.3	1 ± 0.1	3.7 ± 0.2	0.6 ± 0	3.7 ± 0.2	0.7 ± 0.1
1100	34.52	143	27.41	32.3 ± 1.2	5.6 ± 0.2	2.1 ± 0.1	9.7 ± 0.2	1.9 ± 0.1	0.6 ± 0	3.2 ± 0.1	0.5 ± 0	4.3 ± 0.2	1.3 ± 0	4.9 ± 0.2	0.8 ± 0	5.2 ± 0.1	1 ± 0
Station 073 - Filtered (July 26, 2012; 7° 9' 57.6" S; 149° 59' 56.4" E; depth: 5253 m)																	
50	35.06	171	22.66	4 ± 0.1	3.1 ± 0.1	0.9 ± 0	4.1 ± 0.1	0.9 ± 0	0.3 ± 0	1.5 ± 0.1	0.2 ± 0	1.9 ± 0.1	0.5 ± 0	1.7 ± 0.1	0.2 ± 0	1.2 ± 0	0.2 ± 0
170	35.59	141	24.76	4 ± 0.2	2.5 ± 0.1	0.8 ± 0	3.6 ± 0.1	0.7 ± 0	0.2 ± 0	1.4 ± 0.1	0.2 ± 0	1.8 ± 0.1	0.5 ± 0	1.6 ± 0.1	0.2 ± 0	1.2 ± 0	0.2 ± 0
200	35.60	140	24.90	3.6 ± 0.1	11.6 ± 0.1	0.7 ± 0	3.3 ± 0.1	0.7 ± 0	0.2 ± 0	1.3 ± 0.1	0.2 ± 0	1.7 ± 0.1	0.5 ± 0	1.7 ± 0.1	0.2 ± 0	1.2 ± 0	0.2 ± 0
700	34.47	169	27.16	11.2 ± 0.2	1.2 ± 0	1.5 ± 0	7.1 ± 0.1	1.4 ± 0	0.5 ± 0	2.4 ± 0.1	0.4 ± 0	3.5 ± 0.1	1 ± 0	4 ± 0.1	0.6 ± 0	4 ± 0.1	0.7 ± 0
1650	34.61	123	27.62	19.6 ± 0.9	2.2 ± 0.2	2.5 ± 0	11.7 ± 0.2	2.3 ± 0.1	0.7 ± 0	3.8 ± 0	0.6 ± 0	4.8 ± 0.1	1.4 ± 0	5.2 ± 0.1	0.8 ± 0	5.6 ± 0.1	1.1 ± 0

(continued on next page)

Table 2 (continued)

Depth (m)	Salinity (PSU)	O ₂ (μmol/kg)	σ _θ (kg/m ³)	La (pmol/kg)	Ce (pmol/kg)	Pr	Nd	Sm	Eu	Gd	Tb	Dy	Ho	Er	Tm	Yb	Lu
Station 077 (July 28, 2012; 5° 57' 3.6" S, 147° 39' 36" E; depth: 1045 m)																	
25	34.77	191	22.35	9.1 ± 0.2	3.7 ± 0.1	1 ± 0	4.9 ± 0.1	1.1 ± 0	0.4 ± 0	1.8 ± 0.1	0.3 ± 0	2.2 ± 0.1	0.6 ± 0	1.8 ± 0	0.2 ± 0	1.3 ± 0	0.2 ± 0
180	35.61	140	24.85	3.9 ± 0.1	2.3 ± 0	0.7 ± 0	3.4 ± 0	0.8 ± 0	0.2 ± 0	1.3 ± 0	0.2 ± 0	1.7 ± 0	0.5 ± 0	1.6 ± 0	0.2 ± 0	1.1 ± 0	0.2 ± 0
501	34.57	178	26.94	13.2 ± 0.2	5.2 ± 0.5	1.8 ± 0	8 ± 0.1	1.6 ± 0	0.5 ± 0	2.4 ± 0.1	0.4 ± 0	3.3 ± 0.1	1 ± 0	3.6 ± 0.1	0.5 ± 0	3.6 ± 0.1	0.6 ± 0
701	34.48	159	27.20	13.1 ± 0.2	11.6 ± 0.7	1.7 ± 0	7.9 ± 0.1	1.5 ± 0	0.5 ± 0	2.7 ± 0.1	0.4 ± 0	3.7 ± 0.1	1.1 ± 0	4.3 ± 0.1	0.7 ± 0	4.3 ± 0.1	0.8 ± 0
983	34.51	145	27.35	20 ± 0.7	2.9 ± 0.1	2.1 ± 0	9.6 ± 0.2	1.9 ± 0.1	0.6 ± 0	3.1 ± 0.1	0.5 ± 0	4.3 ± 0.2	1.3 ± 0	4.8 ± 0.1	0.8 ± 0	5 ± 0.1	1 ± 0
Station 082- non-filtrated (August 03, 2012; 13° 59' 49.2" S, 156° 0' 25.2" E; depth: 2586 m)																	
25	34.93	197	22.92	6.6 ± 0.2	4.9 ± 0.1	0.9 ± 0	4.2 ± 0.1	0.9 ± 0.1	0.4 ± 0	1.7 ± 0.1	0.2 ± 0	1.9 ± 0.1	0.5 ± 0	1.7 ± 0.1	0.2 ± 0	1.1 ± 0	0.2 ± 0
180	35.79	129	24.65	6.2 ± 0.3	4.6 ± 0.2	0.8 ± 0	3.5 ± 0.1	0.8 ± 0	0.2 ± 0	1.3 ± 0.1	0.2 ± 0	1.6 ± 0.1	0.5 ± 0	1.6 ± 0.1	0.2 ± 0	1.1 ± 0	0.2 ± 0
700	34.47	165	27.13	14 ± 0.6	4.5 ± 0.2	1.9 ± 0.1	8.1 ± 0.2	1.6 ± 0.1	0.5 ± 0	2.9 ± 0.1	0.4 ± 0	3.8 ± 0.2	1.1 ± 0	4.3 ± 0.2	0.7 ± 0	4.1 ± 0.1	0.7 ± 0
800	34.45	163	27.23	15.5 ± 0.7	4.4 ± 0.2	2 ± 0.1	8.6 ± 0.3	1.7 ± 0.1	0.5 ± 0	2.9 ± 0.1	0.5 ± 0	3.9 ± 0.2	1.2 ± 0.1	4.6 ± 0.2	0.7 ± 0	4.5 ± 0.1	0.8 ± 0
1000	34.50	151	27.38	17.3 ± 0.7	1.4 ± 0.3	2.1 ± 0.1	9.5 ± 0.2	1.8 ± 0.1	0.6 ± 0	3.3 ± 0.1	0.5 ± 0	4.2 ± 0.1	1.3 ± 0.1	4.9 ± 0.2	0.8 ± 0	5 ± 0.1	0.9 ± 0
1200 ^a	34.54	145	27.48	20 ± 1.7	6.9 ± 0.9	2.2 ± 0	10 ± 0.2	1.9 ± 0.1	0.6 ± 0	3.3 ± 0	0.5 ± 0	4.6 ± 0.1	1.4 ± 0	5.3 ± 0.1	0.8 ± 0	5.6 ± 0.1	1.1 ± 0
1350	34.57	140	27.53	22.1 ± 1.2	3 ± 0.1	2.4 ± 0.1	11 ± 0.4	2.3 ± 0.1	0.6 ± 0	3.7 ± 0.2	0.6 ± 0	5.1 ± 0.3	1.5 ± 0.1	5.8 ± 0.3	0.9 ± 0	6 ± 0.2	1.2 ± 0.1
2000	34.64	141	27.67	29.1 ± 1.1	10.7 ± 0.4	3.6 ± 0.1	14.5 ± 0.4	2.7 ± 0.2	0.9 ± 0.1	4.7 ± 0.2	0.7 ± 0	6.1 ± 0.2	1.8 ± 0.1	6.8 ± 0.3	1 ± 0	7.3 ± 0.2	1.5 ± 0.1

Square brackets indicate data with low recoveries.

^a Italic values refer to data with its statistical error bar.

Three main processes could condition the distribution of the REE in the Solomon Sea: 1) advection of waters from outside already displaying such vertical shape, consistent with the surface-scavenging and depth-dissolution hypothesis characterizing the fate of these elements along the general circulation (De Baar et al., 1985a; Elderfield et al., 1988; Garcia-Solsona et al., 2014; Sholkovitz et al., 1994; Takebe, 2005); 2) external inputs as for example dissolved or solid material weathered from the surrounding islands or dust of volcanic origin and 3) internal processes specific of this area. Disentangling properly the respective roles of these three processes would require the quantification of the first term by performing an analysis such as the Optimum Multiparameter Analysis (OMP; Tomczak and Large, 1989). Such a method would ideally allow identifying profiles as mixing of a few water types sources, by assuming that parameters such as nutrients and oxygen are conservative. Although promising, this method would be very uncertain in this region and would require significant additional work. Indeed, the Solomon Sea is characterized by a highly variable and complex dynamic, important diapycnal mixing (Germineaud et al., 2016), by water masses sources that are not easily identifiable (Gasparin et al., 2014), and high diazotrophic blooms that question the assumption of conservative parameters (Ganachaud et al., 2017). Therefore, we choose to apply a simple box model to estimate the dNd and dREE enrichments within the Solomon Sea (see Section 5.1).

In any case, beyond the observed general concentration increase, the vertical shape of the profiles shows subtle but interesting variations:

- Down to 3000 m, all the concentrations linearly increase, although the dYb profile is always slightly more convex than the 3 other dREE ones;
- In the southern part of our study (Coral Sea and Solomon Sea entrance, Fig. 3a), a break is observed in the linearity at 3000 m, with dREE concentration values slightly lower between 3000 and 4000 m. In the northern and almost deepest part of the Solomon Sea, at station 60, dREE profiles show a local maximum between 4000 and 5000 m, dREE concentrations being maximal in this layer and then decreasing toward the bottom. The convex shape of dYb is more pronounced at this station (Fig. 3c). This particular shape could be related to the fact that the Solomon Sea is considered as a sealed area below 3000–3500 m, separated from the outer world by islands and sills (Germineaud, 2016; Sokolov and Rintoul, 2000). This topographic constraint might increase the residence time of the waters at these depths, facilitating the scavenging to operate and yielding the slight depletion observed in the deepest part of the profiles;
- On average, dREE concentrations are slightly enriched within the Solomon Sea compared to the sites located outside of it. For example, dNd average value is of -3.5 pmol/kg in the Solomon Sea for the isopycnal layer $24 \text{ kg/m}^3 < \sigma_\theta < 26 \text{ kg/m}^3$ while of 2.5 pmol/kg for the same density layer in the Coral Sea and east of the Solomon archipelago (see station 04, 10, 34 and 71, Fig. 3).
- Fig. 3e shows a slight maximum at station 21, suggesting an input of Solomon Archipelago material into seawater passing through Indispensable Strait.

In addition to these features affecting the profiles, local enrichments are observed at specific stations and depths such as at the surface of stations 36, 57 and 77, very likely reflecting the proximity between these stations and the coast. Within the thermocline some layers also show enriched dREE concentrations (e.g. around 500 m at station 42, 46, 57, 77; in the intermediate waters, around 700 m, at station 13, 21, 34; at 980 m at station 29).

Dissolved cerium (dCe) concentrations are reported in Table 1 and some data will be shown later as part of the discussion. As often observed in seawater where the oxidized Ce(IV) is poorly soluble and then behaves differently to the remaining trivalent REEs, dCe shows a reverse behavior compared to the other dREEs, with high concentrations

Table 3
Average dNd concentration (pmol/kg) in the different layers of the box model.

Water mass	Upper σ_θ (kg/m ³)	Station 34	Station 29	Station 77	Station 57	Station 42
Upper thermocline water (UTW)	24–25.3	0.49 ± 0.01	0.51 ± 0.05	0.49 ± 0.01	0.54 ± 0.02	0.50 ± 0.01
Lower thermocline water (LTW)	25.3–26.9	0.65 ± 0.01	0.57 ± 0.02	1.15 ± 0.01	0.75 ± 0.20	0.72 ± 0.24
Intermediate water (IW)	26.9–27.4	1.21 ± 0.16	1.15 ± 0.14	1.22 ± 0.14	1.08 ± 0.13	1.13 ± 0.20
Upper Circumpolar Deep Water (UCDW) - upper extent	27.4–26.65	2.02 ± 0.12	1.48 ± 0.22	–	1.65 ± 0.04	1.96 ± 0.40
Upper Circumpolar Deep Water (UCDW) - lower extent	27.65–27.76	–	2.44 ± 0.12	–	2.89 ± 0.08	2.87 ± 0.38

at the top of the water column, decreasing at intermediate levels before increasing again slightly in the deep and bottom waters due to its preference for scavenging (see station 29, 42, 71 and 73, Table 1; De Baar et al., 1983; De Baar et al., 1985a; Elderfield et al., 1988; Goldberg et al., 1963; Liu et al., 1988; Piepgras and Jacobsen, 1992; Sholkovitz et al., 1994; Tachikawa et al., 1999). However, consistently with the other dREEs, dCe maxima are observed at some specific locations: in surface layers at station 36 and 77, close to the surface and at 735 m at station 34 and slightly deeper (934 m) at station 29 (Table 1).

4.2. Comparison with previous studies

Two previous studies analyzed samples outside the Solomon Sea and in the Coral Sea (Grenier et al., 2013; Zhang and Nozaki, 1996), allowing us to compare our data with published values. Fig. 4 shows the locations of these stations and the dREE concentrations versus potential density in order to compare the dREE values in the same isopycnal layers. This figure highlights the excellent agreement between our data and these previous results. The minor difference observed between the surface dLa concentrations at SA-7 and at station 82 of our study likely reflects the dissimilarity in our sampling locations and times of the year, in this region of high eddy variability (Keppler et al., 2018).

In Vitiaz Strait, a striking similarity between our results (station 77) and those of Grenier et al. (2013, their station EUC-30) is also observed, despite the difference in sampling times in this highly variable and turbulent region (Fig. 4). This strait is narrow and relatively shallow (1200 m deep) in comparison with Solomon Sea average depth; the continental influence on dREE concentrations is therefore suggested to be high in such location. This constancy of concentration could suggest that the REE concentrations are “buffered” by interplay of different external and internal processes.

4.3. Dissolved REE patterns

Fractionation of the dREEs from each other during oceanic processes (such as particulate scavenging, remineralization, or fresh continental weathering) could be identified using the normalization of dREE concentrations in seawater to those contained in shale, a material representing the average crustal geochemical composition. Here we used the Post-Archean Australian Shale or “PAAS” (McLennan, 1989). The PAAS-normalized REE patterns are presented in Fig. 5.

The main characteristics of the dREE patterns observed in the Coral and Solomon Seas are consistent with those found in the literature: the obvious negative dCe anomalies reflect the impact of the poor solubility and preferential scavenging of this element. The (dNd_n/dYb_n) ratio, which informs about the dLREE versus dHREE slope evolution, is maximum in surface, decreasing from ~0.3 to approximately 0.1 at intermediate level (~1000 m), from where it increases again in the deep and bottom waters. These observations agree with previously published results (Bertram and Elderfield, 1993; De Baar et al., 1985a; Tachikawa et al., 1999; Garcia-Solsona et al., 2014; Grenier et al., 2013, 2018; Zhang and Nozaki, 1996).

dREE patterns are relatively flat in surface waters, which indicates that recent—maybe still ongoing—lithogenic inputs affected these upper layers. The evolution of the pattern shapes with depth reflects the

differential scavenging along the water column. A slight local maximum is often observed for the dMREEs, as already noticed by Grenier et al. (2013) in the same area.

5. Discussion

5.1. Nd and dREE enrichments within the Solomon Sea

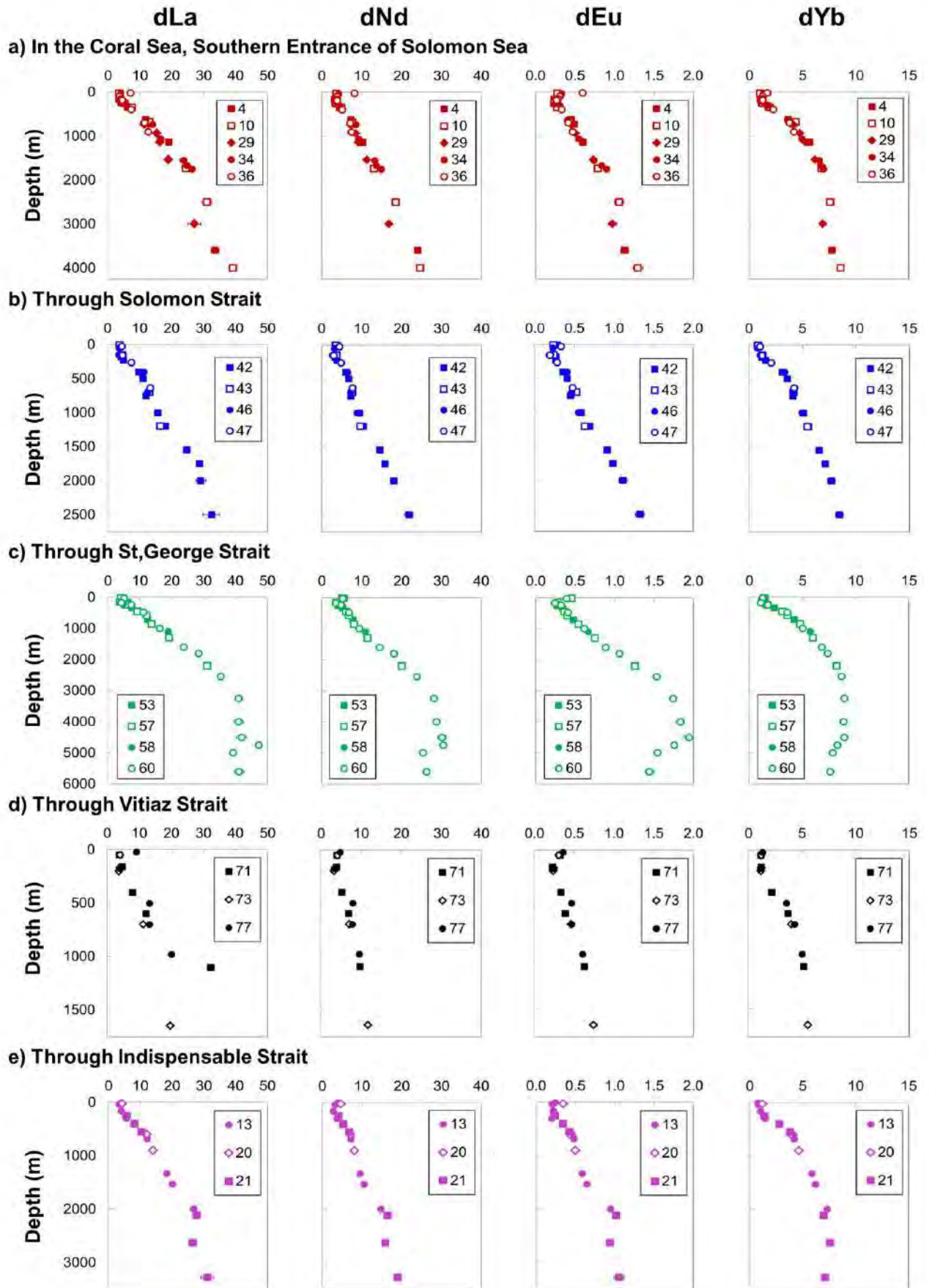
A simple box model was built for the Solomon Sea, allowing us to estimate the dREE budget for different isopycnal layers between its southern entrance (southern section) and its northern exits (Vitiaz Strait, St George's Channel and Solomon Strait). The box model proposed here aims at identifying whether dREE concentrations get enriched, depleted, or stay constant while crossing the Solomon Sea and estimating the associated net fluxes (positive if inputs dominate, negative if outputs dominate, null if inputs and outputs are equivalent). Here we discuss more specifically the Nd budget, results for all the REEs are compiled in Table A in the supplementary material. Further developments that will include the ongoing measurements of Nd isotopic compositions will allow a better quantification of exchange processes, if any. The scheme of the box model is proposed in Fig. 6. This box model is applied to the upper thermocline layer ($\sigma_\theta = 24\text{--}25.3\text{ kg/m}^3$), the lower thermocline layer ($\sigma_\theta = 25.3\text{--}26.9\text{ kg/m}^3$), the intermediate waters ($\sigma_\theta = 26.9\text{--}27.4\text{ kg/m}^3$), and the deeper UCDW waters ($\sigma_\theta = 27.4\text{--}27.65$ and $27.65\text{--}27.76\text{ kg/m}^3$). We also performed the same calculation on a unique box comprising the thermocline and intermediate layers ($\sigma_\theta = 24\text{--}27.4\text{ kg/m}^3$) in order to reveal the enrichment/depletion of dREEs throughout the water column (see Table A in the supplementary material). The lack of water mass transport data for the deep waters prevents us to build the box model down to the bottom (see Table 4).

Our box model considers the Solomon Sea as a closed area at steady state and assumes that incoming and exiting water fluxes are balanced (Fig. 6a). Two upstream sources (incoming NGCU and direct NVJ) are feeding the Solomon Sea across the southern entrance and three downstream fluxes (SGU, NICU and NGCU) are exiting from it through the different straits (NGCU through Vitiaz Strait, SGU through St George's Channel, NICU through Solomon Strait). The required parameters to achieve the model calculation are the water mass transports and the Nd concentrations of each layer. Water flowing equatorward into the Solomon Sea includes the transports of the NGCU (W_E), and of the direct inflow (W_N). Meanwhile, water leaving the Solomon Sea gathers the water fluxes exiting through Solomon Strait (W_S), St. George's Strait (W_G) and Vitiaz Strait (W_V). Respective dissolved Nd concentrations considered here are Nd_E, Nd_N at the southern entrance and Nd_S, Nd_G and Nd_V at the northern exits (Fig. 6a and b). Under the hypothesis that diapycnal mixing is weak in this area, we obtain, for each density layer, the following equation:

$$W_E \cdot [Nd]_E + W_N \cdot [Nd]_N + F_{\text{tot PANDORA}} = W_S \cdot [Nd]_S + W_G \cdot [Nd]_G + W_V \cdot [Nd]_V \quad (1)$$

where $F_{\text{tot PANDORA}}$ is the total net flux into seawater from the surrounding coasts.

The transports are computed for each density layer using the



(caption on next page)

Fig. 3. Profiles of dissolved REE concentrations for La, Nd, Eu and Yb. Stations are gathered into five groups with the color codes consistent with their geographical location as proposed in Fig. 1;

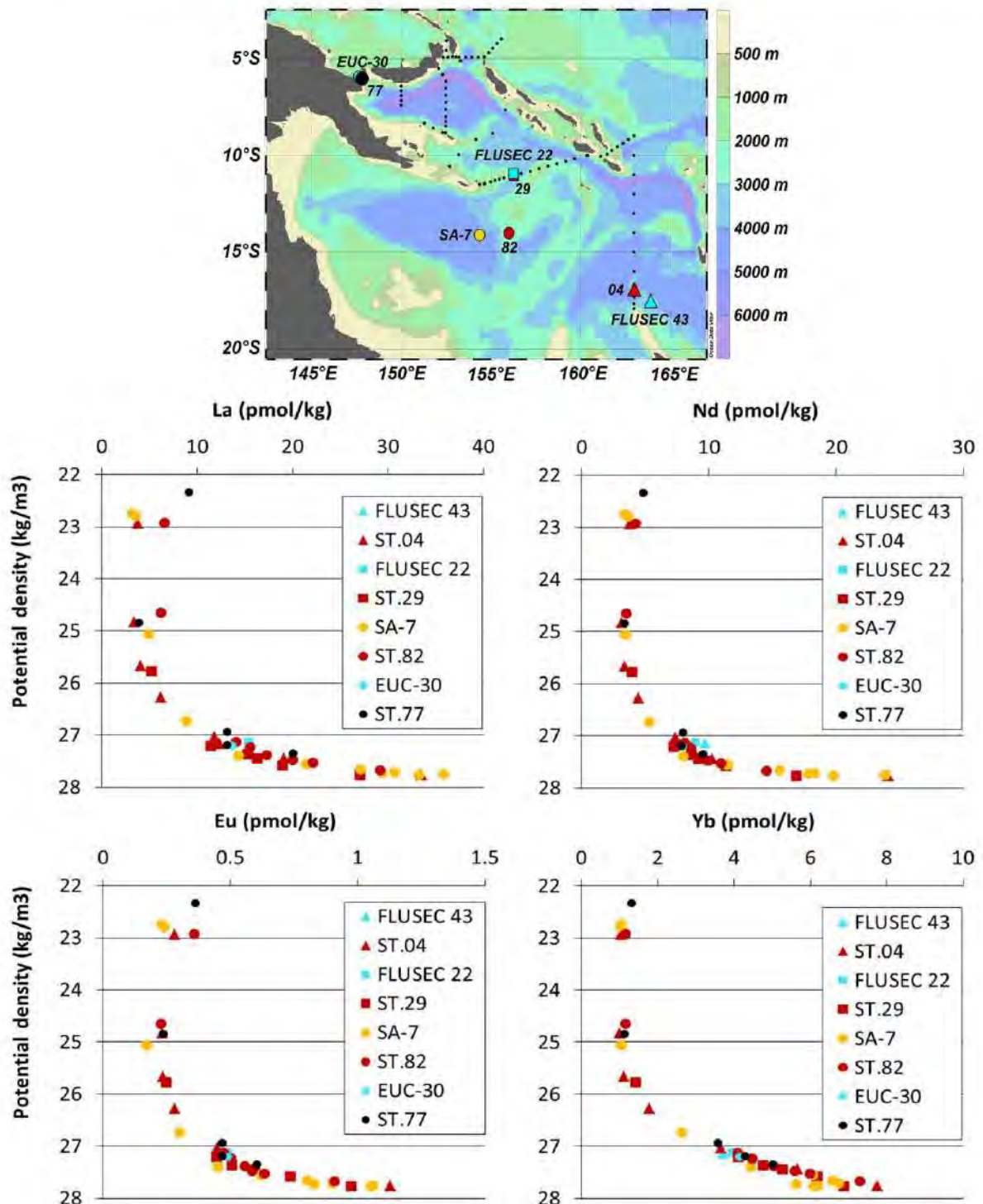


Fig. 4. Comparison of our data with those measured in the framework of preceding studies. Yellow point represent data from station SA-7 (sampled during September–October 1992) located in the middle of the Coral Sea and measured by Zhang and Nozaki (1996). Aqua square, triangle and dot represent data measured at the entrance of Solomon (FLUSEC 22), Coral sea (FLUSEC 43) and at exiting Vitiaz Strait (EUC-30), respectively, measured by Grenier et al. (2013). It is noted that all sample using in study of Grenier was sampled in August–September 2006. Sampling date of our samples are reported in Table 1. (For interpretation of the references to color in this figure legend, the reader is referred to the web version of this article.)

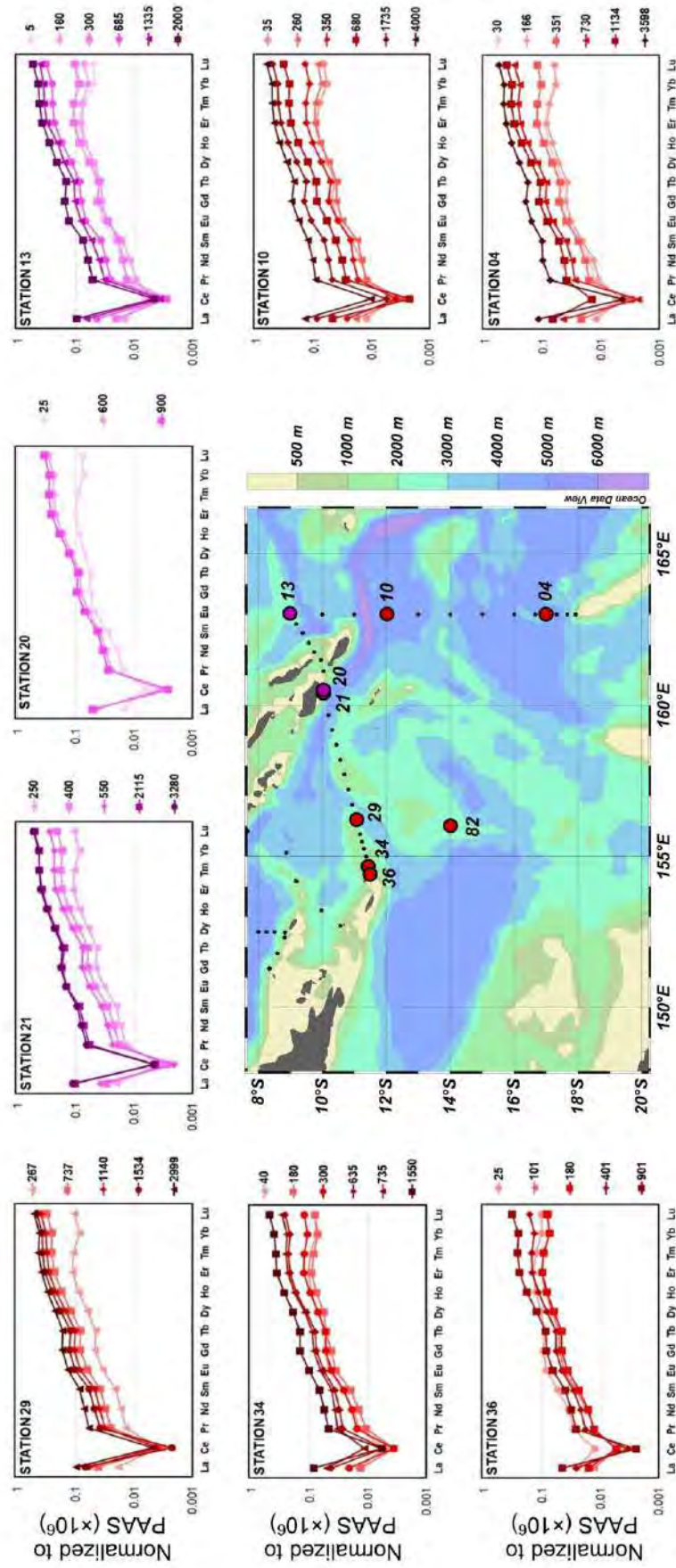


Fig. 5. dREE patterns normalized to PAAS ($\times 10^6$) at different depths for 8 stations sampled in the Coral Sea and at the entrance of Solomon Sea and for 12 stations located in the Solomon Sea and in the different straits. The light colors indicate shallow samples while darker colors represent the deeper ones.

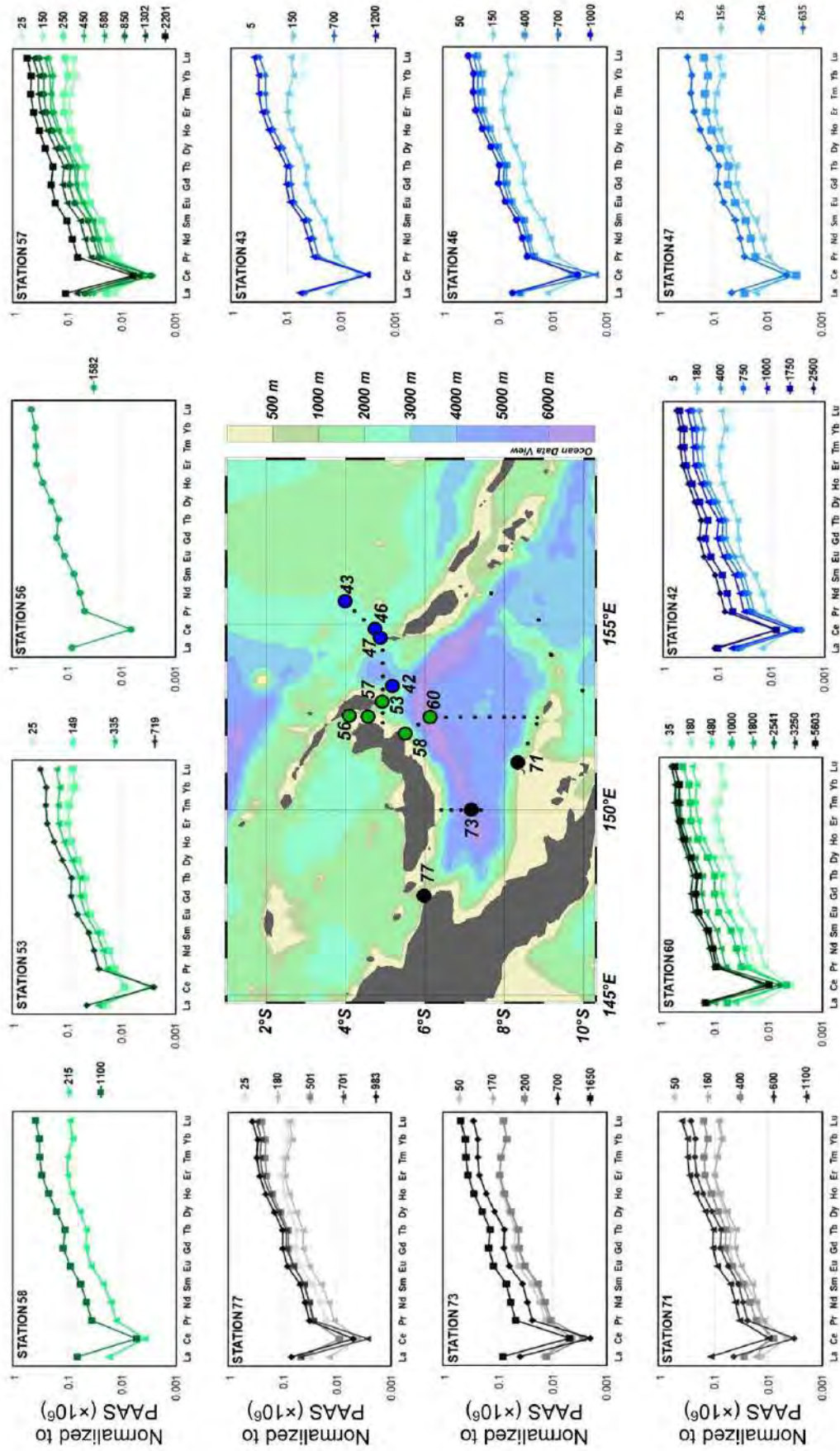


Fig. 5. (continued)

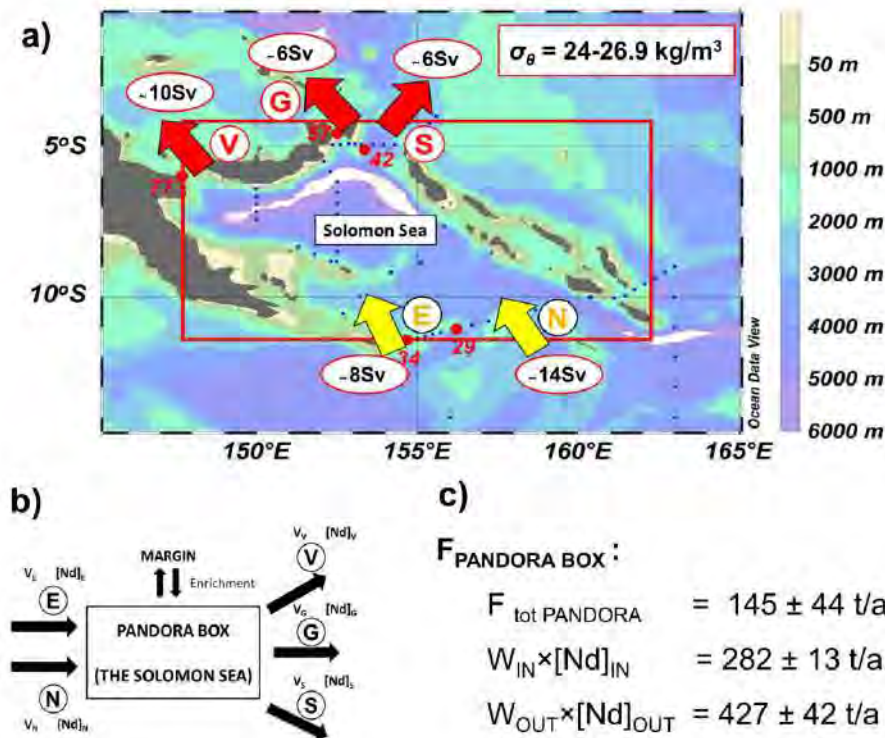


Fig. 6. a) Schematic description of the Pandora box (red rectangular). The water layer is defined in Table 4. Yellow arrows indicate southern input while red arrows characterize output flow through three straits. Meanwhile, colored letters coupled with number indicate different stations together with their transport. E: NGCU transport, N: direct NVJ transport, V, G and S: Vitiaz Strait, St George's Channel and Solomon Strait transports, respectively. b) Enrichment visualizing by simple Pandora box with 2 southern inputs and 3 northern outputs as presented in Fig. 6a. The Nd concentrations taken into account here are $[Nd]_E$, $[Nd]_N$ in the south and $[Nd]_S$, $[Nd]_G$ and $[Nd]_V$ in the north. c) Significant enrichment is observed at Lower Thermocline Water; all fluxes are reported in Table 4. (For interpretation of the references to color in this figure legend, the reader is referred to the web version of this article.)

Table 4

Water masses and associated volume transports (Sv) of different density layers during Pandora. The dNd fluxes were estimated from dNd values compiled in Table 3 and water transports entering and leaving the Solomon Sea.

Water mass	Upper σ_θ (kg/m ³)	Lower σ_θ (kg/m ³)	Incoming NGCU $\{W_{IN}\}$	Direct NVJ $\{W_{S}\}$	Vitiaz $\{W_V\}$	St-Georges $\{W_G\}$	Solomon $\{W_S\}$	dNd flux (ton/year)
UTW	24	25.3	1.5 ± 0.5	3.5 ± 0.5	1.5 ± 0.5	1.5 ± 0.5	2.0 ± 0.5	1 ± 16
LTW	25.3	26.9	9.2 ± 0.5	7.8 ± 0.5	8.0 ± 0.5	4.0	5 ± 0.5	145 ± 45
IW	26.9	27.4	7.2 ± 1.0	1.2 ± 1.0	4.5	1.4	2.5 ± 1.0	-4 ± 51
UCDW - upper extent	27.4	27.65	1.0 ± 0.5	4.5 ± 1.5	-	1.5 ± 0.5	4.0 ± 0.5	49 ± 104
UCDW - lower extent	27.65	27.76	-	3.0 ± 2.0	-	0.5	2.5 ± 2.0	25 ± 138

PANDORA cruise data (Ganachaud et al., 2017; Germinesud et al., 2016). Currents were recorded along the ship track with Shipboard Acoustic Doppler Current Profilers (S-ADCPs) with a vertical extent of around 1000–1300 m. S-ADCPs were rotated to estimate the current perpendicular to each of the box model section (Germinesud et al., 2016). Deeper than 1000 m, they are combined with geostrophic velocities estimated with CTD station pairs, and referenced to 3000 m depth, or to the deepest common level of the station pairs.

Transports computed across the southern entrance do not balance the summed transports at the exits, as they were estimated during instantaneous transects. For the purpose of this study, relying on a steady state hypothesis, velocities are adjusted with an inverse model allowing the mass, salt and heat conservation (Germinesud et al., 2016). The water transports and associated uncertainties are given, for each layer, in Table 4.

The calculation is reported in Fig. 6c for Nd in the lower thermocline layer, and budgets for the other layers are reported in Table 4. The only missing dREE concentration data are for the upper thermocline at station 29. We therefore estimated these values using its neighbor stations due to their similarity in dREE concentrations (stations 04, 34 and 36). The sign of $F_{tot PANDORA}$ indicates whether external input of Nd (when positive) or subtraction by scavenging process (when negative) dominates along the pathways of the different water layers. A Monte Carlo statistic method (normal distribution, $n = 1000$) was used to

estimate uncertainties of the fluxes.

A significant positive net flux ($F_{tot PANDORA} = 145 \pm 46$ t(Nd)/year; Fig. 6c) is estimated in the lower thermocline, suggesting that waters leaving the Solomon Sea export more dNd than waters entering the Solomon Sea, indicating a net gain of dNd in this layer. Grenier et al. (2014) did not show any enrichment of this layer upstream the Solomon Sea while they similarly found a dNd enrichment downstream, more specifically along the Papua New Guinea coast. The present study fills a gap of this preceding work by showing that dNd enrichment also occurs within the Solomon Sea. Both studies demonstrate that the Lower Thermocline is enriched before filling the Equatorial Undercurrent. Enrichments are also observed in the other layers, except for IW. However, the large uncertainties affecting the calculated fluxes prevent us from drawing firm conclusions for these layers (Table 4).

Contrastingly, in the upper thermocline, our results do not show a clear and strong enrichment in Nd content. Our hypothesis is that the dNd (dREE) external inputs, likely weathered from the surrounding islands and discharged into the Solomon Sea, are balanced by the dNd (dREE) removal by scavenging, consistent with the productivity of the area (Radenac et al., 2013; Bonnet et al., 2016). This will be confirmed or disproved by the isotopic Nd measurements.

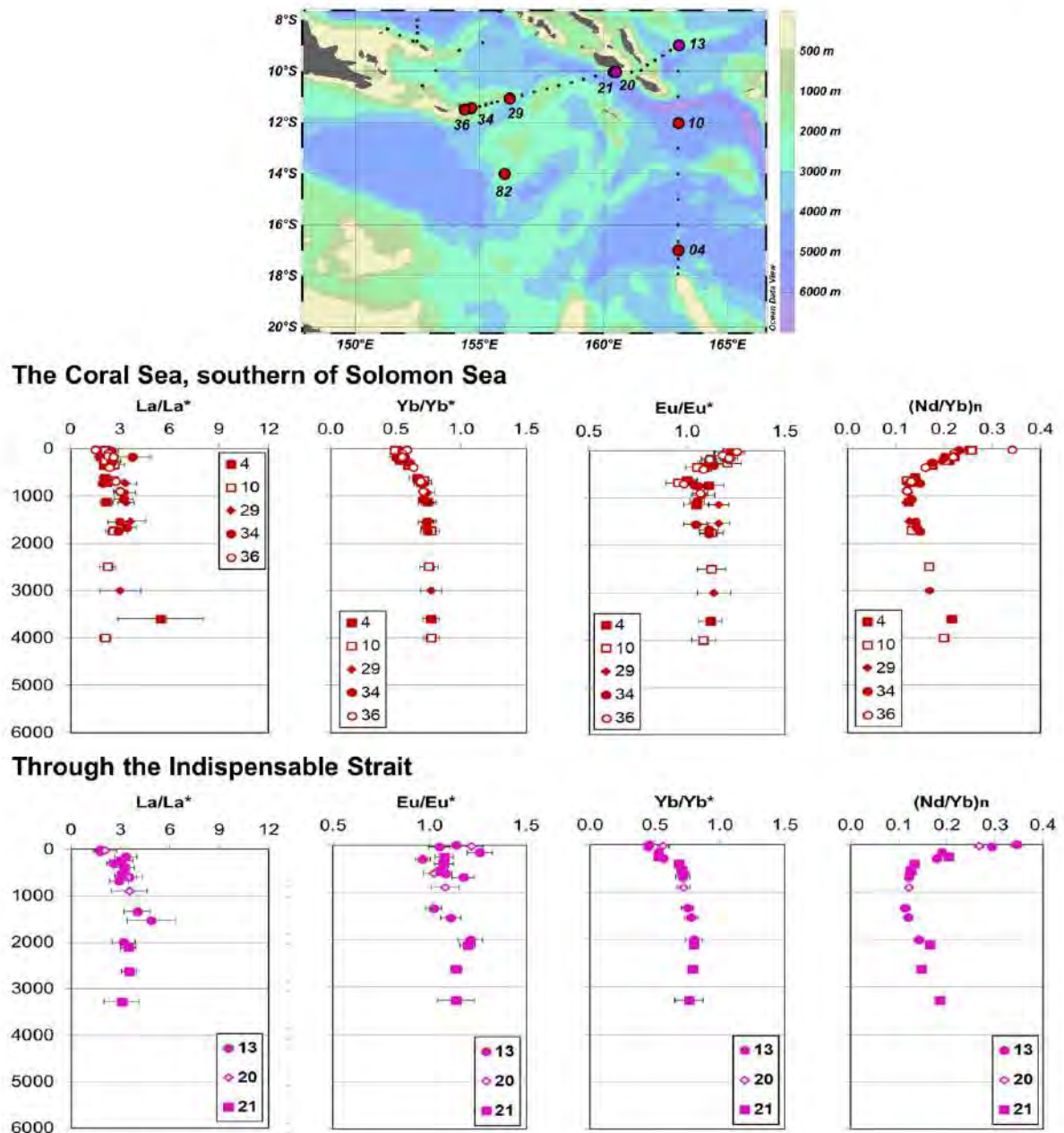


Fig. 7. Vertical profiles of the anomalies of La (La/La^*), Eu (Eu/Eu^*), Yb (Yb/Yb^*) and of ratio $(Nd/Yb)_n$ calculated following Bau et al. (2004), Bau et al. (1996), Friend et al. (2008), and García-Solsona et al. (2014). The color of markers follows the color code of Fig. 1. $(Nd/Yb)_n$ profiles are also reported after normalization to basalt (orange markers), for comparison with the PAAS-normalized ones.

5.2. Interesting features in the dREE profiles

This section discusses more specifically the dREE PAAS-normalized patterns and anomalies. Calculated dREE anomalies allow identifying if, after normalization to the PAAS values, an element is enriched or depleted relatively to its neighbors. Thus, they can bring information about the dominant mechanisms affecting the local marine REE pool. Anomalies are calculated following the equations below (Bau et al., 2004; Bau et al., 1996; Friend et al., 2008; García-Solsona et al., 2014). In the following, we will discuss more specifically the La, Ce, Eu and Yb anomalies. The REE/REE* ratio reveals an enrichment relatively to its neighbors when its value is larger than one, and a depletion in the opposite case.

$$\frac{La}{La^*} = \frac{[La]_n}{3[Pr]_n - 2[Nd]_n} \tag{1}$$

$$\frac{Ce}{Ce^*} = \frac{[Ce]_n}{2[Pr]_n - [Nd]_n} \tag{2}$$

$$\frac{Eu}{Eu^*} = \frac{4 \times [Eu]_n}{3[Sm]_n + [Dy]_n} \tag{3}$$

$$\frac{Yb}{Yb^*} = \frac{[Yb]_n}{2[Er]_n + [Dy]_n} \tag{4}$$

A complementary parameter to the anomalies is the ratio between normalized LREEs and HREEs, expressed as Nd_n/Yb_n , which provides information about the slope of the normalized dREE pattern. Fig. 7 shows the vertical profiles for the La, Eu, Yb anomalies and the Nd_n/Yb_n

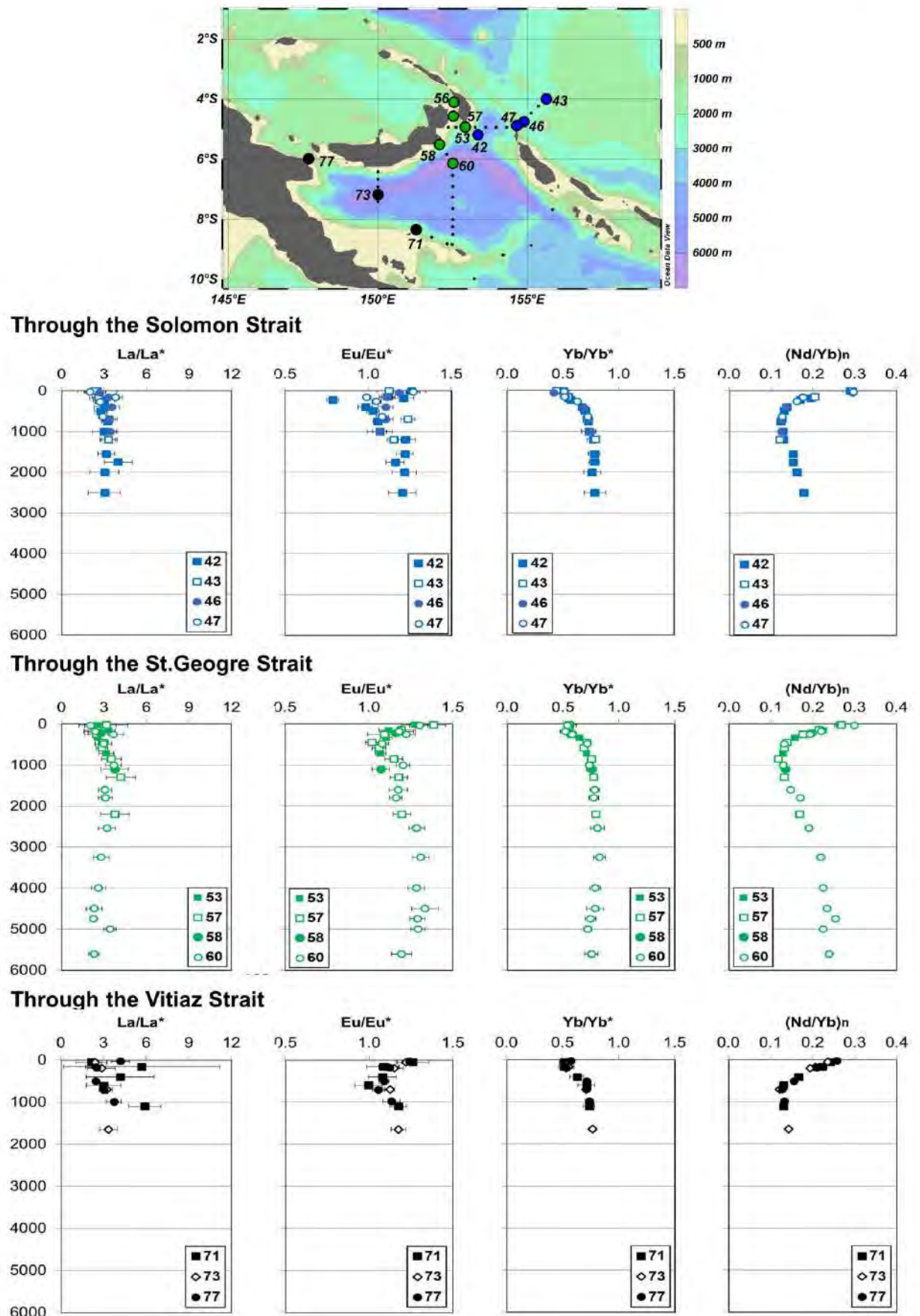


Fig. 7. (continued)

slope. Normalization of the dREEs to PAAS suggests that without any fractionation between the dREEs within the water column, the dREE pattern would be flat $-Nd_n/Yb_n$ equal to 1- or marked by a slight positive Eu anomaly if the lithogenic material is basaltic (Grenier et al., 2013). The full data set is reported in Table 1.

5.2.1. Dissolved lanthanum anomaly

All the dissolved Solomon Sea samples collected during Pandora are characterized by positive La anomalies, with values ranging from 3 to 6 (Fig. 7). Such positive values have been observed elsewhere in the ocean (e.g. Garcia-Solsona et al., 2014; Grenier et al., 2018) and are believed to result from a differential La behavior due to the lacking electron in the 4f shell of the La atom, suspected to increase its stability in seawater, so called the “tetrad” or “double-double” effect (Byrne and Kim, 1990; Byrne and Sholkovitz, 1996; De Baar et al., 1985b; Elderfield et al., 1988; Garcia-Solsona et al., 2014; Grenier et al., 2018; Lee and Byrne, 1993; McLennan, 1994). In particular, while dLa is released from riverine particles when freshwaters are discharged into the ocean, more efficient releasing than scavenging rate could cause local positive dLa anomalies (Lawrence and Kamber, 2006).

Nevertheless, the positive dLa anomalies in the Solomon Sea are observed at all the monitored stations, even those located far from the coastline. The oceanic dREE pattern may result from dissolved-particle exchange also occurring in the open ocean (Byrne and Kim, 1990; Schijf et al., 2015; Tachikawa et al., 1999), so we are seeking if another factor than the “Tetrad effect” only could govern the La behavior in the Coral and Solomon Seas.

Due to the similar atomic size and close chemical properties of barium and lanthanum, they are suspected to display coupled behavior in seawater (Garcia-Solsona et al., 2014; Haley et al., 2014; Grenier et al., 2018). Bishop (1988) and Dehairs et al. (1980) demonstrated that oceanic dBa distribution is governed by the surface biologically driven formation of barite crystal ($BaSO_4$) followed by its dissolution at depth. Coupling between the two elements could therefore occur if dLa is associated to the dBa/barite cycle within the water column (Dehairs et al., 1980; Garcia-Solsona et al., 2014; Grenier et al., 2018; Gulchard et al., 1979). Although significant correlations between dLa and dBa concentrations were observed at some stations in the Solomon Sea, these correlations do not hold when incorporated in a plot representing the world ocean dBa and dLa data, extracted from the GEOTRACES IDP 2017 (see Fig. A3 and A4, supplementary material). We therefore consider that our data do not help assessing the dLa-dBa link.

A third mechanism that could yield La fractionation is of microbial origin. Indeed, Shiller et al. (2017) revealed that some methanotroph bacteria require LREE and more specifically La as enzyme co-factor. However, it seems that this process subtracts La from the water column, while we observe a La enrichment. In any case, this hypothesis needs further investigation.

5.2.2. Dissolved europium anomaly

All normalized dREE patterns display a positive Eu anomaly whatever the water mass type and sample location. Such positive dEu anomalies were observed in previous studies (Amakawa et al., 2000; Nozaki et al., 1999) but were not discussed till the work of Zhang et al. (2008) and the more recent observations of Grenier et al. (2013, 2018). Either on the Kerguelen plateau (Grenier et al., 2018; Zhang et al., 2008) or in the Equatorial Pacific (Grenier et al., 2013) these authors invoke a remaining signature of lithogenic inputs of basaltic origin, local basalts being characterized by a positive Eu anomaly.

In our studied area, the dEu shows maxima in the surface water, reach a minimum at intermediate depths (~500 m) and then slightly increase again toward bottom except in the Coral Sea profiles characterized by fairly constant dEu anomalies at depths below 1000 m (Fig. 7).

The higher dEu anomalies (~1.3) at the surface likely reflect recent enrichments of lithogenic origin, which could be of coastal or

atmospheric source. Indeed, the Solomon Sea is surrounded by volcanic islands whose basaltic material is enriched in Eu (Grenier et al., 2013). Basalt REE patterns (normalized to PAAS) originating from the New Britain (Holm et al., 2013) and (Kelemen et al., 2013). Tonga islands are reported in Fig. A5. While quite different in shape, both displays a marked positive Eu anomaly, confirming the Eu enrichment in these outcropping material. Besides, some volcanoes such as Rabaul, Ulawun and Bagana, are still very active (Lefèvre et al., 2008; Slemons et al., 2010). The variable REE basalt patterns shown in Fig. A5a makes difficult to select one of those to normalize our seawater dREE dataset to the local material. However, Fig. A5b displays the Eu anomaly profiles when normalized to the 3 basalt REE values. The resulting negative anomalies suggest that internal processes modified the relative abundance of Eu to its trivalent neighbors.

Deeper than 1000 m, the positive dEu anomaly increase could result from two non-exclusive processes. The first presumed process is the release of dREE in intermediate and deep layers caused by the dissolution of basaltic sediments deposited on the margins by submarine weathering followed by the advection of the enriched waters (Grenier et al., 2013; Jeandel et al., 2011; Zhang et al., 2008). As already underlined by Grenier et al. (2013), the preservation of this dEu anomaly is made possible by the fact that the residence time of dEu (320–820 years; Alfaro and Nozaki, 1999) is larger than that of the thermocline waters across the studied area (10–15 years, Fukumori et al., 2004). Another explanation was recently suggested by Grenier et al. (2018): the deep positive dEu anomaly may also result from LREE/MREE preferential scavenging onto surface coating of organic particles in surface water followed by their release at depth (Sholkovitz et al., 1994). Ongoing measurements of the filtered particles might help to characterize the importance of such processes in the Solomon Sea.

5.2.3. Dissolved cerium anomalies

Contrasting to dLa and dEu, the marked depletion of dCe is observed at almost all the studied stations, although less pronounced in the surface and subsurface waters above 500 m ($dCe/dCe^* \geq 0.4$). Consistent with the higher dEu anomalies discussed above, these less pronounced dCe anomalies might reflect recent lithogenic inputs, which likely impact preferentially the upper layers. Higher dCe anomalies ($dCe/dCe^* \geq 0.5$) were found mostly in the surface water of stations located around the Solomon archipelago (e.g. stations 42, 43, 60), indicating more recent inputs. Specifically, one sample in the upper thermocline at station 71 (160 m) shows a significantly high positive dCe anomaly (~1.4). However, this station is very close to the coast and was located here to identify any margin input to the waters conveyed by the NGCU through the split between Papua New Guinea main island and Woodlark island; the existence of strong inputs is thus confirmed by the high positive Ce anomaly observed at this station.

5.2.4. HREE behavior

The vertical dHREE profiles show more convex shapes than the other dREE ones (Fig. 3). In addition, the Nd_n/Yb_n slopes are increasing below intermediate depths at a rate of two up to the seafloor (Fig. 7). Such rapid increase was already observed although not always discussed (Grenier et al., 2018; Haley et al., 2014; Jeandel et al., 2013; Molina-Riescher et al., 2014). Bertram and Elderfield (1993) noticed that coupling between dREE and dSi cycle could be more significant for the dHREE than for the dLREE and recent field work of Akagi (2013) and Grenier et al. (2018) seem to confirm this observation. Here we propose to explore deeper the link between dHREE (represented by dYb) and the dSi cycle. In Fig. 8, only the data acquired in this work are reported. Fig. 8a shows that dNd relationship with dSi is dispersed, as shown by the correlation coefficients, ranging from 0.04 above the thermocline to 0.75 below. This contrasts with the better relationship observed between dYb and dSi in Fig. 8b ($R^2 = 0.66$ above the thermocline and 0.93 below). To go further, we extended this comparison to a broader scale (see Fig. A1 and A2 in the supplementary material).

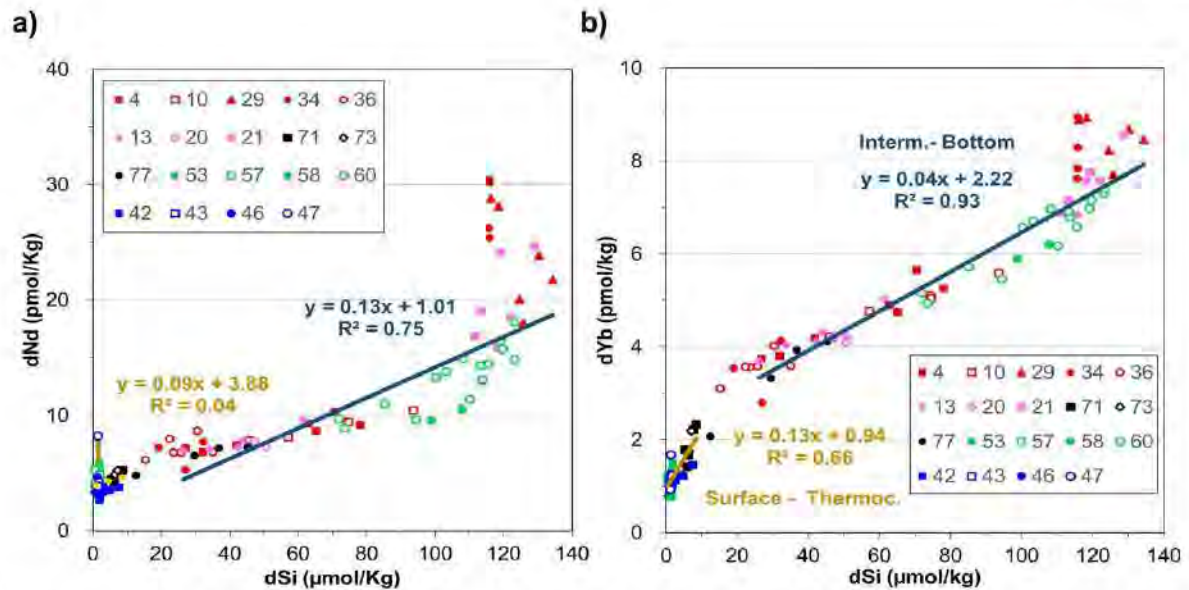


Fig. 8. Relationship between a) dNd and b) dYb (in pmol/kg) versus dSi (in $\mu\text{mol/kg}$) in Surface-Thermocline and Intermediate-Bottom layers in the Solomon Sea.

The comparison of the Solomon Sea data with the dREE data collected over the whole Atlantic Ocean shows the high values of the correlation coefficients ($\sim R^2 = 0.9$). This supports the hypothesis of a coupling between dYb and dSi except in the upper layers: for dSi concentrations below $20 \mu\text{M}$, dSi and dYb data are more dispersed. The dLREE relationship with dSi is clearly different and more scattered than the dHREE one, as illustrated for dNd in Fig. A1. In the deep layers, the observed dYb/dSi slope of the linear fitting curve is consistent with the dEr/dSi one found by Bertram and Elderfield (1993) in the intermediate, deep and bottom waters of the Pacific Ocean ($\Delta\text{dHREE}/\Delta\text{dSi} \sim 0.04$; see Fig. 8b of Bertram and Elderfield, 1993).

The shape of the global and local curves reflects several common features: for $\text{dSi} < 20 \mu\text{M}$, a faster release (rather than a slower removal; see below) of Yb than of Si generates a steep and very scattered slope; deeper, the increase rate of dYb significantly diminishes and is strongly correlated to the Si one. This could reflect differential release of Yb and Si from the particles, a fraction of Yb being adsorbed and easily released, and the remaining part being possibly adsorbed in the silica tests as suggested by Akagi (2013). Another explanation could be that complexation between dREE and silicate (only found to be significant in the deep Pacific water; Patten and Byrne, 2017) could explain this differential behavior with depth between the 2 species. However, Patten and Byrne (2017) underline that we don't have so far the correct thermodynamic data for the whole series of REEs to conclude further. Similar break in the dYb/dSi slope was observed on the Kerguelen plateau (Grenier et al., 2018), but the lack of reliable kinetic and thermodynamic data invite to interpret cautiously the relationship between REE and the opal uptake/remineralization in the different oceanic environments.

Nevertheless, while there is no pronounced difference for the dYb-dSi ratio between the deep Atlantic and Pacific, Fig. 8b shows that for the same dSi content, dYb values are larger in the north Atlantic than in the south Atlantic or in the Pacific. Such gradient likely reflects the fact that the Si cycle is mostly driven by biological uptake-remineralization while Yb one is sensitive to lithogenic external inputs (more important in the Atlantic) and scavenged by different processes (adsorption, possible opal stripping...).

5.3. Origin of the dREE enrichments in the Solomon Sea

Based on features discussed in the preceding Subsection 5.2, the

dNd (dREE) enrichment calculated with our box model (Section 5.1) likely results from the release of dNd (dREEs) from the surface and submarine weathering of the surrounding islands. Several complementary parameters allowed us to confirm the nature of this external dNd source and its signature in the dissolved phase. In this aim, the full set of measured dMn and dAl analyzed by Susanna Michael are proposed in Table C in the Supplementary material (Michael et al., submitted). Surface dEu enrichments and larger dCe values are consistent with similar high concentrations observed in the dAl and dMn profiles (Michael et al., submitted). In addition, consistent maxima of dREEs, dAl and dMn are also observed at some specific points in the thermocline and intermediate layers (i.e. stations 04-1000 m; 10-350 m; 20-700 m; 42-700 m; 71-300 m; 77-500 m). Such consistencies underline that submarine weathering took place along the island margins. The Solomon Sea is an area of strong internal wave activity and associated mixing (Alberty et al., 2017). It has been suggested that when the continental slope is close to a critical angle, the strong bottom shear velocities enhance sediment resuspension and potential release of chemical elements (Cacchione et al., 2002). Nepheloid layers might result from these processes and be advected further from the slope, contributing to the observed enrichments. The exact location of such resuspension events could be an interesting investigation for future studies.

6. Conclusion

This study presented vertical profiles of dREE concentrations for 143 samples and 21 stations collected in the Coral and Solomon Seas as part of the PANDORA cruise (summer 2012). Although the profile shapes display common dREE features -i.e. surface depleted and enriched at depth- the dREE patterns and anomalies could be discussed and lead to interesting results.

A pronounced dissolved positive dLa anomaly is estimated (dLa^*/dLa varying between 3 and 6). Despite the interesting correlation between dBa and dLa in our data, we could not demonstrate that this anomaly was linked to the Ba-Barite cycle. This specific lanthanum behavior likely relates more to the "tetrad" effect. The future analysis of particulate La and biogenic particulate Ba may bring further information.

A ubiquitous europium positive anomaly is also found in the dREE patterns, with higher dEu/dEu⁺ values in the upper layers. This striking

feature agrees with previous observations (Grenier et al., 2013, 2018; Zhang et al., 2008) and suggests that the enrichment calculated with the box model is of basaltic origin, consistent with the geology of the surrounding islands. The lithogenic character of this source is later supported by dCe anomaly.

dHREE behaviour seem to be mostly influenced by the Si cycle as suggested by Akagi (2013) and also observed by Grenier et al. (2018). However, HREE are also scavenged by adsorption on the settling particles, which explains differential fates of both tracers in the upper layers ($dSi < 20 \mu M$).

A box model allowed us to establish the net dNd (dREE) fluxes of the waters flowing equatorward through the Solomon Sea. Significant enrichment is observed for the Lower Thermocline Layer (between 200 and 500 m; $F_{total} PANDORA = 145 \pm 46$ tons of Nd per year). This enrichment is of main interest, as these waters will eventually be advected till the equatorial eastern Pacific through the lower part of the EUC (Slemons et al., 2010; Grenier et al., 2011). By contrast, the lack of clear net enrichment in the upper thermocline is surprising in this area bounded by continental margins and with many potential sources. However, the large error bars prevent us from drawing conclusions about what is happening in other layers. This points to the complexity of boundary exchange processes and to the need of better understanding the removal processes of the oceanic dissolved material. The ongoing analysis of the associated particles and Nd isotopic composition will also help to refine our understanding of these net exchange fluxes.

Acknowledgements

This work is a contribution to the CLIVAR/SPICE and GEOTRACES International programs. We thank the technical division of INSU (DT-INSU) Olivier Desprez de Gesincourt and Lionel Fichen who made possible the various in situ measurements, thereby requiring skills and care. The collaboration with SOPAC/SPC, PI-GOOS, and University of Papua New Guinea was greatly appreciated. We also acknowledge Benjamin Dupont for his volunteering help during the on-board sampling. The accomplishments were made possible through concurrent contributions of national funding agencies. The Pandora cruise has been co-funded by NSF grant OCE1029487, and by ANR project ANR-09-BLAN-0233-01 and INSU/LEFE project Solwara (IDAO and CYBER). All the authors whose work contributed to the database GEOTRACES are acknowledged (<http://www.geotraces.org>; <http://www.solomon-sea-oceanography.org>). Besides of that, we would like to thank the research TIM at LEGOS for insightful comment and encouragement. C. Pradoux and F. Candaudap are thanked for their technical supports.

Appendix A. Supplementary data

Supplementary data to this article can be found online at <https://doi.org/10.1016/j.chemgeo.2019.05.012>.

References

Abbott, A.N., Haley, B.A., McManus, J., Reimers, C.E., 2015. The sedimentary flux of dissolved rare earth elements to the ocean. *Geochim. Cosmochim. Acta.* <https://doi.org/10.1016/j.gca.2015.01.010>.

Akagi, T., 2013. Rare earth element (REE)-silicic acid complexes in seawater to explain the incorporation of REEs in opal and the 'leftover' REEs in surface water: new interpretation of dissolved REE distribution profiles. *Geochim. Cosmochim. Acta.* <https://doi.org/10.1016/j.gca.2013.03.014>.

Akagi, T., Fu, F., Hongo, Y., Takahashi, K., 2011. Composition of rare earth elements in settling particles collected in the highly productive North Pacific Ocean and Bering Sea: Implications for siliceous-matter dissolution kinetics and formation of two REE-enriched phases. *Geochim. Cosmochim. Acta.* <https://doi.org/10.1016/j.gca.2011.06.001>.

Alberty, M.S., Sprintall, J., et al., 2017. Spatial patterns of mixing in the Solomon Sea. *Journal of Geophysical Research: Oceans* 122, 4021–4039. <https://doi.org/10.1002/2016JC012666>.

Alibo, D.S., Nozaki, Y., 1999. Rare earth elements in seawater: particle association, shale-

normalization, and Ce oxidation. *Geochim. Cosmochim. Acta.* [https://doi.org/10.1016/S0016-7037\(98\)00279-8](https://doi.org/10.1016/S0016-7037(98)00279-8).

Amakawa, H., Alibo, D.S., Nozaki, Y., 2000. Nd isotopic composition and REE pattern in the surface waters of the eastern Indian Ocean and its adjacent seas. *Geochim. Cosmochim. Acta* 64, 1715–1727. [https://doi.org/10.1016/S0016-7037\(00\)00333-1](https://doi.org/10.1016/S0016-7037(00)00333-1).

Bai, M., Koschinsky, A., Dulski, P., Helne, J.R., 1996. Comparison of the Partitioning Behaviours of Yttrium, Rare Earth Elements, and Titanium between Hydrothermal Marine Ferromanganese Crusts and Seawater.

Bau, M., Alexander, B., Chesley, J.T., Dulski, P., Brantley, S.L., 2004. Mineral dissolution in the Cape Cod aquifer, Massachusetts, USA: I. Reaction stoichiometry and impact of accessory feldspar and glauconite on strontium isotopes, solute concentrations, and REY distribution. *Geochim. Cosmochim. Acta.* <https://doi.org/10.1016/j.gca.2003.08.015>.

Behrens, M.K., Muratli, J., et al., 2016. Rapid and precise analysis of rare earth elements in small volumes of seawater - Method and intercomparison. *Mar. Chem.* <https://doi.org/10.1016/j.marchem.2016.08.006>.

Bertram, C.J., Elderfield, H., 1993. The geochemical balance of the rare earth elements and neodymium isotopes in the oceans. *Geochim. Cosmochim. Acta.* [https://doi.org/10.1016/0016-7037\(93\)90087-D](https://doi.org/10.1016/0016-7037(93)90087-D).

Bishop, J.K.B., 1988. The barite-opal-organic carbon association in oceanic particulate matter. *Nature* 332, 341–343. <https://doi.org/10.1038/332341a0>.

Bonnet, S., Berthelot, H., et al., 2016. Diazotroph derived nitrogen supports diatom growth in the South West Pacific: a quantitative study using nanoSIMS. *Limnol. Oceanogr.* <https://doi.org/10.1002/lno.10300>.

Bostock, H.C., Opdyke, B.N., Williams, M.J.M., 2010. Characterising the intermediate depth waters of the Pacific Ocean using $\delta^{13}C$ and other geochemical tracers. *Deep-Sea Research Part I: Oceanographic Research Papers.* <https://doi.org/10.1016/j.dsr.2010.04.005>.

Byrne, R., Sholkovitz, E., 1996. Chapter 158 Marine Chemistry and Geochemistry of the Lanthanides. pp. 497–593. doi: [https://doi.org/10.1016/S0168-1273\(96\)23009-0](https://doi.org/10.1016/S0168-1273(96)23009-0) (C).

Byrne, R.H., Kim, K.H., 1990. Rare earth element scavenging in seawater. *Geochim. Cosmochim. Acta.* [https://doi.org/10.1016/0016-7037\(90\)90002-3](https://doi.org/10.1016/0016-7037(90)90002-3).

Cacchione, D.A., Pratson, L.F., Ogston, A.S., 2002. The shaping of continental slopes by internal tides. *Science.* <https://doi.org/10.1126/science.1069803>.

Chung, C.H., Brenner, I., You, C.F., 2009. Comparison of microconcentric and membrane-desolvation sample introduction systems for determination of low rare earth element concentrations in surface and subsurface waters using sector field inductively coupled plasma mass spectrometry. *Spectrochimica Acta - Part B Atomic Spectroscopy* 64, 849–856. <https://doi.org/10.1016/j.sab.2009.06.013>.

Cravatte, S., Ganachaud, A., Duong, Q.P., Kessler, W.S., Eldin, G., Dutrieux, P., 2011. Observed circulation in the Solomon Sea from SADCP data. *Prog. Oceanogr.* <https://doi.org/10.1016/j.poc.2010.12.015>.

Crusius, J., Calvert, S., Pedersen, T., Sage, D., 1996. Rhenium and molybdenum enrichments in sediments as indicators of oxic, suboxic and sulfidic conditions of deposition. *Earth Planet. Sci. Lett.* [https://doi.org/10.1016/S0012-821X\(96\)00204-X](https://doi.org/10.1016/S0012-821X(96)00204-X).

Davis, R.E., Kessler, W.S., Sherman, J.T., Davis, R.E., Kessler, W.S., Sherman, J.T., 2012. Gliders measure western boundary current transport from the South Pacific to the equator*. *J. Phys. Oceanogr.* 42, 2001–2013. <https://doi.org/10.1175/JPO-D-12-022.1>.

De Baar, H.J.W., Bacon, M.P., Brewer, P.G., 1983. Rare-earth distributions with a positive Ce anomaly in the Western North Atlantic Ocean. *Nature* 301, 324–327. <https://doi.org/10.1038/301324a0>.

De Baar, H.J.W., Brewer, P.G., Bacon, M.P., 1985a. Anomalies in rare earth distributions in seawater: Gd and Tb. *Geochim. Cosmochim. Acta.* [https://doi.org/10.1016/0016-7037\(85\)90090-0](https://doi.org/10.1016/0016-7037(85)90090-0).

De Baar, H.J.W., Bacon, M.P., Brewer, P.G., Bruland, K.W., 1985b. Rare earth elements in the Pacific and Atlantic Oceans. *Geochim. Cosmochim. Acta.* [https://doi.org/10.1016/0016-7037\(85\)90089-4](https://doi.org/10.1016/0016-7037(85)90089-4).

Dehairs, F., Chesselet, R., Jedwab, J., 1980. Discrete suspended particles of barite and the barium cycle in the open ocean. *Earth Planet. Sci. Lett.* 49, 528–550. [https://doi.org/10.1016/0012-821X\(80\)90094-1](https://doi.org/10.1016/0012-821X(80)90094-1).

Elderfield, H., 1990. Tracers of ocean paleoproductivity and paleochemistry: an introduction. *Paleoceanography* 5, 711–717. <https://doi.org/10.1029/PA005i005p00711>.

Elderfield, H., Sholkovitz, E.R., 1987. Rare earth elements in the pore waters of reducing nearshore sediments. *Earth Planet. Sci. Lett.* [https://doi.org/10.1016/0012-821X\(87\)90202-0](https://doi.org/10.1016/0012-821X(87)90202-0).

Elderfield, H., Whitfield, M., Burton, J.D., Bacon, M.P., Liss, P.S., 1988. The oceanic chemistry of the rare-earth elements [and discussion]. *Philos. Trans. R. Soc. A Math. Phys. Eng. Sci.* 325, 105–126. <https://doi.org/10.1098/esta.1988.0046>.

Elrod, V.A., Berelson, W.M., Coale, K.H., Johnson, K.S., 2004. The flux of iron from continental shelf sediments: a missing source for global budgets. *Geophys. Res. Lett.* <https://doi.org/10.1029/2004GL020216>.

Fine, R.A., Lukas, R., Bingham, F.M., Warner, M.J., Gammon, R.H., 1994. The western equatorial Pacific: a water mass crossroads. *J. Geophys. Res.* <https://doi.org/10.1029/94JC02277>.

van de Fliedert, T., Pahnke, K., et al., 2012. GEOTRACES intercalibration of neodymium isotopes and rare earth element concentrations in seawater and suspended particles. Part I: Reproducibility of results for the international intercomparison. *Limnol. Oceanogr. Methods.* <https://doi.org/10.4319/lom.2012.10.234>.

Freydier, R., Dupre, B., Polve, M., 1995. Analyses by inductively coupled plasma mass spectrometry of Ba concentrations in water and rock samples. Comparison between isotope dilution and external calibration with or without internal standard. *European Journal of Mass Spectrometry* 1, 283. <https://doi.org/10.1255/ejms.140>.

- Friend, C.R.L., Nutman, A.P., Bennett, V.C., Norman, M.D., 2008. Seawater-like trace element signatures (REE + Y) of Eoarchaean chemical sedimentary rocks from southern West Greenland, and their corruption during high-grade metamorphism. *Contrib. Mineral. Petrol.* <https://doi.org/10.1007/s00410-007-0239-z>.
- Fukumori, I., Lee, T., Cheng, B., Menemenlis, D., 2004. The Origin, Pathway, and Destination of Niño-3 Water estimated by a simulated Passive Tracer and its Adjoint. *J. Phys. Oceanogr.* <https://doi.org/10.1175/2515.1>.
- Ganachaud, A., Cravatte, S., et al., 2014. The Southwest Pacific Ocean circulation and climate experiment (SPICE). *Journal of Geophysical Research: Oceans*. <https://doi.org/10.1002/2013JC009678>.
- Ganachaud, A., Cravatte, S., et al., 2017. The Solomon Sea: its circulation, chemistry, geochemistry and biology explored during two oceanographic cruises. *Elem Sci Anth.* <https://doi.org/10.1525/elementa.221>.
- García-Solsona, E., Jeandel, C., Labatut, M., Lacan, F., Vance, D., Chavagnac, V., Pradoux, C., 2014. Rare earth elements and Nd isotopes tracing water mass mixing and particle-seawater interactions in the SE Atlantic. *Geochim. Cosmochim. Acta.* <https://doi.org/10.1016/j.gca.2013.10.009>.
- Gasparin, F., Ganachaud, A., Maes, C., 2011. A western boundary current east of New Caledonia: Observed characteristics. *Deep-Sea Research Part I: Oceanographic Research Papers*. <https://doi.org/10.1016/j.dsr.2011.05.007>.
- Gasparin, F., Maes, C., Sudre, J., Garçon, V., Ganachaud, A., 2014. Water mass analysis of the Coral Sea through an Optimum Multiparameter method. *Journal of Geophysical Research: Oceans* 119, 7229–7244. <https://doi.org/10.1002/2014JC010246>.
- German, C.R., Elderfield, H., 1989. Rare earth elements in Saanich Inlet, British Columbia, a seasonally anoxic basin. *Geochim. Cosmochim. Acta.* [https://doi.org/10.1016/0016-7037\(89\)90128-2](https://doi.org/10.1016/0016-7037(89)90128-2).
- Germineaud, C., 2016. *Circulation Océanique et Variabilité en Mer Des Salomon*. Université Toulouse 3 Paul Sabatier (UT3 Paul Sabatier) (240 pp).
- Germineaud, C., Ganachaud, A., et al., 2016. Pathways and water mass properties of the thermocline and intermediate waters in the Solomon Sea. *J. Phys. Oceanogr.* 46, 3031–3049. <https://doi.org/10.1175/JPO-D-16-0107.1>.
- Goldberg, E.D., Koide, M., Schmitt, R.A., Smith, R.H., 1963. Rare-Earth distributions in the marine environment. *J. Geophys. Res.* <https://doi.org/10.1029/JZ068i014p04209>.
- Goldstein, S.L., Hemming, S.R., 2003. Long-lived Isotopic Tracers in Oceanography, Paleooceanography, and Ice-sheet Dynamics. In: *Treatise on Geochemistry*. Elsevier, pp. 453–489. <https://doi.org/10.1016/B0-08-043751-6/06179-X>.
- Grenier, M., Cravatte, S., et al., 2011. From the western boundary currents to the Pacific equatorial undercurrent: modeled pathways and water mass evolutions. *Journal of Geophysical Research: Oceans*. <https://doi.org/10.1029/2011JC007477>.
- Grenier, M., Jeandel, C., Lacan, F., Vance, D., Venchiarutti, C., Cros, A., Cravatte, S., 2013. From the subtropics to the central equatorial Pacific Ocean: Neodymium isotopic composition and rare earth element concentration variations. *Journal of Geophysical Research: Oceans*. <https://doi.org/10.1029/2012JC008239>.
- Grenier, M., Jeandel, C., Cravatte, S., 2014. From the subtropics to the equator in the Southwest Pacific: Continental material fluxes quantified using neodymium data along modeled thermocline water pathways. *Journal of Geophysical Research: Oceans*. <https://doi.org/10.1002/2013JC009670>.
- Grenier, M., Garcia-Solsona, E., et al., 2018. Differentiating lithogenic supplies, water mass transport, and biological processes on and off the Kerguelen Plateau using rare earth element concentrations and neodymium isotopic compositions. *Front. Mar. Sci.* <https://doi.org/10.3389/fmars.2018.00426>.
- Guichard, F., Church, T.M., Treuil, M., Jaffreic, H., 1979. Rare earths in barites: distribution and effects on aqueous partitioning. *Geochim. Cosmochim. Acta.* [https://doi.org/10.1016/0016-7037\(79\)90088-7](https://doi.org/10.1016/0016-7037(79)90088-7).
- Haley, B.A., Klinkhammer, G.P., McManus, J., 2004. Rare earth elements in pore waters of marine sediments. *Geochim. Cosmochim. Acta.* <https://doi.org/10.1016/j.gca.2003.09.012>.
- Haley, B.A., Frank, M., Hathorne, E., Pidas, N., 2014. Biogeochemical implications from dissolved rare earth element and Nd isotope distributions in the Gulf of Alaska. *Geochim. Cosmochim. Acta.* <https://doi.org/10.1016/j.gca.2013.11.012>.
- Hanawa, K., Talley, L.D., 2001. Eds. In: Siedler, G., Church, J., Gould, W.J. (Eds.), *Mode Waters. Ocean Circulation and Climate: Observing and Modelling the Global Ocean*. Academic, San Diego, Calif. London, pp. 373–386.
- Holm, R.J., Spandler, C., Richards, S.W., 2013. Melanesian arc far-field response to collision of the Ontong Java Plateau: Geochronology and petrogenesis of the Simuku Igneous complex, New Britain, Papua New Guinea. *Tectonophysics* 603, 189–212. <https://doi.org/10.1016/j.tecto.2013.05.029>.
- Jacquet, S.H.M., Dehairs, F., Cardinal, D., Navez, J., Delille, B., 2005. Barium distribution across the Southern Ocean frontal system in the Crozet–Kerguelen Basin. *Mar. Chem.* 95, 149–162. <https://doi.org/10.1016/j.marchem.2004.09.002>.
- Jeandel, C., et al., 2011. Ocean margins: the missing term in oceanic element budgets? *EOS, Transactions American Geophysical Union* 92 (26), 217–218.
- Jeandel, C., Delattre, H., Grenier, M., Pradoux, C., Lacan, F., 2013. Rare earth element concentrations and Nd isotopes in the Southeast Pacific Ocean. *Geochem. Geophys. Geosyst.* <https://doi.org/10.1029/2012GC004309>.
- Johannesson, K.H., Chevis, D.A., Burdige, D.J., Cable, J.E., Martin, J.B., Roy, M., 2011. Submarine groundwater discharge is an important net source of light and middle REEs to coastal waters of the Indian River Lagoon, Florida, USA. *Geochim. Cosmochim. Acta.* <https://doi.org/10.1016/j.gca.2010.11.005>.
- Johnson, G.C., Toole, J.M., 1993. Flow of Deep and Bottom Waters in the Pacific at 10°N. *Journal of Geophysical Research* 98, 10,339–10,352.
- Johnson, K.S., Elrod, V.A., et al., 2003. Surface ocean-lower atmosphere interactions in the northeast Pacific ocean gyre: aerosols, iron, and the ecosystem response. *Glob. Biogeochem. Cycles*. <https://doi.org/10.1029/2002GB002004>.
- Kawabe, M., Fujio, S., 2010. Pacific ocean circulation based on observation. *J. Oceanogr.* 66, 389–403. <https://doi.org/10.1007/s10872-010-0034-8>.
- Kelemen, P.B., Hanghøj, K., Greene, A.R., 2013. One view of the geochemistry of subduction-related magmatic arcs, with an emphasis on primitive andesite and lower crust. In: *Treatise on Geochemistry*, Second edition. Elsevier, Oxford, pp. 749–806. <https://doi.org/10.1016/B978-0-08-095975-7.00323-5>.
- Keppeler, L., Cravatte, S., Chaigneau, A., Pegliasco, C., Gourdeau, L., Singh, A., 2018. Observed characteristics and vertical structure of Mesoscale Eddies in the southwest tropical Pacific. *Journal of Geophysical Research: Oceans* 123, 2731–2756. <https://doi.org/10.1002/2017JC013712>.
- Kessler, W.S., 1999. Interannual variability of the subsurface high salinity tongue south of the equator at 165°E. *J. Phys. Oceanogr.* 29, 2038–2049. [https://doi.org/10.1175/1520-0485\(1999\)029<2038:IVOTSH>2.0.CO;2](https://doi.org/10.1175/1520-0485(1999)029<2038:IVOTSH>2.0.CO;2).
- Kessler, W.S., Cravatte, S., 2013. Mean circulation of the Coral Sea. *Journal of Geophysical Research: Oceans*. <https://doi.org/10.1002/2013JC009117>.
- Klinkhammer, G.P., Chan, L.H., 1990. Determination of barium in marine waters by isotope dilution inductively coupled plasma mass spectrometry. *Anal. Chim. Acta* 232, 323–329. [https://doi.org/10.1016/S0003-2670\(00\)81249-0](https://doi.org/10.1016/S0003-2670(00)81249-0).
- Lacan, F., Jeandel, C., 2001. Tracing Papua New Guinea imprint on the central equatorial Pacific Ocean using neodymium isotopic compositions and rare earth element patterns. *Earth Planet. Sci. Lett.* [https://doi.org/10.1016/S0012-821X\(01\)00263-1](https://doi.org/10.1016/S0012-821X(01)00263-1).
- Lawrence, M.G., Kamber, B.S., 2006. The behaviour of the rare earth elements during estuarine mixing-revisited. *Mar. Chem.* <https://doi.org/10.1016/j.marchem.2005.11.007>.
- Lee, Jong Hyeon, Byrne, R.H., 1993. Complexation of trivalent rare earth elements (Ce, Eu, Gd, Tb, Yb) by carbonate ions. *Geochim. Cosmochim. Acta.* [https://doi.org/10.1016/0016-7037\(93\)90432-V](https://doi.org/10.1016/0016-7037(93)90432-V).
- Lefèvre, D., Guigou, C., Obernosterer, I., 2008. The metalic balance at two contrasting sites in the Southern Ocean: The iron-fertilized Kerguelen area and HNLC waters. In: *Deep-Sea Research Part II: Topical Studies in Oceanography*, <https://doi.org/10.1016/j.dsr.2.2007.12.006>.
- Liu, Y.G., Miah, M.R.U., Schmitt, R.A., 1988. Cerium: a chemical tracer for paleo-oceanic redox conditions. *Geochim. Cosmochim. Acta.* [https://doi.org/10.1016/0016-7037\(88\)90207-4](https://doi.org/10.1016/0016-7037(88)90207-4).
- Mackey, D.J., O'Sullivan, J.E., Watson, R.J., 2002. Iron in the western Pacific: a riverine or hydrothermal source for iron in the Equatorial Undercurrent? *Deep-Sea Res. Part I: Oceanogr.* 49, 877–893. [https://doi.org/10.1016/S0967-0637\(01\)00075-9](https://doi.org/10.1016/S0967-0637(01)00075-9).
- McCartney, M.S., 1977. Subantarctic Mode Water, George Deacon 70th Anniversary. *Voyage of Discovery*, vol. Volume A. pp. 103–119.
- McLennan, M., 1989. Rare earth elements in sedimentary rocks: influence of provenance and sedimentary processes. *Rev. Mineral. Geochem.* 21 (1), 169–200.
- McLennan, M., 1994. Rare earth element geochemistry and the tetrad effect. *Geochim. Cosmochim. Acta* 58, 2025–2033.
- Michael, S., et al., 2019. Constraining the Solomon Sea as a Source of Al and Mn to the Equatorial Undercurrent. (Submitted in 2019).
- Milliman, J.D., Farnsworth, K.L., Albertin, C.S., 1999. Flux and fate of fluvial sediments leaving large islands in the East Indies. *J. Sea Res.* 41, 97–107. [https://doi.org/10.1016/S1385-1101\(98\)0040-9](https://doi.org/10.1016/S1385-1101(98)0040-9).
- Molina-Kescher, M., Frank, M., Hathorne, E., 2014. South Pacific dissolved Nd isotope compositions and rare earth element distributions: water mass mixing versus biogeochemical cycling. *Geochim. Cosmochim. Acta.* <https://doi.org/10.1016/j.gca.2013.11.038>.
- Nozaki, Y., 1986. 226Ra/222Rn/210Pb systematics in seawater near the bottom of the ocean. *Earth Planet. Sci. Lett.* [https://doi.org/10.1016/0012-821X\(86\)90017-8](https://doi.org/10.1016/0012-821X(86)90017-8).
- Nozaki, Y., Alibo, D.S., 2003a. Dissolved rare earth elements in the Southern Ocean, southwest of Australia: unique patterns compared to the South Atlantic data. *Geochim. J.* <https://doi.org/10.2343/geochemj.37.47>.
- Nozaki, Y., Alibo, D.S., 2003b. Importance of vertical geochemical processes in controlling the oceanic profiles of dissolved rare earth elements in the northeastern Indian Ocean. *Earth Planet. Sci. Lett.* [https://doi.org/10.1016/S0012-821X\(02\)01027-0](https://doi.org/10.1016/S0012-821X(02)01027-0).
- Nozaki, Y., Alibo, D.S., Amakawa, H., Gamo, T., Hasumoto, H., 1999. Dissolved rare earth elements and hydrography in the Sulu Sea. *Geochim. Cosmochim. Acta.* [https://doi.org/10.1016/S0016-7037\(99\)00142-8](https://doi.org/10.1016/S0016-7037(99)00142-8).
- Orsi, A.H., Johnson, G.C., Bullister, J.L., 1999. Circulation, mixing, and production of Antarctic Bottom Water. *Prog. Oceanogr.* 43, 55–109. [https://doi.org/10.1016/S0079-6611\(99\)00004-X](https://doi.org/10.1016/S0079-6611(99)00004-X).
- Pahnke, K., van de Fliert, T., Jones, K.M., Lambelet, M., Hemming, S.R., Goldstein, S.L., 2012. GEOTRACES intercalibration of neodymium isotopes and rare earth element concentrations in seawater and suspended particles. Part 2: Systematic tests and baseline profiles. *Limnol. Oceanogr. Methods*. <https://doi.org/10.4319/lom.2012.10.252>.
- Patten, J.T., Byrne, R.H., 2017. Assessment of Fe(III) and Eu(III) complexation by silicate in aqueous solutions. *Geochim. Cosmochim. Acta* 202, 361–373. <https://doi.org/10.1016/j.gca.2016.12.004>.
- Pieppgras, D.J., Jacobsen, S.B., 1992. The behavior of rare earth elements in seawater: Precise determination of variations in the North Pacific water column. *Geochim. Cosmochim. Acta.* [https://doi.org/10.1016/0016-7037\(92\)90315-A](https://doi.org/10.1016/0016-7037(92)90315-A).
- Qin, X., Menviel, L., Sen Gupta, A., van Sebille, E., 2016. Iron sources and pathways into the Pacific Equatorial Undercurrent. *Geophys. Res. Lett.* <https://doi.org/10.1002/2016GL070501>.
- Qu, T., Lindstrom, E.J., 2002. A climatological interpretation of the circulation in the Western South Pacific*. *J. Phys. Oceanogr.* <https://doi.org/10.1055/s-2007-989442>.
- Qu, T., Lindstrom, E.J., 2004. Northward intrusion of antarctic intermediate water in the Western Pacific*. *J. Phys. Oceanogr.* 34, 2104–2118. [https://doi.org/10.1175/1520-0485\(2004\)034<2104:NIQATW>2.0.CO;2](https://doi.org/10.1175/1520-0485(2004)034<2104:NIQATW>2.0.CO;2).
- Qu, T., Gao, S., Fukumori, I., Fine, R.A., Lindstrom, E.J., 2008. Subduction of South Pacific waters. *Geophys. Res. Lett.* <https://doi.org/10.1029/2007GL032605>.
- Qu, T., Gao, S., Fukumori, I., Fine, R.A., Lindstrom, E.J., 2009. Origin and pathway of

- equatorial 13°C water in the Pacific identified by a simulated passive tracer and its adjoint*. *J. Phys. Oceanogr.* <https://doi.org/10.1175/2009JPO4045.1>.
- Radenac, M.H., Messié, M., Léger, F., Bosc, C., 2013. A very oligotrophic zone observed from space in the equatorial Pacific warm pool. *Remote Sens. Environ.* <https://doi.org/10.1016/j.rse.2013.03.007>.
- Reid, J.L., 1986. On the Total Geostrophic Circulation of the South Pacific Ocean: Flow Patterns, Tracers and Transports.
- Reid, J.L., 1997. On the Total Geostrophic Circulation of the Pacific Ocean: Flow Patterns, Tracers, and Transports.
- Roemmich, D., Hautala, S., Rudnick, D., 1996. Northward abyssal transport through the Samoan passage and adjacent regions. *Journal of Geophysical Research C: Oceans.* <https://doi.org/10.1029/96JC00797>.
- Rousseau, T.C.C., Sonke, J.E., et al., 2013. Rare earth element analysis in natural waters by multiple isotope dilution-sector field ICP-MS. *J. Anal. At. Spectrom.* <https://doi.org/10.1039/c3ja30332b>.
- Rousseau, T.C.C., Sonke, J.E., et al., 2015. Rapid neodymium release to marine waters from lithogenic sediments in the Amazon estuary. *Nat. Commun.* <https://doi.org/10.1038/ncomms8592>.
- Schiff, J., Christenson, E.A., Byrne, R.H., 2015. YREE scavenging in seawater: a new look at an old model. *Mar. Chem.* <https://doi.org/10.1016/j.marchem.2015.06.010>.
- Shiller, A.M., Chan, E.W., Joung, D.J., Redmond, M.C., Kessler, J.D., 2017. Light rare earth element depletion during Deepwater Horizon blowout methanotrophy. *Sci. Rep.* 7, 10389. <https://doi.org/10.1038/s41598-017-11060-z>.
- Sholkovitz, E., Szymczak, R., 2000. The estuarine chemistry of rare earth elements: Comparison of the Amazon, Fly, Sepik and the Gulf of Papua systems. *Earth Planet. Sci. Lett.* [https://doi.org/10.1016/S0012-821X\(00\)00112-6](https://doi.org/10.1016/S0012-821X(00)00112-6).
- Sholkovitz, E.R., Landing, W.M., Lewis, B.L., 1994. Ocean Particle Chemistry: The Fractionation of Rare Earth Elements between Suspended Particles and Seawater.
- Slemons, L.O., Murray, J.W., Resing, J., Paul, B., Dutrieux, P., 2010. Western Pacific coastal sources of iron, manganese, and aluminum to the equatorial undercurrent. *Glob. Biogeochem. Cycles.* <https://doi.org/10.1029/2009GB003693>.
- Sokolov, S., Rintoul, S., 2000. Circulation and water masses of the southwest Pacific: WOCE Section P11, Papua New Guinea to Tasmania. *J. Mar. Res.* <https://doi.org/10.1357/002224000321511151>.
- Tachikawa, K., Athias, V., Jeandel, C., 2003. Neodymium budget in the modern ocean and paleo-oceanographic implications. *J. Geophys. Res.* 108 (C8), 3254. <https://doi.org/10.1029/1999JC000285>.
- Tachikawa, K., Jeandel, C., Roy-Barman, M., 1999. A new approach to the Nd residence time in the ocean: the role of atmospheric inputs. *Earth Planet. Sci. Lett.* 170, 433–446. [https://doi.org/10.1016/S0012-821X\(99\)00127-2](https://doi.org/10.1016/S0012-821X(99)00127-2).
- Takebe, M., 2005. This content downloaded from 142.12.73.66 on Sun, Source: The *Journal of Geology* 113, 201–215. <https://doi.org/10.1086/427669>.
- Talley, L., 2007. Hydrographic Atlas of the World Ocean Circulation Experiment (WOCE). Pacific Ocean, vol. Volume 2.
- Tomczak, M., Godfrey, J.S., 2003. *Hydrology of the Pacific Ocean, Regional Oceanography: An Introduction*, 2nd Improved Edition. Daya Publishing House, Delhi, pp. 137–174.
- Tomczak, M., Hao, D., 1989. Water masses in the thermocline of the coral sea. *Deep Sea Research Part A: Oceanographic Research Papers* 36, 1503–1514. [https://doi.org/10.1016/0198-0149\(89\)90054-X](https://doi.org/10.1016/0198-0149(89)90054-X).
- Tomczak, M., Large, D.G.B., 1989. Optimum multiparameter analysis of mixing in the thermocline of the eastern Indian Ocean. *J. Geophys. Res.* 94, 16141. <https://doi.org/10.1029/JC094C11p16141>.
- Tsimplis, M.N., Bacon, S., Bryden, H.L., 1998. The circulation of the subtropical South Pacific derived from hydrographic data. *Journal of Geophysical Research: Oceans.* <https://doi.org/10.1029/98JC01881>.
- Tsuchiya, M., 1981. The origin of the Pacific equatorial 13°C water. *J. Phys. Oceanogr.* 11, 794–812. [https://doi.org/10.1175/1520-0485\(1981\)011<0794:T001PE>2.0.CO;2](https://doi.org/10.1175/1520-0485(1981)011<0794:T001PE>2.0.CO;2).
- Tsuchiya, M., Lukas, R., Fine, R.A., Firing, E., Lindstrom, E., 1989. Source waters of the Pacific Equatorial Undercurrent. *Prog. Oceanogr.* 23, 101–147. [https://doi.org/10.1016/0079-6611\(89\)90012-8](https://doi.org/10.1016/0079-6611(89)90012-8).
- Wang, Z.L., Yamada, M., 2007. Geochemistry of dissolved rare earth elements in the equatorial Pacific ocean. *Environ. Geol.* <https://doi.org/10.1007/s00254-006-0515-7>.
- Wijffels, S.E., Toole, J.M., Davis, R., 2001. Revisiting the South Pacific subtropical circulation: a synthesis of World Ocean Circulation Experiment observations along 32°S. *Journal of Geophysical Research: Oceans.* <https://doi.org/10.1029/1999JC000118>.
- Zhang, J., Nozaki, Y., 1996. Rare earth elements and yttrium in seawater: ICP-MS determinations in the East Caroline, Coral Sea, and South Fiji basins of the western South Pacific Ocean. *Geochim. Cosmochim. Acta.* [https://doi.org/10.1016/S0016-7037\(96\)00276-1](https://doi.org/10.1016/S0016-7037(96)00276-1).
- Zhang, Y., Lacan, F., Jeandel, C., 2008. Dissolved rare earth elements tracing lithogenic inputs over the Kerguelen Plateau (Southern Ocean). *Deep-Sea Research Part II: Topical Studies in Oceanography.* <https://doi.org/10.1016/j.dsr2.2007.12.029>.

Supplementary Material

Dissolved Rare Earth Elements distribution in the Solomon Sea

Pham V.Q.*, Grenier M., Cravatte S., Michael S., Jacquet S., Belhadj M., Nachez Y.,
Germineaud C. and Jeandel C.*

* **Correspondance:** Catherine JEANDEL : catherine.jeandel@legos.obs-mip.fr; Viet Quoc PHAM: viet.pham@legos.obs-mip.fr

1. The Pandora box comprising the whole water column

In order to assess the input-output fluxes for the whole water column, we built a Solomon Sea box model covering the isopycnal layers $24 < \sigma_\theta < 27.4$. This box model covers the same geographical coordinate as those described in the main document. All the dREE are taken into account in the calculation, although only dLa, dNd, dEu and dYb results only are shown (see table A and figure 3). This model allows estimating a slight REE enrichment on a global Solomon Sea scale, however characterized by large uncertainties. This result underlines the importance of a fine understanding of the isopycnal layer dynamic and modeling. Obviously, lithogenic REE enrichments occur in specific layers. A more detailed study of the processes together with dissolved and particulate ϵ_{Nd} data is an ongoing work.

Table A. dREE flux within the Solomon Sea

Element	Incoming flux (t/a)			Outgoing flux (t/a)		
	Incoming NGCU	Direct NVJ	Vitiaz	St-Georges	Solomon	Flux (t/a)
La	420± 257	695± 371	343± 165	229± 115	660± 356	135± 606
Nd	285± 127	462± 185	228± 91	156± 54	393± 151	33± 287
Eu	19± 7	29± 9	15± 5	11± 3	26± 9	3± 16
Yb	167± 110	258± 132	138± 70	92± 49	230± 113	34± 229

2. The relationship between dissolved Rare Earth Elements and dissolved Si

An extended investigation of the relationship between REE and dSi is proposed here. Thanks to the GEOTRACES data base (www.geotraces.org), dREE and dSi data from the Atlantic and Pacific Oceans were plotted together (see Fig. A1). The three dREE concentrations decrease relatively to the dSi one from the north Atlantic to the Pacific, reflecting the differences of residence times between these species. However, the decrease is less pronounced for Yb, which displays a more homogeneous ratio with dSi between the two basins, more particularly in the deep waters. The dispersion of the dYb/dSi ratios for $dSi < 20 \mu M$ contrasting with the good relationship deeper in the water column ($dSi > 20 \mu M$) is observed both on the Solomon Sea and the global scale.

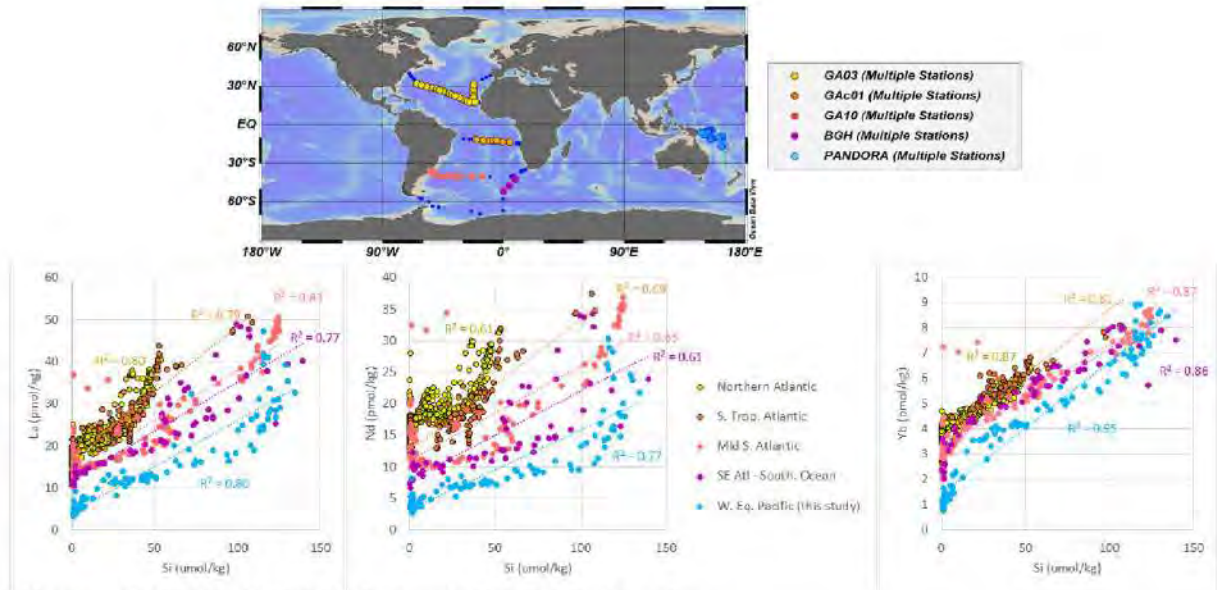


Figure A1. The dREE-dSi correlation global scale

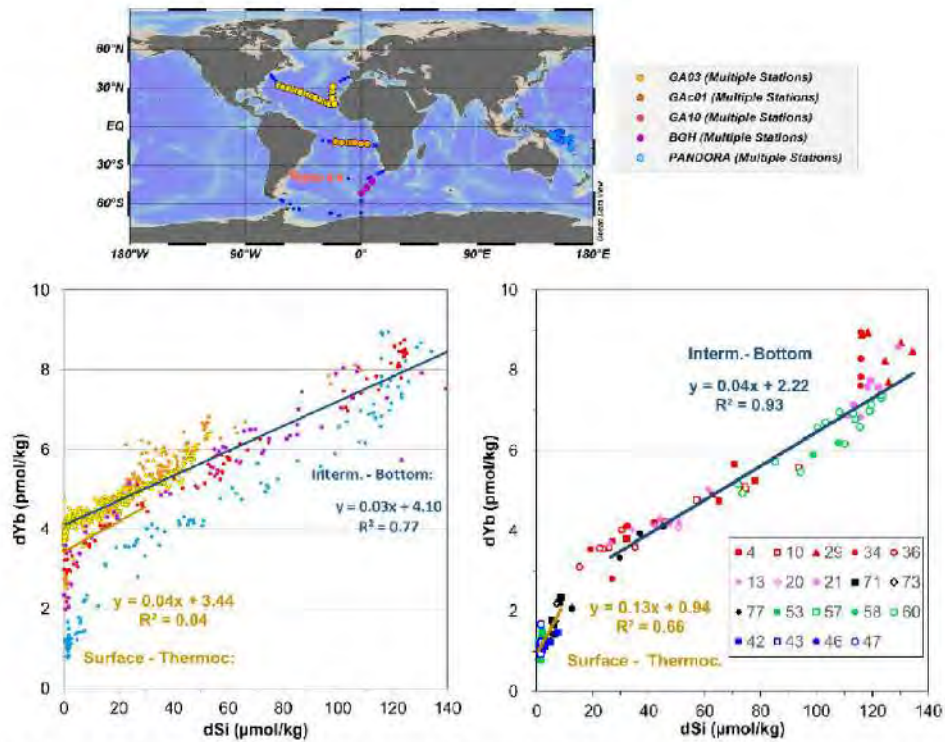


Figure A2. The dYb-dSi correlation in the Solomon Sea and on the global scale

3. The dBa - dLa correlation

Below are reported all the dBa data acquired in the framework of PANDORA cruise (Table B). They allowed us to trace the dLa versus dBa relationship for our data (Figure

A3). As above, we also compared these data to the Atlantic one, using the GEOTRACES IDP 2017 (Schlitzer et al, 2018).

Table B. Dissolved Ba concentration in the Solomon Sea

Depth (m)	Salinity (PSU)	O ₂ ($\mu\text{mol/kg}$)	σ_θ (kg/m^3)	dBa (μM)	Saturation index Ba (Q/K)
Station 004 (July 01, 2012; 17° 0' 10.8" S; 162° 59' 45.6" E ; depth: 4680m)					
35	34.907	199	23.00	27.7300	0.1159
85	35.495	180	23.93	28.6900	0.1242
175	35.636	162	24.92	33.8127	0.1700
265	35.403	159	25.78	31.5033	0.1815
365	35.031	168	26.36	34.3328	0.2305
565	34.466	192	26.97	44.8378	0.3774
735	34.416	179	27.18	58.9650	0.5420
1135	34.51	157	27.44	85.0710	0.7905
1735	34.62	140	27.64	106.6580	0.9285
2205	34.653	144	27.70	111.8670	0.9031
3600	34.687	156	27.76	113.7930	0.7074
Station 010 (July 03, 2012; 12° 0' 0" S; 162° 59' 56.4" E; depth: 5092m)					
5	34.618	192	22.08	29.6497	0.1150
35	34.616	191	22.09	21.6000	0.0833
90	35.182	168	22.59	71.0997	0.2732
140	35.904	138	23.74	32.4469	0.1322
180	36.029	134	24.36	24.3000	0.1069
260	35.523	133	25.58	33.9341	0.1986
465	34.631	153	26.81	37.4700	0.3010
510	34.521	163	26.96	56.2900	0.4832
935	34.511	139	27.38	71.6500	0.6662
1000	34.52	139	27.41	89.3400	0.8361
1335	34.576	130	27.55	92.0500	0.8416
1735	34.613	133	27.63	104.6200	0.9093
1935	34.63	133	27.67	109.0500	0.9212
2500	34.669	145	27.73	110.6900	0.8506
3000	34.679	147	27.76	114.5260	0.8033
4000	34.685	153	27.77	116.2300	0.6698
Station 013 (July 04, 2012; 9° 0' 10.8" S; 162° 59' 56.4" E; depth: 3853m)					
5	34.651	191	21.74	21.4213	0.0796
50	34.676	191	21.77	22.4900	0.0834
150	35.791	130	23.98	23.2000	0.1064
240	35.497	122	25.61	23.8500	0.1187
300	35.188	106	26.07	24.9100	0.1471
365	34.858	111	26.59	31.8800	0.2293
565	34.526	137	27.12	53.0200	0.4782
600	34.515	138	27.16	54.0000	0.4911
685	34.503	138	27.22	76.0500	0.7043
970	34.526	127	27.39	78.5700	0.7377
1335	34.574	126	27.54	92.0100	0.8413
1535	34.595	129	27.60	99.0400	0.8861
2000	34.64	133	27.69	111.7800	0.9393
Station 021 (July 07, 2012; 10° 0' 46.8" S; 160° 21' 25.2" E; depth: 3342m)					
5	34.811	190	21.95	22.2800	0.0836
50	35.172	163	22.27	36.1661	0.1345
60	35.289	157	22.40	23.2000	0.0866
100	35.471	145	23.01	56.9850	0.2178
150	35.627	133	23.79	23.6600	0.1015
250	35.388	127	25.76	36.0082	0.2231
335	34.835	124	26.66	38.3500	0.3015
535	34.493	164	27.09	50.5800	0.4606
550	34.491	163	27.10	61.8717	0.5541

735	34.483	154	27.23	62.3800	0.5839
1065	34.528	138	27.42	76.8100	0.7078
1250	34.566	134	27.52	104.0480	0.9566
1470	34.593	133	27.58	96.4900	0.8696
1865	34.626	135	27.66	104.8100	0.8939
2000	34.634	137	27.67	116.8080	0.9777
2115	34.644	139	27.69	107.2500	0.8802
2625	34.677	150	27.74	105.9300	0.7936
3280	34.7	165	27.77	100.2700	0.6632
Station 034 (July 10, 2012; 11° 27' 7.2" S; 154° 39' 54" E; depth: 2005m)					
50	35.272	157	22.54	28.1802	0.1081
100	35.522	138	23.35	28.1831	0.1169
215	35.609	145	25.24	27.9799	0.1505
340	35.117	161	26.28	33.7535	0.2229
735	34.439	179	27.16	56.1827	0.5049
840	34.45	169	27.25	63.7107	0.5867
1065	34.493	154	27.37	79.9426	0.7316
1465	34.581	138	27.56	97.8179	0.8743
1550	34.6	136	27.60	99.7713	0.8881
1930	34.645	141	27.69	106.9310	0.9068
Station 042 (July 15, 2012; 5° 8' 42" S; 153° 17' 24" E; depth: 3081m)					
5	34.691	192	21.71	25.7700	0.3287
45	34.75	191	21.75	26.4300	0.4132
100	35.464	157	22.68	27.9100	0.5237
200	35.647	140	25.06	26.2500	0.7409
250	35.261	156	26.04	29.3200	0.9161
400	34.644	174	26.84	40.0600	0.9379
500	34.538	158	27.02	47.2700	0.9446
700	34.479	157	27.18	57.2900	0.0803
1000	34.526	137	27.41	79.3200	0.0842
1400	34.595	118	27.58	100.6100	0.0859
1600	34.613	123	27.63	105.5400	0.1077
1800	34.624	124	27.65	109.5600	0.1430
Station 053 (July 19, 2012; 4° 54' 18" S; 152° 52' 12" E; depth: 733m)					
5	34.697	193	21.68	21.8000	0.2276
25	34.879	189	21.99	22.5300	0.4323
50	35.036	182	22.14	23.0000	0.0951
100	35.466	146	23.72	25.0600	0.1011
150	35.61	142	24.72	30.5000	0.1177
335	34.977	161	26.45	32.6000	0.1877
635	34.504	169	27.06	49.4600	0.3046
Station 057 (July 20, 2012; 4° 34' 12" S; 152° 31' 22.8" E; depth: 2552m)					
5	34.768	193	21.91	25.4100	0.3646
75	35.4	163	22.63	26.2700	0.5852
150	35.583	139	24.20	26.3000	0.6963
250	35.268	152	26.00	30.4400	0.9577
400	34.73	171	26.76	38.6600	0.9305
500	34.578	178	26.93	43.5100	0.9264
700	34.486	151	27.24	63.0400	0.8996
1000	34.515	142	27.38	75.5900	0.1009
1400	34.582	127	27.55	106.3300	0.1060
1650	34.611	124	27.62	106.0500	0.1262
1800	34.623	125	27.65	107.6900	0.1523
2200	34.654	135	27.71	111.2800	0.3513
Station 058 (July 21, 2012; 5° 30' 10.8" S; 152° 5' 52.8" E; depth: 1142m)					
25	34.637	193	22.03	26.3300	0.5169
75	35.081	173	22.48	27.6800	0.6686
155	35.645	134	24.48	27.5400	0.7447
220	35.458	138	25.62	28.2900	0.7999

435	34.657	172	26.86	42.9000	0.8156
635	34.488	163	27.15	56.9400	0.1017
835	34.502	145	27.33	71.4900	0.1007
1000	34.536	136	27.44	79.9300	0.1127
1100	34.547	133	27.47	86.0500	0.1092
1185	34.556	131	27.49	88.6500	0.1353
Station 060 (July 22, 2012; 6° 10' 1.2" S; 152° 29' 49.2" E; depth: 5609m)					
10	34.453	193	21.88	26.4700	0.2112
35	34.737	193	22.19	26.4900	0.3171
50	34.854	190	22.38	26.7200	0.5603
75	35.233	164	22.77	27.9600	0.6785
180	35.733	135	24.70	31.6400	0.8234
250	35.325	124	25.86	31.4500	0.8261
400	34.653	151	26.83	41.4800	0.8877
600	34.479	160	27.18	60.8600	0.9586
800	34.498	147	27.32	71.5500	0.9587
1000	34.53	138	27.43	82.6400	0.9357
1100	34.544	135	27.46	87.1600	0.8931
1400	34.591	127	27.58	97.5800	0.8090
1800	34.631	125	27.67	110.6600	0.7655
2000	34.645	129	27.69	113.9000	0.6769
2250	34.657	133	27.72	115.9800	0.6377
2540	34.661	132	27.73	116.8800	0.5725
2750	34.672	141	27.74	110.3100	0.5428
3000	34.684	149	27.76	109.7300	0.4874
3500	34.695	158	27.76	107.3200	0.4625
3770	34.696	159	27.77	106.3700	0.4316
4250	34.696	159	27.77	105.4800	0.1160
4500	34.696	160	27.77	105.1200	0.1394
5000	34.697	161	27.77	104.2500	0.2542
5250	34.697	162	27.77	103.9100	0.2287
5600	34.697	162	27.77	103.9800	0.3396
Station 071 (July 25, 2012; 8° 19' 55.2" S; 151° 17' 27.6" E; depth: 1563m)					
75	35.083	173	22.75	28.7900	0.5588
160	35.659	138	24.60	29.2600	0.7621
200	35.638	124	25.27	48.3800	0.7621
300	35.08	162	26.33	34.1200	0.8131
500	34.65	177	26.84	42.6800	0.1084
700	34.468	173	27.13	62.5900	0.1174
1100	34.522	143	27.41	83.3900	0.1195
1200	34.542	138	27.46	83.3900	0.1350
1205	34.543	137	27.46	89.1600	0.2514
Station 073 (July 26, 2012; 7° 9' 57.6" S; 149° 59' 56.4" E; depth : 5253m)					
5	34.753	195	22.20	26.5500	0.1590
50	35.047	169	22.65	27.7200	0.2213
75	35.15	163	22.78	28.0900	0.3407
150	35.556	144	24.60	60.5300	0.5236
200	35.631	141	24.86	28.1100	0.6085
250	35.474	145	25.56	28.6200	0.7809
300	35.101	161	26.28	32.9700	0.9260
500	34.618	171	26.86	42.0800	1.0561
700	34.474	170	27.16	57.7900	0.1065
900	34.476	159	27.27	68.7500	0.1135
1200	34.538	139	27.46	86.6800	0.1143
1600	34.605	124	27.61	105.0500	0.1142
2000	34.643	129	27.69	136.4800	0.1225
Station 077 (July 28, 2012; 5° 57' 3.6" S; 147° 39' 36" E; depth : 1045m)					
25	34.763	192	22.35	27.0800	0.1760
50	34.891	186	22.51	27.9600	0.3062

75	35.158	162	23.05	28.1600	0.4215
100	35.209	158	23.11	28.1500	0.5595
150	35.457	146	23.90	28.1200	0.6493
250	35.389	149	25.74	30.4300	0.6935
400	34.764	162	26.72	39.7700	0.1132
500	34.525	181	26.99	48.3900	0.1242
700	34.477	160	27.20	61.0400	0.1127
900	34.488	152	27.28	70.2500	0.1232
1005	34.505	145	27.35	75.9400	0.1301
Station 082 (August 03, 2012; 13° 59' 49.2" S; 156° 0' 25.2" E; depth : 2586m)					
25	34.927	197	22.92	27.2900	0.1754
80	34.929	196	22.93	30.1800	0.3451
100	34.951	196	23.01	27.2300	0.5787
150	35.44	174	23.72	28.5800	0.7000
180	35.789	129	24.65	28.3500	0.8403
300	35.38	146	25.81	29.9800	0.9054
500	34.657	148	26.83	43.1500	0.8936
800	34.451	163	27.23	63.0500	0.1179
1000	34.498	151	27.38	75.6700	0.1271
1350	34.565	140	27.53	92.6400	0.1442
1600	34.601	137	27.60	102.4400	0.1296
2000	34.636	141	27.67	107.4100	0.1567

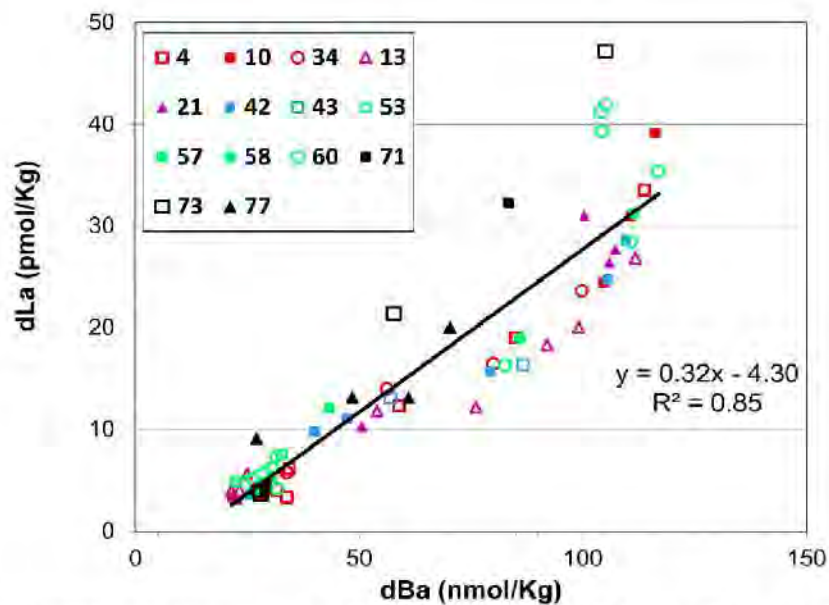


Figure A3. Correlations between dLa (in pmol/kg) and dBa of all Pandora stations. On the scale of the Solomon Basin, the relationship tends to confirm the hypothesis that part of La enrichment is linked to the barium cycle in oceanic water (Garcia-Solsona et al., 2014; Grenier et al., 2018). However, when comparing to other regions (Figure A4), the picture is more complicated: despite the high correlation coefficients (up to 0.93) for some regional relationships, their slopes differ leading to a dispersed “global” distribution. Moreover, the correlation coefficient of the dLa versus dBa relationship along the Atlantic GA03 section is quite low (0.54). All together, these data do not argue for a strong coupling between both tracers. Yet, the ongoing thorough analysis of the

filtered particles might help to explore further if there is any biogeochemical coupling between particulate barite and lanthanum (Garcia-Solsona et al, 2014).

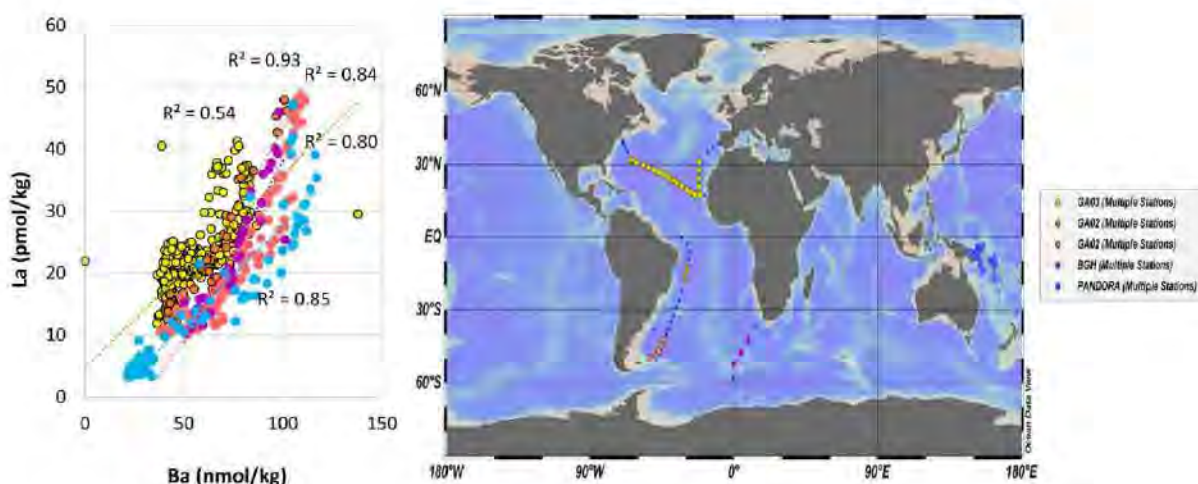


Figure A4. The dREE-dBa correlation on the global scale

4. The Mn and Al data

Dissolved Mn and dissolved Al data acquired in the framework of one of the author thesis (SM) are reported below. Their detailed interpretation is discussed in Michael et al (submitted in 2019).

Table C. Location, depths, hydrological properties, dissolved Mn (dMn) and Al(dAl) data together with total dissolved Mn (TdMn) or Al (TdAl). The total dissolved sample is defined by the lowering of sample's pH by acidification before filtering through membrane while the dissolved one is reversed.

Depth (m)	Salinity (PSU)	O ₂ (μmol/kg)	σ _θ (kg/m ³)	dMn	TdMn	dAl	TdAl
				(nM)			
Station 004 (July 01, 2012; 17° 0' 10.8" S; 162° 59' 45.6" E ; depth: 4680m)							
18	34.76	198	22.76	1.74±0.07	11.2±0.07	11.2±0.36	0±0.36
49	35.05	199	23.17	1.6±0.1	1.7±0.1	13.1±0.4	12.1±0.4
88	35.55	170	24.10	1.2±0	1.3±0.1	10.3±0.4	10.6±0.4
138	35.66	159	24.65	0.5±0	0.7±0	11.5±0.4	10.6±0.4
198	35.62	160	25.16	0.3±0	0.4±0	11±0.4	10.2±0.4
298	35.30	160	25.97	0.3±0	0.4±0	11.6±0.4	9.9±0.4
448	34.72	179	26.72	0.3±0	0.5±0	8.2±0.4	9.8±0.4
620	34.43	192	27.04	0.3±0	0.5±0	6.5±0.4	10.3±0.4
780	34.42	176	27.21	0.3±0	0.5±0	6±0.4	8.8±0.4
1000	34.48	163	27.38	0.4±0	0.7±0	9±0.4	7.1±0.4
1300	34.55	150	27.51	0.4±0	0.8±0	8.7±0.4	10.3±0.4
1320	34.56	147	27.52	0.4±0	0.6±0	8.2±0.4	6.9±0.4
Station 010 (July 03, 2012; 12° 0' 0" S; 162° 59' 56.4" E; depth : 5092m)							
30	34.62	190	22.09	1.6±0.1	1.6±0.1	11.1±0.4	11.1±0.4
95	35.28	159	22.74	1.3±0.1	1.5±0.1	11.9±0.4	12.7±0.4
135	35.83	140	23.58	0.5±0	0.7±0	7.5±0.4	5.4±0.4
175	36.03	132	24.32	0.4±0	0.5±0	5.3±0.4	4.2±0.4
223	35.86	131	25.02	0.3±0	0.4±0	5.1±0.4	4.3±0.4

300	35.22	134	25.99	0.2±0	0.4±0	4.7±0.4	4.3±0.4
397	34.76	140	26.63	0.2±0	0.4±0	6.6±0.4	5.9±0.4
500	34.55	161	26.92	0.2±0	0.4±0	7.2±0.4	7±0.4
502	34.53	162	26.94	0.3±0	0.4±0	6.2±0.4	5.1±0.4
701	34.46	157	27.21	0.3±0	0.5±0	7.6±0.4	6.8±0.4
1001	34.52	139	27.41	0.4±0	0.6±0	8.9±0.4	8.8±0.4
1302	34.57	130	27.54	0.5±0	0.8±0	8.2±0.4	7.5±0.4
Station 013 (July 04, 2012; 9° 0' 10.8" S; 162° 59' 56.4" E; depth : 3853m)							
35	34.68	191	21.77	1±0	1±0	6.9±0.5	10.2±0.5
74	35.24	182	22.26	0.9±0	1±0	9.3±0.5	8.6±0.5
125	35.56	141	23.08	0.5±0	0.6±0	11.3±0.5	9.7±0.5
180	35.85	126	24.80	0.3±0	0.4±0	7.1±0.5	6.5±0.5
181	35.85	126	24.80	0.4±0	0.4±0	6.9±0.5	5.9±0.5
225	35.61	121	25.44	0.3±0	0.4±0	5.8±0.5	4.9±0.5
300	35.19	106	26.07	0.3±0	0.4±0	3.8±0.5	4.7±0.5
400	34.71	127	26.80	0.2±0	0.4±0	6±0.5	6.4±0.5
500	34.56	136	27.05	0.3±0	0.4±0	7.7±0.5	7.8±0.5
700	34.50	136	27.24	0.4±0	0.6±0	9.6±0.5	8.4±0.5
1000	34.53	127	27.41	0.4±0	0.6±0	8.4±0.5	6.1±0.5
1300	34.57	125	27.53	0.4±0	0.7±0	8.2±0.5	9.2±0.5
Station 021 (July 07, 2012; 10° 0' 46.8" S; 160° 21' 25.2" E; depth : 3342m)							
25	34.88	185	21.99	2.2±0.1	2.3±0.1	17.9±0.4	19±0.4
45	35.13	165	22.23	2±0.1	2.2±0.1	17.2±0.4	18.1±0.4
90	35.39	150	22.76	0.5±0	0.9±0	13.7±0.3	17.8±0.4
140	35.60	134	23.68	0.5±0	1.2±0	13.6±0.3	35.9±0.4
199	35.83	131	24.79	0.3±0	0.5±0	7.3±0.3	9.6±0.5
203	35.82	130	24.83	0.3±0	0.5±0	7.2±0.3	11.3±0.3
303	34.93	120	26.51	0.3±0	0.5±0	10.3±0.3	15.1±0.5
401	34.68	140	26.86	0.3±0	0.6±0	10.3±0.3	17.5±0.4
503	34.53	160	27.06	0.3±0	0.6±0	8.6±0.3	18.6±0.5
700	34.48	156	27.22	0.3±0	0.5±0	10.1±0.3	10.9±0.5
1000	34.51	146	27.38	0.5±0	0.9±0	10.7±0.3	17.1±0.5
1300	34.57	134	27.53	0.3±0	0.7±0	10.7±0.3	15.1±0.5
Station 034 (July 10, 2012; 11° 27' 7.2" S; 154° 39' 54" E; depth : 2005m)							
45	35.17	164	22.41	0.9±0.2	1.2±0	14.3±0.3	13.4±0.3
80	35.48	140	23.18	0.5±0	0.8±0	13.7±0.3	13.8±0.3
130	35.79	131	24.15	0.5±0	0.6±0	9.6±0.3	8.2±0.3
180	35.66	144	24.77	0.3±0	0.5±0	12.9±0.3	12.7±0.3
250	35.42	151	25.75	0.2±0	0.4±0	10.7±0.3	10.8±0.3
350	35.09	162	26.32	0.3±0	0.5±0	7.8±0.3	13±0.3
Station 042 (July 15, 2012; 5° 8' 42" S; 153° 17' 24" E; depth : 3081m)							
25	34.74	191	21.73	1.6±0.1	1.9±0.1	13.5±0.3	18.7±0.4
85	35.25	177	22.28	0.5±0	0.8±0	8±0.3	9.9±0.3
127	35.50	152	23.08	0.5±0	0.8±0	13.5±0.3	12.4±0.3
130	35.54	146	23.24	0.5±0	0.9±0	12.9±0.3	13.9±0.3
180	35.64	141	24.84	0.3±0	0.6±0	10.6±0.3	11.9±0.3
225	35.35	152	25.85	0.2±0	0.5±0	7.7±0.3	10.5±0.3
300	35.05	159	26.34	0.2±0	0.4±0	8.4±0.3	8±0.3
400	34.64	174	26.84	0.2±0	0.4±0	9.1±0.3	8.4±0.3
500	34.54	158	27.02	0.2±0	0.4±0	7.1±0.3	8.9±0.3
700	34.48	157	27.18	0.3±0	0.5±0	8.8±0.3	10.7±0.3
1000	34.53	137	27.41	0.5±0	0.9±0	9.5±0.3	14.6±0.3
1300	34.58	126	27.55	0.9±0	1.5±0.1	11.9±0.3	17.9±0.4
Station 043 (July 17, 2012; 3° 59' 52.8" S; 155° 35' 38.4" E; depth : 1925m)							
25	34.69	190	21.73	1.1±0	1.2±0	8.3±0.4	7.7±0.5
55	34.80	190	21.80	1±0	1.1±0	7.2±0.4	7.9±0.5

90	35.55	166	22.63	0.6±0	0.7±0	6±0.4	5.5±0.5
150	35.91	138	23.99	0.4±0	0.5±0	4.5±0.5	2.5±0.3
225	35.19	99	26.09	0.4±0.1	0.4±0	4.2±0.4	3.9±0.5
300	34.72	123	26.78	0.3±0.1	0.4±0	8±0.4	5.8±0.5
400	34.65	120	26.89	0.2±0	0.4±0	8.4±0.5	5.6±0.3
500	34.61	120	26.99	0.3±0	0.4±0	5.4±0.5	6.7±0.3
700	34.51	88	27.18	0.3±0	0.4±0	5.4±0.5	6.4±0.3
1000	34.54	128	27.41	0.4±0	0.5±0	6.7±0.5	5.2±0.3
1300	34.57	108	27.51	0.4±0	0.7±0	4.7±0.5	6.3±0.3
Station 060 (July 22, 2012; 6° 10' 1.2" S; 152° 29' 49.2" E; depth : 5609m)							
23	34.46	108	21.89	1.9±0.1	1.9±0.1	13.3±0.3	12.9±0.3
29	34.60	193	22.05	2±0.1	1.8±0.1	13.3±0.3	12.9±0.3
65	34.96	193	22.51	1.7±0.1	1.8±0.1	12.5±0.3	12.6±0.3
129	35.54	181	23.80	0.5±0	0.7±0	11.9±0.3	12±0.3
177	35.73	143	24.70	0.3±0	0.5±0	7.2±0.3	7.2±0.3
220	35.54	135	25.45	0.3±0	0.5±0	6.4±0.3	7.7±0.3
294	35.08	129	26.26	0.3±0	0.4±0	4.9±0.3	7.4±0.3
400	34.65	125	26.83	0.2±0	0.4±0	8±0.3	7.1±0.3
500	34.50	151	27.07	0.2±0	0.5±0	5.9±0.3	8.8±0.3
700	34.48	170	27.26	0.3±0	0.5±0	5.5±0.3	8.4±0.3
1000	34.53	155	27.43	0.6±0	0.9±0	6.3±0.3	10.9±0.3
1300	34.58	138	27.55	0.6±0	1.1±0	6.6±0.3	12.2±0.3
Station 071 (July 25, 2012; 8° 19' 55.2" S; 151° 17' 27.6" E; depth : 1563m)							
23	34.78	128	22.37	1.8±0.1	1.8±0.1	14.3±0.6	13.9±0.6
69	34.97	194	22.58	0.8±0	0.9±0	12±0.6	12.3±0.6
118	35.74	181	24.33	0.5±0	0.8±0	11.2±0.6	11.4±0.6
170	35.65	134	24.80	0.3±0	0.5±0	5.8±0.6	6.7±0.6
200	35.64	137	25.27	0.3±0	0.5±0	4.3±0.6	6±0.6
300	35.08	124	26.33	0.3±0	0.5±0	8.3±0.6	11.5±0.6
400	34.98	162	26.47	0.2±0	0.4±0	7.7±0.6	11.1±0.6
550	34.52	165	27.00	0.2±0	0.4±0	5.5±0.6	7.8±0.6
730	34.46	180	27.17	0.2±0	0.4±0	5.7±0.6	8.3±0.6
860	34.50	170	27.33	0.3±0	0.7±0	6.2±0.6	10±0.6
1000	34.51	147	27.38	0.4±0	0.7±0	6±0.6	10.2±0.6
1300	34.56	144	27.51	0.5±0	0.9±0	6.5±0.6	11.2±0.6
Station 077 (July 28, 2012; 5° 57' 3.6" S; 147° 39' 36" E; depth : 1045m)							
25	34.77	132	22.35	2.5±0.1	2.7±0.1	20.7±0.4	38.7±0.4
75	35.15	191	23.06	1.3±0.1	1.4±0.1	15.3±0.4	15.7±0.4
82	35.16	163	23.06	1.3±0.1	1.5±0.1	15.4±0.4	15.5±0.4
141	35.42	162	23.63	0.7±0	1.1±0	14.4±0.4	15.6±0.4
174	35.62	146	24.69	0.3±0.1	0.5±0	11±0.4	12±0.4
220	35.42	140	25.69	0.3±0.1	0.5±0	9.9±0.4	11.8±0.4
299	35.10	148	26.28	0.2±0.1	0.5±0	8.9±0.4	10.7±0.4
399	34.78	159	26.69	0.2±0.1	0.4±0	8±0.4	9.9±0.4
501	34.57	165	26.94	0.2±0.1	0.4±0	8.2±0.4	8.4±0.4
701	34.48	178	27.20	0.4±0.1	0.7±0	9.3±0.4	10.4±0.4
902	34.49	159	27.28	0.8±0	1.4±0.1	6.9±0.4	15±0.4
999	34.51	142	27.37	1±0	1.7±0.1	6.8±0.4	15.8±0.4
Station 082 (August 03, 2012; 13° 59' 49.2" S; 156° 0' 25.2" E; depth : 2586m)							
24	34.93	197	22.92	1.7±0.1	1.7±0.1	13±0.4	13±0.4
80	34.93	196	22.93	1.6±0.1	1.7±0.1	13.5±0.4	13.4±0.4
135	35.19	185	23.31	1.5±0.1	1.6±0.1	12.5±0.4	12.5±0.4
175	35.78	128	24.58	0.3±0	0.5±0	7.1±0.4	7.3±0.4
224	35.71	129	25.14	0.3±0	0.4±0	5.6±0.4	6.4±0.4
300	35.38	146	25.81	0.2±0	0.4±0	7.2±0.4	7.8±0.4
447	34.81	134	26.63	0.3±0	0.4±0	5.4±0.4	8.5±0.4

651	34.49	163	27.07	0.2±0	0.4±0	5.9±0.4	7.9±0.4
800	34.45	163	27.23	0.2±0	0.4±0	6.1±0.4	7±0.4
1000	34.50	151	27.38	0.2±0	0.4±0	8.3±0.4	7.1±0.4
1298	34.56	142	27.51	0.3±0	0.4±0	6.5±0.4	7.1±0.4

5. The Basalt-PAAS normalization

Basalt dREE concentrations measured on samples outcropping on Tonga island (table 1a; Kelemen et al., 2013) and New Britain island (SKB04 and SKB11, table 3; Holm et al., 2013) normalized to PAAS (see figure A5-a). Despite their different shapes, all these patterns show a positive Eu anomaly which could be the source of the Eu anomaly observed in our samples (figure A5-b). Profiles of europium anomalies calculated by normalizing to PAAS (green circles) and the 3 basalts described above (filled orange, red and blue circles). The positive Eu value when compared to PAAS confirms the basaltic origin of the material. The negative values when normalized to the 3 basalts suggest that internal processes modified the relative abundance of Eu compared to its trivalent neighbors

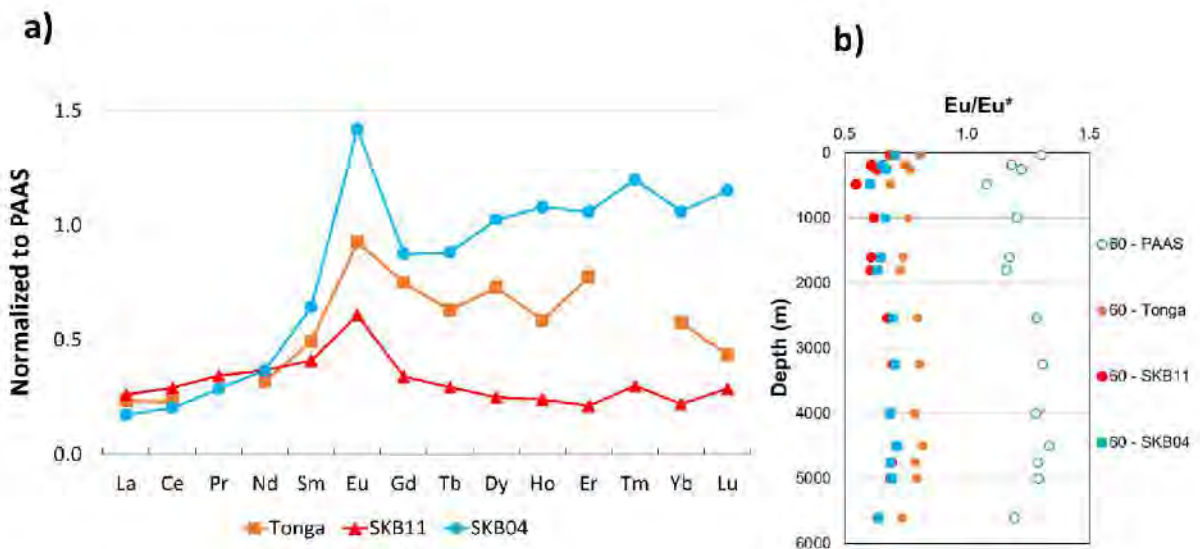


Figure A5: a) Basalt normalized to PAAS pattern. b) Europium anomaly calculated using the REE contents of the different local basaltic sources.

References

- Kelemen, P.B., Hanghøj, K. & Greene, A.R. 2013. One View of the Geochemistry of Subduction-Related Magmatic Arcs, with an Emphasis on Primitive Andesite and Lower Crust. *In: Treatise on Geochemistry: Second Edition*. Oxford, Elsevier, 749–806., <https://doi.org/10.1016/B978-0-08-095975-7.00323-5>.
- Holm, R.J., Spandler, C. & Richards, S.W. 2013. Melanesian arc far-field response to collision of the Ontong Java Plateau: Geochronology and petrogenesis of the

Simuku Igneous Complex, New Britain, Papua New Guinea. *Tectonophysics*, 603, 189–212, <https://doi.org/10.1016/j.tecto.2013.05.029>.

Michael, S. et al., Submitted in 2019. Constraining the Solomon Sea as a source of Al and Mn to the Equatorial Undercurrent.

Chapter 5

The Southwest Pacific Ocean: Neodymium isotopic composition and rare earth element concentration variation

5.1 Introduction

In the previous chapter, the dissolved REE (dREE) concentration distributions in the Coral and Solomon Seas were presented. Their relative enrichments (or not) along the circulation paths across these seas were established. We found that the only layer displaying a significant net enrichment was the lower thermocline one, enriched while crossing the Solomon Sea. We were however unable to identify the processes leading to this net enrichment (location within the Solomon Sea, origin of the enrichment, exchange or net dissolution).

In this chapter, we will consider the dissolved Nd isotopic composition (Nd-IC; ϵ_{Nd}) distribution and discuss what this complementary parameter could bring to the quantification of the transport and transformation of the dREE across the Coral and Solomon Seas. Nd-IC is used as a tracer to characterize the source of lithogenic elements to the ocean. One of the Nd isotopes, ^{143}Nd is formed by α -decay of its parent ^{147}Sm contained in the lithogenic material. The abundance of ^{143}Nd therefore varies with time- and the geological nature of this material, is normally expressed as ϵ_{Nd} :

$$\epsilon_{Nd} = \left(\frac{(^{143}\text{Nd}/^{144}\text{Nd})_{\text{sample}}}{(^{143}\text{Nd}/^{144}\text{Nd})_{\text{CHUR}}} - 1 \right) \times 10^4$$

Where: CHUR = chondritic uniform reservoir, represents the average Earth value ($^{143}\text{Nd}/^{144}\text{Nd}_{\text{CHUR}} = 0.512638$; Wasserburg *et al.*, 1981).

A short reminder on why these parameters are complementary is recalled here (more details in *chapter 1*). Any Nd IC variation observed in a given sample is reflecting either the addition of an external source or the mixing of the sampled water with another water mass, both characterized by different Nd signatures. Changes in Nd concentration could also reflect an external input or a mixing, but also removal by scavenging within the water body. If scavenging equal input –or even if it is removing less Nd than what was added to satisfy the observed (ϵ_{Nd}) change- no Nd (or weak) concentration change will be detected while (ϵ_{Nd}) is keeping the memory of a significant input. All these processes constitute what was named the “Boundary exchange” (BE, Lacan and Jeandel, 2001, 2005)). Exchange can only be revealed and calculated if one gets both ϵ_{Nd} value and Nd concentration of the different concerned reservoirs.

The possible external sources that could explain the variations of Nd-IC and/or Nd concentrations in the Solomon Sea area are: dust deposits, more particularly from the local active volcanoes; river discharges of weathered material; dissolution of sediments deposited on the oceanic margins. Details on these external sources are given in Chapter 1. In addition, the fact that these islands are sparsely populated did not prevent us from considering possible anthropogenic influence too (e.g. mining activity). Following the main pathways of the currents, each layer of water column corresponding to the water masses (Chapter 1) will be considered here.

First, a qualitative description of the changes observed for both Nd IC and Nd concentrations along these pathways is proposed. This helped us to locate where and how inputs or exchange processes are suspected. At last, different oceanic processes influencing the ϵ_{Nd} value and the Nd concentration distribution were then quantified using simple box models.

These calculations were made in the layers for which we gathered enough data to constrain them. The calculated fluxes will help us to estimate the magnitude of the land to ocean transfers, which do not concern the dREE only, but other key elements, among them nutrients of lithogenic origin, as for example Fe, Zn, Cu, Co, Cd, etc. In fact, these vital substances to oceanic water are lithogenic and most of their inputs occur at the land-ocean interface. Characterizing these fluxes is thus a major issue, knowing that they can locally contribute to the development of the biological activity (dominated in the Solomon Sea by nitrogen fixation which requires amounts of Fe) or farther to the enrichment of the EUC cold tongue (Bonnet *et al.*, 2016, 2017). These trace elements are reactive and can rapidly enter in particle-solution exchange processes, be they biologically driven or not. These non-conservative fates often lead to an underestimate of the input fluxes of these vital elements. Identification and quantification of the lithogenic inputs using complementary tracers (ϵ_{Nd} ; dREE) could thus help to better constrain the land-ocean inputs.

5.2 Sampling and analytical procedure

The sampling protocol and the detailed analytical procedure are described in Chapter 2.

Locations of the stations that have been sampled as well as the sample depths and corresponding hydrological properties are reported in *Figure 5-2* and *Table 5-1*. For sake of clarity and to make the reading of this chapter easier, we also reported the published dREE concentration data (see *Figure 2*; Pham *et al.*, 2019).

5.3 Results

5.3.1 Vertical distribution

The neodymium isotopic compositions (ϵ_{Nd}) measured in the Coral Sea, at the entrance, within and at the exit of the Solomon Sea are also compiled in *Table 5-1* and reported in *Figure 5-2*. Vertical Nd-IC profiles as a function of depth and as a function of density are also shown in *Figure 5-1*. All the profiles display high ϵ_{Nd} values at the surface, the highest value reaching +3 (Station 53). On a regional scale, the surface waters collected within the Solomon Sea (e.g: 29, 42, 60, etc) show more radiogenic values than those located outside of the Solomon Sea (e.g: 4, 10 and 13), (*Figure 5-1b*).

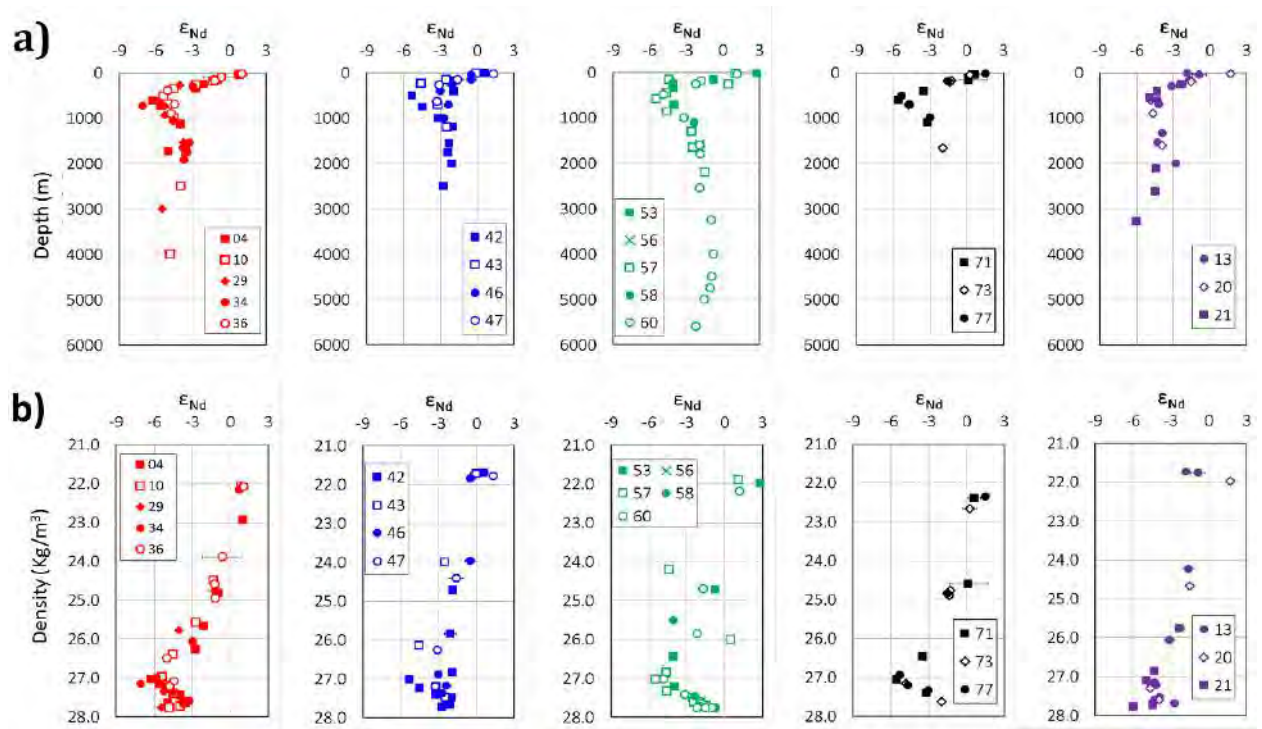


Figure 5-1 Vertical distribution of ϵ_{Nd} measured at all the stations shown in figure 5.0, as a function of a) depth and b) sigma

A pronounced minimum of the Nd-IC signature (ϵ_{Nd} values around -6) is found at 500-700m, which corresponds to the intermediate water layer (Figure 5-1a). It is observed at all the stations studied although it is slightly more negative in the south than in the north of the Solomon Sea. The thermocline layers (100-400m; $\sim\sigma_{\theta} = 24-26.9$) display a Nd IC gradient between the surface and intermediate values. This gradient is quite homogeneous except in the St George's channel (green color) which shows more dispersed values.

The deeper layers ($\sigma_{\theta} > 27.4$) display more radiogenic signal than the intermediate ones with a smooth maximum around 2000m before diminishing again in the bottom waters. Between 2000m and the bottom, a slight decrease of ϵ_{Nd} values is observed at the entrance of the Coral Sea (stations 4 and 10). A marked drop of ϵ_{Nd} values is also observed at the same depth of station 21 which corresponds to the entrance of the Solomon Sea via the Indispensable Strait). Note that these depths also show enriched Nd concentrations (Figure 5-2)

Table 5-1 Locations, depths, hydrological properties, Eu Anomalies, Nd Concentrations, Nd-IC ($^{143}\text{Nd}/^{144}\text{Nd}$) and ϵ_{Nd} of the samples analyzed in this study. All the errors are reported within 2 sigma

Depth (m)	Salinity (PSU)	Pot.temp (θ) ($^{\circ}\text{C}$)	Pot. dens σ_{θ} (kg/m^3)	Eu/Eu*	[Nd] (pmol/kg)	$^{143}\text{Nd}/^{144}\text{Nd}$	ϵ_{Nd}
Station 004 (July 01, 2012; 17° 0' 10.8" S; 162° 59' 45.6" E; depth: 4680m)							
30	34.84	25.9	22.94	1.21 ± 0.07	3.8 ± 0.1	0.512687 ± 12	1 ± 0.2
166	35.63	21.5	24.83	1.12 ± 0.05	3.2 ± 0.1	0.512588 ± 17	-1 ± 0.3
250	35.46	17.8	25.67	1.11 ± 0.05	3.4 ± 0.1	0.512528 ± 13	-2.1 ± 0.3
351	35.10	13.9	26.28	1.09 ± 0.04	4.5 ± 0.1	0.512497 ± 14	-2.8 ± 0.3
621	34.43	6.5	27.04	1 ± 0.05	7.3 ± 0.2	0.512318 ± 08	-6.2 ± 0.2
730	34.42	5.4	27.17	1.11 ± 0.08	7.7 ± 0.4	0.512352 ± 07	-5.6 ± 0.2
1134	34.51	3.6	27.44	1.05 ± 0.06	10.3 ± 0.3	0.512434 ± 12	-4 ± 0.2
1734	34.62	2.4	27.64	-	-	0.512384 ± 14	-5 ± 0.3

3598	34.69	1.5	27.76	1.12 ± 0.06	24.1 ± 0.7	-	-
Station 010 (July 03, 2012; 12° 0' 0" S; 162° 59' 56.4" E; depth : 5092m)							
35	34.62	28.1	22.09	1.21 ± 0.07	3.6 ± 0.1	0.512682 ± 12	0.9 ± 0.2
185	36.03	24.5	24.50	-	-	0.51257 ± 17	-1.3 ± 0.3
260	35.52	18.4	25.58	1.21 ± 0.07	3.6 ± 0.1	0.512498 ± 18	-2.7 ± 0.4
350	34.92	12.7	26.40	1.05 ± 0.06	4.9 ± 0.2	0.512407 ± 11	-4.5 ± 0.2
515	34.51	7.4	26.98	-	-	0.512363 ± 09	-5.4 ± 0.2
680	34.46	5.4	27.20	0.95 ± 0.06	7.7 ± 0.2	0.512379 ± 07	-5.1 ± 0.2
1000	34.52	4.0	27.41	-	-	0.512408 ± 06	-4.5 ± 0.2
1735	34.61	2.4	27.63	1.12 ± 0.06	13.1 ± 0.3	0.512457 ± 09	-3.5 ± 0.2
2500	34.67	1.8	27.73	1.13 ± 0.07	18.5 ± 0.6	0.512435 ± 12	-4 ± 0.2
4000	34.69	1.4	27.77	1.08 ± 0.06	24.6 ± 0.7	0.51239 ± 11	-4.8 ± 0.2
Station 013 (July 04, 2012; 9° 0' 10.8" S; 162° 59' 56.4" E; depth : 3853m)							
5	34.65	29.2	21.74	1.14 ± 0.06	3.9 ± 0.1	0.512545 ± 18	-1.8 ± 0.4
40	34.68	29.2	21.77	1.05 ± 0.06	3.3 ± 0	0.512595 ± 30	-0.8 ± 0.6
160	35.83	24.1	24.24	1.26 ± 0.07	2.8 ± 0.1	0.512556 ± 19	-1.6 ± 0.4
300	35.19	15.2	26.07	0.96 ± 0.04	3.7 ± 0.1	0.51248 ± 19	-3.1 ± 0.4
600	34.52	6.1	27.16	1.08 ± 0.03	7.2 ± 0.1	0.51242 ± 07	-4.3 ± 0.2
685	34.50	5.5	27.22	1.18 ± 0.06	7.2 ± 0.2	0.512425 ± 16	-4.2 ± 0.3
1335	34.57	3.1	27.54	1.02 ± 0.04	9.6 ± 0.2	0.51244 ± 08	-3.9 ± 0.2
1535	34.60	2.7	27.60	1.11 ± 0.05	10.6 ± 0.3	0.51242 ± 07	-4.3 ± 0.2
2000	34.64	2.0	27.69	1.21 ± 0.06	14.8 ± 0.4	0.512499 ± 07	-2.7 ± 0.2
Station 020 (July 06, 2012; 9° 59' 56.4" S; 160° 25' 1.2" E; depth : 2910m)							
25	34.83	28.9	21.97	1.21 ± 0.06	4.7 ± 0.2	0.512727 ± 15	1.7 ± 0.3
190	35.82	22.6	24.67	-	-	0.512561 ± 18	-1.5 ± 0.4
600	34.49	6.2	27.12	1.02 ± 0.06	7.2 ± 0.2	0.512391 ± 07	-4.8 ± 0.2
900	34.49	4.8	27.30	1.08 ± 0.07	8.2 ± 0.3	0.5124 ± 09	-4.6 ± 0.2
1600	34.60	2.7	27.60	-	8.2 ± 0.3	0.512438 ± 07	-3.9 ± 0.2
Station 021 (July 07, 2012; 10° 0' 46.8" S; 160° 21' 25.2" E; depth : 3342m)							
250	35.39	17.2	25.76	1.08 ± 0.05	4.1 ± 0.1	0.512519 ± 20	-2.3 ± 0.4
400	34.68	9.0	26.86	1.07 ± 0.05	5.3 ± 0.1	0.512418 ± 07	-4.3 ± 0.2
550	34.49	6.4	27.10	1.06 ± 0.03	6.8 ± 0.1	0.512385 ± 14	-4.9 ± 0.3
2115	34.64	2.1	27.69	1.18 ± 0.04	15.3 ± 0.7	0.512414 ± 08	-4.4 ± 0.2
2625	34.68	1.8	27.74	1.21 ± 0.1	18.1 ± 0.9	0.512411 ± 12	-4.4 ± 0.2
3280	34.70	1.6	27.77	1.14 ± 0.1	19 ± 0.7	0.512331 ± 13	-6 ± 0.3
Station 029 (July 09, 2012; 11° 3' 39.6" S; 156° 12' 54" E; depth : 3856m)							
267	35.38	17.1	25.78	1.1 ± 0.05	4 ± 0.1	0.51243 ± 16	-4.1 ± 0.3
737	34.47	5.3	27.21	1.07 ± 0.05	7.2 ± 0.2	0.512368 ± 13	-5.3 ± 0.3
934	34.50	4.3	27.36	1.08 ± 0.06	8.6 ± 0.2	0.512369 ± 11	-5.3 ± 0.2
1140	34.54	3.7	27.45	1.16 ± 0.05	9.2 ± 0.2	0.512434 ± 07	-4 ± 0.2
1534	34.59	2.8	27.59	1.16 ± 0.06	11.4 ± 0.3	0.512446 ± 07	-3.7 ± 0.2
2999	34.70	1.7	27.77	1.14 ± 0.08	16.9 ± 0.9	0.512357 ± 11	-5.5 ± 0.2
Station 034 (July 10, 2012; 11° 27' 7.2" S; 154° 39' 54" E; depth : 2005m)							
40	34.93	28.5	22.17	1.21 ± 0.04	4.2 ± 0.1	0.512676 ± 12	0.7 ± 0.2
180	35.66	21.8	24.77	1.21 ± 0.03	3.4 ± 0	0.512578 ± 26	-1.2 ± 0.5
300	35.25	15.4	26.08	1.14 ± 0.05	4.5 ± 0.1	0.512485 ± 11	-3 ± 0.2
635	34.49	7.1	27.00	1.01 ± 0.04	7.2 ± 0.1	0.512339 ± 07	-5.8 ± 0.2
735	34.44	5.6	27.16	1.04 ± 0.04	8.6 ± 0.2	0.512276 ± 06	-7.1 ± 0.2
1065	34.49	4.1	27.37	1.05 ± 0.04	9.3 ± 0.2	0.512404 ± 07	-4.6 ± 0.2
1550	34.60	2.7	27.60	1.05 ± 0.06	13.3 ± 0.5	0.512472 ± 07	-3.2 ± 0.2
1665	34.61	2.6	27.62	1.11 ± 0.05	13.8 ± 0.3	0.512447 ± 07	-3.7 ± 0.2
1750	34.63	2.4	27.65	1.11 ± 0.04	15 ± 0.4	0.512463 ± 07	-3.4 ± 0.2
1920	34.65	2.1	27.69	-	15 ± 0.4	0.51245 ± 13	-3.7 ± 0.3
Station 036 (July 11, 2012; 11° 30' 7.2" S; 154° 23' 24" E; depth : 1168m)							
25	34.49	27.8	22.09	1.25 ± 0.04	8.2 ± 0.1	0.512693 ± 17	1.1 ± 0.3
100	35.43	24.3	23.89	1.18 ± 0.04	3.9 ± 0	0.512606 ± 8	-0.6 ± 1.6
160	35.61	22.3	24.60	1.22 ± 0.04	3.8 ± 0	0.512576 ± 17	-1.2 ± 0.3

180	35.64	21.1	24.96	1.11 ± 0.04	3.8 ± 0	0.512579 ± 15	-1.2 ± 0.3
400	34.94	12.2	26.51	1.08 ± 0.04	5.2 ± 0.1	0.512381 ± 11	-5 ± 0.2
700	34.46	6.3	27.09	0.98 ± 0.03	7.2 ± 0.1	0.51241 ± 10	-4.5 ± 0.2
900	34.46	5.1	27.24	1.07 ± 0.04	7.5 ± 0.1	0.512394 ± 1	-4.8 ± 0.2
Station 042 (July 15, 2012; 5° 8' 42" S; 153° 17' 24" E; depth : 3081m)							
5	34.69	29.4	21.71	1.26 ± 0.09	3.9 ± 0.2	0.512669 ± 14	0.6 ± 0.3
180	35.65	22.0	24.72	1.21 ± 0.06	3.4 ± 0.1	0.512543 ± 16	-1.9 ± 0.3
225	35.35	16.8	25.85	0.79 ± 0.04	3.8 ± 0.1	0.512533 ± 25	-2.1 ± 0.5
400	34.64	9.0	26.84	0.98 ± 0.04	6.1 ± 0.1	0.512542 ± 13	-1.9 ± 0.3
500	34.54	7.3	27.02	1.03 ± 0.04	6.8 ± 0.1	0.512366 ± 12	-5.3 ± 0.2
750	34.48	5.3	27.23	1.06 ± 0.03	7.3 ± 0.1	0.512408 ± 08	-4.5 ± 0.2
1000	34.53	4.0	27.41	1.07 ± 0.08	9.4 ± 0.3	0.512476 ± 11	-3.2 ± 0.2
1200	34.56	3.5	27.49	1.22 ± 0.06	10.4 ± 0.2	0.512537 ± 12	-2 ± 0.2
1550	34.61	2.6	27.62	1.22 ± 0.05	14.5 ± 0.3	0.51252 ± 07	-2.3 ± 0.2
1750	34.62	2.4	27.64	1.16 ± 0.05	15.8 ± 0.5	0.512516 ± 08	-2.4 ± 0.2
2000	34.64	2.1	27.68	1.22 ± 0.07	18 ± 0.8	0.512532 ± 08	-2.1 ± 0.2
2500	34.66	1.8	27.73	1.2 ± 0.08	21.8 ± 0.9	0.512498 ± 09	-2.7 ± 0.2
Station 043 (July 17, 2012; 3° 59' 52.8" S; 155° 35' 38.4" E; depth : 1925m)							
5	34.66	29.3	21.72	1.13 ± 0.07	3.5 ± 0.1	0.512635 ± 24	-0.1 ± 0.5
150	35.91	25.1	23.99	1.11 ± 0.05	3.8 ± 0.2	0.512509 ± 12	-2.5 ± 0.2
230	35.16	14.8	26.14	1.19 ± 0.06	5.2 ± 0.1	0.512404 ± 09	-4.6 ± 0.2
700	34.51	5.9	27.18	1.24 ± 0.04	7.6 ± 0.1	0.512473 ± 07	-3.2 ± 0.2
1200	34.56	3.7	27.47	1.15 ± 0.04	9.6 ± 0.2	0.512511 ± 08	-2.5 ± 0.2
Station 046 (July 18, 2012; 4° 42' 0" S; 154° 52' 48" E; depth : 3117m)							
50	34.79	29.2	21.85	1.19 ± 0.04	3.3 ± 0	0.512615 ± 15	-0.5 ± 0.3
150	35.97	25.4	23.97	1.11 ± 0.03	2.6 ± 0	0.512613 ± 20	-0.5 ± 0.4
400	34.65	8.7	26.89	1.11 ± 0.04	6.5 ± 0.1	0.512483 ± 10	-3 ± 0.2
700	34.54	6.0	27.19	1.1 ± 0.05	7.2 ± 0.2	0.512518 ± 18	-2.3 ± 0.4
1000	34.54	4.3	27.39	1.07 ± 0.04	8.9 ± 0.2	0.512499 ± 08	-2.7 ± 0.2
Station 047 (July 18, 2012; 4° 56' 2.4" S; 154° 38' 52.8" E; depth : 1004m)							
25	34.67	29.1	21.78	1.27 ± 0.04	4.4 ± 0.1	0.512707 ± 17	1.3 ± 0.3
156	36.02	24.0	24.41	0.99 ± 0.02	3 ± 0	0.512556 ± 28	-1.6 ± 0.6
264	35.08	14.0	26.27	1.05 ± 0.03	4.8 ± 0.1	0.512479 ± 12	-3.1 ± 0.2
635	34.52	5.9	27.20	1.09 ± 0.04	7.7 ± 0.1	0.512471 ± 10	-3.3 ± 0.2
Station 053 (July 19, 2012; 4° 54' 18" S; 152° 52' 12" E; depth : 733m)							
25	34.88	29.0	21.99	1.27 ± 0.08	5.7 ± 0.3	0.512783 ± 10	2.8 ± 0.2
149	35.61	21.9	24.72	1.12 ± 0.05	4 ± 0.1	0.512599 ± 12	-0.8 ± 0.2
335	34.98	12.6	26.45	1.1 ± 0.03	5.3 ± 0.1	0.512431 ± 10	-4 ± 0.2
719	34.48	5.4	27.22	1.07 ± 0.03	7.8 ± 0.1	0.512434 ± 10	-4 ± 0.2
Station 056 (July 20, 2012; 4° 4' 37.2" S; 152° 32' 20.4" E; depth : 1580m)							
1582	34.60	2.8	27.59	1.08 ± 0.04	14.3 ± 0.3	0.512543 ± 06	-1.9 ± 0.2
Station 057 (July 20, 2012; 4° 34' 12" S; 152° 31' 22.8" E; depth : 2552m)							
25	34.77	29.0	21.91	1.39 ± 0.08	5.2 ± 0.1	0.512693 ± 07	1.1 ± 0.2
150	35.58	23.6	24.20	1.19 ± 0.08	3.7 ± 0.1	0.512413 ± 10	-4.4 ± 0.2
250	35.27	15.8	26.00	1.09 ± 0.1	4.2 ± 0.1	0.512662 ± 17	0.5 ± 0.3
450	34.65	9.0	26.85	1.02 ± 0.04	6.2 ± 0.1	0.512402 ± 09	-4.6 ± 0.2
580	34.51	7.1	27.02	1.06 ± 0.04	6.8 ± 0.1	0.512359 ± 1	-5.4 ± 0.2
850	34.50	4.6	27.33	1.15 ± 0.05	8.1 ± 0.2	0.512405 ± 16	-4.5 ± 0.3
1302	34.57	3.4	27.51	1.18 ± 0.05	11.5 ± 0.3	0.512509 ± 06	-2.5 ± 0.2
1650	34.61	2.6	27.62	-	-	0.512513 ± 05	-2.4 ± 0.2
2201	34.65	2.0	27.71	1.2 ± 0.05	20 ± 0.5	0.512562 ± 07	-1.5 ± 0.2
Station 058 (July 21, 2012; 5° 30' 10.8" S; 152° 5' 52.8" E; depth : 1142m)							
215	35.50	18.6	25.51	1.16 ± 0.06	3.9 ± 0.1	0.512431 ± 13	-4 ± 0.3
1100	34.55	3.7	27.47	1.07 ± 0.05	11 ± 0.3	0.512519 ± 05	-2.3 ± 0.2
Station 060 (July 22, 2012; 6° 10' 1.2" S; 152° 29' 49.2" E; depth : 5609m)							
35	34.74	28.0	22.19	1.26 ± 0.06	4.6 ± 0.2	0.512699 ± 13	1.2 ± 0.3
180	35.73	22.3	24.70	1.18 ± 0.09	3.4 ± 0.1	0.512551 ± 14	-1.7 ± 0.3

250	35.33	16.6	25.86	1.28 ± 0.06	5.1 ± 0.1	0.512527 ± 09	-2.2 ± 0.2
480	34.53	7.2	27.03	1.04 ± 0.04	6.5 ± 0.2	0.512391 ± 08	-4.8 ± 0.2
1000	34.53	3.9	27.43	1.2 ± 0.04	9.4 ± 0.1	0.512476 ± 07	-3.2 ± 0.2
1600	34.61	2.6	27.62	1.3 ± 0.05	14.3 ± 0.5	0.512542 ± 2	-1.9 ± 0.4
1800	34.63	2.3	27.67	1.2 ± 0.03	16.5 ± 0.7	0.512545 ± 05	-1.8 ± 0.2
2541	34.66	1.7	27.73	1.23 ± 0.04	24.3 ± 0.8	0.512542 ± 05	-1.9 ± 0.2
3250	34.69	1.7	27.76	1.29 ± 0.06	27.8 ± 1.1	0.512591 ± 04	-0.9 ± 0.2
4000	34.70	1.7	27.77	1.28 ± 0.06	28.8 ± 0.8	0.5126 ± 05	-0.7 ± 0.2
4500	34.70	1.7	27.77	1.26 ± 0.08	30 ± 0.9	0.512593 ± 04	-0.9 ± 0.2
4750	34.70	1.7	27.77	1.29 ± 0.04	30.4 ± 0.4	0.512587 ± 03	-1 ± 0.2
5000	34.70	1.7	27.77	1.29 ± 0.04	25.4 ± 0.3	0.51256 ± 03	-1.5 ± 0.2
5603	34.70	1.6	27.77	1.19 ± 0.06	26.3 ± 0.7	0.512527 ± 06	-2.2 ± 0.2
Station 071 (July 25, 2012; 8° 19' 55.2" S; 151° 17' 27.6" E; depth : 1563m)							
50	34.80	27.6	22.39	1.26 ± 0.1	4 ± 0.2	0.512668 ± 26	0.6 ± 0.5
160	35.66	22.4	24.60	1.09 ± 0.1	3.9 ± 0.2	0.512645 ± 78	0.1 ± 1.5
400	34.98	12.6	26.47	1.08 ± 0.08	5.2 ± 0.2	0.51246 ± 11	-3.5 ± 0.2
600	34.49	6.7	27.06	1 ± 0.08	6.9 ± 0.4	0.512354 ± 07	-5.5 ± 0.2
1100	34.52	4.1	27.41	1.17 ± 0.05	9.7 ± 0.2	0.512476 ± 07	-3.2 ± 0.2
Station 073 (July 26, 2012; 7° 9' 57.6" S; 149° 59' 56.4" E; depth : 5253m)							
50	35.06	27.3	22.66	1.22 ± 0.05	4.1 ± 0.1	0.512651 ± 27	0.2 ± 0.5
170	35.59	21.7	24.76	1.33 ± 0.18	8.6 ± 0.9	0.512573 ± 15	-1.3 ± 0.3
200	35.60	21.2	24.90	1.15 ± 0.05	3.3 ± 0.1	0.512567 ± 13	-1.4 ± 0.3
700	34.47	5.9	27.16	1.01 ± 0.05	12.9 ± 0.4	0.512393 ± 11	-4.8 ± 0.2
1650	34.61	2.6	27.62	1.15 ± 0.07	28.1 ± 1.2	0.512544 ± 04	-2 ± 0.2
Station 077 (July 28, 2012; 5° 57' 3.6" S; 147° 39' 36" E; depth : 1045m)							
25	34.77	27.6	22.35	1.24 ± 0.04	4.9 ± 0.1	0.512716 ± 14	1.5 ± 0.3
180	35.61	21.4	24.85	1.12 ± 0.03	3.4 ± 0	0.512561 ± 21	-1.5 ± 0.4
501	34.57	8.0	26.94	1.09 ± 0.03	8 ± 0.1	0.512367 ± 13	-5.3 ± 0.3
701	34.48	5.5	27.20	1.05 ± 0.03	7.9 ± 0.1	0.512401 ± 06	-4.6 ± 0.2
983	34.51	4.5	27.35	1.13 ± 0.05	9.6 ± 0.2	0.512484 ± 07	-3 ± 0.2

Contrastingly, the deep water samples collected inside the Solomon Sea (station 60) reveal a gradual increase of ϵ_{Nd} values down to 4000m followed by a decrease of ϵ_{Nd} values toward the bottom, from -1 at (4000m) to -3 at (5600m). The station 60 dNd vertical profile shows a concomitant Nd concentration depletion in these bottom waters.

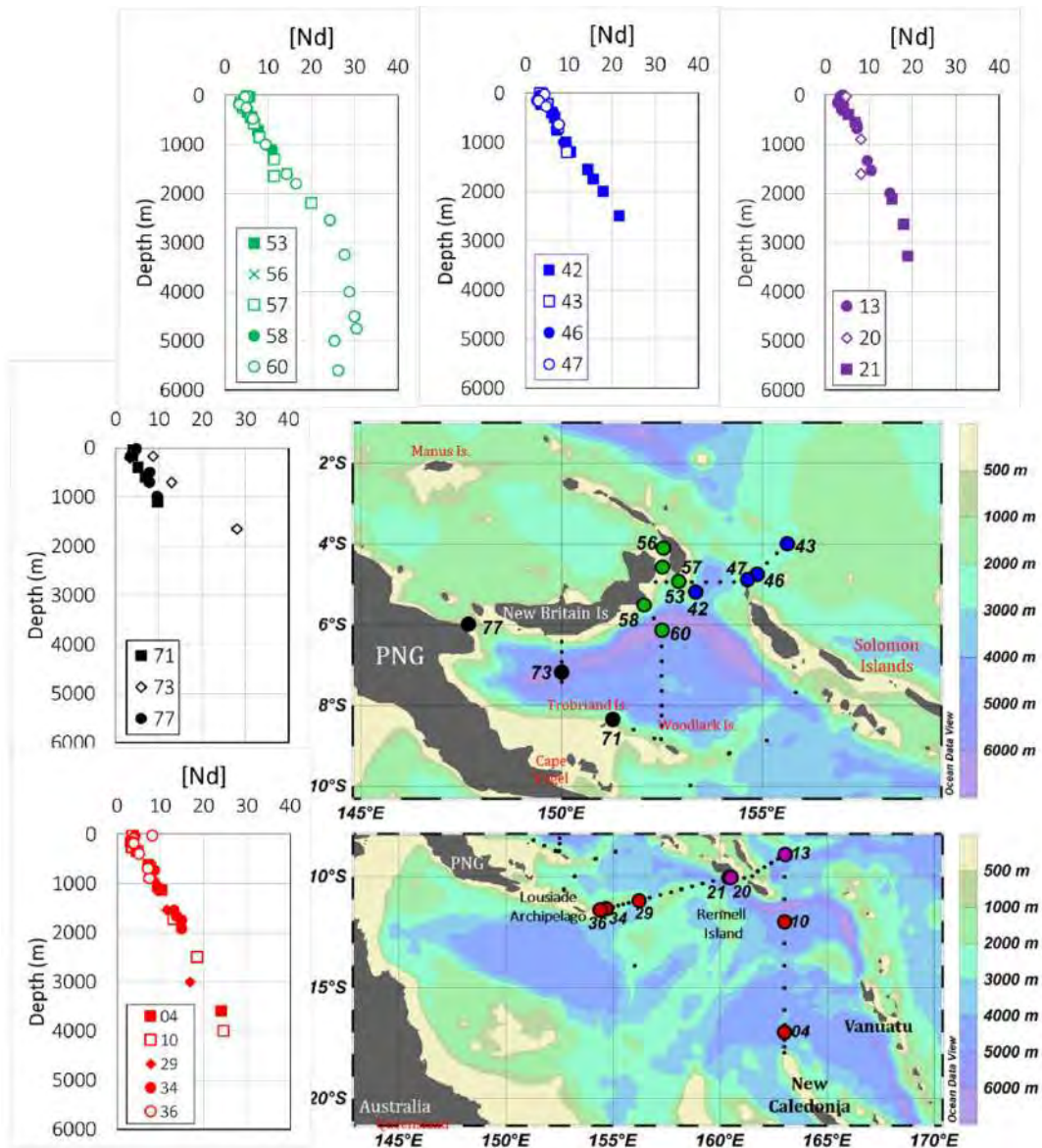


Figure 5-2 Location of the sampling stations dedicated to the Nd isotopic composition measurements during Pandora. Different colors are used to “cluster” the different sampling areas, as in Pham *et al.*, (2019). The red points correspond to the southern entrance of the Solomon Sea. Samples collected in waters flowing through four straits (Indispensable, Vitiaz, St George’s and Solomon), are colored with violet, black, green and dark blue, respectively. These color criteria will be kept all along this study. In addition, dissolved Nd concentration vertical profiles (pmol/kg) are also reported, using colors consistent with the sampling location ones.

5.3.2 Comparison with previous studies

Grenier *et al.*, (2013) analyzed samples at stations located in the Coral Sea, in the North Caledonian Jet core (station Flusec 43), at the entrance of the Solomon Sea (Flusec 29) and in the Vitiaz Strait (EUC -30) allowing us to compare our data with published value. *Figure 5-3* allows locating these stations together with the PANDORA ones. Comparisons of the Nd isotopic values are made along the potential densities in order to avoid any bias due to possible temporal variability affecting the isopycnal depths.

An excellent agreement is observed between the data obtained in this work and Grenier's results. Our analytical protocols were also initially validated by the GEOTRACES international intercalibration exercise (van de Flierdt *et al.*, 2012). Here, the good consistency between results from two different cruises and obtained by two different providers in the same laboratory reinforces our trust in our data. This consistency is also indicating that in the open ocean Nd IC could be considered as a conservative tracer of the water masses on this geographical scale and because the stations are far from any lithogenic inputs (Tachikawa *et al.*, 2017). The only slight difference is observed in the surface layer of the Vitiaz Strait. Such small Nd IC variations at different sampling times likely reflect surface water natural variability, either due to variable external sources or highly variable circulation. This will be discussed in the following section.

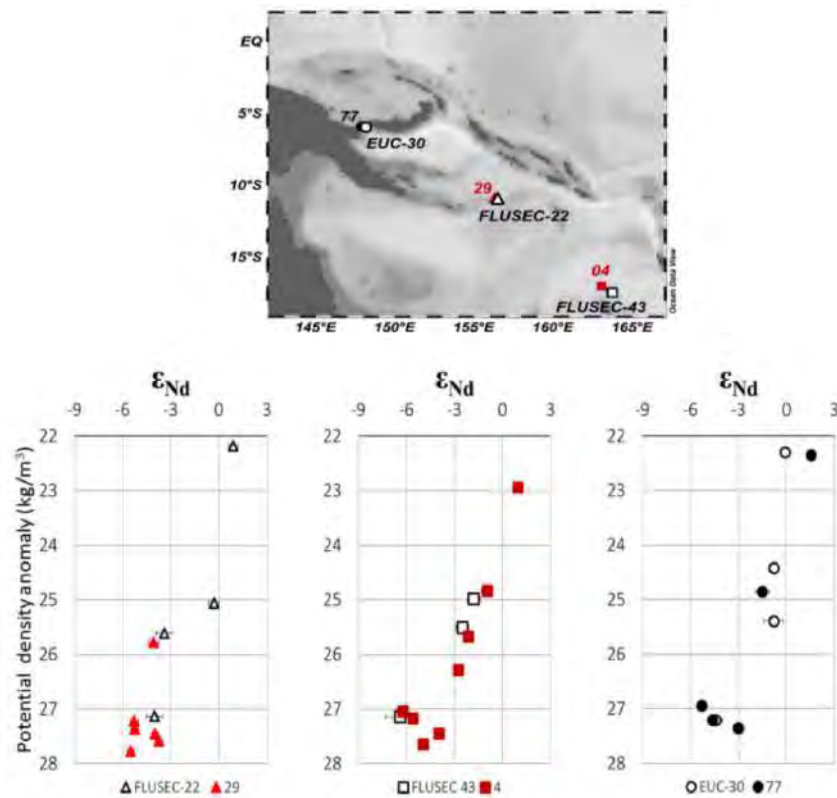


Figure 5-3 Comparison of our data with those measured in the framework of preceding studies (Grenier *et al.*, 2013).

5.4 Discussion

5.4.1 Geochemical characteristics of the lithogenic source

Figure 5-5 displays the ϵ_{Nd} data of the geological materials outcropping at the surface of the continent (Australia) and islands surrounding the studied area. Published data on rocks, beach sand and detrital lithogenic particles have been considered when reading the literature following the strategy adopted by Jeandel *et al.*, (2007). Similarly, Figure 5-6 shows the data for the bottom sediments of the Coral and Solomon Seas. These dataset were extracted using the EarthChem portal (<http://www.earthchem.org>). Altogether 28 articles were downloaded and thoroughly read to extract values representative of surfaces large enough to generate a

significant amount of particles (Jeandel *et al.*, 2007). The list of references is provided in Annex B of this manuscript.

New and fresh basaltic dusts could be emitted from the numerous active volcanoes characterizing this area. They are potential sources of very radiogenic Nd-IC inputs to the surrounding areas (solid earth as seawater surfaces). Therefore, recent erupted volcanoes were also identified in *Figure 5-5*. The volcano list was extracted from Global Volcanism Program (http://volcano.si.edu/gvp_vo_tw.cfm). Their emissions are the most radiogenic of this area.

Another possible source of lithogenic material entering seawater is extractive activities. Dust originating from mining heap together with muddy mine wastes could be a significant source of terrigenous sediment to seawater (*Figure 5-4*; Jupiter *et al.*, 2018). The PNG mining industry is driving the economy of this area, with broad and highly mechanized operation recorded in 2018 (<http://pngchamberminpet.com.pg/industrybenefits/economiccontributions>). A significant amount of lithogenic particles could be brought to the sea each year by these extracting activities. This influence is supposed to be more severe in surface layer. On the PNG island, Edie Creek mines is particularly important (*Figure 5-5*; <http://pngchamberminpet.com.pg/our-resource-industry/mining>). Belonging to PNG country but located east of the New Britain Island, Lihir is also one of biggest mine of PNG and goldmine on a worldwide scale. This extensive activity may leave a significant imprint on water passing along Lihir island.

The Solomon archipelago is also displaying many various mining activities including i) nickel mines in Choiseul and Santa Isabel islands, ii) Gold Ridge mine at the Guadalcanal island and ii) bauxite mine at Rennel island (Allen, 2018). This high density of mines surrounding the Solomon Sea which were intensively exploited (some of them are even re-opening as Gold Ridge for example) locally accelerated the weathering potentially generating a significant source of lithogenic material. This anthropogenic activity could also modify the Nd parameters (concentration and IC) of the seawater.

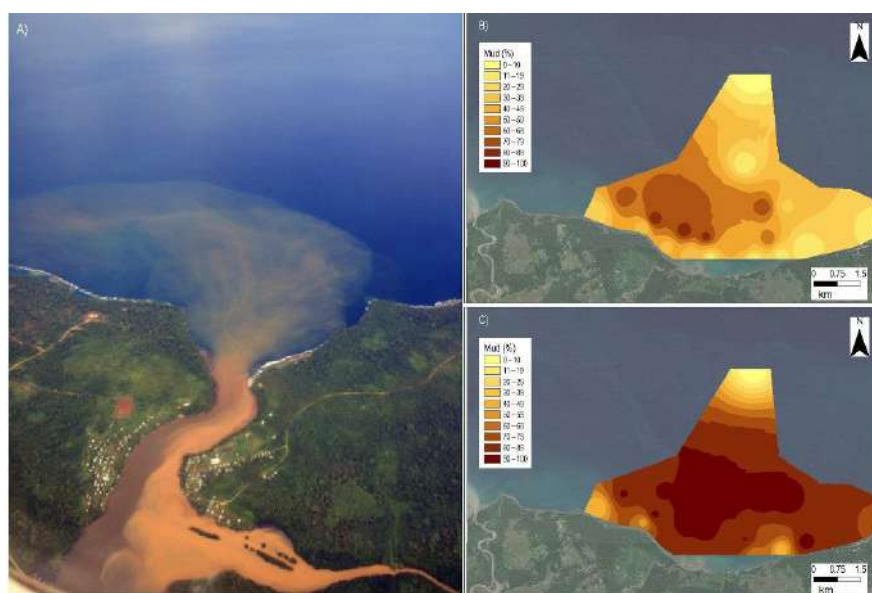


Figure 5-4 (A) Suspended sediment runoff at estuary of New Georgia Island, Solomon archipelago. Mud distribution in Tetere Bay, Guadalcanal Island in (B) 1977 and in (C) 2016, 20 years' after Gold Ridge mine development. Data from Jupiter *et al.*, (2018).

Most of the ϵ_{Nd} data reveal highly radiogenic sources consistent with the back-arc tectonic and volcanic structures of the studied area. However, some specific areas are displaying negative ϵ_{Nd} values (Australian and south Papua New Guinea coast essentially).

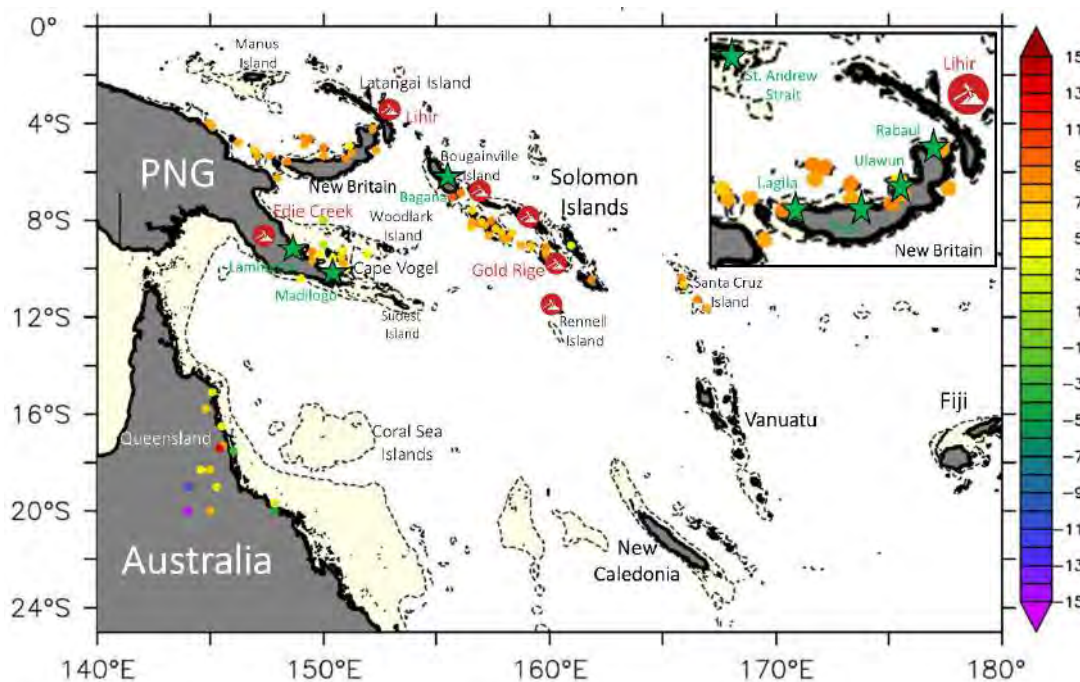


Figure 5-5 ϵ_{Nd} value of samples of rocks and continent material extracted from the geochemical data set of EarthChem portal (<http://www.earthchem.org>). Recent active volcanoes are marked by green stars. The volcano names are also highlighted by green color. The areas where the bathymetry is shallower than 1000m depth are shaded in beige. Mine locations are displayed on the map by red pixel icon (Data from PNG Chamber of Mines and Petroleum, <http://pngchamberminpet.com.pg/our-resource-industry/mining>)

In more details, the mostradiogenic Nd-IC signatures are observed in the north of New Britain (ϵ_{Nd} values up to +7; Cunningham *et al.*, 2009, 2012). On this island, some recent volcanic eruptions were recorded including Pago in 2003; Rabaul in 2006, Ulawun in 2005, Lagila in 2006 (http://volcano.si.edu/gvp_votw.cfm). High radiogenic material is also observed on dozens of islands of the Solomon archipelago, from Rennelle to Bougainville Island where some active volcanos were also found (e.g: Bagana; Schuth *et al.*, 2004, 2009).

At the southern tip of PNG, the Nd isotopic signatures are slightly less radiogenic than in the north and east, displaying ϵ_{Nd} values around +3. Moreover, Cameron, McCulloch and Walker, (1983) revealed that material outcropping at Cape Vogel could show negative ϵ_{Nd} values down to -12. Discussing in details the geological reason of this observation is beyond the scope of this chapter, although it corresponds to the reworking of old crustal material by the more recent tectonic.

Australian eastern coast appears as a patchwork of different lithogenic materials which reveal both positive and negative ϵ_{Nd} values (Rudnick *et al.*, 1986; Ewart, Chappell and Menzies,

1988; Allen, 2000; Zhang, 2001; Handler, Bennett and Carlson, 2005). The Proterozoic and Paleozoic basins covering the eastern Queensland display the most negative ϵ_{Nd} values of the studied area (down to -15; *Shaping a Nation: A Geology of Australia*, 2012). However, the coastal region extending from -18°S to -16°S results of interlacing between Paleozoic and Mesozoic materials which led to fluctuating ϵ_{Nd} values, ranging from -5 to +5.

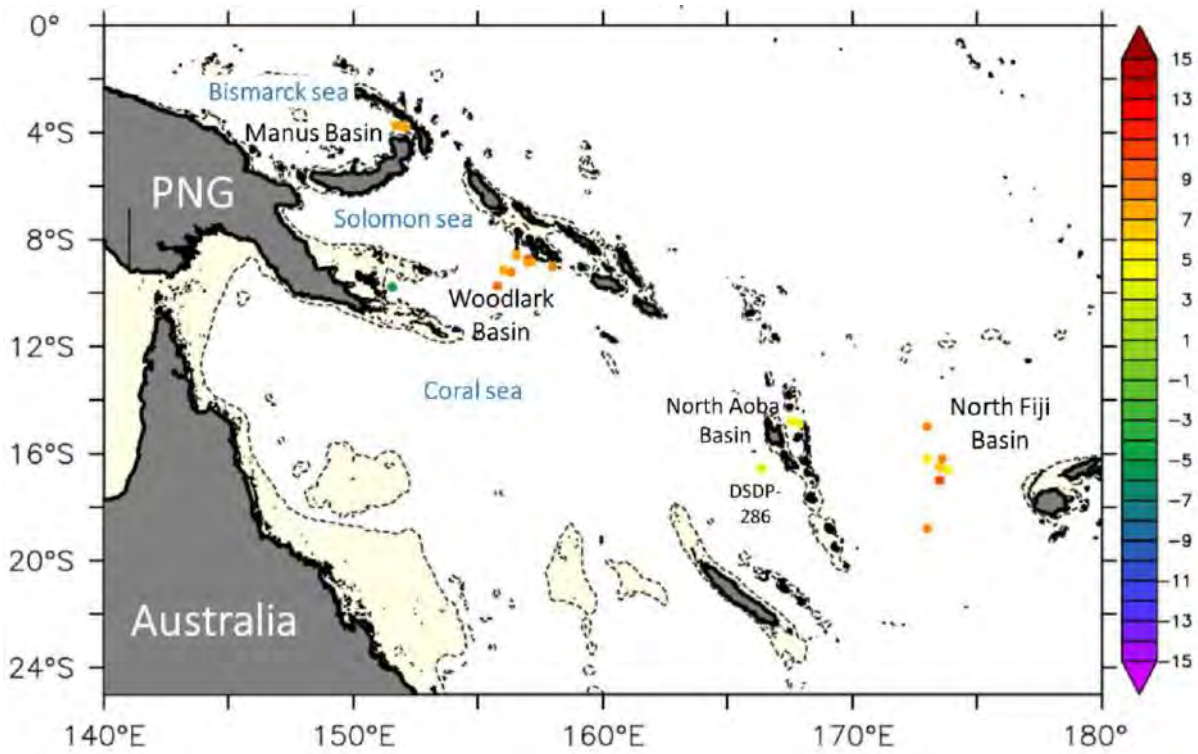


Figure 5-6 ϵ_{Nd} of sediment particles collected in different basins from Fiji to the north of New Britain Island. Data from the EarthChem portal (<http://www.earthchem.org>).

The sediment Nd IC data are still very scarce in this remote area despite our thorough investigation (Figure 5-6). From the north Fiji Basin to the eastern part of Manus Basin, high radiogenic signals are identified, the highest ϵ_{Nd} values reaching +10 (Briqueu *et al.*, 1994; Nohara *et al.*, 1994; Kamenetsky *et al.*, 2001; Beier *et al.*, 2015). At the southern entrance of the Solomon Sea, sediments of the Woodlark basin show radiogenic values close to the Solomon Islands (ϵ_{Nd} ranging between +7 and +9) while negative values (down to -4.8) are observed at the western end of the section, in the eastern PNG's bay (Chadwick *et al.*, 2009; Speckbacher *et al.*, 2012). The later likely reflect deposits of metamorphic materials outcropping on a large part of Cape Vogel. (Figure 5.5; <http://exploringtheearth.com/2018/04/30/exploration-papua-new-guinea/png-geology/>)

5.4.2 Seawater modification through the Solomon Sea

In this section, the distribution of the Nd isotopic signatures will be discussed following the main oceanic pathways along the different layers described in Chapter 1. In order to provide a broader coverage of our area, we reported the results obtained at stations FLUSEC 43, EUC-15, EUC-24, EUC-25 and EUC-28 (Grenier *et al.*, 2013) and St47 (Behrens *et al.*, unpublished).

Four main sections were considered: 1) From the Coral Sea to the southern entrance of the Solomon Sea, 2) from the Solomon Sea Southern entrance to the Woodlark- Trobriand islands,

3) from inside to outside the Solomon Sea through the three Straits (Vitiaz, St. George's and Solomon Straits), 4) more specifically, water entering the Solomon Sea through the Indispensable Strait. The variation of ϵ_{Nd} values and the Nd concentrations will be discussed using maps drawn for each layer and the identification of the potential sources for land-ocean inputs will be provided by the geological frame presented above (*Figure 5-5; Figure 5-6*).

Before entering into detailed descriptions the general trend is that more radiogenic waters (higher ϵ_{Nd} values) were generally found in the northern parts and exits of the Solomon Sea compared to the southern ones (below 10°S). However, the Nd concentrations remain fairly stable while ϵ_{Nd} values are changing, suggesting that boundary exchange processes might occur inside the Solomon Sea. A recurrent feature is the observation of noticeable high Nd concentrations in different layers of station 73 (*Figures 5-10, 5-13 and 5-14* below). Although one cannot exclude an analytical contamination, the location of this station off Lae harbor could also reflect anthropogenic inputs from rivers draining mines in land. In any case, we did not consider this station in our discussion, but left the data, reported in brackets. For some layers for which we could gather enough information to constrain flux calculation, specific quantification of the external inputs and scavenging fluxes will be proposed.

a) Surface waters

Horizontal distributions of ϵ_{Nd} values together with dissolved Nd concentrations are reported in the maps of *Figure 5-7*. In general, surface waters flowing close to the islands, especially active volcanic islands are characterized by a strong radiogenic signal.

The Nd-IC of materials brought to the surface waters could originate from two vectors mainly: atmospheric dust deposition (volcanic or extractive activities origin, see above) and fine particles carried to seawater by rivers and/or diffused streaming resulting from i) the active weathering characterizing these volcanic islands (Milliman, Farnsworth and Albertin, 1999), ii) the waste water or mud from operating mines (Jupiter *et al.*, 2018).

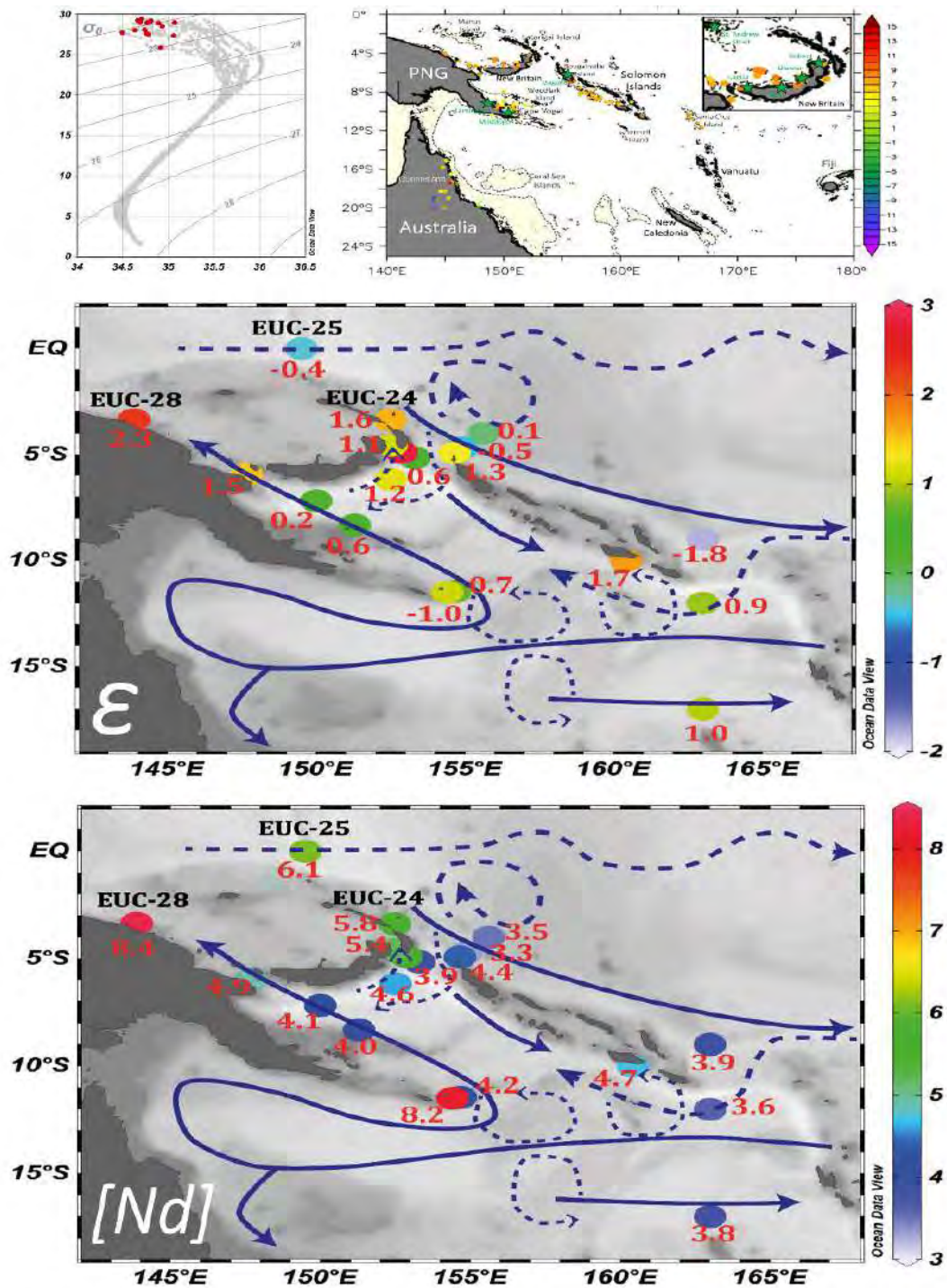


Figure 5-7 Neodymium data, hydrographic properties and main circulation scheme of the surface waters (5-40m). The data reported here are identified by the red dots on the adjacent θ - S plot. The ε_{Nd} data of the potential geological sources (Figure 5-5) are also recalled at the right corner of the top panel. Main currents are determined from Ceccarelli et al., (2013) and represented by continuous dark blue arrow. In addition, water current observed during Pandora are represented by dashed-arrow.

- At the entrance of the Solomon Sea, Nd-IC and Nd concentrations of the surface waters at station 34 show the same values as at station 10. Getting closer to the PNG's coast, more negative ε_{Nd} values are found at station 36 ($\varepsilon_{Nd} = -1$) while Nd concentration doubles compared to the value found at station 34, reaching 8.2 pmol/kg. These observed values

could result from: i) a modification of the water signature while flowing along the Australian coast characterized by negative fields ii) more likely recent local inputs from the extreme southern tip of PNG. The former is the only geological structure displaying unradiogenic outcroppings while the later would be consistent with the high Nd concentrations (*Figures 5-5*). However, the lack of precise Nd-IC of this PNG extreme tip prevents us to conclude farther.

- In general, surface waters in the three northern straits are more radiogenic than in the south, the most radiogenic ones being observed in the eastern St. George's channel and Solomon Straits where the surface waters are coming from the north, in other words are entering within the Solomon Sea. This likely reflects inputs from the most radiogenic fields, corresponding to the active volcanoes located on New Britain or influence of Lihir mine (*Figure 5-5*)(Schuth *et al.*, 2004, 2009). From station 71 (Trobriand-Woodlark islands) toward the Vitiaz passage, an increase of ϵ_{Nd} value is observed while Nd concentration remain stable. This could reflect BE process along the PNG coast. In addition, waters are flowing along the Cape Vogel (*Figure 5.5*), location of active mining: deforestation and land extraction could favor dust inputs of anthropic origin. Downstream Vitiaz Strait, station EUC-28 display even more radiogenic Nd-IC signals ($\epsilon_{Nd} = +2.3$), reflecting inputs of PNG margin origin, mostly linked to the Sepik river discharge (Jeandel *et al.*, 2013). In the western part of the Solomon Strait, surface water was entering the Solomon Sea Strait during PANDORA (*Figure 4a of Germaineaud et al.*, 2016)). The high ϵ_{Nd} value observed at the surface of station 53 (+2.8) could thus result from BE process along the New Ireland's margin since surface waters arriving from upstream indicates less radiogenic signal ($\epsilon_{Nd} = +1.6$; st EUC 24, Grenier *et al.*, 2013), while Nd concentrations between these two stations reveal no significant modification. The source of high radiogenic material here could arrive from regular weathering or wastes discharged from Lihir mine (*Figure 5-5*). At the eastern end of the Solomon strait, a surprising drop of the Nd-IC signal is seen at station 46 with a value of -0.5 while this station is sandwiched between stations 43 and 47 characterized by ϵ_{Nd} values of -0.1 and 1.3, respectively. Actually, this negative value corresponds to the incursion of colder water brought by a small eddy located at 4°S. Station 46 surface water is also characterized by a lower Nd concentration than its neighbors. (*Figure 5-8*)
- Regarding the Indispensable strait, the surface waters collected downstream the strait (stations 20 & 21) display a significative increase of +3 units compared to station 13 (from $\epsilon_{Nd} = -1.8$ to +1.7) together with a slight enrichment of Nd concentration from 3.9 pmol/Kg to 4.7 pmol/Kg, respectively. This is consistent with the fact that this narrow strait is surrounded by very radiogenic fields (*Figure 5-5*). We hypothesize that both Nd and ϵ_{Nd} increases reflect lithogenic inputs from the island, noticeably the high extracting activity of Gold Ridge mine at the Guadalcanal island (See section 5.4.1)

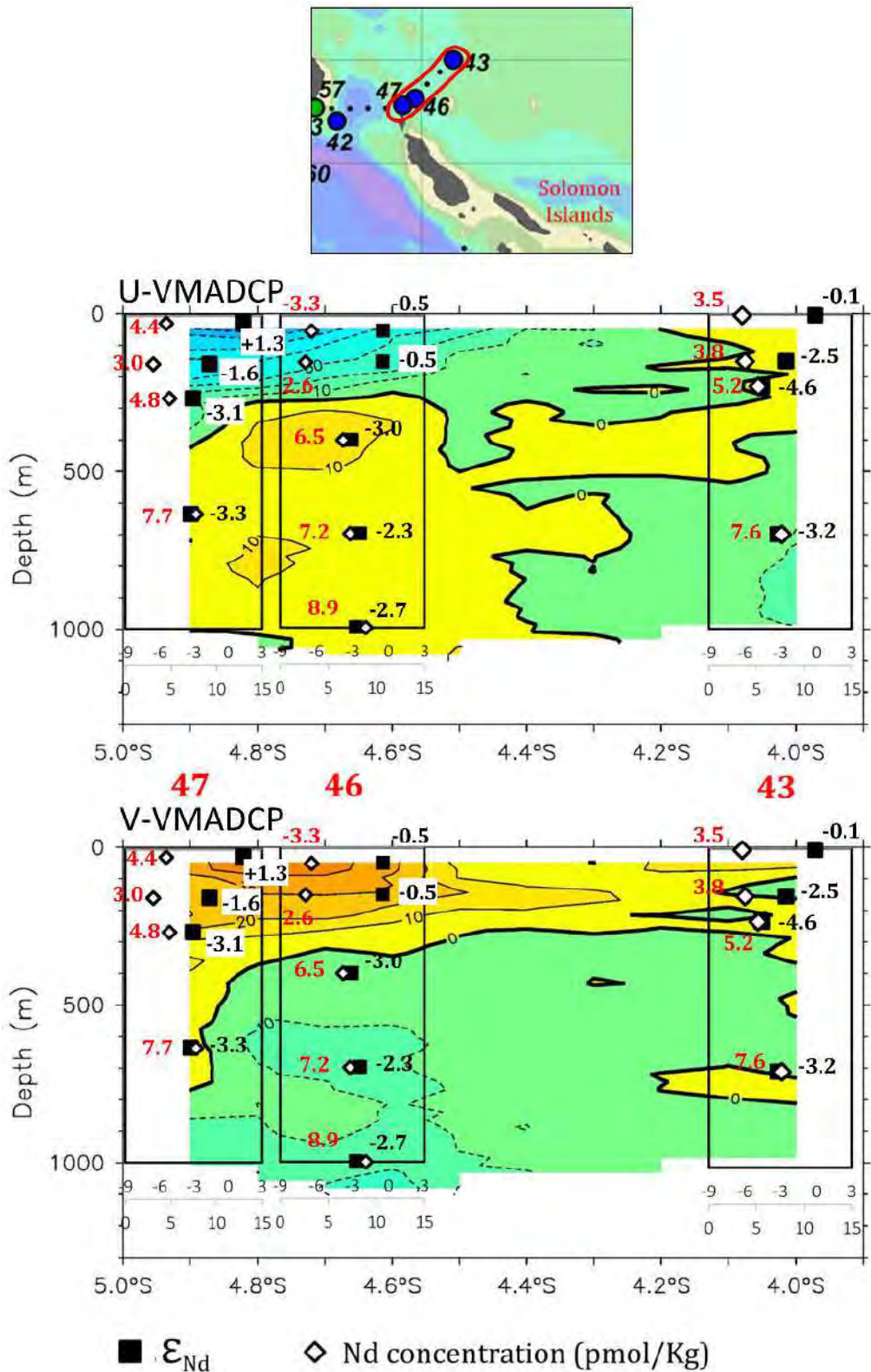


Figure 5-8 Zonal cross-section S-ADCP velocities from station 43 to station 47 on which we reported vertical data of ϵ_{Nd} and Nd concentrations. Red numbers correspond to the sampled stations. Yellow color indicates positive value, representing northward and eastward directions. ϵ_{Nd} values and Nd concentrations are reported on the sections by black and red numbers, respectively –courtesy of Gerard Eldin, Chief Scientist of PANDORA). Note that the currents here are dominated by tidal variability at semi-diurnal periods, and reverse.

Figure 5-9 shows the Eu anomalies versus ϵ_{Nd} values measured in the surface waters. The Eu anomalies data are taken in Pham *et al.*, (2019). The quasi linear positive correlation between both parameters is consistent with an enrichment of the waters by dissolution of material of basaltic origin while flowing from outside (stations 13, 43 and 46 less radiogenic and less pronounced Eu anomaly) to inside the Solomon Sea (remaining stations with more radiogenic and higher Eu anomaly). Grenier *et al.*, (2013, 2018) already discussed the interest of using the dissolved Eu anomaly as tracer of the local basalts. This was recently confirmed by Pham *et al.*, (2019) and reinforced here with ϵ_{Nd} values.

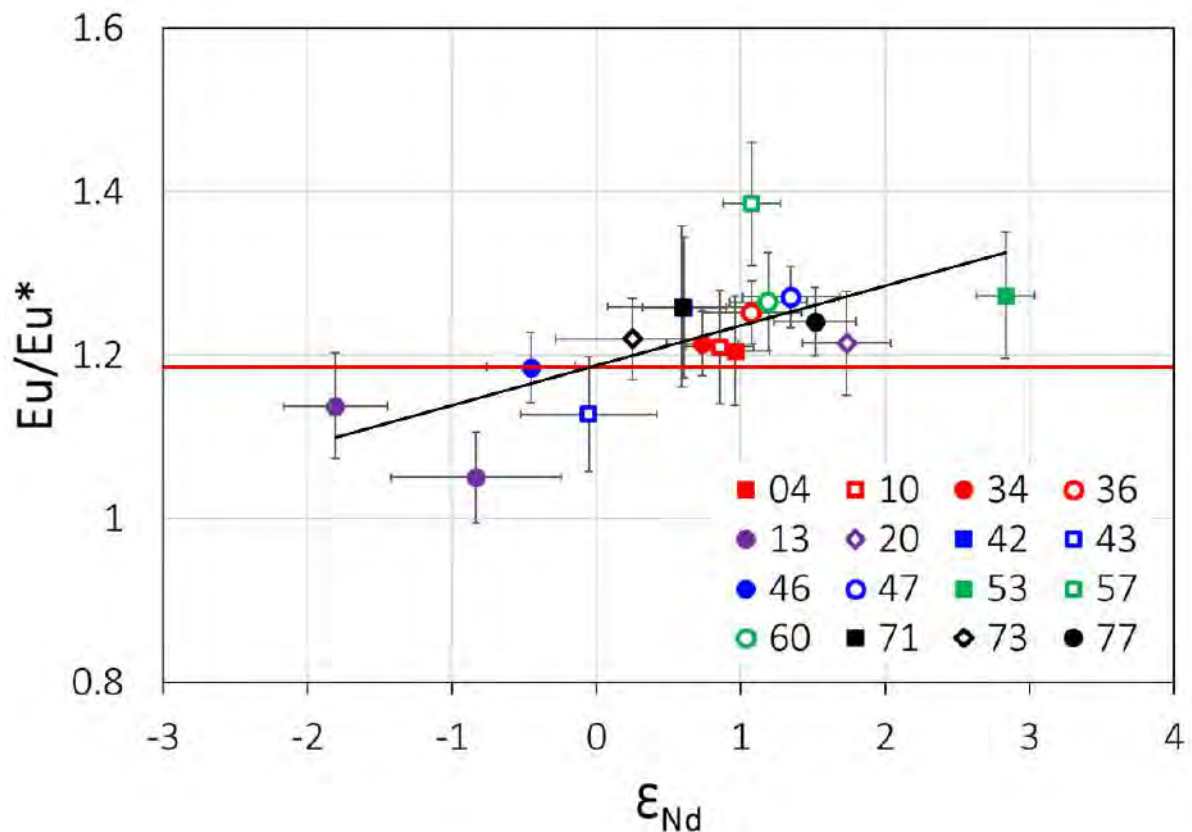


Figure 5-9 Plot of the Eu anomalies as a function of ϵ_{Nd} of the surface waters, for all the stations documented during Pandora. Higher values ($Eu/Eu^* \geq 1.2$ and $\epsilon_{Nd} > 0$) are observed for stations located inside the Solomon sea. Eu anomalies data are extracted from Pham *et al.*, (2019).

As a consequence, surface waters passing through the Solomon Sea were imprinted by high positive Nd-IC signal of the basaltic-origin material arriving from volcanic area; however, this lithogenic material intrusion mostly happens at some specific locations.

b) Upper Thermocline Layer (UTW)

The distribution of Nd-IC of Tropical Water (TW) in the UTW is shown in Figure 5-10. As a whole, this layer is relatively homogeneous, ϵ_{Nd} values ranging within -1.9 and -0.8. However, this relative constancy of the signal is perturbed by some local features discussed below.

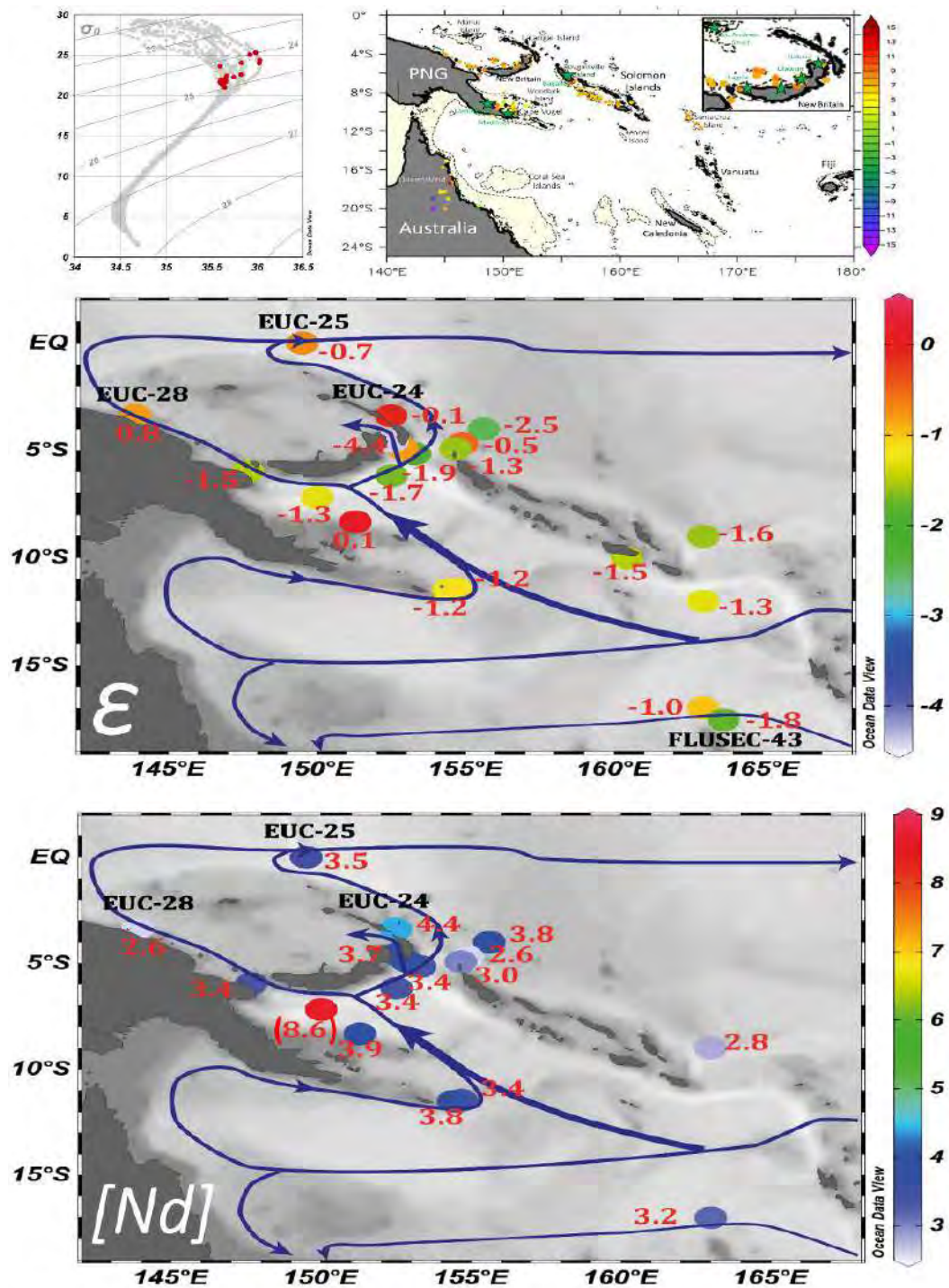


Figure 5-10 As figure 5.7 for UTW-Tropical Waters ($\sigma_\theta = 24-25.3\text{Kg/m}^3$). Value in bracket indicate possible contaminating sample.

- From the Coral to the southern entrance of the Solomon Sea, the seawater displays constant ϵ_{Nd} values and Nd concentrations, around -1.2 and 3.5, respectively. Between stations 34 and 36 (at the extreme tip of the PNG coast), the influence of potential recent inputs seems no longer significant since we observe a remarkable similarity of their Nd parameters.
- Between the Woodlark and Trobriand Islands, station 71 shows a slight increase of Nd-IC signal (from -1.2 to 0.1) while its Nd concentration remains equal to the upstream one (~ 3.8 pmol/Kg). This could reflect that boundary exchange (BE) processes occur along the

PNG's coast, altering the ϵ_{Nd} values but not the Nd concentration ones; although the uncertainty affecting the data (*Table 5-1*) prevents us to conclude further.

- Regarding the three northern straits: a) the ϵ_{Nd} value of UTW passing through Vitiaz Strait is marked by a decrease from station 71 to station 77, reaching a minimum at -1.5 in the middle of Vitiaz passage. Further north, at EUC-28, Nd-IC signature rises up again, to reach +0.8 (Grenier *et al.*, 2013); these authors suggested that the impact of Sepik river discharge could still be active at these depths. Contrastingly, Nd concentrations show continuous decrease from Vitiaz (3.4 pmol/kg) to EUC-28 (2.6 pmol/Kg). Although we cannot exclude a sample contamination at station 73 (discussed in Pham *et al.*, (2019) and mentioned above), its high Nd concentration could also reflect an external input. In such case, its Nd signature might be negative ($\epsilon_{Nd} \leq -2.5$) in order to change the ϵ_{Nd} value of +0,1 at station 71 to -1.3 at station 73. to -. b) In St. George's channel and Solomon Strait the UTW are less radiogenic with a striking minimum recorded at Station 57 ($\epsilon_{Nd} = -4.4$ in the midpoint of the narrow St.George). The stable Nd concentration distribution reflects the possibility that BE takes place in this strait. However, the negative source of Nd-IC remains unknown since this strait is located next to the volcanic and radiogenic New Britain. Nevertheless, the number of faults and active tectonic at play in the channel and between both New Britain and New Ireland could lead to the reworking of older materials at certain depths of this narrow area (Lindley, 2006). c) In the eastern part of the Solomon Strait, the mesoscale eddy is still active at this depth, expressed by station 46 parameters different from its neighbor's ones (*Figure 5-8*). Interestingly, unlike at the surface, station 46 is now more radiogenic than the two others.
- No major change is observed in the Indispensable Strait: the water kept its negative ϵ_{Nd} value observed upstream (station 13; -1.6) during its trajectory.

c) *The Lower Thermocline Layer (LTW)*

As described in chapter 1, this layer comprises different water masses with distinct hydrological properties: The Central Waters (CW) and the SubAntarctic Mode Waters (SAMW) However, they also display markedly different Nd signatures, reflecting their area of formation (Grenier *et al.*, 2013). While CW are relatively radiogenic (ϵ_{Nd} around -2.5), the SAMW of southern origin are more negative (ϵ_{Nd} around -4.5). Thus, we decided to subdivide the LTW in 2 layers: The Upper LTW (ULTW, $\sigma_\theta = 25.3-26.4$) and the lower LTW (LLTW, $\sigma_\theta = 26.4-26.9$) transporting the CW and SAMW respectively. (Chapter 1)

i. ULTW ($\sigma_\theta = 25.3-26.4$)

The ϵ_{Nd} values of ULTW increase from $\epsilon_{Nd} = -4.1$ at station 29 to approximately -2 in the north (e.g: station 42, 60). Besides, the Nd concentration distribution is relatively homogeneous, which could reflect occurrence of BE on the scale of the Solomon Sea for this layer. (*Figure 5-11*)

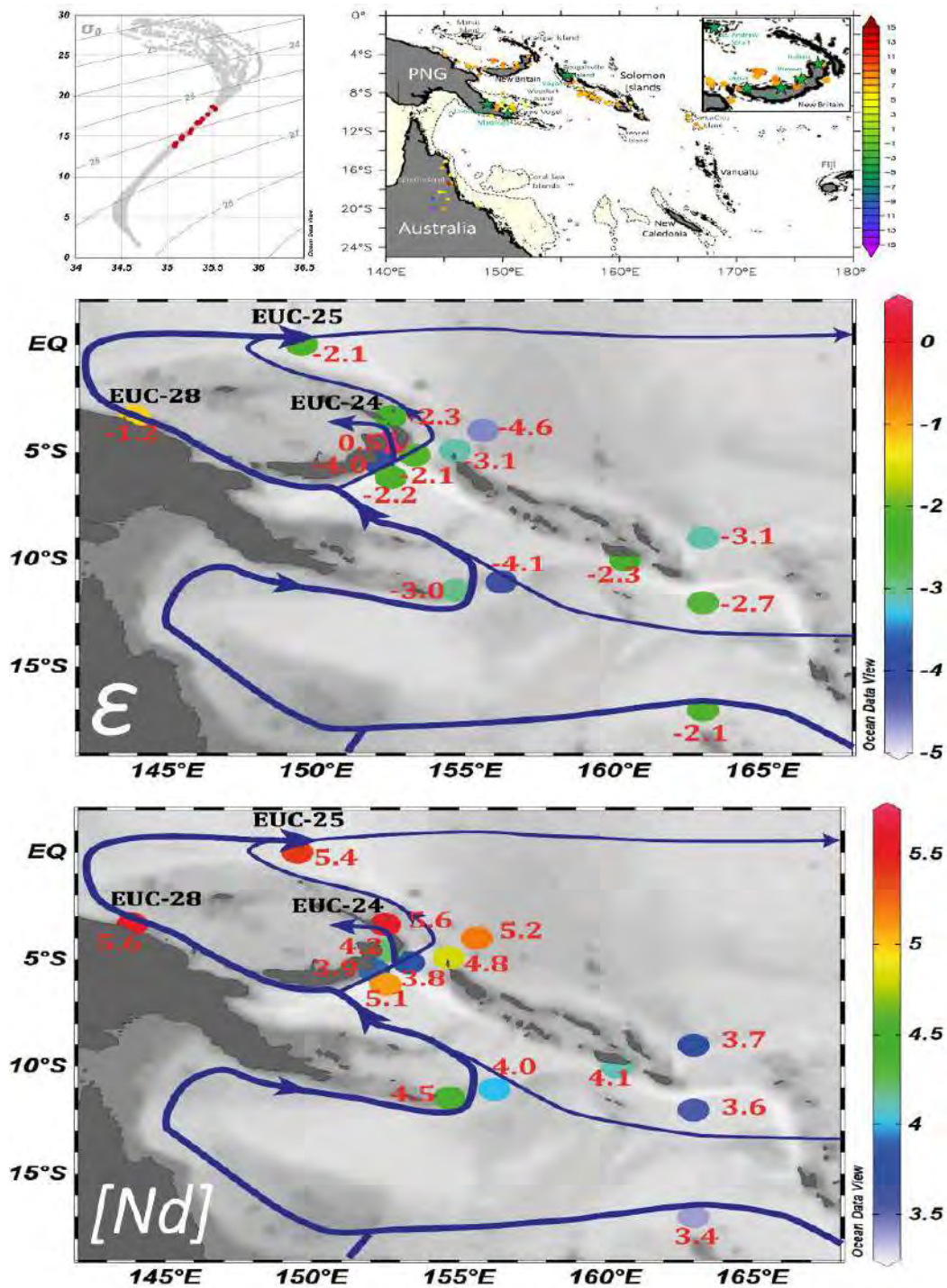


Figure 5-11 As figure 5.7, for ULTW-CW ($\sigma_\theta = 25.3-26.4 \text{ Kg/m}^3$)

- Together with a slight concentration increase, the more negative seawater found at station 29 ($\varepsilon_{Nd} = -4.1$) compared to the upstream station located in the eastern of the Coral Sea (station 10; $\varepsilon_{Nd} = -2.7$) could reflect an enrichment from negative sources along the Australian coast. This is consistent with the Australian rocks IC shown in *Figure 5-5*.
- Regarding the three northern straits: This layer is not documented for the Vitiaz Strait. The high ε_{Nd} found downstream at station EUC-28 reflects margin inputs near the Sepik river mouth as discussed in Grenier *et al.*, (2013). In the middle of the St. George's channel, station 57 is marked by significant increase of Nd IC signature ($\varepsilon_{Nd} = +0.5$) when compared to the upstream station 58 ($\varepsilon_{Nd} = -4.0$). This high value corresponds likely to

local processes. However, the Nd concentration does not show any significant input which leads us to hypothesize that BE took place here. Finally, the Nd-IC signal of ULTW passing through the western end of the Solomon Strait stays constant around -2.2 (station 42; EUC-24). The more negative values found outside likely corresponds to water transported from station 13 to the north by the South Equatorial Current (SEC).

- More radiogenic water was found after passing through the Indispensable strait (station 21; $\epsilon_{Nd} = -2.3$), compared to station 13 ($\epsilon_{Nd} = -3.1$). In addition, the slight Nd concentration increase between both stations is consistent with external input in this narrow Strait, with energetic currents.

ii. Lower LTW-SAMW ($\sigma_{\theta} = 26.4-26.9$)

Figure 5-12 shows the distribution of Nd-IC and Nd concentration in the lower LTW. As for the ULTW we observe a south-north general increase of the ϵ_{Nd} values excepted at Vitiaz strait.

- At the southern entrance of the Solomon Sea, negative Nd IC are observed, ranging within -4.5 (station 10) to -5.0 (Station 36).
- At station 71 (off Cape Vogel; Figure 5.5), a radiogenic Nd-IC signal higher than in the south ($\epsilon_{Nd} = -3.5$) is observed while the Nd concentration remains stable. This suggests that BE is occurring along the PNG margin for this layer.
- At the exit of Vitiaz strait, ϵ_{Nd} values of LLTW are similar to those observed at the southern entrance, ($\epsilon_{Nd} = -5.3$ at station 77), likely reflecting that the branch of the NGCU flowing from station 36 to Vitiaz was not impacted by the lithogenic input observed at station 71. The LLTW exiting the St. George's channel shows a signature close to what is observed in the same channel in the UTW, which could indicate a local effect of similar origin. More radiogenic and richer in Nd concentration, radiogenic waters were found downstream of the eastern Solomon Strait (up to $\epsilon_{Nd} = -1.9$) suggesting fresh basaltic lithogenic inputs

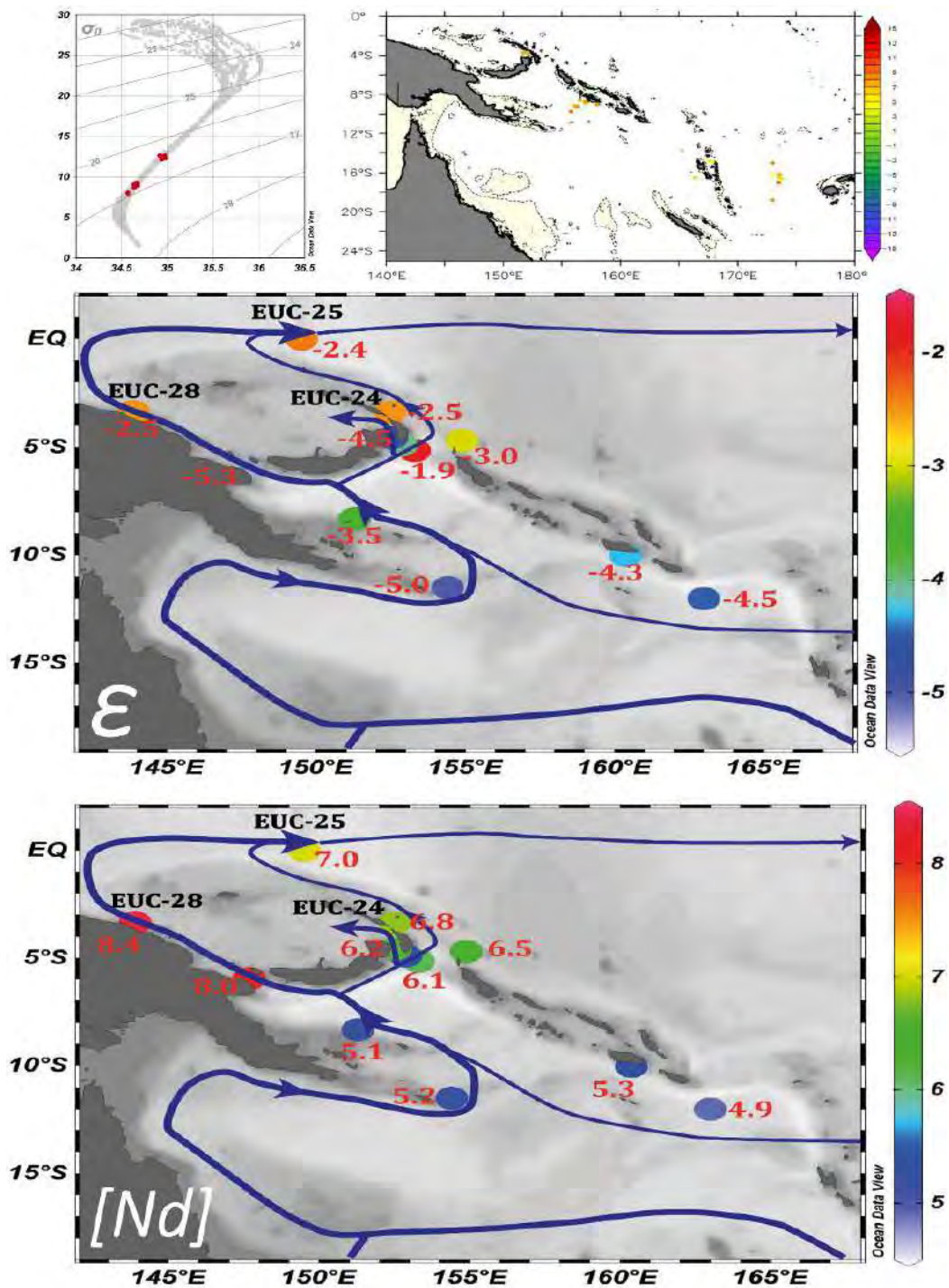


Figure 5-12 As figure 5.7, for LLTW-SAMW (σ_{θ} =26.4-26.9 Kg/m³)

d) Intermediate layer (IW)

The two water masses identified in this layer are the Antarctic Intermediate Water (AAIW) and the Equatorial Pacific Intermediate Water (EqPIW; Chapter 1). A strong contrast is observed between waters upstream and inside the Solomon Sea, and waters outside of the northern straits. Nd-IC ranges from approximately -5.0 at the entrance of Coral Sea up to -2.3 in the northern area (around 4°S). The Nd concentrations however, stay relatively constant.

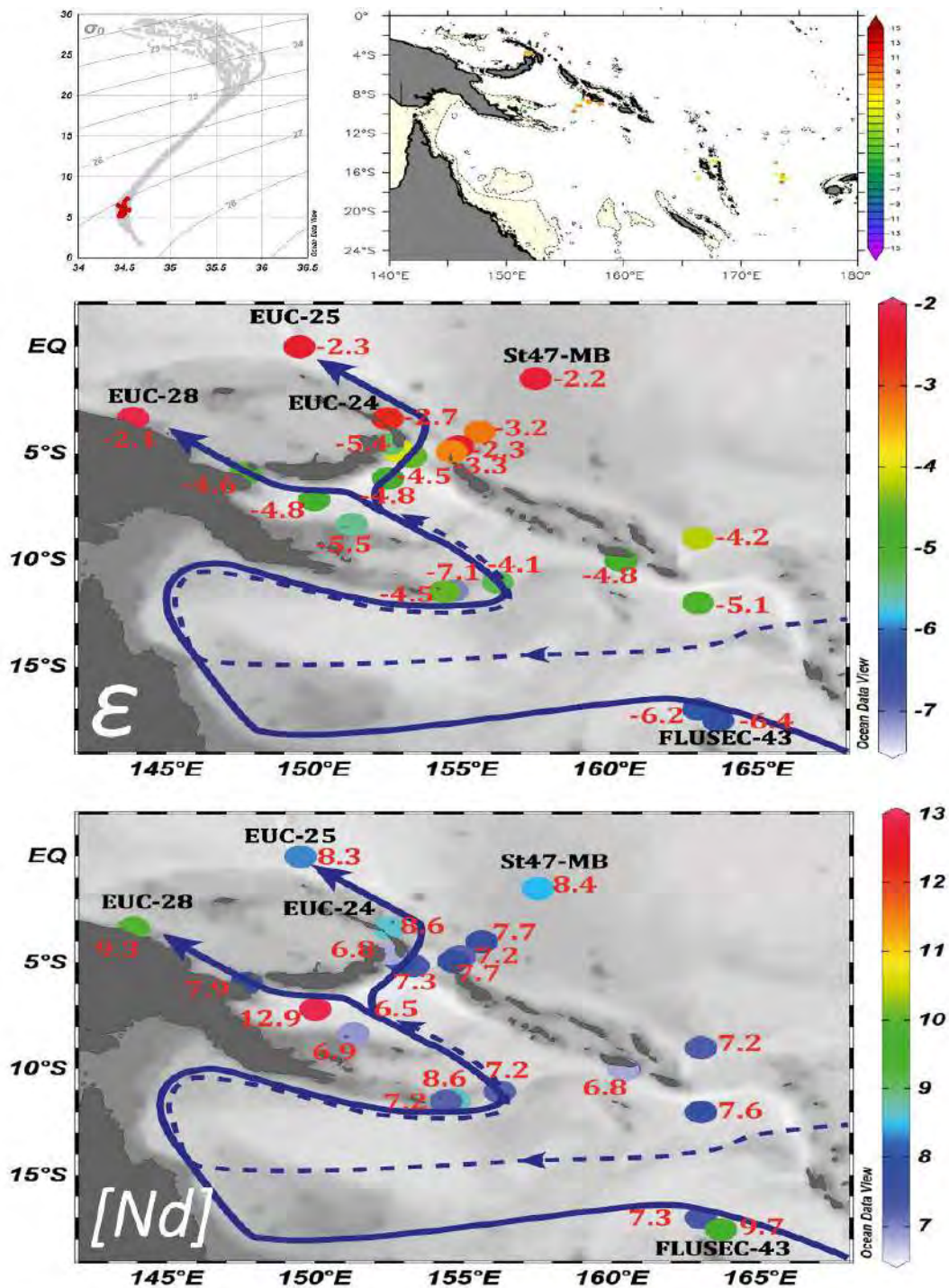


Figure 5-13 As figure 5.6, for Intermediate water ($\sigma_\theta = 26.9-27.4 \text{ Kg/m}^3$). The dark blue arrows (both continuous and dashed) indicate the AAIW current. The ϵ_{Nd} data of the sediments (Figure 5-6) are also displayed at the right corner of the top panel

- In the Coral Sea, the AAIW follows the loop made by the NCJ from North Caledonia to the South West entrance of the Solomon Sea, flowing close to the Queensland coast on its way. This likely explains why the water is slightly more negative at station 34 than at station 4 or FLUSEC-43 (Grenier *et al.*, 2013): this layer could have been modified by an influence of the Australian negative Nd-IC fields (Figure 5-5). More radiogenic intermediate water found at station 4 and FLUSEC 43 could result from exchange with margin of active Vanuatu Island. Then, the difference of ϵ_{Nd} values measured at station 34 (-7.1) and its

neighbor stations 29 and 36 ($\sim \epsilon_{Nd} = -4.3$) could reflect that the same layer sticking the sediments weathered from the South East of the island and deposited on the shelf of station 36 is influenced by local lithogenic inputs, the latter being clearly radiogenic. (see *Figure 5-6*).

- When arriving to Woodlark-Trobriand islands, slightly less radiogenic water found at station 71 ($\epsilon_{Nd} = -5.5$) together with the stable Nd concentration likely reflect two possible processes there i) intermediate water from station 71 results from the mixing of station 34 and 29. However, the nonlinear T-S plot does not support this hypothesis ii) occurrence of BE process again, exchanging with negative Nd-IC material from the bottom of western Woodlark basin – eastern bays of PNG (*Figure 5-6*)
- Regarding the three straits: from the Solomon Sea to the St. George's channel and Vitiaz strait, ϵ_{Nd} values of IW are roughly comparable to what is observed at the southern entrance (from -5.5 to -4.5). This stable Nd-IC signal is also observed at the beginning of the Solomon strait exit, at station 42 ($\epsilon_{Nd} = -4.5$). Contrastingly, a significant ϵ_{Nd} value increase is observed in the northeastern part of the Solomon Strait likely reflecting the mixing between AAIW and the EqPIW, identified as very radiogenic (Bostock, Opdyke and Williams, 2010; Grenier *et al.*, 2013). Outside, station 46 is again different from its neighbor stations displaying more radiogenic value ($\epsilon_{Nd} = -2.3$). This suggests an intrusion of water coming from the equator, probably still a consequence of the vortex mentioned above. This influence could end up around 7°S since station 13 IW display a clear AAIW signature (*Figure 5-8*). Downstream of Vitiaz Strait (where $\epsilon_{Nd} = -4.6$), radiogenic values observed at station EUC-28 ($\epsilon_{Nd} = -2.1$), together with an increase in the Nd concentration, suggest inputs near the Sepik river mouth since no occurrence of EqPIW could be found there, according to mooring data (Alberty *et al.*, 2019).
- IW passing through Indispensable Strait shows that Nd parameters are relatively stable suggesting no significant lithogenic inputs.

e) Upper Circumpolar Deep Water

For these depths, the bottom bathymetry is becoming a strong circulation constraint, motivating a detailed report of the submarine relief in *Figures 5-14 and 5-15*. The Nd-IC signal and Nd concentration are both slightly increasing inside of the Solomon Sea compared to their outside values (*Figure 5-14*). Following the UCDW pathway in the eastern Coral Sea, we first suspected that the different branches flowing at stations 04 and 13 with distinct Nd-IC signatures (-5.0 and -2.7, respectively), are joining up at station 10, which shows an intermediate value. However, the T-S diagram does not support this hypothesis, underlining that a third water mass is required in this mixing, for which we don't have ϵ_{Nd} value. The southern entrance of the Solomon Sea, is characterized by ϵ_{Nd} values relatively homogeneous and ranging from -3.4 (station 34) to -3.9 (Station 21)

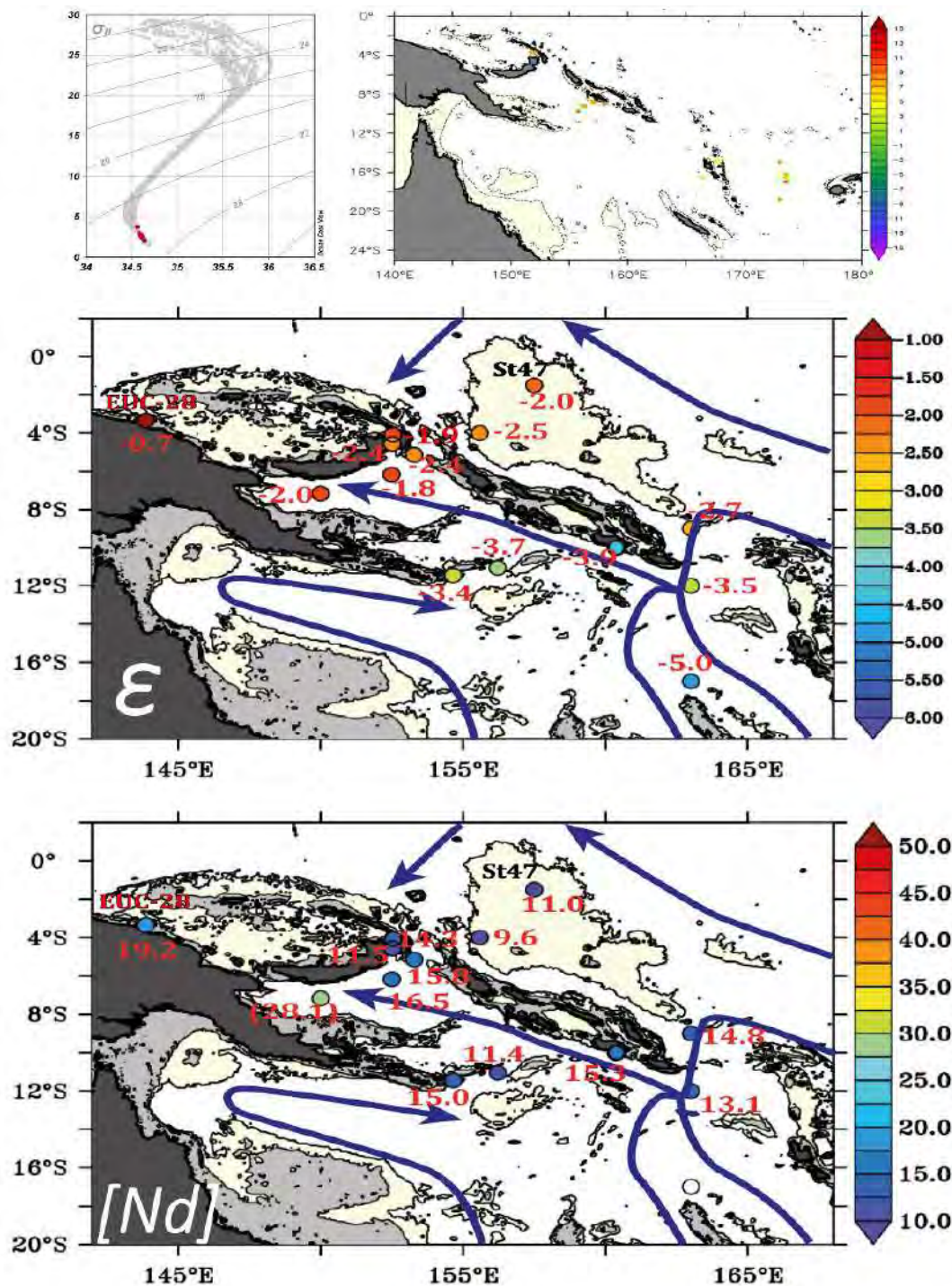


Figure 5-14 As figure 5.13, for UCDW (σ_{θ} =27.4-27.76 Kg/m³). The bathymetry shallower than 1200m is colored in light grey, in yellow if shallower than 2200 m. Value in bracket indicate possible contaminating sample

The most radiogenic ϵ_{Nd} values are observed at all stations located north of $\sim 10^{\circ}\text{S}$ (e.g: -1.8 at station 60). This radiogenic Nd-IC signature is kept beyond the Solomon Sea, as observed at station St47-MB (Behrens et al., unpublished). However, the pathway of the exiting water remains unknown. Regarding the Nd concentration, it is quasi homogeneous between the southern entrance and the output of the Solomon Sea through the straits. Thus, BEs processes are suspected and will be quantified later.

f) Lower Circumpolar Deep Water (LCDW)

We only have 3 samples to characterize the LCDW but it's worth discussing them, in this largely unexplored water mass. From 3500m down to the bottom, the Nd-IC signal of LCDW is negative outside of the Solomon Sea with values around -6. This is contrasting with the radiogenic value of -1 observed at station 60 inside the sea. Dissolved Nd concentration is also increasing from 22 pmol/Kg outside to 30 pmol/Kg at the bottom of station 60. In addition, the oxygen profile of station 60 suggests that relatively ventilated waters are penetrating the Solomon Sea from the south (Figure 2 of Ganachaud *et al.*, 2017; Pham *et al.*, 2019). The processes that might have modified the LCDW value while penetrating the Solomon Sea through the complex topography of the southern sill is likely input from the sediment deposited on the bottom, since the sediment deposited in the Woodlark basin (8-10°S) is definitely basaltic and radiogenic. (Figure 5-6; Chadwick *et al.*, 2009; Speckbacher *et al.*, 2012).

The high dNd concentrations characterizing the deepest part of the station 60 likely reflect an influence of the bottom sediments, which could be through diagenetic processes or dissolution of re-suspended sediments.

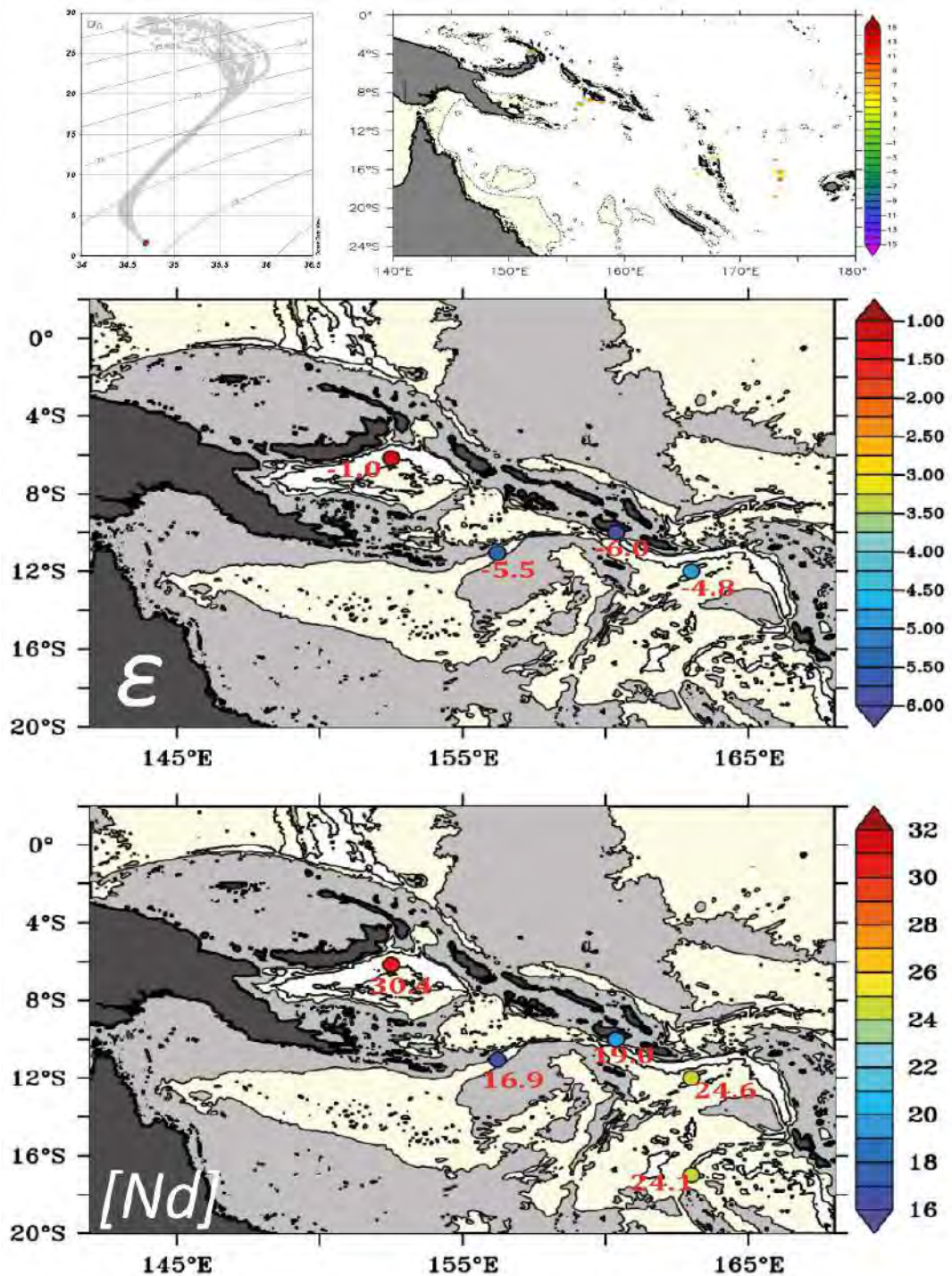


Figure 5-15 As Figure 5.14, for LCDW ($\sigma_\theta \geq 27.76 \text{ Kg/m}^3$). The bathymetry shallower than 3000m is colored in light grey, in yellow if shallower than 4750 m

5.4.3 Quantifying the Boundary exchange process

The evolution of the Nd parameters along the different layers revealed different cases of water signature modification. This could be very local as for example at Indispensable Strait or on larger scale covering the whole Solomon Sea, the most striking illustration being the UCDW. Changes in Nd-IC are accompanied by Nd concentration changes or not. Boundary Exchange quantification requires the Nd concentration, Nd isotopic composition but also the water transport of the considered layer. Thus the box model calculations proposed in the following

paragraphs are restricted to the two layers for which we could gather the three parameter values for each entrance and exits sections of the box_models. We drew two box models, one for the local scale (named “local box”, applied to the LLTW) and the second for the Solomon Sea scale (named ‘Pandora box’, applied to the UCDW; *Figure 5-16*). The box models applied here are similar to what was proposed by (Lacan and Jeandel, 2001, 2005; Garcia-Solsona *et al.*, 2014; Grenier, Jeandel and Cravatte, 2014). All the water mass flows (W) were estimated applying the inverse model developed by Germaineaud *et al.*, (2016) and extended to deeper layers as in Pham *et al.*, (2019). Calculations are made assuming that the balance between input and output terms is at steady state and that no diapycnal mixing occurs within the defined boxes, which is a strong hypothesis.

Local box (Lower thermocline layers) : As mentioned above, the eastern branch of the LLTW is likely impacted by BE processes, from station 71 ($\epsilon_{Nd} = -3.5$) to 42 ($\epsilon_{Nd} = -1.9$). We propose to quantify the exchanged fluxes considering the water layer between stations 71 and 42 as defined by Germaineaud *et al.* (2016) and using the “local box” described in *Figure 5-16a*. The evolution of the Nd parameters within the box follows the equations (1) and (2)

$$W \times [Nd]_{71} + F_{net\ flux} = W \times [Nd]_{42} \quad (1)$$

$$W \times [Nd]_{71} \times \epsilon_{71} + F_{ex} \times \epsilon_{ex} - F_{sc} \times \epsilon_{sc} = W \times [Nd]_{42} \times \epsilon_{42} \quad (2)$$

Where: $F_{net\ flux} = F_{ex} - F_{sc}$

F_{ex} is the external flux or material coming from the neighbor island margin;

F_{sc} is the “scavenging” flux- exported from the water mass toward the sediments due to adsorption of dissolved Nd on the particles

W is the water transport, taken at 1.7 Sv

$[Nd]_{71}$ and ϵ_{71} are the input Nd parameter values

$[Nd]_{42}$ and ϵ_{42} are the output Nd parameter values

Calculation of F_{ex} and F_{sc} requires to constrain ϵ_{ex} and ϵ_{sc} , the isotopic signatures of the external source and of the scavenged particles respectively. The ϵ_{ex} value is taken here at +4.9, which is the average value of all lithogenic material (e.g: rock chips, beach sand) collected along this water pathway (Hegner and Smith, 1992; König *et al.*, 2007). The ϵ_{sc} value is assumed to be similar to the exiting one (here equal to ϵ_{42}) following Grenier, Jeandel and Cravatte, (2014).

Table 5.2 compiles both the numerical values used in the calculations and the results. For the local box, we estimate an external flux of $8 \pm 2 \text{ T Nd/yr}$, a scavenging one of $2 \pm 2 \text{ T Nd/yr}$ and thus a net flux of $6 \pm 2 \text{ T Nd/yr}$ satisfying both the Nd concentration and ϵ_{Nd} variations.. At this depth, it is likely that particle remineralization already occurs which could explain the low scavenging compared to the external input. The ongoing analyses of the particles will help to conclude farther. The net flux represents one tenth of the one observed in Pham *et al.*, (2019) for the whole LTW across the whole Solomon Sea. This indicates that most of the external inputs are

occurring at other locations for this layer, which the scarcity of the data prevented us to calculate.

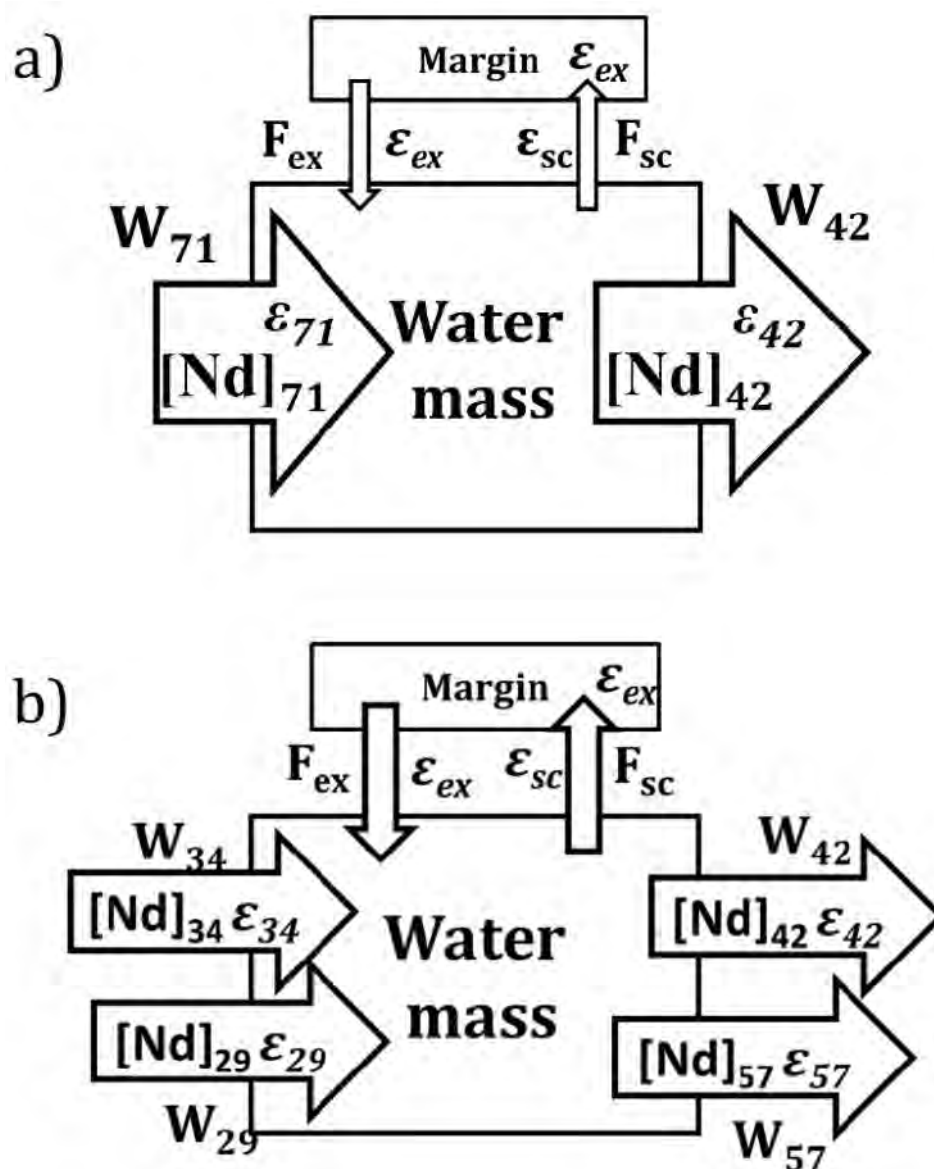


Figure 5-16 Representations of the box models used to calculate the Nd exchanged fluxes at the land-ocean interface for a) local application (LLTW) and b) the whole Solomon Sea (UCDW). Note that for the later, Vitiaz Strait is closed.

Pandora box (Deep water layer): The significant increase of the ϵ_{Nd} values while the Nd concentrations remain constant observed along the south-north pathway of the UCDW clearly suggests that BE is impacting this layer. We applied the ‘Pandora box model’ to estimate the exchange intensity.

The ‘Pandora box’ for UCDW represented in Figure 5-16b is similar to that described in Pham *et al.*, (2019). The striking feature here is that we had to split the calculation in 2 parts because there is no water transport below 2000m at station 34 upon topography blocking. The evolution of the Nd parameters within the box follows the equations (3) and (4) below.

$$W_{29} \times [Nd]_{29} + W_{34} \times [Nd]_{34} + F_{net\ flux} = W_{42} \times [Nd]_{42} + W_{57} \times [Nd]_{57} \quad (3)$$

$$W_{29} \times [Nd]_{29} \times \varepsilon_{29} + W_{34} \times [Nd]_{34} \times \varepsilon_{34} + F_{ex} \times \varepsilon_{ex} - F_{sc} \times \varepsilon_{sc} = W_{42} \times [Nd]_{42} \times \varepsilon_{42} + W_{57} \times [Nd]_{57} \times \varepsilon_{57} \quad (4)$$

Where: $F_{net\ flux} = F_{ex} - F_{sc}$

F_{ex} and F_{sc} : see definition above

$[Nd]_{29} \varepsilon_{29}$ and $[Nd]_{34} \varepsilon_{34}$ represented for the input Nd parameter values of station 29 and 34, respectively.

$[Nd]_{42} \varepsilon_{42}$ and $[Nd]_{57} \varepsilon_{57}$ represented for the output Nd parameter values of station 42 and 57, respectively.

The only missing Nd parameters data are for the lower extent of UCDW ($\sigma_{\theta} = 27.65-27.76$) at station 29. We therefore estimated these values using its neighbor stations (stations 04, 34) due to their similarity in dNd and Nd-IC values (see vertical profile, *Figure 5-1* and *5-2*). Here, the ε_{ex} was taken as +5.1 which is average value of sediment collected at the bottom of the Solomon Sea (*Figure 5-6*; Chadwick *et al.*, 2009; Speckbacher *et al.*, 2012). The ε_{sc} value was calculated by averaging the value of all exiting stations.

The results show similar external inputs of 42 T Nd/yr for both layers of UCDW. Scavenging fluxes are affected by large error bars; however, they are clearly lower than the external input. The negative value estimated in the upper layer should indicate that desorption from the particles is required to balance the Nd concentration variation. The total net flux for the whole UCDW is 105 ± 50 T Nd/yr. This value is consistent with what was found in Pham *et al.*, (2019), although we gained in precision and information. Indeed, satisfying the ε_{Nd} variation requires a significant external input providing radiogenic dissolved material (partly balanced by scavenging) into the UCDW while crossing the Solomon Sea. The origin of this flux is likely the submarine weathering of suspended particles from the local sediments. Considering the average Nd concentration of the surrounding basalts (deduced from the geological articles listed in annex B), we calculate that this Nd flux corresponds to a weathered flux of basaltic sediments of 14 MT Basalt/yr. Milliman, (1995) estimated that about 403 MT of sediment are weathered and transported to the Solomon Sea each year via river streaming (See figure 7 of this study). Thus, we estimate here that the dissolution (release) of less than 3% of this annual flux could explain the UCDW external enrichment. This proportion is consistent with the previous results of Tachikawa, (2003); Arsouze *et al.*, (2009); Grenier, Jeandel and Cravatte, (2014).

Table 5-2 Fluxes calculated from local-LLTW and Pandora-UCDW box models. Entering and exiting branches of the model corresponds to what was identified by Figure 5-17. The water masses and Nd concentrations were taken from Table 3 and 4 of Pham *et al.*, (2019).

Layer		Water mass transport (Sv)	Nd conc. (pmol/Kg)	ϵ_{Nd}	ϵ_{sc}	ϵ_{ex}	Net flux- $F_{net\ total}$ (T Nd/yr)	Scavenging flux- F_{sc} (T Nd/yr)	External flux - F_{ex} (T Nd/yr)
The 'Local box'									
LLTW ($\sigma_\theta = 25.3$ - 26.4 kg/m ³)	Enter	W71: 1.7	0.8 ± 0.0	-3.5 ± 0.2					
	Exit	W42: 1.7	0.9 ± 0.0	-1.9 ± 0.3	-1.9	+4.9	6 ± 2	2 ± 2	8 ± 2
The Pandora box'									
UCDW-Upper extent ($\sigma_\theta = 27.4$ - 27.65 kg/m ³)	Enter	W29: 4.5	1.5 ± 0.2	-3.9 ± 0.2					
		W34: 1.0	2.0 ± 0.1	-3.5 ± 0.2					
	Exit	W42: 4.0	2.0 ± 0.1	-2.2 ± 0.2	-2.3	+5.1	43 ± 18	-24 ± 26	68 ± 31
		W57: 1.5	1.7 ± 0.0	-2.5 ± 0.2					
UCDW- Lower extent ($\sigma_\theta = 27.65$ - 27.76 kg/m ³)	Enter	W29: 3.0	2.4 ± 0.4	-3.8 ± 0.2					
	Exit	W42: 2.5	2.9 ± 0.4	-2.4 ± 0.5	-2.1	+5.1	42 ± 25	5 ± 36	37 ± 39
		W57: 0.5	2.9 ± 0.0	-1.5 ± 0.2					

5.5 Conclusion

The seawater Nd-IC data collected during the Pandora cruise (July-August 2012) were presented for 132 samples at 20 stations. All the vertical profiles show similar shapes, with high ϵ_{Nd} values at the surface (up to +3), a minimum at intermediate depths (down to 1100m) and an increase again in the upper deep layers, a slight decrease again being observed in the deepest part of the Solomon Sea core (station 60 from 4000 m to the bottom). Our data compared well with those published by Grenier *et al.*, (2013), which assessed their quality.

Maps of the Nd parameter horizontal distributions in the different water layers flowing in the Coral and Solomon Sea helped us to identify variations of their composition along their pathways.

As a whole, waters exiting from the Solomon Sea show a higher Nd-IC signal than at the southern entrance. The release of radiogenic ϵ_{Nd} by dissolution of continental margin material could explain the ϵ_{Nd} modification along these pathways. Thus detailed ϵ_{Nd} maps of the material outcropping on the fields surrounding the area and that could constitute external sources including human impact were established (i.e: atmospheric dust, volcanoes, extensive weathering, mining activity).

Surface waters are marked by lithogenic material input as expressed by their radiogenic Nd-IC signatures and their good correlation with the Eu anomalies of the same samples. The most

important increment was found in the Indispensable strait where we observed an increase of +3 of the ϵ_{Nd} value. However, the strong tide occurring there prevented us to do the BE process calculation. The thermocline layer is marked by a slight increase of Nd-IC between the southern entrance and the exiting straits. Local BE processes were suspected at some specific areas, which we quantified applying a local box model for the lower layer of the lower thermocline. Explain both the ϵ_{Nd} and Nd concentration variations required an external flux of 8 ± 2 T Nd/y slightly balanced by a scavenging flux of 2 ± 2 TNd/y .

Intermediate waters show the imprint of the negative AAIW that enters the Solomon Sea in the South. This layer is keeping a quasi-homogeneous Nd-IC across the Solomon Sea ($\epsilon_{Nd} \sim -4.5$) until reaching the northern exiting passages. This AAIW predominance is broken just at the Solomon Strait with the intrusion of EqPIW marked by more radiogenic signature ($\epsilon_{ex} \sim -2.0$).

The slight Nd concentration increase and significant Nd-IC increase observed along the pathway of the UCDW are quantified applying a 'Pandora' box model. A total external flux of 105 TNd/y is estimated while the scavenging flux does not look significant. The ongoing analyses of the suspended particle profiles collected at the same station will give more insight on the particle-solution exchange mechanisms.

Many small-scale ϵ_{Nd} contrasts were observed between close stations at certain depths, as in the Indispensable strait, near the PNG southern tip (e.g between stations 34 and 36 for intermediate waters), or inside the Solomon Strait (e.g. for LLTW waters). The processes leading to these contrasts remain to be constrained. Fine-scale oceanic features, or high-frequency variability might influence the ϵ_{Nd} signature. This would deserve more investigation of both the circulation and geochemical processes.

ANNEX B: LIST OF REFERENCES USED TO BUILD THE MAP OF LITHIOGENIC GEOCHEMICAL SIGNATURES AROUND AND AT THE BOTTOM OF THE CORAL AND SOLOMON SEAS

This annex provides all the references which published ϵ_{Nd} data of the geological materials outcropping at the surface of the Australian continent and the Islands surrounding the Coral and Solomon seas (section B.1) and those characterizing the bottom sediments (section B.2) of the southwest Pacific Ocean. These articles were extracted using the EarthChem portal (<http://www.earthchem.org>).

B.1 List of reference using for *Figure 5.5* of chapter 5

- Allen, C. M. (2000) 'Evolution of a post-batholith dike swarm in central coastal Queensland, Australia: Arc-front to backarc?', *Lithos*, 51(4), pp. 331–349. doi: 10.1016/S0024-4937(99)00068-7.
- Baker, M. J., Crawford, A. J. and Withnall, I. W. (2010) 'Geochemical, Sm-Nd isotopic characteristics and petrogenesis of Paleoproterozoic mafic rocks from the Georgetown Inlier, north Queensland: Implications for relationship with the Broken Hill and Mount Isa Eastern Succession', *Precambrian Research*. Elsevier, 177(1–2), pp. 39–54. doi: 10.1016/j.precamres.2009.11.003.
- Basu, A. R. and Tatsumoto, M. (1980) 'Nd-isotopes in selected mantle-derived rocks and minerals and their implications for mantle evolution', *Contributions to Mineralogy and Petrology*. Springer-Verlag, 75(1), pp. 43–54. doi: 10.1007/BF00371888.
- Cameron, W. E., McCulloch, M. T. and Walker, D. A. (1983) 'Boninite petrogenesis: chemical and Nd-Sr isotopic constraints', *Earth and Planetary Science Letters*, 65(1), pp. 75–89. doi: 10.1016/0012-821X(83)90191-7.
- Cunningham, H. et al. (2012) 'Rapid magmatic processes accompany arc-continent collision: The Western Bismarck arc, Papua New Guinea', *Contributions to Mineralogy and Petrology*. Springer-Verlag, 164(5), pp. 789–804. doi: 10.1007/s00410-012-0776-y.
- Cunningham, H. S. et al. (2009) 'Temporal Variations in U-series Disequilibria in an Active Caldera, Rabaul, Papua New Guinea', *Journal of Petrology*. Narnia, 50(3), pp. 507–529. doi: 10.1093/petrology/egp009.
- Davidson, G. J., Stolz, A. J. and Eggins, S. M. (2001) 'Geochemical anatomy of silica iron exhalites: Evidence for hydrothermal oxyanion cycling in response to vent fluid redox and thermal evolution (Mt. Windsor subprovince, Australia)', *Economic Geology*, 96(5), pp. 1201–1226. doi: 10.2113/gsecongeo.96.5.1201.
- Ewart, A., Chappell, B. W. and Menzies, M. A. (1988) 'An Overview of the Geochemical and Isotopic Characteristics of the Eastern Australian Cainozoic Volcanic Provinces', *Journal of Petrology*, Special_Vo(1), pp. 225–273. doi: 10.1093/petrology/Special_Volume.1.225.
- Handler, M. R., Bennett, V. C. and Carlson, R. W. (2005) 'Nd, Sr and Os isotope systematics in young, fertile spinel peridotite xenoliths from northern Queensland, Australia: A unique

- view of depleted MORB mantle?', *Geochimica et Cosmochimica Acta*, 69(24), pp. 5747–5763. doi: 10.1016/j.gca.2005.08.003.
- Hegner, E. and Smith, I. E. M. (1992) 'Isotopic compositions of late Cenozoic volcanics from southeast Papua New Guinea: Evidence for multi-component sources in arc and rift environments', *Chemical Geology*, 97(3–4), pp. 233–249. doi: 10.1016/0009-2541(92)90078-J.
- König, S. et al. (2007) 'The role of slab melting in the petrogenesis of high-Mg andesites: Evidence from Simbo Volcano, Solomon Islands', *Contributions to Mineralogy and Petrology*. Springer-Verlag, 153(1), pp. 85–103. doi: 10.1007/s00410-006-0136-x.
- Rudnick, R. L. et al. (1986) 'Lower crustal xenoliths from Queensland, Australia: Evidence for deep crustal assimilation and fractionation of continental basalts', *Geochimica et Cosmochimica Acta*, 50(6), pp. 1099–1115. doi: 10.1016/0016-7037(86)90391-1.
- Schuth, S. et al. (2004) 'Geochemical constraints on the petrogenesis of arc picrites and basalts, New Georgia Group, Solomon Islands', *Contributions to Mineralogy and Petrology*, 148(3), pp. 288–304. doi: 10.1007/s00410-004-0604-0.
- Schuth, S. et al. (2009) 'Petrogenesis of Lavas along the Solomon Island Arc, SW Pacific: Coupling of Compositional Variations and Subduction Zone Geometry', *Journal of Petrology*. Narnia, 50(5), pp. 781–811. doi: 10.1093/petrology/egp019.
- White, W. M. and Patchett, J. (1984) 'HfNdSr isotopes and incompatible element abundances in island arcs: implications for magma origins and crust-mantle evolution', *Earth and Planetary Science Letters*. Elsevier, 67(2), pp. 167–185. doi: 10.1016/0012-821X(84)90112-2.
- Woodhead, J. et al. (2010) 'The big crunch: Physical and chemical expressions of arc/continent collision in the Western Bismarck arc', *Journal of Volcanology and Geothermal Research*. Elsevier, 190(1–2), pp. 11–24. doi: 10.1016/j.jvolgeores.2009.03.003.
- Woodhead, J. D., Eggins, S. M. and Johnson, R. W. (1998) 'Magma Genesis in the New Britain Island Arc: Further Insights into Melting and Mass Transfer Processes', *Journal of Petrology*. Oxford University Press, 39(9), pp. 1641–1668. doi: 10.1093/etroj/39.9.1641.
- Woodhead, J. D. and Johnson, R. W. (1993) 'Isotopic and trace-element profiles across the New Britain island arc, Papua New Guinea', *Contributions to Mineralogy and Petrology*. Springer-Verlag, 113(4), pp. 479–491. doi: 10.1007/BF00698317.
- Zhang, M. (2001) 'Petrogenesis and Geodynamic Implications of Late Cenozoic Basalts in North Queensland, Australia: Trace-element and Sr-Nd-Pb Isotope Evidence', *Journal of Petrology*, 42(4), pp. 685–719. doi: 10.1093/etrology/42.4.685.

B.2 List of reference using for *Figure 5.6* of chapter 5

- Beier, C. et al. (2010) 'Influence of subducted components on back-arc melting dynamics in the Manus Basin', *Geochemistry, Geophysics, Geosystems*, 11(6), p. n/a-n/a. doi: 10.1029/2010GC003037.

- Beier, C. et al. (2015) 'Origin of Silicic Magmas at Spreading Centres—an Example from the South East Rift, Manus Basin', *Journal of Petrology*, 56(2), pp. 255–272. doi: 10.1093/petrology/egu077.
- Briqueu, L. et al. (1994) 'Temporal Magmatic Evolution of the Aoba Basin, Central New Hebrides Island Arc: Pb, Sr, and Nd Isotopic Evidence for the Coexistence of Two Mantle Components beneath the Arc', in *Proceedings of the Ocean Drilling Program, 134 Scientific Results. Ocean Drilling Program*. doi: 10.2973/odp.proc.sr.134.019.1994.
- Chadwick, J. et al. (2009) 'Arc lavas on both sides of a trench: Slab window effects at the Solomon Islands triple junction, SW Pacific', *Earth and Planetary Science Letters*, 279(3–4), pp. 293–302. doi: 10.1016/j.epsl.2009.01.001.
- Kamenetsky, V. S. et al. (2001) 'Parental basaltic melts and fluids in eastern Manus backarc Basin: Implications for hydrothermal mineralisation', *Earth and Planetary Science Letters*, 184(3–4), pp. 685–702. doi: 10.1016/S0012-821X(00)00352-6.
- Nohara, M. et al. (1994) 'The North Fiji Basin basalts and their magma sources: Part II. Sr-Nd isotopic and trace element constraints', *Marine Geology*, 116(1–2), pp. 179–195. doi: 10.1016/0025-3227(94)90175-9.
- Speckbacher, R. et al. (2012) 'Fluid flow and metasomatic fault weakening in the Moresby Seamount detachment, Woodlark Basin, offshore Papua New Guinea', *Geochemistry, Geophysics, Geosystems*. Blackwell Publishing Ltd, 13(11). doi: 10.1029/2012GC004407.
- Vervoort, J. D., Plank, T. and Prytulak, J. (2011) 'The Hf-Nd isotopic composition of marine sediments', *Geochimica et Cosmochimica Acta*, 75(20), pp. 5903–5926. doi: 10.1016/j.gca.2011.07.046.

Chapter 6

Conclusion and Perspective

6.1 Conclusion

In the framework of my thesis, I studied the southwest Pacific Ocean, an important crossroad area for the Equatorial Pacific Ocean. More specifically, the Coral and Solomon Sea are key pathways for the waters from the southern hemisphere which eventually join the Equator. The strong dynamic characterizing the semi-closed Solomon Sea is leading to the transformations of the water hydrological properties. It was also suspected that its complex geography and bathymetry coupled to this dynamic exert a strong influence on the macro and micro nutrient contents of these waters (Ganachaud *et al.*, 2014a, 2017; Germaineaud *et al.*, 2016; Albery *et al.*, 2017; Cravatte *et al.*, 2017; Kessler *et al.*, 2017). Indeed, most of the islands surrounding the Solomon Sea are high, submitted to intense precipitations and thus strongly weathered, likely leading important inputs at the land-ocean interface. This potential water mass modification during the passage through the Solomon Sea could influence the marine productivity within the sea itself and then later in the Equatorial current system, participating to its productivity and thus to the regulation of the concentration of atmospheric carbon dioxide. Several previous studies focused on the Coral Sea or on the equatorial current systems, but what happened within the Solomon Sea remained so far the missing piece of the whole picture.

Identifying the sources of these land-ocean fluxes and quantifying them using geochemical tracers was the main objective of this thesis. The samples studied were collected during the PANDORA cruise (July-August, 2012) as a part of the SOLWARA project-which was labeled by CLIVAR-(SPICE) and GEOTRACES programs. The thesis goal required to: i) analyze the geochemical tracers which are the dissolved Rare Earth Element (dREE) and Nd isotopic composition (Nd-IC) of samples collected during the Pandora cruise; bearing the mission of developing a new analytical protocol, ii) characterize the water mass transformation by coupling hydrological and geochemical data, revealing the influence of surrounding volcanic-arc, and iii) quantify this geochemical enrichment in the different layers of the water column in the Solomon Sea. An important mission of my thesis was to build a preconcentration system for dREE concentration analysis, thanks to which we could improve our experiment data quality. The manifold will be then applied in further studies and especially for developing countries (e.g: Vietnam) in which its low-cost characteristic could improve their analytical procedures, and reinforce their research possibilities in marine geochemistry

The dREE analytical protocol was improved by the development of a handcrafted manifold using NOBIAS® resin packed in precleaning column. In fact, the classical protocol that had been used for years in LEGOS revealed some weaknesses, including: i) high sample volume as compromise between the measured signal and the chemical blank, ii) relatively long experiment time consumption due to multiple steps. The new analytical protocol applying the preconcentration system (a.k.a: seaSLOW) inspired by Hatje, Bruland and Flegal, (2014) was thus developed. The seaSLOW provides us the ability to analyze 8 samples simultaneously with competing matrix blank, all the undesirable salt removed and affordable signal for SF-ICP-MS measurement. The accuracy and precision of the protocol using seaSLOW are better than those provided by classical protocol. In addition, the coupling with the isotopic dilution method is warrants an excellent control of the recoveries. Lesser steps and easy to use procedures? are also considered as the advantages of this seaSLOW. About fabrication cost, the full system cost

around 6000 euro to set up including column fabrication. This represents one fifteenth of the seaFAST-the commercial system for trace element preconcentration.

Next, the first study conducted on the PANDORA cruise samples was to establish the dissolved REE (dREE) distributions in the Coral and Solomon Seas (Chapter 4). This provided a better view on the surface to deep, and horizontal variations of the dREE in these seas, complementing the preceding studies of Zhang and Nozaki, (1996) and Grenier *et al.*, (2013) who did not document the Solomon Sea. The quantified positive flux of dREE from the Solomon box model also suggested that a significant amount of macro and micro nutrients could enter the seawater and then possibly regulate its biological productivity. The dREE concentrations were normalized to a reference crust material value (PAAS) in order to identify any fractionation or anomaly that help tracing geochemical processes. Among others, significant Europium (Eu) positive anomalies revealed an imprint of basaltic material confirming observations by Zhang, Lacan and Jeandel, (2008); Grenier *et al.*, (2013, 2018) and consistent with the geochemical characteristics of the surrounding lands. This lithogenic impact was also supported by the Cerium (Ce) anomalies, clearly positive at the surface and decreasing deeper in the water column. An extremely high positive lanthanum anomalies (La; range from 3 to 6) were hypothesized to be related to the barium/barite cycle; however, no clear explanation allowed us to link both La and Ba cycles; iii) the correlation between REE and Si cycle is more pronounced with the heavy REE than with the light ones, consistent with theoretical preceding works (Akagi, 2013; Patten and Byrne, 2017) but also field observations (Bertram and Elderfield, 1993; Grenier *et al.*, 2018).

Quantification of the dREE concentration variations in the different water layers along their pathways across the Solomon Sea was done using a simple box model, and transport computed from velocity data collected during PANDORA cruise. Unfortunately, large error bars on transports prevented us from quantifying unambiguously the enrichment in most of the layers. The only significant observed enrichment is affecting the lower thermocline layer, and gave us a first indication about the location and magnitude of trace element fluxes of continental origin. The analysis of the Nd-isotopic compositions of Pandora samples, together with the previous Nd concentration data, allowed tracing the lithogenic inputs within the Solomon Sea. Maps of ϵ_{Nd} and Nd concentration distributions for each layer from surface to the deepest layer allowed us to describe how its Nd parameter signals are varying from the Coral Sea to the exits of the Solomon Sea. In general, the waters exiting the Solomon Sea show higher Nd-IC signals than those entering from the Coral Sea, likely reflecting the influence of external inputs during the transit. In details, the surface water reveals the significant impact of land to ocean inputs, which impact mostly their Nd-IC signatures, which become more radiogenic when getting closer to volcanic islands characterized by positive ϵ_{Nd} value. In the thermocline layers, a slight increase of both Nd parameters between the southern entrance and the exiting straits was observed. The BE process was quantified in this layer on a 'local' scale, for a circulation branch flowing from the middle of the Solomon Sea to the Solomon Strait. An external flux of 8 ± 2 T Nd/yr was found together with scavenging flux at 2 ± 2 T Nd/yr, Intermediate layers of the Solomon Sea revealed the dominance of AAIW marked by a negative Nd-IC signal ($\sim \epsilon_{Nd} = -4.5$) which is kept across the Solomon Sea until reaching the exit straits, where it mixes with the

intrusion of EqPIW from the eastern Pacific characterized by a different dNd-IC ($\sim \varepsilon_{Nd} = -2.0$). The deeper water layers (UCDW), displayed significant increase of Nd-IC with a small increase of Nd concentration between the southern entrance and the northern exits, likely reflecting Boundary Exchange processes occurring at the 'Solomon Sea' scale. The box model designed for this scale allowed us estimating a significant external flux of 105 TNd/yr while scavenging flux stayed relatively weak.

As a whole, the dREE concentrations together with the dNd-IC of samples collected during the Pandora cruise were successfully analyzed as part of this thesis. This allowed improving our understanding on how the seawater modified its characteristics (in this case, trace element content) during the transit toward the Equatorial region. All the possible external sources (i.e: weathering, local stream or anthropogenic activities) were considered to explain the observed modification in the different layers of the water column. Boundary exchange process was also quantified to estimate the magnitude of the "continental" influence. Similar application could be proposed to understand the fate of other trace elements or to provide a complementary quantification of their SS budgets. A new and more efficient pre-concentration system was built, tested and is ready for further applications in further researches. Last but not least, the concentration data was published (Pham et al., 2019) and data were made available publicly in the data base of GEOTRACE program, contributing to the global-scale database of trace element distribution in the ocean. The same is ongoing for the Nd IC data.

6.2 Perspectives

6.2.1 Better constraining the elemental fluxes at land-ocean interface and the fate of particles in seawater

In chapter 4, the net dissolved Rare Earth Elements (REEs) flux at land-ocean contact within the Solomon Sea had been quantified, suggesting a significant enrichment in the Lower thermocline layer (LTL). Other layers also indicate positive enrichments despite large uncertainties. With the Nd-IC data in chapter 5, we were able to trace that Boundary Exchange was likely occurring at many places and we could quantify it for some specific cases. Despite the high resolution of the sampling done during PANDORA, the high variability of water transport, leading to the uncertainties on the mean lagrangian connections within the Solomon Sea together with the lack of isotope data at some key locations were the main reasons that prevented us to quantify further the Nd fluxes. Applying Lagrangian trajectories in a high-resolution model could help to better constrain the water pathways by identifying the contribution of the various water body sources and trajectories to a given station (Grenier, Jeandel and Cravatte, 2014). It would offer us a chance to quantify some of the missing parts and get better understanding of the BE processes.

Another fruitful following of this work could be to apply the box models designed for the whole Solomon Sea and for local areas to other elements which had also been sampled during the Pandora cruise (i.e: Al, Mn, Fe, Hg). The fluxes calculated could confirm the observed enrichment for other elements than for the REE, providing knowledge on how waters are modified during their passage through the Solomon Sea and to which extent they contribute to feed the Equatorial 'Cold Tongue'. Establishing correlations between different elemental fluxes could also contribute to understand how lithogenic particle dissolve and release chemical species at the contact with seawater.

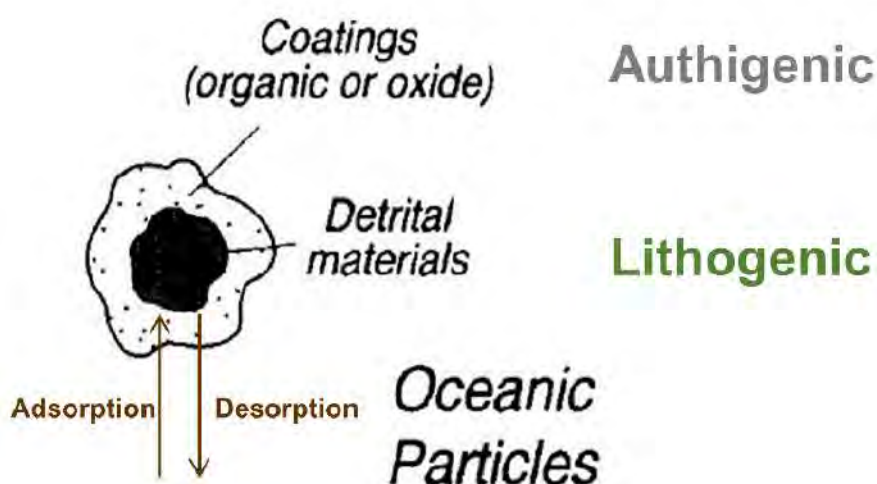


Figure 6-1 Authigenic and lithogenic phases of the particle during its sinking in oceanic water. Model taken from Sholkovitz et al., (1994)

In further study, it will also be very important to seek for the information about the fate of particles while they settle to the bottom of the Solomon Sea. In chapter 1, we introduced the

oceanic processes that contribute to the formation of the two main fractions composing a marine particle and how the REE dissolved-particulate exchanges are controlled by these fractions, leading to their distribution in the different main phases within the water column (a.k.a: dissolved, authigenic and lithogenic; *Figure 6-1*). During the Pandora cruise, suspended particles were collected on SUPOR filter membrane (142mm diameter; 0.8 μ m pore size) using in situ pumps at all the stations at which dREE and dNd IC was measured. The REE concentration of the lithogenic fraction will be identified by using ^{232}Th , conservative tracer of lithogenic sources. In fact, the very-long lived primordial isotope ^{232}Th ($t^{1/2} = 1.4 \times 10^{10}$ years) represents $\sim 99.98\%$ of all natural Th and it is supplied to the ocean almost exclusively by the continental material transported by streams, rivers, wind and continental shelf sediments (Pérez-Tribouillier *et al.*, 2013). The authigenic fraction will be subsequently calculated via total REE content to which the lithogenic fraction will be subtracted. The horizontal and vertical distributions of REE and ϵ_{Nd} in both fractions will inform us about the behavior of lithogenic particles after entering the seawater and refine our identification of the possible external sources (e.g: hydrothermal, bottom reflux).

6.2.2 Deep waters inside the Solomon Sea

Surprisingly, the oxygen profile of station 60 –the deepest one of PANDORA, located in the core of the Solomon Sea trench- shows a constant increase from 3000m toward the bottom (*Figure 2*, Pham *et al.*, 2019) while an oxygen depletion could have been expected if the waters were effectively locked between 3000 and 7000 m, as suggested by the topography. This non-depleted oxygen feature suggests that ventilation of seawater from outside occurs, renewing the deep water within the Solomon Sea. Another surprising observation comes from the comparison of nutrient profiles between station 60 and others stations located outside of the Solomon Sea: they show striking similarities, likely tracing the same water mass origin (*Figure 6-4*). Finally, the quasi-homogeneous nutrient distribution below 3000m is also observed in the dREE vertical profiles (*Chapter 4*) and could result from the strong turbulence mixing due to the internal waves in this layer (*Figure 6-3*). The high tidal currents and the seamount and rough topography in *Figure 6-2b* explain the generation and propagation of such waves inside the Solomon Sea, especially in the straits and close to the eastern tip of PNG coast, at the entrance of the Solomon Sea (Tchilibou *et al.*, 2019). The dissipation of tides could explain the mixing, as suggested by Alberty *et al.*, (2017), which showed a direct link between the dissipation in the deep layers, the tide power input and the topographic roughness within the Solomon Sea.

The abyssal water layers in the Pacific Ocean are originating from the Southern Ocean. The water mass that dominated in the deep Pacific Ocean is the Circumpolar Deep Water (CDW) and it is a result from the mixing between Antarctic Bottom Water (AABW) and shallower waters from 1000 to 2000 m layers, mixing occurring at the northern edges of the Antarctic Circumpolar Current (ACC) (Orsi, Johnson and Bullister, 1999). The CDW spreads through the South Pacific along the east of New Zealand and then finds its way to the North Pacific basin (Kawabe *et al.*, 2009). The presence of CDW in the Southwest Pacific had been first noticed by Wyrski, (1961) and then Sokolov and Rintoul, (2000). The later study also proposed a pathway of this water mass through the Solomon Sea (described in the Chapter 1 of this thesis). However,

the lower part of this water body (below 3000m) was supposed to stay outside the Solomon Sea due to the bathymetry of this part of the Southwest Pacific.

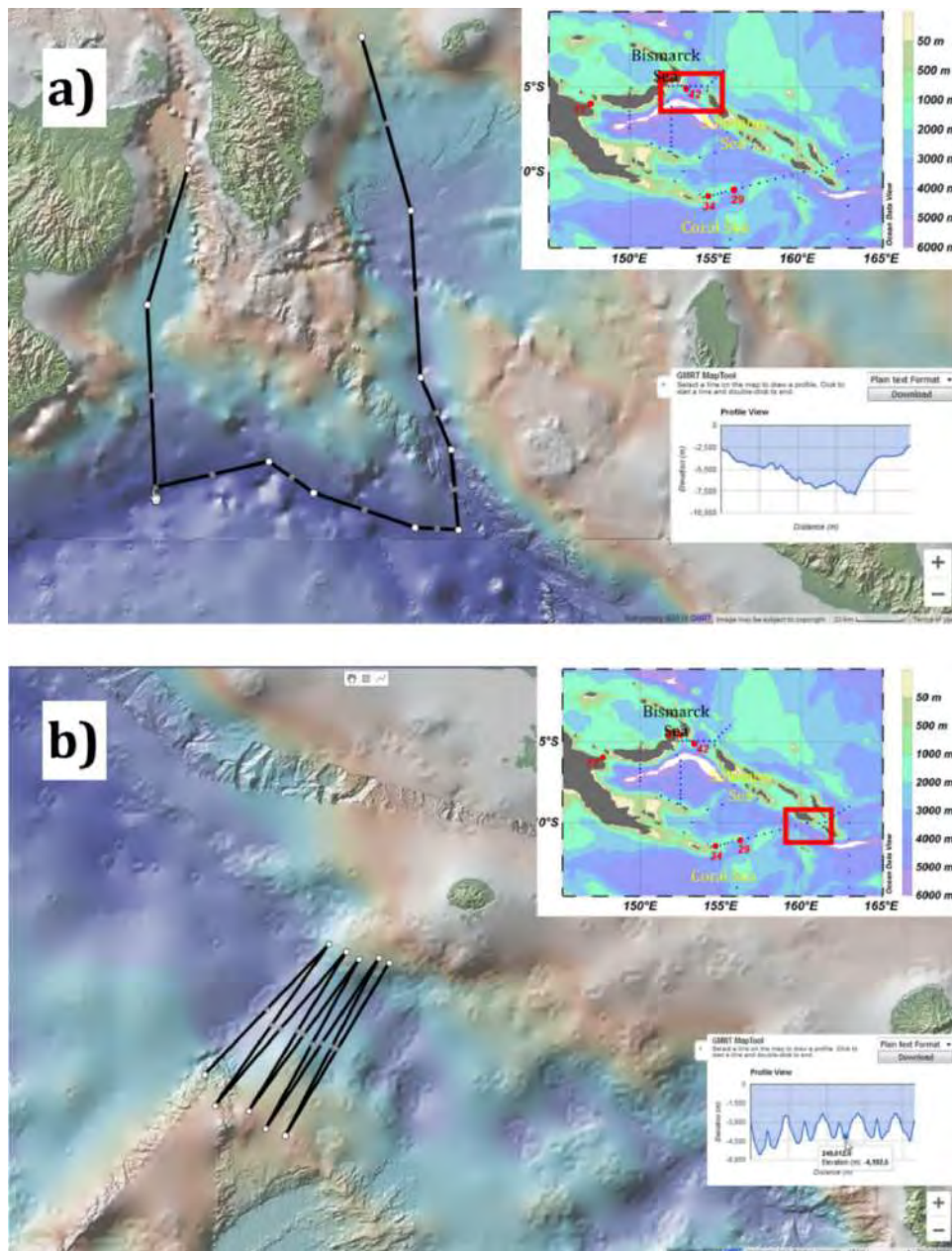


Figure 6-2 Map of the bathymetry of a) the northern area of the Solomon Sea, from St. George to Solomon Straits and b) the southern trench at eastern Woodlark basin. The red rectangular on the map located on the upper right corner shows the location of the working area in the Solomon Sea. The insets show the details of the bottom topography along the sections identified by the black lines on the maps.

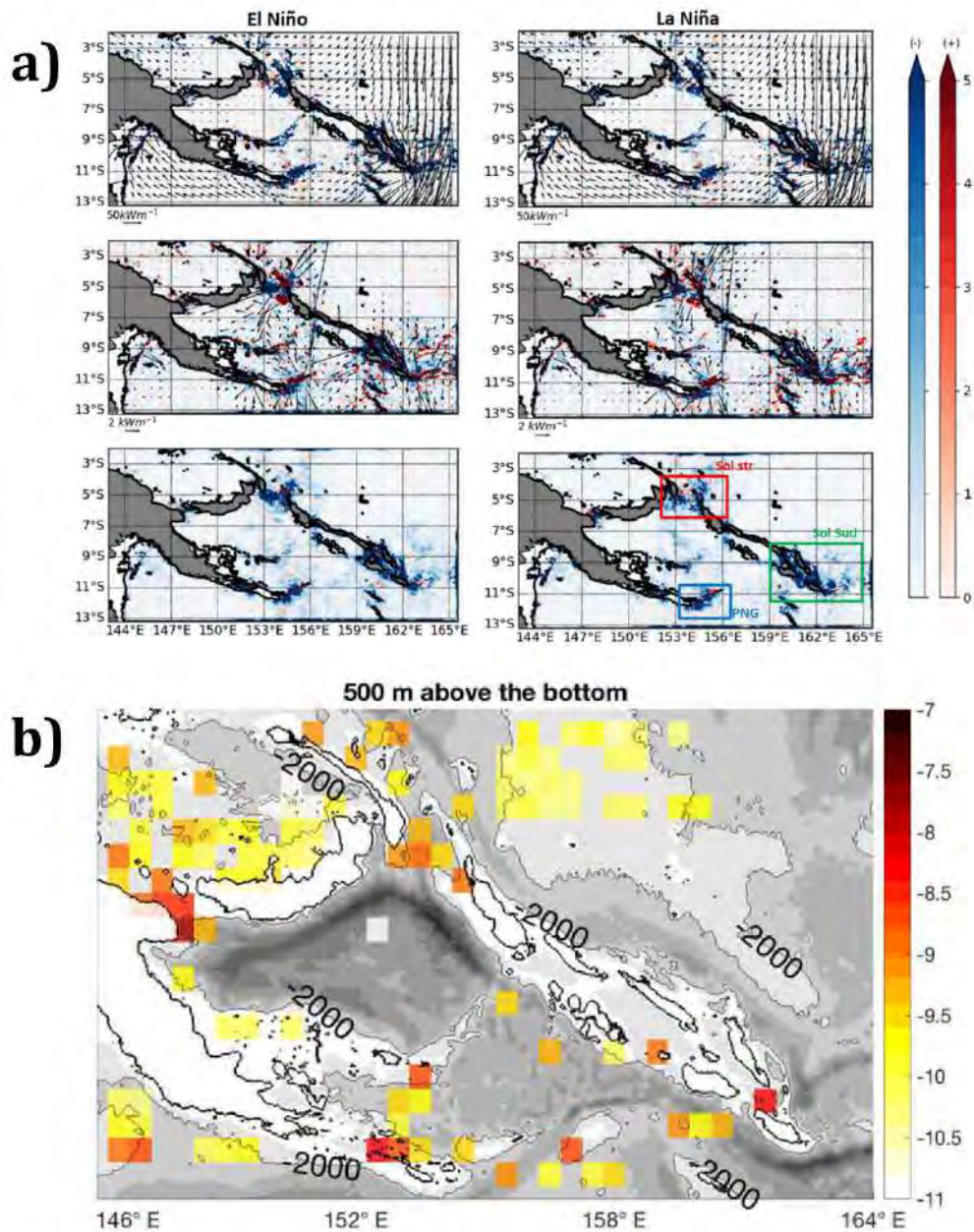


Figure 6-3 Indication for internal wave generation, and dissipation in the Solomon Sea by internal tides a) barotropic to baroclinic tide conversion rate (top) (negative values mean that internal tides are generated), baroclinic flux divergence (middle), and baroclinic dissipation rate (bottom) for the M2 harmonic (negative values shaded in blue, positive values in red, unit: W/m^2). The left column corresponds to the El Niño period and the right column to the La Niña period. Results from a High-resolution model from Tchilibou et al., (2019); b) The log of median dissipation [W/kg] from combined cruise and Argo data sets using the finescale method within 500 m above the bottom. Bathymetry is contoured at 1000 m intervals and the coast is drawn in black. The 2000 m isobath is also contoured and labeled in black. Data from Alberty et al., (2017)

By working on the bathymetry of the Solomon Sea using GMRTmapprool thanks to the help of Melanie Grenier, we identified a small trench inside the Woodlark Basin that could open a “leak” and allow a source of bottom water inside the Solomon Sea. It is noticeable that this trench reaches down to 5500m (Figure 6-2b). However, in the northern side of the Solomon Sea, the bathymetry of Vitiaz, St. George’s and Solomon straits prevent any water below 3000m to

escape northward (*Figure 62-a*). It is therefore suggested that a small southern gate could provide abyssal water to the Solomon Sea, this water could circulate around the Solomon Sea before exiting at the same place but in another trench. At last, it raises the issue “How do we bring to light this circulation?”. To answer this question, we have to consider the vertical profiles of the different tracers (e.g: Ra, Th) observed at station 60 located inside the Solomon Sea. Future collaboration with Pieter van Beek, Melanie Grenier and Francois Roger is then required to gather and discuss these data. C. Germaineaud is also working on describing the deep circulation within the Solomon Sea. Putting all this information together will help understanding the whole dynamic of the Solomon Sea.

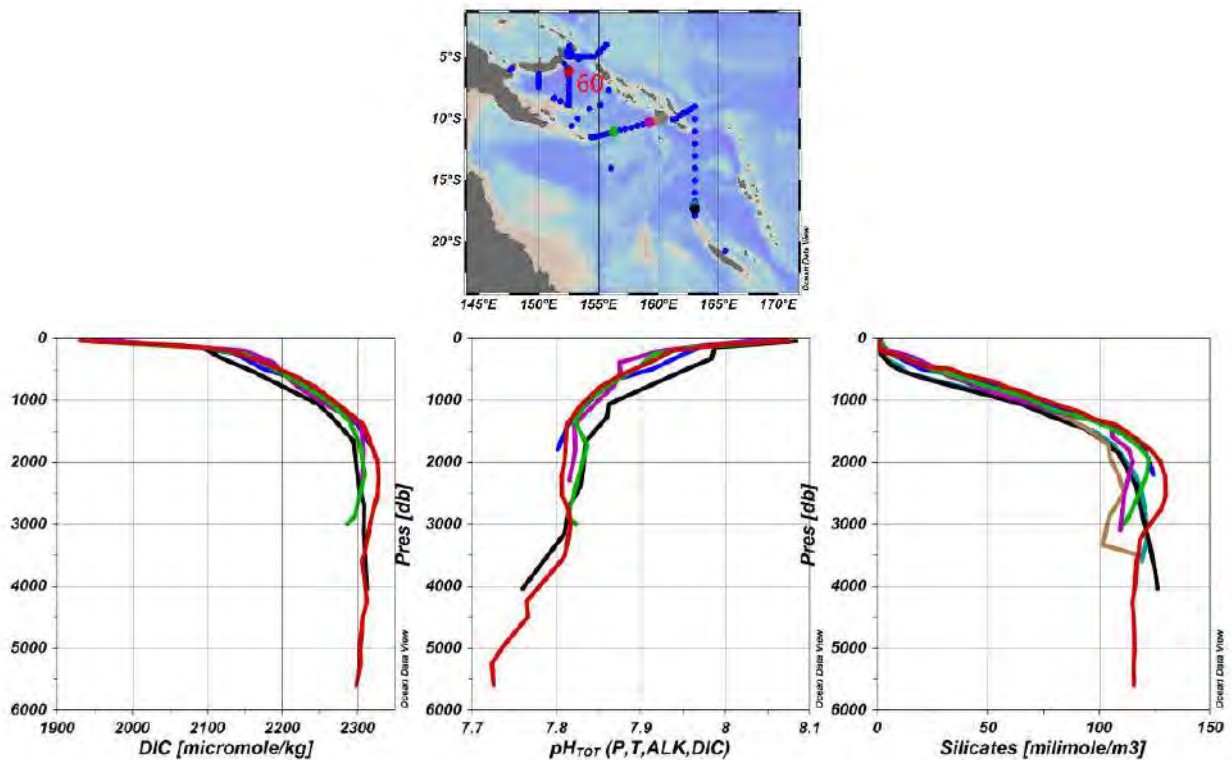


Figure 6-4 Vertical distributions of dissolved inorganic carbon(DIC), pH and Silicate (SiO_4) between different stations located in the Coral Sea, at the entrance and in the core (st 60) of the Solomon Sea. Profile colors relate to the stations on the map, station 60 (middle of the Solomon Sea) is highlighted in red.

6.2.3 Future collaboration between Vietnam-France: project PLUME

At present, several French laboratories investigate the flow of riverine water into the estuarine-coastal adjacent waters in Vietnam together with close partnership with Vietnamese laboratories. PLUME project was then proposed in collaboration between French and Vietnamese scientists. This project aims at studying the transport and fate of natural and anthropogenic material, as well as their influence on the water composition. This includes the two major classes of anthropogenic carbonaceous particles, plastics and Black Carbon from the Mekong and Red River deltas and the Saigon Dongnai system to the ocean and other contaminants, and their impact on planktonic productivity and community structure. The impact of these materials on biological production and community structure is of great interest in

Vietnam, where the threats of anthropogenic materials are increasing vertiginously and are worsened by climate change derived effects such as coastal erosion, sea level rise and warming.

In Vietnam, there is no civil oceanographic research vessel available to undertake this research. The cruises organized by the French researchers and their Vietnamese partners usually depend on the rental of small touristic boats, which restrains enormously the working efficiency. The research teams concerned are thus determined to organize a proper oceanographic cruise focusing on three river plumes and their impact on the coastal zone (Red River Delta, Saigon Dongnai Estuary, Mekong Delta). Through dedicated sampling in each of these areas, the scientists will collect invaluable set of data that will allow them to map the spatial variability of the natural physical, chemical and biological characteristics and their evolution as river waters meet the ocean, as well as those of contaminants including black carbon, plastics, emerging contaminants, mercury and trace metals. The cruise is planned to take place in the summer monsoon, when rivers experience their most voluminous discharge. Importantly, this cruise will produce a unique calibration dataset to feed sediment-hydrodynamics-biogeochemical coupled models used to complement the observational results obtained from our target study zones.

One of the main question will be to quantify dissolved-particulate exchanges. After finishing my PhD thesis, I will be able to analyze the REE and Nd-IC and other trace metals, among them contaminants and to study the processes at play at the land-ocean interface. Rivers, one of the carriers that transport dissolved and particulate material to seawater will be considered. Within the estuaries, the mixing between fresh and salt water could result in removing dissolved elements to particulate phase and trapping them the bottom sediment (e.g: Fe by coagulation; (Eckert and Sholkovitz, 1976; Sholkovitz, 1980). The analysis of REE concentration and Nd-IC in both dissolved and particulate phase could bring to light some interesting information, including: i) distribution of dREE and Nd-IC in both horizontal and vertical axis, contributing in global data set of trace element; ii) understanding the interaction between dissolved/particulate phase during the estuarine mixing. By coupling the dissolved and particulate REE data, the information about authigenic and lithogenic fraction of the sinking particle will be brought to light, result in better understanding on scavenging process happening at the fresh-salt water interface; iii) Nd parameters could be used as complementary element to quantify the amount of nutrient (e.g: Si) and also major elements (Fe, Zn) brought to ocean; iv) the anthropogenic anomaly of Gd in the environment could be used to traced back to the increasing use of Gd-based contrast agents (Gd-CAs) used in magnetic resonance imaging (MRI).

Reference

- Akagi, T. *et al.* (2011) 'Composition of rare earth elements in settling particles collected in the highly productive North Pacific Ocean and Bering Sea: Implications for siliceous-matter dissolution kinetics and formation of two REE-enriched phases', *Geochimica et Cosmochimica Acta*, 75(17), pp. 4857–4876. doi: 10.1016/j.gca.2011.06.001.
- Akagi, T. (2013) 'Rare earth element (REE)-silicic acid complexes in seawater to explain the incorporation of REEs in opal and the "leftover" REEs in surface water: New interpretation of dissolved REE distribution profiles', *Geochimica et Cosmochimica Acta*, 113, pp. 174–192. doi: 10.1016/j.gca.2013.03.014.
- Alberty, M. *et al.* (2019) 'Moored Observations of Transport in the Solomon Sea', *Journal of Geophysical Research: Oceans*. Blackwell Publishing Ltd, 124(11), pp. 8166–8192. doi: 10.1029/2019JC015143.
- Alberty, M. S. *et al.* (2017) 'Spatial patterns of mixing in the Solomon Sea', *Journal of Geophysical Research: Oceans*. Blackwell Publishing Ltd, 122(5), pp. 4021–4039. doi: 10.1002/2016JC012666.
- Alibo, D. S. and Nozaki, Y. (1999) 'Rare earth elements in seawater: Particle association, shale-normalization, and Ce oxidation', *Geochimica et Cosmochimica Acta*, 63(3–4), pp. 363–372. doi: 10.1016/S0016-7037(98)00279-8.
- Allen, C. M. (2000) 'Evolution of a post-batholith dike swarm in central coastal Queensland, Australia: Arc-front to backarc?', *Lithos*, 51(4), pp. 331–349. doi: 10.1016/S0024-4937(99)00068-7.
- Allen, M. G. (2018) 'Mining in Contemporary Solomon Islands', in *Resource Extraction and Contentious States*. Springer Singapore, pp. 105–126. doi: 10.1007/978-981-10-8120-0_5.
- Arsouze, T. *et al.* (2008) 'A modeling sensitivity study of the influence of the Atlantic meridional overturning circulation on neodymium isotopic composition at the Last Glacial Maximum', *Climate of the Past*. European Geosciences Union, 4(3), pp. 191–203. doi: 10.5194/cp-4-191-2008.
- Arsouze, T. *et al.* (2009) 'Reconstructing the Nd oceanic cycle using a coupled dynamical-Biogeochemical model', *Biogeosciences*. doi: 10.5194/bg-6-2829-2009.
- De Baar, H. J. W., Brewer, P. G. and Bacon, M. P. (1985) 'Anomalies in rare earth distributions in seawater: Gd and Tb', *Geochimica et Cosmochimica Acta*, 49(9), pp. 1961–1969. doi: 10.1016/0016-7037(85)90090-0.
- Bedinger, G. M., Kohler, J. J. and Wallace, G. J. (2018) *Titanium - 2015 [Advance Release]*, U.S. Geological Survey Minerals Yearbook 2015: Volume I, Metals and Minerals. Reston, VA. doi: 10.3133/mybvI.
- Behrens, M. K. *et al.* (2016) 'Rapid and precise analysis of rare earth elements in small volumes of seawater - Method and intercomparison', *Marine Chemistry*. Elsevier B.V., 186, pp. 110–120. doi: 10.1016/j.marchem.2016.08.006.

- Behrens, M. K. *et al.* (2018) 'Rare earth element distributions in the West Pacific: Trace element sources and conservative vs. non-conservative behavior', *Earth and Planetary Science Letters*. Elsevier B.V., 486, pp. 166–177. doi: 10.1016/j.epsl.2018.01.016.
- Beier, C. *et al.* (2015) 'Origin of Silicic Magmas at Spreading Centres—an Example from the South East Rift, Manus Basin', *Journal of Petrology*, 56(2), pp. 255–272. doi: 10.1093/petrology/egu077.
- Bertram, C. J. and Elderfield, H. (1993) 'The geochemical balance of the rare earth elements and neodymium isotopes in the oceans', *Geochimica et Cosmochimica Acta*, 57(9), pp. 1957–1986. doi: 10.1016/0016-7037(93)90087-D.
- Billier, D. V. and Bruland, K. W. (2012) 'Analysis of Mn, Fe, Co, Ni, Cu, Zn, Cd, and Pb in seawater using the Nobias-chelate PA1 resin and magnetic sector inductively coupled plasma mass spectrometry (ICP-MS)', *Marine Chemistry*. Elsevier B.V., 130–131, pp. 12–20. doi: 10.1016/j.marchem.2011.12.001.
- Bonnet, S. *et al.* (2016) 'Diazotroph derived nitrogen supports diatom growth in the South West Pacific: A quantitative study using nanoSIMS', *Limnology and Oceanography*. Wiley Blackwell, 61(5), pp. 1549–1562. doi: 10.1002/lno.10300.
- Bonnet, S. *et al.* (2017) 'Hot spot of N₂ fixation in the western tropical South Pacific pleads for a spatial decoupling between N₂ fixation and denitrification', *Proceedings of the National Academy of Sciences of the United States of America*. National Academy of Sciences, pp. E2800–E2801. doi: 10.1073/pnas.1619514114.
- Bostock, H. C., Opdyke, B. N. and Williams, M. J. M. (2010) 'Characterising the intermediate depth waters of the Pacific Ocean using $\delta^{13}\text{C}$ and other geochemical tracers', *Deep-Sea Research Part I: Oceanographic Research Papers*, 57(7), pp. 847–859. doi: 10.1016/j.dsr.2010.04.005.
- Briqueu, L. *et al.* (1994) 'Temporal Magmatic Evolution of the Aoba Basin, Central New Hebrides Island Arc: Pb, Sr, and Nd Isotopic Evidence for the Coexistence of Two Mantle Components beneath the Arc', in *Proceedings of the Ocean Drilling Program, 134 Scientific Results*. Ocean Drilling Program. doi: 10.2973/odp.proc.sr.134.019.1994.
- Byrne, R. H. and Kim, K. H. (1990) 'Rare earth element scavenging in seawater', *Geochimica et Cosmochimica Acta*, 54(10), pp. 2645–2656. doi: 10.1016/0016-7037(90)90002-3.
- Cameron, W. E., McCulloch, M. T. and Walker, D. A. (1983) 'Boninite petrogenesis: chemical and Nd-Sr isotopic constraints', *Earth and Planetary Science Letters*, 65(1), pp. 75–89. doi: 10.1016/0012-821X(83)90191-7.
- Ceccarelli, D. M. *et al.* (2013) 'The Coral Sea. Physical Environment, Ecosystem Status and Biodiversity Assets.', in *Advances in Marine Biology*. Academic Press, pp. 213–290. doi: 10.1016/B978-0-12-408096-6.00004-3.
- Chadwick, J. *et al.* (2009) 'Arc lavas on both sides of a trench: Slab window effects at the Solomon Islands triple junction, SW Pacific', *Earth and Planetary Science Letters*, 279(3–4), pp. 293–302. doi: 10.1016/j.epsl.2009.01.001.

- Chavagnac, V. *et al.* (2007) 'Anti-Atlas Moroccan Chain as the source of lithogenic-derived micronutrient fluxes to the deep Northeast Atlantic Ocean', *Geophysical Research Letters*, 34(21). doi: 10.1029/2007GL030985.
- Chavagnac, V. *et al.* (2008) 'Tracing dust input to the Mid-Atlantic Ridge between 14°45'N and 36°14'N: Geochemical and Sr isotope study', *Marine Geology*. Elsevier, 247(3–4), pp. 208–225. doi: 10.1016/j.margeo.2007.09.003.
- Chavagnac, V. *et al.* (2018) 'Spatial Variations in Vent Chemistry at the Lucky Strike Hydrothermal Field, Mid-Atlantic Ridge (37°N): Updates for Subseafloor Flow Geometry From the Newly Discovered Capelinhos Vent', *Geochemistry, Geophysics, Geosystems*. Blackwell Publishing Ltd, 19(11), pp. 4444–4458. doi: 10.1029/2018GC007765.
- Chelgani, S. C. *et al.* (2015) 'A review of rare earth minerals flotation: Monazite and xenotime', *International Journal of Mining Science and Technology*. China University of Mining and Technology, 25(6), pp. 877–883. doi: 10.1016/j.ijmst.2015.09.002.
- Cravatte, S. *et al.* (2011) 'Observed circulation in the Solomon Sea from SADC data', *Progress in Oceanography*, 88(1–4), pp. 116–130. doi: 10.1016/j.pocean.2010.12.015.
- Cravatte, S. *et al.* (2017) 'Subthermocline and Intermediate Zonal Currents in the Tropical Pacific Ocean: Paths and Vertical Structure', *Journal of Physical Oceanography*, 47(9), pp. 2305–2324. doi: 10.1175/jpo-d-17-0043.1.
- Cravatte, S., Kessler, W. S. and Marin, F. (2012) 'Intermediate Zonal Jets in the Tropical Pacific Ocean Observed by Argo Floats*', *Journal of Physical Oceanography*, 42(9), pp. 1475–1485. doi: 10.1175/jpo-d-11-0206.1.
- Cunningham, H. *et al.* (2012) 'Rapid magmatic processes accompany arc-continent collision: The Western Bismarck arc, Papua New Guinea', *Contributions to Mineralogy and Petrology*. Springer-Verlag, 164(5), pp. 789–804. doi: 10.1007/s00410-012-0776-y.
- Cunningham, H. S. *et al.* (2009) 'Temporal Variations in U-series Disequilibria in an Active Caldera, Rabaul, Papua New Guinea', *Journal of Petrology*. Narnia, 50(3), pp. 507–529. doi: 10.1093/petrology/egp009.
- Deacon, G. (1937) *The hydrology of the southern ocean*. London ;New York: Cambridge University Press ;;Macmillan.
- Eckert, J. M. and Sholkovitz, E. R. (1976) 'The flocculation of iron, aluminium and humates from river water by electrolytes', *Geochimica et Cosmochimica Acta*. Pergamon, 40(7), pp. 847–848. doi: 10.1016/0016-7037(76)90036-3.
- Elderfield, H. (1990) 'Tracers of ocean paleoproductivity and paleochemistry: An introduction', *Paleoceanography*, 1 October, pp. 711–717. doi: 10.1029/PA005i005p00711.
- Elderfield, H., Upstill-Goddard, R. and Sholkovitz, E. R. (1990) 'The rare earth elements in rivers, estuaries, and coastal seas and their significance to the composition of ocean waters', *Geochimica et Cosmochimica Acta*, 54(4), pp. 971–991. doi: 10.1016/0016-7037(90)90432-K.
- Elrod, V. A. *et al.* (2004) 'The flux of iron from continental shelf sediments: A missing source for

- global budgets', *Geophysical Research Letters*, 31(12). doi: 10.1029/2004GL020216.
- Ewart, A., Chappell, B. W. and Menzies, M. A. (1988) 'An Overview of the Geochemical and Isotopic Characteristics of the Eastern Australian Cainozoic Volcanic Provinces', *Journal of Petrology*, Special_Vo(1), pp. 225–273. doi: 10.1093/petrology/Special_Volume.1.225.
- Fabre, S. *et al.* (2019) 'An Overlooked Silica Source of the Modern Oceans: Are Sandy Beaches the Key?', *Frontiers in Earth Science*. Frontiers Media S.A., 7, p. 231. doi: 10.3389/feart.2019.00231.
- Fine, R. A. *et al.* (1994) 'The western equatorial Pacific: A water mass crossroads', *Journal of Geophysical Research*, 99(C12), p. 25063. doi: 10.1029/94JC02277.
- van de Fliedt, T. *et al.* (2012) 'GEOTRACES intercalibration of neodymium isotopes and rare earth element concentrations in seawater and suspended particles. Part 1: Reproducibility of results for the international intercomparison', *Limnology and Oceanography: Methods*. doi: 10.4319/lom.2012.10.234.
- Ganachaud, A. *et al.* (2007) *Southwest Pacific Ocean Circulation and Climate Experiment (SPICE) Part I. Scientific Background*.
- Ganachaud, A. *et al.* (2014a) 'The Southwest Pacific Ocean circulation and climate experiment (SPICE)', *Journal of Geophysical Research: Oceans*, 119(11), pp. 7660–7686. doi: 10.1002/2013JC009678.
- Ganachaud, A. *et al.* (2014b) 'The Southwest Pacific Ocean circulation and climate experiment (SPICE)', *Journal of Geophysical Research: Oceans*, 119(11), pp. 7660–7686. doi: 10.1002/2013JC009678.
- Ganachaud, A. *et al.* (2017) 'The Solomon Sea: its circulation, chemistry, geochemistry and biology explored during two oceanographic cruises', *Elem Sci Anth*. University of California Press, 5(0), p. 33. doi: 10.1525/elementa.221.
- Ganachaud, P. (2008) 'Southwest Pacific Ocean Circulation and Climate Experiment (SPICE): Part II. Implementation Plan'. International CLIVAR Project Office. Available at: <http://eprints.soton.ac.uk/id/eprint/65402> (Accessed: 30 April 2020).
- Garcia-Solsona, E. *et al.* (2014) 'Rare earth elements and Nd isotopes tracing water mass mixing and particle-seawater interactions in the SE Atlantic', *Geochimica et Cosmochimica Acta*. doi: 10.1016/j.gca.2013.10.009.
- Gasparin, F., Ganachaud, A. and Maes, C. (2011) 'A western boundary current east of New Caledonia: Observed characteristics', *Deep-Sea Research Part I: Oceanographic Research Papers*, 58(9), pp. 956–969. doi: 10.1016/j.dsr.2011.05.007.
- Germineaud, C. (2016) *Circulation Océanique et Variabilité en Mer des Salomon*. Université Toulouse 3 Paul Sabatier (UT3 Paul Sabatier).
- Germineaud, C. *et al.* (2016) 'Pathways and Water Mass Properties of the Thermocline and Intermediate Waters in the Solomon Sea', *Journal of Physical Oceanography*, 46(10), pp. 3031–3049. doi: 10.1175/jpo-d-16-0107.1.

- Goldstein, S. L. and Hemming, S. R. (2003) 'Long-lived Isotopic Tracers in Oceanography, Paleooceanography, and Ice-sheet Dynamics', in *Treatise on Geochemistry*. Elsevier, pp. 453–489. doi: 10.1016/B0-08-043751-6/06179-X.
- Grenier, M. *et al.* (2011) 'From the western boundary currents to the Pacific Equatorial Undercurrent: Modeled pathways and water mass evolutions', *Journal of Geophysical Research: Oceans*, 116(12). doi: 10.1029/2011JC007477.
- Grenier, M. (2012) *Le rôle du Pacifique Tropical Sud-Ouest dans la fertilisation du Pacifique Équatorial: couplage dynamique et multi-traceur*. Université Toulouse 3 Paul Sabatier (UT3 Paul Sabatier).
- Grenier, M. *et al.* (2013) 'From the subtropics to the central equatorial Pacific Ocean: Neodymium isotopic composition and rare earth element concentration variations', *Journal of Geophysical Research: Oceans*, 118(2), pp. 592–618. doi: 10.1029/2012JC008239.
- Grenier, M. *et al.* (2018) 'Differentiating Lithogenic Supplies, Water Mass Transport, and Biological Processes On and Off the Kerguelen Plateau Using Rare Earth Element Concentrations and Neodymium Isotopic Compositions', *Frontiers in Marine Science*, 5. doi: 10.3389/fmars.2018.00426.
- Grenier, M., Jeandel, C. and Cravatte, S. (2014) 'From the subtropics to the equator in the Southwest Pacific: Continental material fluxes quantified using neodymium data along modeled thermocline water pathways', *Journal of Geophysical Research: Oceans*, 119(6), pp. 3948–3966. doi: 10.1002/2013JC009670.
- Haley, B. A. *et al.* (2014) 'Biogeochemical implications from dissolved rare earth element and Nd isotope distributions in the Gulf of Alaska', *Geochimica et Cosmochimica Acta*, 126, pp. 455–474. doi: 10.1016/j.gca.2013.11.012.
- Haley, B. A., Klinkhammer, G. P. and McManus, J. (2004) 'Rare earth elements in pore waters of marine sediments', *Geochimica et Cosmochimica Acta*, 68(6), pp. 1265–1279. doi: 10.1016/j.gca.2003.09.012.
- Hanawa, K. and Talley, L. D. (2001) 'Chapter 5.4 Mode waters', *International Geophysics*. Academic Press, 77(C), pp. 373–386. doi: 10.1016/S0074-6142(01)80129-7.
- Handler, M. R., Bennett, V. C. and Carlson, R. W. (2005) 'Nd, Sr and Os isotope systematics in young, fertile spinel peridotite xenoliths from northern Queensland, Australia: A unique view of depleted MORB mantle?', *Geochimica et Cosmochimica Acta*, 69(24), pp. 5747–5763. doi: 10.1016/j.gca.2005.08.003.
- Hasson, A. *et al.* (2012) 'The origin and fate of mode water in the southern Pacific Ocean', *Ocean Dynamics*, 62(3), pp. 335–354. doi: 10.1007/s10236-011-0507-3.
- Hathorne, E. C. *et al.* (2012) 'Online preconcentration ICP-MS analysis of rare earth elements in seawater', *Geochemistry, Geophysics, Geosystems*. Wiley Online Library, 13(1). doi: 10.1029/2011GC003907.
- Hatje, V., Bruland, K. W. and Flegal, A. R. (2014) 'Determination of rare earth elements after pre-

- concentration using NOBIAS-chelate PA-1@resin: Method development and application in the San Francisco Bay plume', *Marine Chemistry*, 160, pp. 34–41. doi: 10.1016/j.marchem.2014.01.006.
- Hegner, E. and Smith, I. E. M. (1992) 'Isotopic compositions of late Cenozoic volcanics from southeast Papua New Guinea: Evidence for multi-component sources in arc and rift environments', *Chemical Geology*, 97(3–4), pp. 233–249. doi: 10.1016/0009-2541(92)90078-J.
- Homoky, W. B. *et al.* (2013) 'Distinct iron isotopic signatures and supply from marine sediment dissolution', *Nature Communications*. Nature Publishing Group, 4(1), pp. 1–10. doi: 10.1038/ncomms3143.
- Homoky, W. B. *et al.* (2016) 'Quantifying trace element and isotope fluxes at the ocean-sediment boundary: A review', *Philosophical Transactions of the Royal Society A: Mathematical, Physical and Engineering Sciences*. Royal Society of London. doi: 10.1098/rsta.2016.0246.
- Hristova, H. G. and Kessler, W. S. (2012) 'Surface circulation in the solomon sea derived from lagrangian drifter observations', *Journal of Physical Oceanography*, 42(3), pp. 448–458. doi: 10.1175/JPO-D-11-099.1.
- Jeandel, C. (1993) 'Concentration and isotopic composition of Nd in the South Atlantic Ocean', *Earth and Planetary Science Letters*. Elsevier, 117(3–4), pp. 581–591. doi: 10.1016/0012-821X(93)90104-H.
- Jeandel, C. *et al.* (2007) 'Isotopic Nd compositions and concentrations of the lithogenic inputs into the ocean: A compilation, with an emphasis on the margins', *Chemical Geology*, 239(1–2), pp. 156–164. doi: 10.1016/j.chemgeo.2006.11.013.
- Jeandel, C. *et al.* (2013) 'Rare earth element concentrations and Nd isotopes in the Southeast Pacific Ocean', *Geochemistry, Geophysics, Geosystems*, 14(2), pp. 328–341. doi: 10.1029/2012GC004309.
- Jeandel, C. (2016) 'Overview of the mechanisms that could explain the “Boundary Exchange” at the land-ocean contact', *Philosophical Transactions of the Royal Society A: Mathematical, Physical and Engineering Sciences*. Royal Society of London. doi: 10.1098/rsta.2015.0287.
- Jeandel, C., Bishop, J. K. and Zindler, A. (1995) 'Exchange of neodymium and its isotopes between seawater and small and large particles in the Sargasso Sea', *Geochimica et Cosmochimica Acta*. Pergamon, 59(3), pp. 535–547. doi: 10.1016/0016-7037(94)00367-U.
- Johannesson, K. H. *et al.* (2017) 'Rare earth element behavior during groundwater–seawater mixing along the Kona Coast of Hawaii', *Geochimica et Cosmochimica Acta*. Elsevier Ltd, 198, pp. 229–258. doi: 10.1016/j.gca.2016.11.009.
- Johnson, G. C. and McPhaden, M. J. (1999) 'Interior Pycnocline Flow from the Subtropical to the Equatorial Pacific Ocean*', *Journal of Physical Oceanography*. doi: 10.1175/1520-0485(1999)029<3073:IPFFTS>2.0.CO;2.
- Johnson, K. S. *et al.* (1994) 'Iron photochemistry in seawater from the equatorial Pacific', *Marine Chemistry*. Elsevier, 46(4), pp. 319–334. doi: 10.1016/0304-4203(94)90029-9.

- Jupiter, S. *et al.* (2018) 'Solomon Islands: Coastal and marine ecosystems', in *World Seas: An Environmental Evaluation Volume II: The Indian Ocean to the Pacific*. Elsevier, pp. 855–874. doi: 10.1016/B978-0-08-100853-9.00043-9.
- Kamenetsky, V. S. *et al.* (2001) 'Parental basaltic melts and fluids in eastern Manus backarc Basin: Implications for hydrothermal mineralisation', *Earth and Planetary Science Letters*, 184(3–4), pp. 685–702. doi: 10.1016/S0012-821X(00)00352-6.
- Kawabe, M. *et al.* (2009) 'Water masses and currents of deep circulation southwest of the Shatsky Rise in the western North Pacific', *Deep-Sea Research Part I: Oceanographic Research Papers*. doi: 10.1016/j.dsr.2009.06.003.
- Kawabe, M. and Fujio, S. (2010) 'Pacific ocean circulation based on observation', *Journal of Oceanography*. Springer Netherlands, 66(3), pp. 389–403. doi: 10.1007/s10872-010-0034-8.
- Kessler, W. *et al.* (2017) 'The Solomon Sea: its circulation, chemistry, geochemistry and biology explored during two oceanographic cruises', *Elem Sci Anth*, 5, p. 33. doi: 10.1525/elementa.221.
- Kessler, W. S. (1999) 'Interannual Variability of the Subsurface High Salinity Tongue South of the Equator at 165°E*', *Journal of Physical Oceanography*, 29(8), pp. 2038–2049. doi: 10.1175/1520-0485(1999)029<2038:IVOTSH>2.0.CO;2.
- Kessler, W. S. and Cravatte, S. (2013a) 'ENSO and Short-Term Variability of the South Equatorial Current Entering the Coral Sea', *Journal of Physical Oceanography*. doi: 10.1175/JPO-D-12-0113.1.
- Kessler, W. S. and Cravatte, S. (2013b) 'Mean circulation of the Coral Sea', *Journal of Geophysical Research: Oceans*. doi: 10.1002/2013JC009117.
- Klaver, G. *et al.* (2014) 'Anthropogenic Rare Earth Element in rivers: GADOLINIUM and lanthanum. Partitioning between the dissolved and particulate phases in the Rhine River and spatial propagation through the Rhine-Meuse Delta (the Netherlands)', *Applied Geochemistry*. Elsevier Ltd, 47, pp. 186–197. doi: 10.1016/j.apgeochem.2014.05.020.
- König, S. *et al.* (2007) 'The role of slab melting in the petrogenesis of high-Mg andesites: Evidence from Simbo Volcano, Solomon Islands', *Contributions to Mineralogy and Petrology*. Springer-Verlag, 153(1), pp. 85–103. doi: 10.1007/s00410-006-0136-x.
- Kulaksiz, S. and Bau, M. (2011) 'Rare earth elements in the Rhine River, Germany: First case of anthropogenic lanthanum as a dissolved microcontaminant in the hydrosphere', *Environment International*. Elsevier Ltd, 37(5), pp. 973–979. doi: 10.1016/j.envint.2011.02.018.
- Kulaksiz, S. and Bau, M. (2013) 'Anthropogenic dissolved and colloid/nanoparticle-bound samarium, lanthanum and gadolinium in the Rhine River and the impending destruction of the natural rare earth element distribution in rivers', *Earth and Planetary Science Letters*. Elsevier, 362, pp. 43–50. doi: 10.1016/j.epsl.2012.11.033.
- Labatut, M. *et al.* (2014) 'Iron sources and dissolved-particulate interactions in the seawater of

- the Western Equatorial Pacific, iron isotope perspectives', *Global Biogeochemical Cycles*. doi: 10.1002/2014GB004928.
- Lacan, F. and Jeandel, C. (2001) 'Tracing Papua New Guinea imprint on the central Equatorial Pacific Ocean using neodymium isotopic compositions and rare earth element patterns', *Earth and Planetary Science Letters*. doi: 10.1016/S0012-821X(01)00263-1.
- Lacan, F. and Jeandel, C. (2004) 'Neodymium isotopic composition and rare earth element concentrations in the deep and intermediate Nordic Seas: Constraints on the Iceland Scotland Overflow Water signature', *Geochemistry, Geophysics, Geosystems*. John Wiley & Sons, Ltd, 5(11), p. n/a-n/a. doi: 10.1029/2004GC000742.
- Lacan, F. and Jeandel, C. (2005) 'Neodymium isotopes as a new tool for quantifying exchange fluxes at the continent-ocean interface', *Earth and Planetary Science Letters*. doi: 10.1016/j.epsl.2005.01.004.
- Lambelet, M. *et al.* (2016) 'Neodymium isotopic composition and concentration in the western North Atlantic Ocean: Results from the GEOTRACES GA02 section', *Geochimica et Cosmochimica Acta*. Elsevier Ltd, 177, pp. 1–29. doi: 10.1016/j.gca.2015.12.019.
- Lindley, I. D. (2006) 'Extensional and vertical tectonics in the New Guinea islands: Implications for island arc evolution', *Annals of Geophysics*, 49(1 SUPPL.), pp. 403–426.
- Mackey, D. J., O'Sullivan, J. E. Os. and Watson, R. J. (2002) 'Iron in the western Pacific: a riverine or hydrothermal source for iron in the Equatorial Undercurrent?', *Deep Sea Research Part I: Oceanographic Research Papers*. Pergamon, 49(5), pp. 877–893. doi: 10.1016/S0967-0637(01)00075-9.
- McCartney (1977) 'Subantarctic Mode Water', *George Deacon 70th, Anniversar*, pp. 103–119.
- Meija, J. *et al.* (2016) 'Atomic weights of the elements 2013 (IUPAC Technical Report)', *Pure and Applied Chemistry*. Walter de Gruyter GmbH, pp. 265–291. doi: 10.1515/pac-2015-0305.
- Melet, A. *et al.* (2010) 'Thermocline Circulation in the Solomon Sea: A Modeling Study*', *Journal of Physical Oceanography*. doi: 10.1175/2009JPO4264.1.
- Milliman, J. D. (1995) 'Sediment discharge to the ocean from small mountainous rivers: The New Guinea example', *Geo-Marine Letters*. Springer-Verlag, 15(3–4), pp. 127–133. doi: 10.1007/BF01204453.
- Milliman, J. D., Farnsworth, K. L. and Albertin, C. S. (1999) *Flux and fate of fluvial sediments leaving large islands in the East Indies*, *Journal of Sea Research*. Elsevier. doi: 10.1016/S1385-1101(98)00040-9.
- Moffett, J. W. (1990) 'Microbially mediated cerium oxidation in sea water', *Nature*. doi: 10.1038/345421a0.
- Moffett, J. W. (1994) 'A radiotracer study of cerium and manganese uptake onto suspended particles in Chesapeake Bay', *Geochimica et Cosmochimica Acta*. doi: 10.1016/0016-7037(94)90499-5.
- Morel, F. M. M. and Price, N. M. (2003) 'The biogeochemical cycles of trace metals in the oceans',

- Science*. American Association for the Advancement of Science, pp. 944–947. doi: 10.1126/science.1083545.
- Nohara, M. *et al.* (1994) 'The North Fiji Basin basalts and their magma sources: Part II. Sr-Nd isotopic and trace element constraints', *Marine Geology*, 116(1–2), pp. 179–195. doi: 10.1016/0025-3227(94)90175-9.
- Nozaki, Y. *et al.* (1999) 'Dissolved rare earth elements and hydrography in the Sulu Sea', *Geochimica et Cosmochimica Acta*. doi: 10.1016/S0016-7037(99)00142-8.
- Nozaki, Y. and Alibo, D. S. (2003) 'Importance of vertical geochemical processes in controlling the oceanic profiles of dissolved rare earth elements in the northeastern Indian Ocean', *Earth and Planetary Science Letters*. doi: 10.1016/S0012-821X(02)01027-0.
- Officer, C. B. and Ryther, J. H. (1980) 'The Possible Importance of Silicon in Marine Eutrophication', *Marine Ecology Progress Series*. Inter-Research Science Center, pp. 83–91. doi: 10.2307/24813305.
- Ogata, T. and Terakado, Y. (2006) 'Rare earth element abundances in some seawaters and related river waters from the Osaka Bay area, Japan: Significance of anthropogenic Gd', *Geochemical Journal*, 40(5), pp. 463–474. doi: 10.2343/geochemj.40.463.
- Olmez, I. *et al.* (1991) 'Rare Earth Elements in Sediments off Southern California: A New Anthropogenic Indicator', *Environmental Science and Technology*. American Chemical Society, 25(2), pp. 310–316. doi: 10.1021/es00014a015.
- Orsi, A. H. *et al.* (1995) *On the meridional extent and fronts of the Antarctic Circumpolar Current, Deep Sea Research Part I: Oceanographic Research Papers*. Pergamon. doi: 10.1016/0967-0637(95)00021-W.
- Orsi, A. H., Johnson, G. C. and Bullister, J. L. (1999) 'Circulation, mixing, and production of Antarctic Bottom Water', *Progress in Oceanography*. Pergamon, 43(1), pp. 55–109. doi: 10.1016/S0079-6611(99)00004-X.
- Patten, J. T. and Byrne, R. H. (2017) 'Assessment of Fe(III) and Eu(III) complexation by silicate in aqueous solutions', *Geochimica et Cosmochimica Acta*, 202, pp. 361–373. doi: 10.1016/j.gca.2016.12.004.
- Pedreira, R. M. A. *et al.* (2018) 'Tracking hospital effluent-derived gadolinium in Atlantic coastal waters off Brazil', *Water Research*. Elsevier Ltd, 145, pp. 62–72. doi: 10.1016/j.watres.2018.08.005.
- Pérez-Tribouillier, H. *et al.* (2013) 'Quantifying lithogenic inputs to the North Pacific Ocean using the long-lived thorium isotopes', *Earth and Planetary Science Letters*. Frontiers, 383, pp. 16–25. doi: 10.1016/j.epsl.2013.09.025.
- Persson, P. O. *et al.* (2011) 'Determination of Nd isotopes in water: A chemical separation technique for extracting Nd from seawater using a chelating resin', *Analytical Chemistry*, 83(4), pp. 1336–1341. doi: 10.1021/ac102559k.
- Pham, V. (2015) *Tracing the land to ocean inputs: focus on the Coral and the Solomon Seas*.

- Pham, V. Q. *et al.* (2019) 'Dissolved rare earth elements distribution in the Solomon Sea', *Chemical Geology*. Elsevier, 524(May), pp. 11–36. doi: 10.1016/j.chemgeo.2019.05.012.
- Qu, T. *et al.* (2008) 'Subduction of South Pacific waters', *Geophysical Research Letters*. doi: 10.1029/2007GL032605.
- Qu, T. *et al.* (2009) 'Origin and Pathway of Equatorial 13°C Water in the Pacific Identified by a Simulated Passive Tracer and Its Adjoint*', *Journal of Physical Oceanography*. doi: 10.1175/2009JPO4045.1.
- Qu, T., Gao, S. and Fine, R. A. (2013) 'Subduction of South Pacific Tropical Water and Its Equatorward Pathways as Shown by a Simulated Passive Tracer', *Journal of Physical Oceanography*, 43(8), pp. 1551–1565. doi: 10.1175/JPO-D-12-0180.1.
- Qu, T. and Lindstrom, E. J. (2002) 'A Climatological Interpretation of the Circulation in the Western South Pacific*', *Journal of Physical Oceanography*. doi: 10.1055/s-2007-989442.
- Qu, T. and Lindstrom, E. J. (2004) 'Northward Intrusion of Antarctic Intermediate Water in the Western Pacific*', *Journal of Physical Oceanography*, 34(9), pp. 2104–2118. doi: 10.1175/1520-0485(2004)034<2104:nioaiw>2.0.co;2.
- Raven, J. A., Evans, M. C. W. and Korb, R. E. (1999) 'The role of trace metals in photosynthetic electron transport in O₂-evolving organisms', *Photosynthesis Research*. Springer Netherlands, pp. 111–150. doi: 10.1023/A:1006282714942.
- Reid, J. L. (1986) *On the Total Geostrophic Circulation of the South Pacific Ocean: Flow Patterns, Tracers and Transports*, *Prog. Oceanog.*
- Reid, J. L. (1997) 'On the total geostrophic circulation of the Pacific Ocean: Flow patterns, tracers, and transports', *Progress in Oceanography*. Elsevier Ltd, pp. 263–352. doi: 10.1016/S0079-6611(97)00012-8.
- Rousseau, T. C. C. *et al.* (2013) 'Rare earth element analysis in natural waters by multiple isotope dilution-sector field ICP-MS', *Journal of Analytical Atomic Spectrometry*, 28(4), pp. 573–584. doi: 10.1039/c3ja30332b.
- Rousseau, T. C. C. *et al.* (2015) 'Rapid neodymium release to marine waters from lithogenic sediments in the Amazon estuary', *Nature Communications*. doi: 10.1038/ncomms8592.
- Rudnick, R. L. *et al.* (1986) 'Lower crustal xenoliths from Queensland, Australia: Evidence for deep crustal assimilation and fractionation of continental basalts', *Geochimica et Cosmochimica Acta*, 50(6), pp. 1099–1115. doi: 10.1016/0016-7037(86)90391-1.
- Schoffman, H. *et al.* (2016) 'Iron-nutrient interactions within phytoplankton', *Frontiers in Plant Science*. Frontiers Research Foundation. doi: 10.3389/fpls.2016.01223.
- Schott, F. A., Wang, W. and Stammer, D. (2007) 'Variability of Pacific subtropical cells in the 50-year ECCO assimilation', *Geophysical Research Letters*. John Wiley & Sons, Ltd, 34(5). doi: 10.1029/2006GL028478.
- Schuth, S. *et al.* (2004) 'Geochemical constraints on the petrogenesis of arc picrites and basalts, New Georgia Group, Solomon Islands', *Contributions to Mineralogy and Petrology*, 148(3),

pp. 288–304. doi: 10.1007/s00410-004-0604-0.

- Schuth, S. *et al.* (2009) 'Petrogenesis of Lavas along the Solomon Island Arc, SW Pacific: Coupling of Compositional Variations and Subduction Zone Geometry', *Journal of Petrology*. Narnia, 50(5), pp. 781–811. doi: 10.1093/petrology/egp019.
- SCOR (2007) 'GEOTRACES - An international study of the global marine biogeochemical cycles of trace elements and their isotopes', *Chemie der Erde*. Elsevier GmbH, 67(2), pp. 85–131. doi: 10.1016/j.chemer.2007.02.001.
- Shabani, M. B., Akagi, T. and Masuda, A. (1992) 'Preconcentration of Trace Rare-Earth Elements in Seawater by Complexation with Bis(2-ethylhexyl) Hydrogen Phosphate and 2-Ethylhexyl Dihydrogen Phosphate Adsorbed on a C18 Cartridge and Determination by Inductively Coupled Plasma Mass Spectrometry', *Analytical Chemistry*, 64(7), pp. 737–743. doi: 10.1021/ac00031a008.
- Shaping a Nation: A Geology of Australia* (2012) *Shaping a Nation: A Geology of Australia*. ANU Press. doi: 10.22459/sn.08.2012.
- Sholkovitz, E. R. (1980) 'Removal of "soluble" iron in the Potomac River estuary: Comments', *Estuarine and Coastal Marine Science*. Academic Press, pp. 585–587. doi: 10.1016/S0302-3524(80)80010-7.
- Sholkovitz, E. R. *et al.* (1999) 'Island weathering: River sources of rare earth elements to the Western Pacific Ocean', *Marine Chemistry*. Elsevier, 68(1–2), pp. 39–57. doi: 10.1016/S0304-4203(99)00064-X.
- Sholkovitz, E. R., M Landing, W. and Lewis, B. L. (1994) *Ocean particle chemistry: The fractionation of rare earth elements between suspended particles and seawater*, *Geochimica et Cosmochimica Acta*.
- Slemons, L. O. *et al.* (2010) 'Western Pacific coastal sources of iron, manganese, and aluminum to the Equatorial Undercurrent', *Global Biogeochemical Cycles*. doi: 10.1029/2009GB003693.
- Sohrin, Y. *et al.* (2008) 'Multielemental determination of GEOTRACES key trace metals in seawater by ICPMS after preconcentration using an ethylenediaminetriacetic acid chelating resin', *Analytical chemistry*, 80(16), p. 16.
- Sokolov, S. and Rintoul, S. (2000) 'Circulation and water masses of the southwest Pacific: WOCE Section P11, Papua New Guinea to Tasmania', *Journal of Marine Research*. doi: 10.1357/002224000321511151.
- Song, H. *et al.* (2017) 'Anthropogenic rare earth elements and their spatial distributions in the Han River, South Korea', *Chemosphere*. Elsevier Ltd, 172, pp. 155–165. doi: 10.1016/j.chemosphere.2016.12.135.
- Speckbacher, R. *et al.* (2012) 'Fluid flow and metasomatic fault weakening in the Moresby Seamount detachment, Woodlark Basin, offshore Papua New Guinea', *Geochemistry, Geophysics, Geosystems*. Blackwell Publishing Ltd, 13(11). doi: 10.1029/2012GC004407.
- Tachikawa, K. (2003) 'Neodymium budget in the modern ocean and paleo-oceanographic implications', *Journal of Geophysical Research*, 108(C8). doi: 10.1029/1999jc000285.

- Tachikawa, K. *et al.* (2017) 'The large-scale evolution of neodymium isotopic composition in the global modern and Holocene ocean revealed from seawater and archive data', *Chemical Geology*. Elsevier B.V., 457, pp. 131–148. doi: 10.1016/j.chemgeo.2017.03.018.
- Tachikawa, K., Jeandel, C. and Roy-Barman, M. (1999) 'A new approach to the Nd residence time in the ocean: the role of atmospheric inputs', *Earth and Planetary Science Letters*. Elsevier, 170(4), pp. 433–446. doi: 10.1016/S0012-821X(99)00127-2.
- Talley, L. (2007) *Hydrographic Atlas of the World Ocean Circulation Experiment (WOCE) Volume 2: Pacific Ocean*.
- Talley, L. D. (1996) 'Antarctic Intermediate Water in the South Atlantic', in *The South Atlantic*, pp. 219–238. doi: 10.1007/978-3-642-80353-6_11.
- Tchilibou, M. *et al.* (2019) 'Internal tides in the Solomon Sea in contrasted ENSO conditions', *Ocean Science Discussions*, pp. 1–40. doi: 10.5194/os-2019-94.
- Tomczak, M. and Godfrey, J. S. (2003) *Regional Oceanography: an Introduction*. 2nd edn. Daya Publishing House.
- Tomczak, M. and Hao, D. (1989) 'Water masses in the thermocline of the coral sea', *Deep Sea Research Part A. Oceanographic Research Papers*, 36(10), pp. 1503–1514. doi: 10.1016/0198-0149(89)90054-X.
- Tsimplis, M. N., Bacon, S. and Bryden, H. L. (1998) 'The circulation of the subtropical South Pacific derived from hydrographic data', *Journal of Geophysical Research: Oceans*, 103(C10), pp. 21443–21468. doi: 10.1029/98JC01881.
- Tsuchiya, M. (1981) 'The Origin of the Pacific Equatorial 13°C Water', *Journal of Physical Oceanography*, 11(6), pp. 794–812. doi: 10.1175/1520-0485(1981)011<0794:TOOTPE>2.0.CO;2.
- Tsuchiya, M. *et al.* (1989) 'Source waters of the Pacific Equatorial Undercurrent', *Progress in Oceanography*, pp. 101–147. doi: 10.1016/0079-6611(89)90012-8.
- Tsuchiya, M. and Talley, L. D. (1998) 'A Pacific hydrographic section at 88°W: Water-property distribution', *Journal of Geophysical Research C: Oceans*. John Wiley & Sons, Ltd, 103(3336), pp. 12899–12918. doi: 10.1029/97jc03415.
- Wasserburg, G. J. *et al.* (1981) 'Precise determination of Sm Nd ratios, Sm and Nd isotopic abundances in standard solutions', *Geochimica et Cosmochimica Acta*, 45(12), pp. 2311–2323. doi: 10.1016/0016-7037(81)90085-5.
- Wen, B., Shan, X. and Xu, S. (1999) 'Preconcentration of ultratrace rare earth elements in seawater with 8-hydroxyquinoline immobilized polyacrylonitrile hollow fiber membrane for determination by inductively coupled plasma mass spectrometry', pp. 621–626.
- Wijffels, S. E., Toole, J. M. and Davis, R. (2001) 'Revisiting the South Pacific subtropical circulation: A synthesis of World Ocean Circulation Experiment observations along 32°S', *Journal of Geophysical Research: Oceans*. doi: 10.1029/1999JC000118.
- Winter, J. D. (John D. (2010) *Principles of igneous and metamorphic petrology*. Prentice Hall.

- Wyrтки, K. (1961) 'The subsurface water masses in the Western South Pacific Ocean', *Marine and Freshwater Research*, 13(1), pp. 18–47. doi: 10.1071/MF9620018.
- Zhang, J. and Nozaki, Y. (1996) 'Rare earth elements and yttrium in seawater: ICP-MS determinations in the East Caroline, Coral Sea, and South Fiji basins of the western South Pacific Ocean', *Geochimica et Cosmochimica Acta*, 60(23), pp. 4631–4644. doi: 10.1016/S0016-7037(96)00276-1.
- Zhang, J. and Nozaki, Y. (1998) 'Behavior of rare earth elements in seawater at the ocean margin: a study along the slopes of the Sagami and Nankai troughs near Japan', *Geochimica et Cosmochimica Acta*, 62(8), pp. 1307–1317. doi: 10.1016/S0016-7037(98)00073-8.
- Zhang, M. (2001) 'Petrogenesis and Geodynamic Implications of Late Cenozoic Basalts in North Queensland, Australia: Trace-element and Sr-Nd-Pb Isotope Evidence', *Journal of Petrology*, 42(4), pp. 685–719. doi: 10.1093/petrology/42.4.685.
- Zhang, Y., Lacan, F. and Jeandel, C. (2008) 'Dissolved rare earth elements tracing lithogenic inputs over the Kerguelen Plateau (Southern Ocean)', *Deep-Sea Research Part II: Topical Studies in Oceanography*, 55(5–7), pp. 638–652. doi: 10.1016/j.dsr2.2007.12.029.